Superconductivity in impurity systems with a lower density of charge carriers and with strong electron correlations

M. E. Palistrant*

Institute of Applied Physics, Academy of Sciences of Moldova, ul. Akademicheskaya 5, 2028 Kishinev, Moldova

(Submitted June 26, 2001; revised October 3, 2001)
Fiz. Nizk. Temp. **28**, 157–167 (February 2002)

The influence of a paramagnetic impurity on the superconducting transition temperature T_c, energy gap Ω_g, and order parameter Δ at $T=0$ is investigated in systems with a lower density of charge carriers and with strong electron correlations. It is shown that, since the Migdal theorem is violated in these systems, taking the vertex and ''crossing'' functions into account in the weak-coupling approximation explains the substantial change in the calculated quantities, in particular, the increase of T_c and of the critical impurity concentrations. The decrease of T_c, Δ, and Ω_g with increasing impurity concentration is slowed considerably in comparison with the case of conventional superconductors on account of nonadiabaticity effects. © *2002 American Institute of Physics.* [DOI: 10.1063/1.1461922]

1. INTRODUCTION

One of the important problems of the modern theory of superconductivity is to study the influence of impurities (nonmagnetic and magnetic) on the thermodynamic properties of high-T_c superconducting (HTSC) materials. This problem is one of real importance, since the free charge carriers and, hence, the superconductivity in these systems arises on account of doping, which leads to substantial disordering of the system. In addition, nonmagnetic and magnetic impurities can exist in real systems.

The difficulties of solving this problem stem from the unusual nature of the objects of study, which have a complex crystal structure, features in the electron energy spectrum, a lower density of charge carriers, strong electron correlations, etc. Taking all of these factors into account makes the problem unsolvable at this stage. Therefore, in our view, it is of interest to take the Fermi-liquid approach, which is based on the fact that at a certain carrier density a metallic state arises in which the electronic state is modified but not destroyed by the electron correlations. Consequently, a transition to a superconducting state can occur, with the formation of Cooper pairs (the BCS scenario) or local pairs (the Schafroth scenario).

In this approach (adopting the standard theory of Abrikosov and Gor'kov for systems with a randomly distributed impurity) one studies the influence of a nonmagnetic impurity on the superconducting transition temperature T_c in different models that enable one to take into account the overlap of the energy bands at the Fermi surface in the case of phonon[1,2] and nonphonon mechanisms of superconductivity,[3] the anisotropy of the electron–phonon interaction and the $d_{x^2-y^2}$ symmetry of the order parameter,[4] the mechanism of pair tunneling with s pairing,[5] etc. In all these studies the dependence of T_c on the concentration of the nonmagnetic impurity arises on account of various anisotropic properties of the particular system. In an isotropic system with s pairing, according to the Anderson theorem,[6] the thermodynamic properties of the superconductor are independent of the concentration of a nonmagnetic impurity.

Let us also mention Refs. 7 and 8, where, in a study of the influence of a nonmagnetic impurity on the properties of disordered systems, an attempt was made to go beyond the framework of the Abrikosov–Gor'kov approach by taking into account the spatial variation of the order parameter.

At the same time, a magnetic impurity in an isotropic system substantially suppresses the superconductivity on account of the exchange interaction and the breaking of Cooper pairs.[9]

The studies mentioned above were based on the use of the Migdal theorem,[10] which allows one to ignore the vertex corrections in determining the mass operators and the normal and anomalous Green's functions. This theory works in the region of large values of the Fermi energy ($\varepsilon_F \gg \omega_0$, where ω_0 is the characteristic boson frequency) and large values of the momentum transfer ($q \sim 2p_F$).

In oxide ceramics, organic superconductors, and fullerenes, the values of ε_F and ω_0 can be of the same order, and the momentum transfer $q \ll 2p_F$ because of the strong electron correlations.[11,12] As a result, the Migdal theorem is violated, and it becomes necessary to take into account additional many-particle effects determined by the vertex and ''crossing'' diagrams. Taking these (nonadiabaticity) effects into account in pure superconductors[13,14] leads, at small values of q, to positive values of the vertex functions and to the possibility of obtaining values of T_c corresponding to HTSC materials at moderate values of the electron–phonon interaction constant ($\lambda \sim 0.5-1$). Thus the lower concentration of charge carriers and the strong electron correlations in HTSC materials may be one of the reasons for their high-temperature superconductivity. Since nonadiabaticity effects are so substantial, it is unquestionably of interest to study the influence of an impurity on the value of T_c with these effects taken into account.

Here we solve this problem on the basis of a Hamiltonian of the Fröhlich type supplemented by an interaction of the electrons with a magnetic impurity. This interaction contains magnetic and nonmagnetic parts of the impurity scattering and, consequently, allows one to investigate a nonmagnetic impurity as a limiting case. Our task is to generalize the Abrikosov–Gor'kov theory[9] on the influence of a magnetic impurity on the superconducting transition temperature to systems with small values of the Fermi energy ($\varepsilon_F \sim \omega_0$) and momentum $q \ll 2p_F$, in which the Migdal theorem[10] is violated. This study will further our understanding of the processes of impurity scattering in oxide ceramics, fullerenes, and organic superconductors, which are nonadiabatic systems with strong electron correlations. We shall consider a three-dimensional system with a variable density of charge carriers (arbitrary filling of the energy band).

This paper is organized as follows. In Sec. 2 we give the Hamiltonian of the system and obtain the basic equations of the theory of superconductivity for a nonadiabatic system containing a paramagnetic impurity. Section 3 is devoted to the determination of the temperature of the superconducting transition: an equation is obtained for determining the value of T_c, analytical expressions are found in the region of small and large impurity concentrations, and analytical formulas are given for determining the vertex functions. In Sec. 4 we obtain equations for determining the order parameter Δ at $T=0$, the energy gap Ω_g, and the critical impurity concentration at which gapless superconductivity sets in. In Sec. 5 we carry out numerical calculations and analyze the results.

2. BASIC EQUATIONS

The Hamiltonian of a two-band system with a randomly distributed magnetic impurity is written in the form

$$H = H_0 + \sum_{\sigma} \int d\mathbf{x} \Psi_{\sigma}^{+}(\mathbf{x}) \Psi_{\sigma}(\mathbf{x}) \varphi(\mathbf{x}) + \sum_{\alpha\beta} \int d\mathbf{x} \Psi_{\alpha}^{+}(\mathbf{x}) V_{\alpha\beta}(\mathbf{x}) \Psi_{\beta}(\mathbf{x}), \tag{1}$$

where H_0 is the Hamiltonian of the free electrons and bosons, the second term corresponds to the electron–boson interaction responsible for the superconductivity, the third term describes the interaction of electrons with the magnetic impurity, $\psi_{\alpha}(\mathbf{x})$ is the annihilation operator for an electron with spin α at a point $\mathbf{x}$, $\varphi(\mathbf{x})$ is the boson operator, and

$$V_{\alpha\beta}(\mathbf{x}) = \sum_{n} V_{\alpha\beta}(\mathbf{x} - \mathbf{R}_n) = V_1(\mathbf{x}) \delta_{\alpha\beta} + \frac{1}{2} \mathbf{S} \sigma_{\alpha\beta} V_2(\mathbf{x}), \tag{2}$$

where $\mathbf{R}_n$ is the position of the impurity, $\mathbf{S}$ is the spin of the impurity, σ is the spin-matrix vector, and V_1 and V_2 are the nonmagnetic and magnetic parts of the scattering potential for electrons on the impurity.

We introduce the temperature electron and boson Green's functions

$$\begin{aligned} G_{\beta\alpha}(xx') &= -\langle T\Psi_{\beta}(x)\Psi_{\alpha}^{+}(x')\rangle; \\ \overline{F}_{\alpha\alpha'}(xx') &= -\langle T\Psi_{\alpha}^{+}(x)\Psi_{\alpha'}^{+}(x')\rangle; \\ \overline{F}_{\beta\beta'}(xx') &= -\langle T\Psi_{\beta}(x)\Psi_{\beta'}(x')\rangle; \\ D(xx') &= -\langle T\sqrt{2}(x)\varphi(x')\rangle; x = (x,\tau). \end{aligned} \tag{3}$$

We shall consider the joint influence of the electron–boson and electron–impurity interactions on the electron functions (3). With this goal we go over to the interaction representation and use perturbation theory,[15] treating both the electron–boson perturbation and the electron–impurity interaction. In the resulting perturbation series we perform an averaging over the positions of the randomly distributed impurities and over orientations of their spins in analogy with what is done in conventional superconductors,[2,9,16] taking into account, in addition to the usual diagrams (corresponding to the adiabatic theory), diagrams with a crossing of two electron–boson or of one electron–boson and one electron–impurity interaction lines. After this we sum over spin variables and obtain a system of equations for determining the Green's functions $\overline{G}(\mathbf{p}\Omega)$ and $\overline{F}(\mathbf{p}\Omega)$ averaged over the positions of the impurity.

Near the superconducting transition temperature ($T \sim T_c$) in the $\mathbf{p}\Omega$ representation the solution of these equations gives

$$\begin{aligned} \overline{G}(p\Omega) &= \frac{1}{i\Omega - \varepsilon_{\mathbf{p}} - \Sigma_N(\mathbf{p}\Omega)}; \\ \overline{F}(\mathbf{p}\Omega) &= \overline{G}(-\mathbf{p}, -\Omega)\Sigma_S(\mathbf{p}\Omega)\overline{G}(\mathbf{p}\Omega). \end{aligned} \tag{4}$$

Here the expressions for the mass operators in the graphical representation have the form [see (5) and (6)].

Here $\Sigma_N^0(\mathbf{p}\Omega)$ and $\Sigma_S^0(\mathbf{p}\Omega)$ contain diagrams corresponding to the electron–boson interaction, including diagrams with a crossing of two lines of the electron–boson interaction.[14] However, unlike the corresponding lines of Ref. 14, the solid lines in the definition of these quantities, just as in expressions (5) and (6), represent the total electron Green's functions averaged over the positions of the randomly distributed impurity and over orientations of the spins. The wavy lines refer to the electron–boson interaction, and the dashed lines to the electron–impurity interaction.

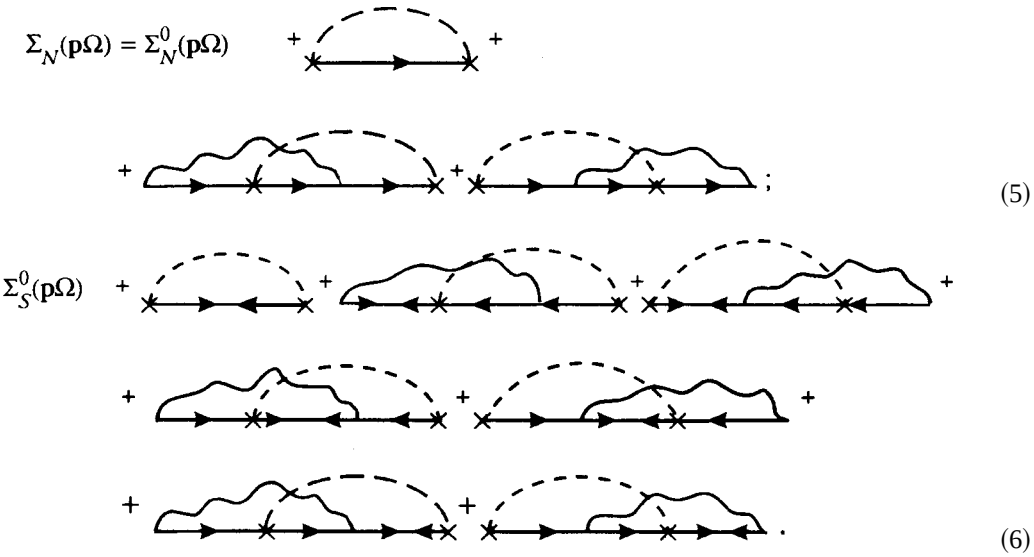

(5)

(6)

Now we use a model representation for the electron–boson and electron–impurity interactions:

$$|g_{\mathbf{pp}_1}|^2 = g^2\left(\frac{2p_F}{q_c}\right)^2 \theta(q_c - |\mathbf{p}-\mathbf{p}_1|); \tag{7}$$

$$U_\pm(\mathbf{p}-\mathbf{p}_1) = U_\pm\left(\frac{2p_F}{q_{c1}}\right)^2 \theta(q_{c1} - |\mathbf{p}-\mathbf{p}_1|), \tag{8}$$

where

$$U_\pm = c\left[V_1^2 \pm \frac{1}{4}S(S+1)V_2^2\right].$$

Here c is the concentration of the magnetic impurity, and q_c and q_{c1} are the cutoff momenta of the electron–boson and electron–impurity interactions.

The electron–boson interaction constant (7) is chosen in accordance with the theory of Refs. 13 and 14, according to which for $q_c \ll 2p_F$ the vertex and ''crossing'' functions are positive, which leads to an upward renormalization of the electron–boson interaction constant and, hence to an increase in the superconducting transition temperature. The smallness of the parameter q_c in turn is due to the presence of strong electron correlations in the system. Expression (7) is an approximate reflection of the results of the studies of the the influence of strong electron correlations on the electron–phonon interaction in Refs. 11, 12, and 17: the electron–phonon interaction increases weakly at small values of the momentum transfer $|\mathbf{p}-\mathbf{p}_1|$ and is sharply suppressed at larger values of $|\mathbf{p}-\mathbf{p}_1|$ on account of electron correlations. The factor $(2p_F/q_c)^2$ is introduced so that g^2 will be obtained as a result of the averaging. Consequently, in this model the constant $\lambda = N_0 g^2$ is independent of q_c, in agreement with the result of Ref. 11.

A similar situation also arises for other scattering mechanisms, such as impurity scattering, for example. Formula (8) reflects the suppression of the electron–impurity interaction for $|\mathbf{p}-\mathbf{p}_1| > q_{c1}$. The case $q_{c1} \ll 2p_F$ corresponds to the presence of strong electron correlations in the system.[11] We assume that the cutoff momenta q_c and q_{c1} are independent quantities.

With (7) and (8) taken into account, the expressions for the the quantities in (5) and (6), averaged over the Fermi surface, can be written in the form

$$\langle\langle \Sigma_N(\mathbf{p},\Omega)\rangle\rangle_{FS} = \Sigma_N(\Omega) = \frac{1}{\beta V}\sum_{\mathbf{p}_1\Omega_1} \overline{V}_N(\Omega\Omega_1)\overline{G}(\mathbf{p}_1\Omega_1) + \frac{1}{V}\sum_{\mathbf{p}_1} \overline{U}_+\overline{G}(\mathbf{p}_1\Omega); \tag{9}$$

$$\langle\langle \Sigma_S(\mathbf{p},\Omega)\rangle\rangle_{FS} = \Sigma_S(\Omega) = \frac{1}{\beta V}\sum_{\mathbf{p}_1\Omega_1} \overline{V}_S(\Omega\Omega_1)\overline{F}(\mathbf{p}_1\Omega_1) + \frac{1}{V}\sum_{\mathbf{p}_1} \overline{U}_-\overline{F}(\mathbf{p}_1\Omega), \tag{10}$$

where

$$\overline{V}_N(\Omega\Omega_1) = -g^2 D(\Omega\Omega_1)[1 + \lambda\overline{P}_V(Q_c\Omega\Omega_1)]; \tag{11}$$

$$\overline{V}_S(\Omega\Omega_1) = -g^2 D(\Omega\Omega_1)[1 + 2\lambda\overline{P}_V(Q_c\Omega\Omega_1) + \lambda\overline{P}_c(Q_c\Omega\Omega_1)] - \lambda D(\Omega\Omega_1) \times [2R_V^I(Q_{c1}\Omega\Omega_1) + R_c^I(Q_c\Omega\Omega_1) + R_c^{II}(Q_{c1}\Omega\Omega_1)]; \tag{12}$$

$$\overline{U}_\pm = U_\pm[1 + 2\lambda\overline{P}_V(Q_c\Omega\Omega)];$$

$$\overline{P}_V(Q_c\Omega\Omega) = \overline{P}_V(Q_c\Omega\Omega_1)|_{\Omega_1=\Omega}. \tag{13}$$

In (11)–(13) we have used the definitions

$$\overline{P}_V(Q_c\Omega\Omega_1) = -\frac{1}{\beta V}\left\langle\left\langle \sum_{\mathbf{p}_2\Omega_2}\left(\frac{2p_F}{q_c}\right)^2 \frac{1}{N_0}\theta(q_c - |\mathbf{p}-\mathbf{p}_2|) \times \overline{G}(\mathbf{p}_2\Omega_2)\overline{G}(\mathbf{p}_1+\mathbf{p}_2-\mathbf{p}, \Omega_1+\Omega_2-\Omega)D(\Omega\Omega_2)\right\rangle\right\rangle_{FS}; \tag{14}$$

$$\overline{P}_c(Q_c\Omega\Omega_1)=-\frac{1}{\beta V}\left\langle\left\langle\sum_{\mathbf{p}_2\Omega_2}\left(\frac{2p_F}{q_c}\right)^2\frac{1}{N_0}\theta(q_c-|\mathbf{p}-\mathbf{p}_2|)\times\overline{G}(\mathbf{p}_2\Omega_2)\overline{G}(\mathbf{p}_2-\mathbf{p}-\mathbf{p}_1,\ \Omega_2-\Omega-\Omega_1)D(\Omega\Omega_2)\right\rangle\right\rangle_{FS};\quad(15)$$

$$\overline{R}_V(Q_{c1}\Omega\Omega_1)=U_+\left\langle\left\langle\sum_{\mathbf{p}_2}\left(\frac{2p_F}{q_{c1}}\right)^2\frac{1}{N_0V}\theta(q_{c1}-|\mathbf{p}-\mathbf{p}_2|)\times\overline{G}(\mathbf{p}_1+\mathbf{p}_2-\mathbf{p},\ \Omega_1)\overline{G}(\mathbf{p}_2\Omega)\right\rangle\right\rangle_{FS};\quad(16)$$

$$R_c^I(Q_c\Omega\Omega_1)=U_-\left\langle\left\langle\sum_{p_2}\left(\frac{2p_F}{q_c}\right)^2\frac{1}{N_0V}\theta(q_c-|\mathbf{p}-\mathbf{p}_2|)\times\overline{G}(\mathbf{p}_2\Omega_1)\overline{G}(\mathbf{p}_2-\mathbf{p}_1-\mathbf{p},-\Omega)\right\rangle\right\rangle_{FS};\quad(17)$$

R_c^{II} is obtained from R_c^I by the substitutions $Q_c\to Q_{c1}$ and $\Omega\to\Omega_1$ ($Q_c=q_c/2p_F$, $Q_{c1}=q_{c1}/2p_F$). Here $\overline{P}_V$ and $\overline{P}_c$ are the vertex and ''crossing'' functions relating to the electron–boson interaction, and R_V and R_c are the corresponding functions determined by the electron–impurity interaction. If in accordance with the Migdal theorem[10] we assume that $\overline{P}_V=\overline{P}_c=R_V=R_c=0$, we obtain for the Green's function (4) and for formulas (9) and (10) the corresponding expressions of the adiabatic theory[15,16] for superconductors with a randomly distributed paramagnetic impurity. In the nonadiabatic systems investigated here ($\varepsilon_F\sim\omega_0$, $q\ll 2p_F$) the Migdal theorem is violated, and it becomes necessary to take into account the contribution of additional many-particle effects: vertex and ''crossing'' functions in the definition of the mass operators. We have expressions for the operators Σ_N (9) and Σ_S (10) containing the total Green's functions, which take into account the electron–boson and electron–impurity interactions in all orders of perturbation theory. Unlike the adiabatic theory, they contain additional diagrams with a crossing of two electron–boson or one electron–boson and one electron–impurity interaction lines (see Eqs. (5) and (6); this is the first order in the nonadiabaticity). If discussion is limited to the contributions linear in the nonadiabaticity, the evaluation of the vertex and ''crossing'' functions (14)–(17) is done using the Green's functions $\overline{G}$ in the adiabatic approximation (see Appendix).

We write the boson propagator $D(\Omega\Omega_1)$ and the electron Green's function (4) in the form

$$D(\Omega\Omega_1)=-\frac{\omega_0^2}{(\Omega-\Omega_1)^2+\omega_0^2};\quad(18)$$

$$\overline{G}(\mathbf{p}\Omega)=[i\tilde{\Omega}-\tilde{\varepsilon}_{\mathbf{p}}]^{-1},\quad(19)$$

where $\tilde{\Omega}=\Omega-\mathrm{Im}\,\Sigma_N(\Omega)$; $\tilde{\varepsilon}_{\mathbf{p}}=\varepsilon_{\mathbf{p}}+\mathrm{Re}\,\Sigma_N(\Omega)$.

Substituting expression (19) into formulas (9) and (10) and doing the integration over energy between the limits $-\mu<\varepsilon_{\mathbf{p}_2}<W-\mu$ (W is the width of the energy band and μ is the chemical potential) in the usual way, we obtain

$$\overline{\Delta}=\frac{\pi N_0}{\beta}\sum_{\Omega_1}\overline{V}_S(\Omega\Omega_1)\frac{\tilde{\Delta}(\Omega_1)}{\tilde{\Omega}_1}\varphi(\tilde{\Omega}_1,\tilde{\mu}):\quad(20)$$

$$\tilde{\Omega}=\Omega+\frac{\pi N_0}{\beta}\sum_{\Omega_1}\overline{V}_N(\Omega\Omega_1)\varphi(\tilde{\Omega}_1,\tilde{\mu})+\pi N_0\overline{U}_+\varphi(\tilde{\Omega},\tilde{\mu};$$
$$\tilde{\Delta}(\Omega)=\Sigma_S(\Omega)=\overline{\Delta}+\pi N_0\overline{U}_-\varphi(\tilde{\Omega},\tilde{\mu}),\quad(21)$$

where

$$\tilde{\mu}=\mu-\mathrm{Re}\,\Sigma_N(\Omega)=\mu-\frac{N_0}{\beta}\sum_{\Omega_1}\overline{V}_N(\Omega\Omega_1)\Psi(\tilde{\Omega}_1,\tilde{\mu})+\overline{U}_+\Psi(\tilde{\Omega},\tilde{\mu});$$
$$\varphi(\tilde{\Omega},\tilde{\mu})=\frac{1}{\pi}\left[\arctan\frac{W-\tilde{\mu}}{\tilde{\Omega}}+\arctan\frac{\tilde{\mu}}{\tilde{\Omega}}\right];\quad(22)$$
$$\Psi(\tilde{\Omega},\tilde{\mu})=\frac{1}{2}\ln\frac{(W-\tilde{\mu})^2+\tilde{\Omega}^2}{\tilde{\mu}^2+\tilde{\Omega}^2}.$$

Because we have taken into account the vertex corrections, the self-consistent system of basic equations of superconductivity (20), (21) contains the renormalized quantities $\overline{V}_N$, $\overline{V}_S$, and $\overline{U}_\pm$. The dependence in (22) is due to the asymmetric limits of integration over energies in (9) and (10), which is characteristic for systems with low densities of charge carriers and narrow energy bands.

3. TEMPERATURE OF THE SUPERCONDUCTING TRANSITION

From now on we shall consider the weak coupling approximation ($\lambda\ll 1$) and replace the vertex functions in (20) and (21) by their values at $\Omega=0$, $\Omega_1=\omega_0$ (Ref. 14). Then, after determining the ratio $\tilde{\Delta}/\tilde{\Omega}$ from Eqs. (21) in a manner similar to how this is done in adiabatic impurity systems, we obtain in this approximation an equation for the order parameter $\overline{\Delta}$ near the superconducting transition temperature:

$$Z\overline{\Delta}(\Omega)=\lambda_\Delta\frac{\pi}{\beta}\times\sum_{\Omega_1}\frac{\omega_0^2}{(\Omega-\Omega_1)^2+\omega_0^2}\frac{\overline{\Delta}(\Omega_1)}{\Omega_1+\Gamma f_c\,\mathrm{sgn}\,\Omega_1}\varphi(\tilde{\Omega}_1,\tilde{\mu}),\quad(23)$$

where

$$\lambda_\Delta=\lambda[1+2\lambda\tilde{P}_V(Q_c,0,\omega_0)+\lambda\tilde{P}_c(Q_c,0,\omega_0)+2R_V(Q_{c1},0,\omega_0)+R_c^I(Q_c,0,\omega_0)+R_c^{II}(Q_c,0,\omega_0)]: \tag{24}$$

$$Z=Z_0-\Gamma[1+\lambda\overline{P}_V(Q_c,\Omega,\Omega)]\times\left[\frac{W-\tilde{\mu}}{(W-\tilde{\mu})^2+\Gamma_1^2}+\frac{\tilde{\mu}}{\tilde{\mu}^2+\Gamma_1^2}\right];$$

$$Z_0=1+\lambda_z\frac{\pi}{\beta\Omega}\sum_{\Omega_1}\frac{\omega_0^2}{(\Omega-\Omega_1)^2+\omega_0^2}\varphi(\tilde{\Omega}_1,\tilde{\mu}); \tag{25}$$

$$\lambda_z=\lambda[1+\lambda\overline{P}_V(Q_c,0,\omega_0)];$$

$$\Gamma=\Gamma_1-\Gamma_2=\pi N_0 c V_2^2\frac{1}{2}S(S+1);\ \ \Gamma_{1,2}=\pi N_0 c U_\pm;$$

$$f_c=\frac{1}{Z}[1+2\lambda\overline{P}_V(Q_c,0,0)]\times\left[1-\frac{1}{\pi}\left(\arctan\frac{\Gamma_1}{W-\tilde{\mu}}+\arctan\frac{\Gamma_1}{\tilde{\mu}}\right)\right]. \tag{26}$$

We now perform a series of transformations in Eq. (23), as this is done in systems in which retardation is taken into account.[20,21] In this way we obtain an equation for determining the superconducting transition temperature T_c:

$$\ln\frac{T_c}{T_{c0}}=\Psi\left(\frac{1}{2}\right)-\Psi\left(\frac{1}{2}+\rho\right)-\frac{Z}{\lambda_\Delta}+\frac{Z_0}{\lambda_\Delta^0}-J_1(c,\mu)+J_2(c,\mu), \tag{27}$$

where Ψ is the Euler psi function, $Z_0=Z|_{c=0}$, $\lambda_\Delta^0=\lambda_\Delta|_{c=0}$, and

$$J_1(c,\mu)=\frac{1}{\pi}\int_0^\infty\frac{dx}{x^2+1}\left[\frac{\varphi_1(x+\Gamma_1,\mu)}{x+\Gamma f_c/\omega_0}-\frac{\varphi_1(x,\mu)}{x}\right]; \tag{28}$$

$$J_2(c,\mu)=\frac{1}{\pi}\int_0^\infty\frac{x^2dx}{(x^2+1)^2}\left[\frac{\varphi_1(x+\Gamma_1,\mu)}{x+\Gamma f_c/\omega_0}-\frac{\varphi_1(x,\mu)}{x}\right],$$

where

$$\varphi_1(x,\mu)=\frac{1}{\pi}\left[\arctan\frac{x}{W-\mu}+\arctan\frac{x}{\mu}\right].$$

The impurity scattering parameter ρ is defined by the relation

$$\rho=\frac{\Gamma f_c}{2\pi T_c}, \tag{29}$$

where $1/2\Gamma$ corresponds to the relaxation time of the scattering of electrons on the magnetic part of the impurity potential for adiabatic systems,[9,16] and the factor f_c (26) corresponds to a renormalization of this parameter due to nonadiabaticity effects.

The superconducting transition temperature for a pure substance is given by the expression[18,19]

$$T_{c0}=\frac{2\omega_0\gamma_e}{\pi\sqrt{e}}\left[\frac{(W-\mu)\mu}{(W-\mu+\omega_0)(\mu+\omega_0)}\right]^{1/2}\times\exp\left\{-\frac{Z_0}{\lambda_\Delta^0}+\frac{1}{4}\left(\frac{\omega_0}{W-\mu+\omega_0}+\frac{\omega_0}{\mu+\omega_0}\right)\right\}. \tag{30}$$

The dependence of T_c on the impurity is contained in the scattering parameter ρ, the quantities in Eq. (28), and in λ_Δ (24) and λ_z (25). It becomes necessary to evaluate all of the vertex and ''crossing'' functions and to determine their dependence on the impurity concentration and density of charge carriers. To calculate these quantities we employ the technique developed in Refs. 14 and 21 (see Appendix). For values $2EQ_c^2<\mu$, $q_c/2p_F=Q_c\ll1$, and $\Gamma_{1,2}/\omega_0\ll1$ we obtain

$$\overline{P}_V(Q_c,0,\omega_0)=P_V(Q_c,0,\omega_0)+O(\Gamma_1/\omega_0);$$

$$\overline{P}_c(Q_c,0,\omega_0)=P_c(Q_c,0,\omega_0)+O(\Gamma_2/\omega_0);$$

$$R_V(Q_c,0,\omega_0)\sim\Gamma_1/\omega_0;\ \ R_c^I(Q_c,0,\omega_0)\sim\Gamma_2/\omega_0, \tag{31}$$

where $P_{V,c}$ are the values of the corresponding functions for the pure substance,[18,19] which are determined by the expression

$$P_V(Q_c,0,\omega_0)=\omega_0B(0,\omega_0)+\left[\frac{A(0,\omega_0)}{\omega_0}-\omega_0B(0,\omega_0)\right]\left[1-\frac{E^2}{\omega_0^2}\frac{1}{2}Q_c^4\right];$$

$$P_c(Q_c,0,\omega_0)=\omega_0B(0,-\omega_0)+\left[\frac{A(0,-\omega_0)}{\omega_0}-\omega_0B(0,-\omega_0)\right]\times\left[1-\frac{E^2}{\omega_0^2}\frac{11}{6}Q_c^4\right]+\frac{E}{\omega_0}C(0,-\omega_0)Q_c^2, \tag{32}$$

where

$$\frac{A(0,\omega_0)}{\omega_0}=\frac{\pi}{4}-\frac{1}{2}\arctan\frac{\omega_0}{\omega_0+\mu}-\frac{1}{2}\arctan\frac{\omega_0}{W-\mu+\omega_0};$$

$$\omega_0B(0,\omega_0)=-\frac{1}{2}\left\{\frac{(\omega_0+\mu)[(\omega_0+\mu)^2+2\omega_0^2]}{[(\omega_0+\mu)^2+\omega_0^2]^2}+\frac{(W-\mu+\omega_0)[(W-\mu+\omega_0)^2+2\omega_0^2]}{[(W-\mu+\omega_0)^2+\omega_0^2]^2}\right\};$$

$$\omega_0C(0,\omega_0)=\frac{1}{2}\left\{\ln\frac{W-\mu+\omega_0}{\omega_0+\mu}-\frac{1}{2}\ln\frac{(W-\mu+\omega_0)^2+\omega_0^2}{(\omega_0+\mu)^2+\omega_0^2}-\frac{\omega_0^2}{(\omega_0+\mu)^2+\omega_0^2}+\frac{\omega_0^2}{(W-\mu+\omega_0)^2+\omega_0^2}\right\}; \tag{33}$$

in addition,

$$P_V(Q_c\Omega\Omega)=-\frac{\omega_0}{2}\left[\frac{\mu+\omega_0}{(\mu+\omega_0)^2+\Omega^2}+\frac{W-\mu+\omega_0}{(W-\mu+\omega_0)^2+\Omega^2}\right]; \tag{34}$$

$$Z_0(0)=1+\lambda_z\left[\frac{W-\mu}{W-\mu+\omega_0}+\frac{\mu}{\mu+\omega_0}\right]. \tag{35}$$

It is easy to see on the basis of results (31) and definitions (24), (25) and (28) that for Γ_1/ω_0, $\Gamma_1/\mu \ll 1$ we have $\lambda_\Delta \approx \lambda_\Delta^0$, $Z \approx Z_0$, and $J_i(c,\mu)\approx 0$, and Eq. (27) takes the form

$$\ln\frac{T_c}{c0}=\Psi\left(\frac{1}{2}\right)-\Psi\left(\frac{1}{2}+\rho\right). \tag{36}$$

As a result, we find that for $\mu \sim \omega_0$ or $\mu \gg \omega_0$ and $\Gamma_{1,2}/\omega_0 \ll 1$ the form of the equation for T_c coincides with the corresponding equation in the Abrikosov–Gor'kov theory[9] (see also Ref. 16). The difference lies in the expressions for the superconducting transition temperature T_{c0} for the pure substance (30) and for the impurity scattering parameter ρ (29), (26). The quantity T_{c0} in (30) in the nonadiabatic theory can reach values characteristic for HTSC materials at moderate values of the constant λ,[14,18] and the parameter ρ (29) contains renormalizations due to nonadiabaticity effects through the quantities f_c and T_c. Here $f_c=1-\lambda[\omega_0/(\omega_0-\mu)+\omega_0/(W+\omega_0+\mu)]<1$, and T_c for this same impurity concentration is significantly larger than its value in the adiabatic theory. Consequently, there is a substantial decrease of the impurity scattering parameter on account of nonadiabaticity effects.

In the limiting case of a nonmagnetic impurity ($\Gamma=0$) Eq. (36) gives $T_c=T_{c0}$, in agreement with the Anderson theorem[6] that T_c is independent of the concentration of a nonmagnetic impurity. Consequently, the model representation we have introduced for the electron–impurity interaction (8) is consistent with the main proposition of the theory of superconductivity in isotropic impurity systems.

At small μ ($\mu \sim \Gamma_1$) the value of T_c is determined by Eq. (27). In the limit $\Gamma \to 0$ the influence of the impurity in this equation is preserved because of the dependence of the quantities appearing in it on the parameters Γ_1 and Γ_2, which contain the scattering of electrons on the nonmagnetic part of the impurity potential (see Eq. (28), for example). A violation of the Anderson theorem[6] occurs which is not due to the momentum cutoff of the electron–impurity interaction (8) but is a consequence of the electron–hole asymmetry (because of the asymmetry of the limits of integration over energy in expressions (9) and (10), which vanishes for $\mu = W/2$. This asymmetry can be regarded as the appearance of anisotropy in the system; the presence of any anisotropy will lead to violation of the Anderson theorem.

On the basis of (36) we have in the region $\mu \sim \omega_0$ or $\mu \gg \omega_0$

$$T_c=T_{c0}-\frac{\pi^2}{2}\frac{\Gamma}{2\pi}f_c \quad \text{for} \quad p\ll 1;$$

$$T_c^2=6\frac{\Gamma^2}{\pi^2}f_c^2\ln\frac{\pi T_{c0}}{\gamma_e\Gamma f_c} \quad \text{for} \quad p\gg 1. \tag{37}$$

These formulas contain a weaker dependence on the impurity concentration than in the case of conventional superconductors on account of nonadiabaticity effects, which lead to the presence of the function $f_c<1$.

Consequently, the pair-breaking effect of the paramagnetic impurity has a weaker influence on the superconductivity because of the additional electron–phonon interaction arising from diagrams with a crossing of impurity and phonon lines. On the basis of Eq. (37) we obtain the following expression for the critical impurity concentration at which the superconductivity vanishes ($T_c=0$):

$$\Gamma_{\rm cr}=\frac{\pi T_{c0}}{\gamma_e f_c}. \tag{38}$$

The large values of T_{c0} and the function $f_c<1$ make for large values of the critical impurity concentration in comparison with adiabatic systems.

4. ORDER PARAMETER Δ AT $T=0$ AND THE ENERGY GAP Ω_g

For $T<T_c$ the expression for the mass operators (5) and (6) should be supplemented with diagrams containing two anomalous Green's functions, and this leads to an additional contribution to the quantities $\overline{V}_N(\Omega\Omega_1)$ and $\overline{V}_S(\Omega\Omega_1)$. However, in the weak-coupling approximation ($\omega_0 \gg \Delta$), which we are considering in this paper, the contribution of these diagrams is small. Furthermore, the calculation of the functions $P_{V,c}$ and $R_{V,c}$ for $\omega_0 \gg \Delta$ and $T=0$ leads to the same results as in the case $T=T_c$. Consequently, in the weak-coupling approximation the parameters λ_Δ, Z, and λ_z are determined by the expressions given above for $T=T_c$.

Let us start from the definitions of the mass operators (5), (6) and generalize the calculational technique of Refs. 9 and 16 for $T=0$ to the case of nonadiabatic systems. In the limit $\Gamma_{1,2}/\omega_0, \Gamma_{1,2}/\mu \ll 1$ and $\omega_0 \gg \Delta$, we obtain for the order parameter

$$\ln\frac{\Delta}{\Delta_0}=-\frac{\Gamma f_c}{\Delta}\frac{\pi}{4} \quad \text{for} \quad \frac{\Gamma f_c}{\Delta}<1;$$

$$\ln\frac{\Delta}{\Delta_0}=\ln\left\{\left[\left(\frac{\Gamma f_c}{\Delta}\right)^2-1\right]^{1/2}+\left(\frac{\Gamma f_c}{\Delta}\right)\right\}-\frac{\left[\left(\frac{\Gamma f_c}{\Delta}\right)^2-1\right]^{1/2}}{\frac{2\Gamma f_c}{\Delta}}$$

$$-\frac{\Gamma f_c}{2\Delta}\frac{1}{\left[\left(\frac{\Gamma f_c}{\Delta}\right)^2-1\right]^{1/2}} \quad \text{for} \quad \frac{\Gamma f_c}{\Delta}>1, \tag{39}$$

where Δ_0 is the order parameter of the pure substance:

$$\Delta_0=\frac{2\omega_0}{\sqrt{e}}\left[\frac{(W-\mu)\mu}{(W-\mu+\omega_0)(\mu+\omega_0)}\right]^{1/2}\times\exp\left\{-\frac{Z_0}{\lambda_\Delta^0}+\frac{1}{4}\left[\frac{\omega_0}{W-\mu+\omega_0}+\frac{\omega_0}{\mu+\omega_0}\right]\right\}. \tag{40}$$

Expressions (39) at ω_0/μ and $(W-\mu)/\mu \to 0$ go over to the corresponding expressions for adiabatic systems.[9,16] Here

we have substantial renormalization of Δ_0 and of the scattering parameter owing to nonadiabaticity effects and the electron–hole asymmetry.

To determine the energy gap we consider the electron density of states in analogy to what was done in Refs. 9 and 16. We have

$$N_S(\Omega)=N_0\,\mathrm{Re}\frac{u}{\sqrt{u^2-1}}; \tag{41}$$

$$\Delta u=\Omega+i\Gamma f_c\frac{u}{\sqrt{u^2-1}}, \tag{42}$$

where $u=\tilde{\Omega}/\tilde{\Delta}$.

The maximum value of Ω, at which the electron density of states is equal to zero, corresponds to the value of the energy gap Ω_g in the energy spectrum. We find $u(\Omega_g)$ from the condition $d\Omega/du=0$. In accordance with (39) we have

$$\begin{aligned} u(\Omega_g)&=[1-(\Gamma f_c/\Delta)^{2/3}]^{1/2};\\ \Omega_g&=[1-(\Gamma f_c/\Delta)^{2/3}]^{3/2}. \end{aligned} \tag{43}$$

It follows from this equation that for $\Gamma f_c=\Delta$ the energy gap $\Omega_g=0$.

Using the definition of Δ (39), we obtain

$$\Gamma_{\Omega_g=0}\frac{\Delta_0}{f_c}\exp\left(-\frac{\pi}{4}\right). \tag{44}$$

This last formula determines the critical impurity concentration at which gapless superconductivity arises. This value is considerably higher than the corresponding value for adiabatic systems on account of the large values of Δ_0 and the function $f_c<1$.

5. NUMERICAL CALCULATIONS AND ANALYSIS OF THE RESULTS

From the formulas obtained above it is seen that the values of T_c, Δ, and Ω_g depend substantially on the values of the chemical potential μ. For $\mu\sim\omega_0\gg\Gamma$, Γ_1 the equations for determining these quantities look the same as the corresponding expressions in the Abrikosov–Gor'kov theory.[9,16] Here there is a substantial renormalization of T_{c0} and Δ_0 and of the scattering parameter ρ on account of the inclusion of the vertex and ''crossing'' functions. The expressions for T_{c0} (30) and Δ_0 (40) hold the possibility of obtaining values characteristic of oxide ceramics[18,19] at intermediate values of the electron–boson interaction constant. The suppression of superconductivity with increasing magnetic impurity concentration due to the breaking of Cooper pairs is slowed considerably.

Figure 1 shows the dependence of the ratios T_c/T_{c0}, Δ/Δ_0, and Ω_g/Δ_0 on the concentration of impurities (on the parameter Γ/Δ_0^0, where Δ_0^0 is the order parameter of an adiabatic impurity-free system) for $\mu=W/2$, $Q_c=q_c/2p_F=0.1$, and $\lambda=0.5$. The solid curves in the figure correspond to the case of adiabatic systems ($m=\omega_0/\mu=2\omega/W=0$), and the dashed lines to the case of nonadiabatic systems for $m=1$. This figure makes it possible to compare the behavior of the quantities indicated above in conventional superconductors (curves *1–3*) and in HTSCs (curves *1′–3′*).

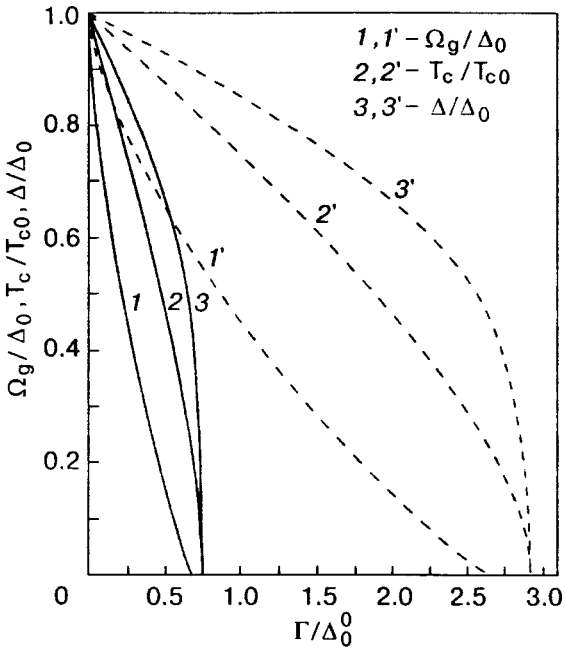

FIG. 1. Energy gap Ω_g, critical temperature T_c, and order parameter Δ at $T=0$ as functions of the impurity concentration.

Thus the following results have been obtained.

1. In nonadiabatic systems T_c, Δ, and Ω_g fall off more slowly with increasing concentration of magnetic impurity in comparison with conventional superconductors.

2. The critical impurity concentration Γ_{cr} at which the superconductivity vanishes and the critical concentration $\Gamma_{\Omega_g=0}$ at which the gapless state arises are increased significantly owing to nonadiabaticity effects.

3. The region of the gapless state $\Gamma_{\mathrm{cr}}-\Gamma_{\Omega_g=0}$ widens substantially in the nonadiabatic systems considered above in comparison with adiabatic systems. We find $\Gamma_{\mathrm{cr}}-\Gamma_{\Omega_g=0}=0.066\Delta_0^0$ for $m=0$, and $\Gamma_{\mathrm{cr}}-\Gamma_{\Omega_g=0}=0.257\Delta_0^0$ for $m=1$.

The model considered here is rather simple for describing the superconducting properties of such complex systems as HTSC materials, which, in addition to the presence of strong electron correlations and a low density of charge carriers, are highly anisotropic systems. However, it does enable one to obtain a qualitative picture of the influence of nonadiabaticity on the behavior of Δ, T_c, and Ω_g as functions of the magnetic impurity concentration and also to determine the values of the critical impurity concentrations Γ_{cr} and $\Gamma_{\Omega_g=0}$ in these systems.

Our results agree qualitatively with the experimental data from studies of the corresponding superconducting properties of lanthanum and yttrium ceramics (see, e.g., Refs. 22 and 23).

In the region of small μ ($\mu\sim\Gamma_1\ll\omega_0$) the equation for determining T_c (27) contains additional impurity dependence through the dependence of the quantities appearing in it on the parameters $\Gamma_{1,2}$, which are determined by the scattering on both the magnetic and nonmagnetic parts of the impurity potential (26), (8). In the limiting case of a nonmagnetic impurity ($\Gamma\to 0$) the impurity dependence on the parameter $\Gamma_{1,2}$ remains in Eq. (27), and that leads to an impurity dependence of T_c. Consequently, in this case the Anderson

theorem[6] is violated. This result is consistent with the main propositions of the theory of superconductivity in impurity systems, since here we are dealing with an anisotropic system (because of the presence of electron–hole asymmetry at small μ). It is known that the Anderson theorem does not hold in anisotropic systems.

In the present paper, following Refs. 13 and 14, we have taken into account the terms linear in the nonadiabaticity (diagrams containing the crossing of two interaction lines) for an impurity system. For this we did a direct evaluation of the vertex and ''crossing'' functions at small values of the momentum transfer for the electron–phonon and electron–impurity interactions. At the present time there are also other approaches, and various methods have been developed for taking nonadiabaticity into account. A detailed analysis of these methods is done in Ref. 24, in which it is shown that the method of direct evaluation of the vertex functions, which was used by Migdal[10] and also by Pietronero, Grimaldi, and Strässler,[13,14] is the most correct. In particular, it gives a correct estimate of the value and sign of the nonadiabatic correction to the self-energy. Consequently, it can be assumed that the theory of the superconductivity of nonadiabatic impurity systems developed in the present study, which is based on direct evaluation of the vertex functions, is a correct theory.

In closing, the author thanks F. G. Kochorbé for a discussion of the results and for assistance in the numerical calculations and in the organization of this paper.

APPENDIX

In evaluating the vertex and ''crossing'' functions, which depend on Ω and q, the technique of Refs. 13 and 14 was generalized to the case of a superconductor with a randomly distributed paramagnetic impurity. We start from definitions (14)–(17) and the expression for the Green's function $\overline{G}(\mathbf{p},\Omega)$ (19) for $\tilde{\Omega}=\Omega+\Gamma_1 \operatorname{sgn}\Omega$ and $\tilde{\varepsilon}_{\mathbf{p}}=\varepsilon_{\mathbf{p}}$, which corresponds to a conventional superconductor containing a paramagnetic impurity at $T=T_c$. This approach gives the first-order result in the nonadiabaticity in the definition of the mass operators (5), (6).

The calculations were done in several steps.

1. The product of the corresponding Green's functions, $\overline{GG}$, which appears in the definition of the functions $P_{V,c}$, is decomposed into simple fractions[13] and a summation over Ω_2 is done, which is replaced by integration, as is done for $T=0$. This approximation is justified for the weak-coupling case ($T_c \ll \omega_0$) considered here.

2. A quadratic dispersion relation of the electron energy is considered; here it is assumed that the momentum cutoff $q_c \ll 2p_F$. For such values of q_c one has $\mathbf{p}\approx\mathbf{p}_1$ and $\mathbf{p}_1 \approx \mathbf{p}_2$. This approach allows one to express the values $\varepsilon_{\mathbf{p}_2+\mathbf{p}_1-\mathbf{p}}$ and $\varepsilon_{\mathbf{p}_2-\mathbf{p}_1-\mathbf{p}}$ in terms of expressions containing $\varepsilon_{\mathbf{p}_2}$ and the angular dependences:

$$\varepsilon_{\mathbf{p}_2+\mathbf{p}_1-\mathbf{p}}=\varepsilon_{\mathbf{p}_2}+EQ\alpha\cos\varphi;$$

$$\varepsilon_{\mathbf{p}_2-\mathbf{p}_1-\mathbf{p}}=\varepsilon_{\mathbf{p}_2}+E(1-Q^2)\frac{\alpha^2}{2}-EQ\sqrt{1-Q^2}\alpha\cos\varphi,$$

where $E=4E_F$, $q=|\mathbf{p}-\mathbf{p}_1|$, $Q=q/2p_F$, and α is the angle between $\mathbf{p}$ and $\mathbf{p}_2$.

3. Integration is done over the energy $\varepsilon_{\mathbf{p}_2}$ (the electron density of states $N(\varepsilon)=N_0$) and then the angular integration over α and φ on the basis of the relation

$$\frac{1}{V}\sum_{\mathbf{p}_2} \rightarrow N_0\int_0^{2\pi}\frac{d\varphi}{2\pi}\int_0^{\pi}\frac{\sin\alpha d\alpha}{2}\int_{\mu}^{W-\mu}d\varepsilon_{\mathbf{p}_2}.$$

4. An averaging is done over the Fermi surface according to the formula

$$P_V(Q_c,0,\omega_0)=\left(\frac{2k_F}{q_c}\right)^2\int\frac{d\Omega_{\mathbf{p}}}{4\pi}\int\frac{d\Omega_{p_1}}{4\pi}\times\theta(q_c-|\mathbf{p}_F-\mathbf{p}_{1F}|)P_{V,c}(\mathbf{p}_F-\mathbf{p}_{1F},0,\omega_o)$$

$$=\frac{2}{Q_c^2}\int QdQP_V(Q,Q_c,0,\omega_0);\quad Q_c=\frac{q_c}{2p_F}.$$

The results of these calculations are presented in the text above. We have used an analogous procedure for evaluation the impurity vertices $R_{V,c}$ (see Ref. 21 for details).

*E-mail: statphys@asm.md

[1] V. A. Moskalenko, M. E. Palistrant, and V. M. Vakalyuk, Usp. Fiz. Nauk **161**, 155 (1991) [Sov. Phys. Usp. **34**, 717 (1991)]; Solid State Commun. **69**, 747 (1989).
[2] V. A. Moskalenko, L. Z. Kon, and M. E. Palistrant, *Low-Temperature Properties of Metals with Features of the Band Spectrum* [in Russian], Shtiintsa, Kishinev (1989).
[3] M. E. Palistrant and F. G. Kochorbé, Fiz. Nizk. Temp. **26**, 1077 (2000) [Low Temp. Phys. **26**, 799 (2000)].
[4] R. Fehrenbacher and R. M. Norman, Phys. Rev. B **50**, 3495 (1994).
[5] J. Bang, Phys. Rev. B **52**, 1279 (1995).
[6] P. W. Anderson, J. Phys. Chem. Solids **11**, 26 (1959).
[7] M. Franz, C. Kollin, A. J. Berlinsky, and M. J. Salkola, Phys. Rev. B **56**, 7882 (1997).
[8] V. M. Loktev and Yu. G. Pogorelov, Physica C **272**, 151 (1996).
[9] A. A. Abrikosov and L. P. Gor'kov, Zh. Éksp. Teor. Fiz. **39**, 1781 (1960) [Sov. Phys. JETP **12**, 1243 (1961)].
[10] A. B. Migdal, Zh. Éksp. Teor. Fiz. **34**, 1438 (1958) [Sov. Phys. JETP **7**, 996 (1958)].
[11] M. L. Kulic and R. Zeyher, Phys. Rev. B **49**, 4395 (1994).
[12] R. Zeyher and M. L. Kulic, Phys. Rev. B **53**, 2850 (1996).
[13] L. Pietronero, S. Strässler, and C. Grimaldi, Phys. Rev. B **52**, 10516 (1995).
[14] C. Grimaldi, L. Pietronero, and S. Strässler, Phys. Rev. B **52**, 10530 (1995).
[15] A. A. Abrikosov, L. P. Gor'kov, and I. E. Dzyaloshinskiĭ, *Methods of Quantum Field Theory in Statistical Physics* [Prentice-Hall, Englewood Cliffs, NJ (1963); Fizmatgiz, Moscow (1962)].
[16] S. Scalski, O. Betbeder-Matibet, and P. R. Weiss, Phys. Rev. **136**, 1500 (1964).
[17] M. Grilli and C. Castellani, Phys. Rev. B **50**, 16880 (1995).
[18] M. E. Palistrant and F. G. Kochorbe, J. Phys.: Condens. Matter **12**, 2217 (2000).
[19] M. E. Palistrant, Fiz. Nizk. Temp. **26**, 557 (2000) [Low Temp. Phys. **26**, 407 (2000)].
[20] W. L. McMillan, Phys. Rev. **167**, 331 (1968).
[21] M. E. Palistrant, Teor. Mat. Fiz. **119**, 455 (1999).
[22] N. Babushkina, A. Inushkin, V. Ozhogin, A. Taldenkov, I. Kobrin, T. Vorob'eva, L. Molchanova, L. Damyanets, T. Uvarova, A. Kuzakov, Physica C **185–189**, 901 (1991).
[23] J. M. Taracson, P. Bartoux, P. F. Miceli, L. H. Greene, and G. W. Hull, Phys. Rev. B **37**, 7458 (1988).
[24] O. V. Danylenko and O. V. Dolgov, Phys. Rev. B **63**, 094506 (2001)

Translated by Steve Torstveit

LOW-TEMPERATURE MAGNETISM

Magnetization dynamics of electron–impurity systems at paramagnetic resonance

E. A. Ivanchenko*

Kharkov Institute of Physics and Technology, National Science Center, Institute for Theoretical Physics, 1 ul. Akademicheskaya, 61108 Kharkov, Ukraine

(Submitted September 27, 2001)
Fiz. Nizk. Temp. **28**, 168–175 (February 2002)

The equation for the magnetization is obtained on the basis of the kinetic equation for an isotropic distribution function of electrons scattering on massive impurity centers in the presence of magnetic and electric fields. The analytical solution of the Cauchy problem for a given initial distribution of the magnetization under conditions of paramagnetic resonance is obtained. The exact solutions are found for magnetization dynamics in samples having the forms of an ellipsoid of revolution and a cylinder, as well. The influence of magnetic exchange on the surface of the cylinder (III boundary value problem) is taken into account. The dependence of the magnetization on the static electric field is exponentially decreasing with time, with an exponent proportional to the electric field squared times the diffusion coefficient. For a fixed instant of time the magnetization depends nonlocally on the magnitude and direction of the electric field. The estimated dynamic shift of the forced precession has a nonlocal and nonlinear dependence on the nonuniform distribution of the initial magnetization. This shift is estimated with boundary conditions taken into account and is caused by a field similar to the Suhl–Nakamura field in a paramagnetic medium. The dynamic shift of the free precession has only a nonlocal character. The time and space dependence of the internal field is obtained. All results are expressed in terms of the initial distribution of the magnetization without specifying its functional form and in terms of the propagation function, which depends on the shape of the sample. These results may be used for analysis of spin diffusion in natural and manmade materials and also in magnetometry.
[DOI: 10.1063/1.1461923]

1. INTRODUCTION

A system of electrons interacting among themselves and with motionless potential impurity centers randomly distributed in uniform external fields is described by a distribution function f obeying the kinetic equation[1,2]

$$\frac{\partial}{\partial t}f+i[w,f]_-+\mathbf{v}\frac{\partial}{\partial \mathbf{x}}f+e\mathbf{E}\frac{\partial}{\partial \mathbf{p}}f+\frac{q}{c}[\mathbf{v}\times\mathbf{B}]\frac{\partial}{\partial \mathbf{p}}f = Lf+L^{ee}f, \tag{1}$$

where $f\equiv f_{\mathbf{p}}(\mathbf{x},t)$ is the distribution function of the electrons, which is a matrix in the electron spin space; q and $\mathbf{v}=\partial e_{\mathbf{p}}/\partial \mathbf{p}$ are the electron charge and velocity, respectively; L and L^{ee} are the electron–impurity and electron–electron collision integrals; $\mathbf{B}$ is the magnetic field, $\mathbf{E}$ is the static electric field; $w=-\mu_0\sigma\cdot\mathbf{B}$ (μ_0 is the Bohr magneton and σ are the Pauli matrices). We assume that the massive charged impurities, whose kinetics is not considered here, form a neutralizing electrical background.

We shall define the distribution function of electrons over energy e (Ref. 3),

$$n(e,\mathbf{x},t)=\langle f\rangle=\frac{1}{\rho(e)}\int dV_{\mathbf{p}}f_{\mathbf{p}}(\mathbf{x},t)\,\delta(e-e_{\mathbf{p}}),$$

$$dV_{\mathbf{p}}=\frac{d^3p}{(2\pi)^3}, \tag{2}$$

where

$$\rho(e)=\int dV_{\mathbf{p}}\delta(e-e_{\mathbf{p}})$$

is the electron density of states, and the brackets mean the averaging defined by formula (2). It follows from Eq. (2) that $\langle \bar{L}f\rangle=0$, where

$$\bar{L}=L+L'(\mathbf{B}),\quad L'(\mathbf{B})=-\frac{q}{c}[\mathbf{v}\times\mathbf{B}]\frac{\partial}{\partial \mathbf{p}}. \tag{3}$$

Indeed, the electron–impurity collision integral has the form

$$(Lf)(\mathbf{p})=2\pi N\int dV_{\mathbf{p}'}\,w\,(\mathbf{p},\mathbf{p}')\,\delta(e_{\mathbf{p}}-e_{\mathbf{p}'})(f_{\mathbf{p}'}-f_{\mathbf{p}}),$$

and hence $\langle Lf\rangle=0$. Here N is the impurity density, $w\,(\mathbf{p},\mathbf{p}')$ is the probability per unit time of electron scattering on the impurity center. As $\varepsilon_{ikl}(\partial v_k/\partial p_i)=\varepsilon_{ikl}(\partial^2 e_{\mathbf{p}}/\partial p_i p_k)=0$, hence the mean

$$\left\langle [\mathbf{v}\times\mathbf{B}]\cdot\left(\frac{\partial}{\partial\mathbf{p}}f\right)\right\rangle = \varepsilon_{ikl}\frac{1}{\rho(e)} \times\int dV_{\mathbf{p}} v_k B_l\left(\frac{\partial}{\partial p_i}f\right)\delta(e-e_{\mathbf{p}}),$$

and after integration by parts we have $\langle\overline{L}f\rangle=0$.

The operator $\overline{L}$ has the property

$$\overline{L}(\mathbf{B})=\overline{L}^{+}(-\mathbf{B}), \tag{4}$$

where + means the conjugate operation, defined by the formula $(x,y)\equiv\langle x,y\rangle$. By virtue of the definition of the operators L and L', we have $(Lx,y)=(x,Ly)$, $(L'(\mathbf{B})x,y)=(x,L'(-\mathbf{B})y)$, i.e., Eq. (4) is valid.

As the result of averaging Eq. (1), we obtain the equation for the distribution function $n(e,\mathbf{x},t)$:

$$\frac{\partial}{\partial t}n+i[\varpi,n]_{-}=\langle L^{ee}f\rangle-\frac{\partial}{\partial x_k}j_k - qE_k\frac{1}{\rho(e)}\frac{\partial}{\partial e}(\rho(e)j_k). \tag{5}$$

To close this equation one has to express the current j_k in terms of n. This can be done if the frequency of electron–impurity collisions $\tau_{e\ \mathrm{imp}}^{-1}$ is much greater than the frequencies of electron-electron collisions τ_{ee}^{-1} and if the times t are large in comparison with the corresponding relaxation time $\tau_{e\ \mathrm{imp}}$; then the electron distribution function becomes some functional of n, i.e., the electron distribution function becomes independent of the electron momentum direction due to the collisions of electrons with impurities. On this basis it is possible to show that in the linear approximation with respect to the gradients and electric field, the diffusion current is[4]:

$$j_k=-D_{ki}(\mathbf{B})\left(\frac{\partial}{\partial x_i}n+qE_i\frac{\partial}{\partial e}n\right), \tag{6}$$

where $D_{ki}(\mathbf{B})=\langle\overline{L}^{-1}v_k,v_i\rangle$ is the diffusion coefficient of electrons in a magnetic field having the property $D_{ki}(\mathbf{B})=D_{ik}(-\mathbf{B})$, which follows from (4).

In case of an isotropic electron dispersion relation $e_{\mathbf{p}}=e_{|\mathbf{p}|}$ we get

$$D_{ki}=d[\delta_{ki}+b_k b_i\omega_c^2\tau_{e\ \mathrm{imp}}+\varepsilon_{ikl}b_i\omega_c],$$

$$d=\frac{\tau_{e\ \mathrm{imp}}\mathbf{v}^2}{3(1+\omega_c^2)},\quad \mathbf{b}=\frac{\mathbf{B}}{|\mathbf{B}|},\quad \omega_c=\tau_{e\ \mathrm{imp}}\Omega_c. \tag{7}$$

The cyclotron frequency Ω_c is equal to $\Omega_c=(q|\mathbf{v}|B)/c|\mathbf{p}|$,

$$\tau_{e\ \mathrm{imp}}^{-1}\equiv 2\pi N\int dV_{\mathbf{p}'}\,\varpi(\mathbf{p},\mathbf{p}')\delta(e_{\mathbf{p}}-e_{\mathbf{p}'})\left(1-\frac{\mathbf{p}\mathbf{p}'}{|\mathbf{p}\mathbf{p}'|}\right). \tag{8}$$

Equations (5) and (6) together determine a closed equation for the distribution function $n(e,\mathbf{x},t)$, which is isotropic with respect to the moments.[4]

2. MACROSCOPIC EQUATION FOR MAGNETIZATION

We define the macroscopic density of the electron magnetic moment $\mathbf{M}=(M_1,M_2,M_3)$, the magnetization, by the formula

$$\mathbf{M}(\mathbf{x},t)=2\mu_0\mathrm{Tr}\frac{1}{2}\sigma\int dV_{\mathbf{p}}n(e,\mathbf{x},t). \tag{9}$$

In view of the relation for Pauli matrixes $\sigma_j\sigma_k-\sigma_k\sigma_j=2i\varepsilon_{jkl}\sigma_l$, the kinetic equation (5), after multiplication by $\mu_0\sigma$, taking the trace on the spin variables, and integration over $dV_{\mathbf{p}}$, takes the form

$$\frac{\partial}{\partial t}\mathbf{M}_i+2\mu_0[\mathbf{B}\times\mathbf{M}]_i+\frac{\partial}{\partial x_k}I_{ik}=0, \tag{10}$$

where the flux density of the electron magnetic moment is equal to

$$I_{ik}\equiv-2\mu_0\mathrm{Tr}\frac{1}{2}\sigma_i\int dV_{\mathbf{p}}D_{kp}\left(\frac{\partial n}{\partial x_p}+qE_p\frac{\partial n}{\partial e}\right). \tag{11}$$

In order to obtain a closed equation for the magnetization we assume that the function D_{kp} is smooth over e, and it is therefore possible to take it out from under the integral sign. We integrate the second term in (11) by parts on e, and assume that the surface terms are small at $e=0$ and at $e=e_F$, where e_F is the Fermi energy. This approximation allows us to write down the equation for the magnetization as

$$\frac{\partial}{\partial t}\mathbf{M}+2\mu_0[\mathbf{B}\times\mathbf{M}]-D_{kp}\left(\frac{\partial^2}{\partial x_k\partial x_p}-\frac{e}{2e_F}E_p\frac{\partial}{\partial x_k}\right)\mathbf{M}=0. \tag{12}$$

Equation (12) without allowance for spatial inhomogeneity corresponds to the Bloch equation and forms the basis of the theory of paramagnetic resonance. The incorporation of inhomogeneity is carried out in Refs. 1 and 5 without specifying the character of the diffusion mechanism. The nonlinear equation describing a collision dynamics of magnetization in the absence of external fields is obtained in Ref. 6.

The purpose of the present work is to study the magnetization dynamics of electron–impurity systems on the basis of Eq. (12) under conditions of paramagnetic resonance with boundary conditions taken into account.

3. PARAMAGNETIC RESONANCE IN ELECTRON–IMPURITY SYSTEMS

We consider the magnetization behavior in the case when the external magnetic field in Eq. (12) consists of two terms:

$$\mathbf{B}=\mathbf{B}_0+\mathbf{h}(t),$$

where $\mathbf{B}_0$ is the static field and $\mathbf{h}(t)$ is the alternating field.

To find the solution of Eq. (12) we shall develop the scheme described by Bar'yakhtar and Ivanov in Ref. 7. For this purpose, we shall present the solution for the magnetization [see Eq. (12)] as an expansion in powers of the amplitude of the external alternating magnetic field:

$$\mathbf{M}(\mathbf{x},t)=\sum_{k=0}^{\infty}\mathbf{m}^{(k)}(\mathbf{x},t). \tag{13}$$

After substituting Eq. (13) into Eq. (12) we have an infinite system of equations for $\mathbf{m}^{(k)}$:

$$\frac{\partial}{\partial t}\mathbf{m}^{(k)}+2\mu_0[\mathbf{B}\times\mathbf{m}^{(k)}]-D\mathbf{m}^{(k)} = -2\mu_0[\mathbf{h}(t)\times\mathbf{m}^{(k-1)}],$$

$$k=0,1,2,\ldots;\ \mathbf{m}^{(-1)}\equiv 0,\ \mathbf{B}=(0,0,B), \tag{14}$$

$$D\equiv d_F\left(\frac{\partial^2}{\partial x^2}+\frac{\partial^2}{\partial y^2}+(1+\omega_c^2)\frac{\partial^2}{\partial z^2}-\frac{q}{2e_F}\times(E_1+\omega_c E_2)\frac{\partial}{\partial x}-\frac{q}{2e_F}(E_2-\omega_c E_1)\times\frac{\partial}{\partial y}-\frac{q}{2e_F}E_3(1+\omega_c^2)\frac{\partial}{\partial z}\right). \tag{15}$$

At first we find the solution $\mathbf{m}^{(0)}$ of the Cauchy problem with the help of the change of dependent variables

$$m_i^{(0)}(\mathbf{x},\ t)=(2\pi)^{-3/2}\int d^3k e^{-i\mathbf{kx}}m_i^{(0)}(\mathbf{k},t)(i=1,2,3). \tag{16}$$

For the Fourier components $\mathbf{m}_i^{(0)}(\mathbf{k},t)$ we get a system of differential equations of first order in time. This system is easily solved. Carrying out the inverse transformation,

$$m_i^{(0)}(\mathbf{k},t)=(2\pi)^{-3/2}\int d^3x' e^{i\mathbf{kx}'}m_i^{(0)}(\mathbf{x},t), \tag{17}$$

we find the solution for the magnetization in the form of free precession in constant fields,

$$\mathbf{m}^{(0)}(\mathbf{x},t)=\int d^3x' g(t,\mathbf{x}',\mathbf{x})(m(\mathbf{x}')\cos(\Omega t+\varphi(\mathbf{x}')), -m(\mathbf{x}')\sin(\Omega t+\varphi(\mathbf{x}')),m_3(\mathbf{x}')) \tag{18}$$

on the set of the known initial data of the form

$$\mathbf{m}^{(0)}(\mathbf{x},t=0)=(m(\mathbf{x})\cos\varphi(\mathbf{x}),-m(\mathbf{x})\sin\varphi(\mathbf{x}),m_3(\mathbf{x})). \tag{19}$$

with a propagation function equal to

$$g(\mathbf{x}',\mathbf{x})=\frac{1}{(1+\omega_c^2)^{1/2}}\left(\frac{1}{2(\pi d_F t)^{1/2}}\right)^3\times\exp\left[-\left(\frac{x'-x}{2\sqrt{d_F t}}+\frac{q}{2e_F}\frac{E_1+\omega_c E_2}{2}\sqrt{d_F t}\right)^2-\left(\frac{y'-y}{2\sqrt{d_F t}}+\frac{q}{2e_F}\frac{E_2-\omega_c E_1}{2}\sqrt{d_F t}\right)^2-\left(\frac{z'-z}{2(1+\omega_c^2)^{1/2}\sqrt{d_F t}}+\frac{q}{2e_F}\frac{(1+\omega_c^2)^{1/2}E_3}{2}\sqrt{d_F t}\right)^2\right], \tag{20}$$

$$\Omega=2\mu_0 B,\quad d_F=\frac{v_F^2\tau_{e\ \mathrm{imp}}}{3(1+\omega_c^2)},$$

where v_F is the Fermi velocity.

This function obeys the equation

$$\frac{\partial}{\partial t}g-Dg=0 \tag{21}$$

and also has the properties

$$\lim_{t\to 0^-} g(t,\mathbf{x}',\mathbf{x})=\delta(\mathbf{x}'=\mathbf{x}), \tag{22}$$

$$\lim_{t\to 0^+}\frac{\partial}{\partial t}g(t,\mathbf{x}',\mathbf{x})=D\,\delta(\mathbf{x}'-\mathbf{x}). \tag{23}$$

An important property of the propagation function is that it satisfies the Smolukhowski–Chapman–Kolmogoroff equation

$$\int d^3x' g(t-t',\mathbf{x}',\mathbf{x})g(t',\mathbf{x}'',\mathbf{x})=g(t,\mathbf{x}'',\mathbf{x}). \tag{24}$$

The particular solution $\mathbf{m}^{(1)}$ of Eq. (14) with the right-hand side $-2\mu_0\ [\mathbf{h}(t)\times\mathbf{m}^{(0)}(\mathbf{x},t)]$ can be obtained, using the semigroup property of the function $g(t,\mathbf{x}',\mathbf{x})$ (24):

$$m_1^{(1)}(\mathbf{x},t)+im_2^{(1)}(\mathbf{x},t)=\int_0^t dt' e^{i\Omega(t'-t)}\int d^3x' g(t,\mathbf{x}',\mathbf{x})\times[(h_1(t')+ih_2(t'))m_3(\mathbf{x}')-h_3(t')e^{-i(\Omega t'+\varphi(\mathbf{x}'))}m(\mathbf{x}')], \tag{25}$$

$$m_3^{(1)}(\mathbf{x},t)=\int_0^t dt'\int d^3x' g(t,\mathbf{x}',\mathbf{x})m(\mathbf{x}')\times[h_1(t')\sin(\Omega t'+\varphi(\mathbf{x}'))+h_2(t')\times\cos(\Omega t'+\varphi(\mathbf{x}'))]. \tag{26}$$

It is seen from formulas (25) and (26), that the magnetization at the time t is determined by the field $\mathbf{h}(t)$ at all previous times, starting at the instant it is turned on.

We choose left rotation for the external alternating magnetic field, which is perpendicular to the static field $\mathbf{B}_0$: $\mathbf{h}(t)=h(\cos\omega t,-\sin\omega t,0)$, where h is the amplitude of the field and ω is the frequency of the alternating magnetic field. Since at the paramagnetic resonance $\omega=\Omega$, we find from formulas (25) and (26) that the particular solution for the magnetization in the approximation linear in the field is the forced precession

$$m_1^{(1)}(\mathbf{x},t)=\omega_1 t m_3^{(0)}(\mathbf{x},t)\cos(\Omega t-\pi/2),$$
$$m_2^{(1)}(\mathbf{x},t)=-\omega_1 t m_3^{(0)}(\mathbf{x},t)\sin(\Omega t-\pi/2), \tag{27}$$
$$m_3^{(1)}(\mathbf{x},t)=\omega_1 t A(\mathbf{x},t),$$

$$A(\mathbf{x},t)\equiv\int d^3x' g(t,\mathbf{x}',\mathbf{x})m(\mathbf{x}')\sin\sigma(\mathbf{x}'),\quad \omega_1=2\mu_0 h, \tag{28}$$

lagging in phase behind the phase of the alternating magnetic field by $\pi/2$.

Having continued the procedure of iteration, we can sum the series on $\omega_1 t$ and find the general exact solution for the magnetization dynamics (12) at paramagnetic resonance:

$$\mathbf{M}(\mathbf{x},t)=\mathbf{m}^{(0)}(\mathbf{x},t)+\mathbf{m}(\mathbf{x},t), \tag{29}$$

$$\mathbf{m}(\mathbf{x},t)=([A(\mathbf{x},t)(1-\cos\omega_1 t)+m_3^{(0)} \times(\mathbf{x},t)\sin\omega_1 t]\sin\Omega t,$$

$$[A(\mathbf{x},t)(1-\cos\omega_1 t)+m_3^{(0)}(\mathbf{x},t)\sin\omega_1 t]\cos\Omega t,$$

$$A(\mathbf{x},t)\sin\omega_1 t+m_3^{(0)}(\mathbf{x},t)(\cos\omega_1 t-1)).$$

At $h=0$ this solution transforms into $\mathbf{M}(\mathbf{x},t)=\mathbf{m}^{(0)}(\mathbf{x},t)$; see Eq. (18). As is seen from the solution (29), there is no divergence in time. Finally we come to the conclusion that the solution of the Cauchy problem of Eq. (12) with the initial distribution (19) in the class of square-integrable functions is completely determined by the propagation function and the shape of the sample, i.e., by the integration volume. For an unbounded medium under conditions of paramagnetic resonance the solution of the Cauchy problem takes the form of Eq. (29).

The magnetization projection $M_3(\mathbf{x},t)$ oscillates. This fact implies that a population inversion occurs in the system considered.

For the analysis of the forced precession we write the solution (29) for M_1, M_2 as

$$M_1(\mathbf{x},t)=a\cos(\Omega t+\phi),$$

$$M_2(\mathbf{x},t)=-a\sin(\Omega t+\phi), \tag{30}$$

where the local amplitude and phase of precession are equal to

$$a(\mathbf{x},t)=\sqrt{[-A(\mathbf{x},t)\cos\omega_1 t+m_3^{(0)}(\mathbf{x},t)\sin\omega_1 t]^2+A_1^2(\mathbf{x},t)},$$

$$\phi(\mathbf{x},t)=\arctan\frac{A(\mathbf{x},t)\cos\omega_1 t-m_3^{(0)}(\mathbf{x},t)\sin\omega_1 t}{A_1(\mathbf{x},t)},$$

$$A_1(\mathbf{x},t)\equiv\int d^3x' g(t,\mathbf{x}',\mathbf{x})m(\mathbf{x}')\cos\varphi(\mathbf{x}'). \tag{31}$$

Expanding the phase $\phi(\mathbf{x},t)$ (31) in a series with respect to t and restricting ourselves to the term linear in t, we get, in view of the property (23), the local dynamic shift of the forced frequency Ω' with respect to the Larmor precession frequency Ω.

$$\phi(\mathbf{x},t)=\varphi(\mathbf{x})+\Omega'(\mathbf{x},0)t+\ldots,$$

$$\Omega'(\mathbf{x},0)=\frac{1}{m^2(\mathbf{x})}\left\{\left[-\omega_1 m_3(\mathbf{x})+\int d^3x'(D\delta(\mathbf{x}-\mathbf{x}')) \times m(\mathbf{x}')\sin\varphi(\mathbf{x}')\right]m(\mathbf{x})\cos\varphi(\mathbf{x}) -\left[\int d^3x'(D\delta(\mathbf{x}-\mathbf{x}'))m(\mathbf{x}')\cos\varphi(\mathbf{x}')\right] \times(m(\mathbf{x})\sin\varphi(\mathbf{x})-\omega_1 m_3(\mathbf{x}))\right\}. \tag{32}$$

the cause of which has the meaning of the internal field at the point $\mathbf{x}$ (an analog of the Suhl–Nakamura field[8] in a paramagnetic medium, coordinated with the boundary conditions). This field depends on an initial nonuniform magnetization distribution at all points of the sample and on the shape of the sample, that is, it has a nonlocal character. Without nonlocality being taken into account, this shift is proportional to the amplitude of the forced field and has the simple form

$$\Omega'(\mathbf{x},0)=-2\mu_0 h\frac{m_3(\mathbf{x})\cos\varphi(\mathbf{x})}{m(\mathbf{x})}. \tag{33}$$

As is seen from formula (33), this shift depends nonlinearly on the initial distribution. This result coincides with that of Ref. 8 in view of heterogeneity. It follows from formula (32) that the dynamic shift of the free precession $\Omega'_{\text{free}}(\mathbf{x},0)$ is completely nonlocal:

$$\Omega'_{\text{free}}(\mathbf{x},0)=-\frac{1}{m(\mathbf{x})}\int d^3x'(D\delta(\mathbf{x}-\mathbf{x}'))m(\mathbf{x}') \times\sin(\varphi(\mathbf{x})-\varphi(\mathbf{x}')). \tag{34}$$

Now it is obvious that in the general case the dependence of the dynamic shift on time and coordinates is

$$\Omega'(\mathbf{x},t)=\frac{\phi(\mathbf{x},t)-\varphi(\mathbf{x})}{t}. \tag{35}$$

We find the maximal amplitude of the forced precession $a^{\max}$ from the condition $M_3=0$, i.e.,

$$A\sin\omega_1 t+m_3^{(0)}\cos\omega_1 t=0. \tag{36}$$

After substituting (36) in (31), we get

$$a^{\max}=\left(\frac{m_3^{(0)2}}{\sin^2\omega_1 t}+A_1^2\right)^{1/2}, \tag{37}$$

and the times $t^{(k)}$ are determined by the solution of Eq. (36), which can be written in equivalent form as

$$\sin(\omega_1 t+\delta)=0,\quad \delta=\arctan\frac{m_3^{(0)}}{A}. \tag{38}$$

In the simplest case we find $\delta=-\pi/4$, $\omega_1 t\approx k\pi+\pi/4$, $k=0, 1, 2, \ldots$

$$t^{(0)}\approx\frac{\pi}{4\omega_1},\quad t^{(1)}\approx\frac{5\pi}{4\omega_1},\ldots, \tag{39}$$

$$a^{\max}_{t=t^{(0)}}\approx\sqrt{3}|m_3^{(0)}|_{t=t^{(0)}}.$$

Decaying bursts of precession amplitude $a^{\max}$ are observed.

To take into account the particular shape of the sample it is necessary to use the eigenfunctions of the Laplace operator in cylindrical, spherical, or other coordinates as well. The general formulas (29) and the formulas related to them retain their form under replacement of the propagation function and volume of integration. The propagation functions for the cylinder and ellipsoid of revolution are given in Appendix 1. The general exact solution of the equation (12) is given in Appendix 2.

4. CONCLUSIONS

The dynamics of the evolution of a system of electrons and impurities placed in static electric and magnetic fields is investigated under the influence of an alternating magnetic field under conditions of paramagnetic resonance. The general formulas for all three magnetization components in their evolutionary interrelation are obtained with the shape of the

sample (cylinder, ellipsoid of revolution) taken into account, since experimental engineering allows one to measure these components.[9] The behavior of forced precession in samples is theoretically investigated. The dynamic shift of the frequency of paramagnetic resonance caused by a nonuniform distribution of initial magnetization is found. All results are expressed in terms of the initial magnetization distribution and a propagation function dependent on the shape of the sample. The results obtained are applied to the analysis of spin diffusion in natural and manmade materials[10,11] and also in magnetometry.[9]

The author thanks Prof. S. V. Peletminskii for interest in the research and for a helpful discussion.

APPENDIX 1

Cylinder (III boundary value problem) [Ref. 12]

$\mathbf{E}=(0,0,E_3)$,

$$x=r\cos\varphi,\quad y=r\sin\varphi,\quad \frac{z}{\sqrt{1+\omega_c^2}}=u;$$

$$0\leqslant r\leqslant r_0,\quad 0\leqslant\varphi\leqslant 2\pi,\quad 0\leqslant z\leqslant l,\quad 0\leqslant t\leqslant\infty,$$

$$d^3x'=r'dr'd\varphi'du'.$$

The boundary conditions are

$$\left[\frac{\partial}{\partial z}\mathbf{M}-h_1\mathbf{M}\right]_{z=0}=0,$$

$$\left[\frac{\partial}{\partial z}\mathbf{M}+h_2\mathbf{M}\right]_{z=l}=0,$$

$$\left[\frac{\partial}{\partial r}\mathbf{M}+H_3\mathbf{M}\right]_{z=l}=0,$$

where h_1, h_2, H_3 are the surface magneto-exchange factors.

The initial conditions are

$\mathbf{M}_{t=0}=(m(\mathbf{x})\cos\varphi(\mathbf{x}),-m(\mathbf{x})\sin\varphi(\mathbf{x}),m_3(\mathbf{x}))$:

The propagation function is

$$g(t,r',\varphi',r,\varphi,u)$$

$$=\frac{4}{\pi r_0^2}\exp\left(-\frac{qE_3}{4e_F}\sqrt{1+\omega_c^2}(u'-u)-\frac{(1+\omega_c^2)q^2E_3^2}{16e_F^2}d_Ft\right)$$

$$\times\sum_{n=0;\ m,k=1}^{\infty}\left[l+\frac{(H_1H_2+\nu_m^2)(H_1+H_2)}{(H_1^2+\nu_m^2)(H_2^2+\nu_m^2)}\right]^{-1}$$

$$\times\left(1+\frac{r_0^2H_3-n^2}{(\mu_k^{(n)})^2}\right)^{-1}$$

$$\times J_n^{-2}(\mu_k^{(n)})J_n\left(\frac{\mu_k^{(n)}}{r_0}r\right)J_n\left(\frac{\mu_k^{(n)}}{r_0}r'\right)$$

$$\times\exp\left(-\left[\left(\frac{\mu_k^{(n)}}{r_0}\right)^2+\nu_m^2\right]d_Ft\right)$$

$$\times(\varepsilon_n^{-1}\cos n\varphi\cos n\varphi'+\sin n\varphi\sin n\varphi')\sin(\nu_mu+z_m)$$

$$\times\sin(\nu_mu'+z_m),$$

$\varepsilon_n=2$ if $n=0$ and $\varepsilon_n=1$ if $n\neq 0$, J_n are the Bessel functions, $\mu_k^{(n)}$, ν_m are the positive roots according to the equations

$$\mu_k^{(n)}J'(\mu_k^{(n)})+r_0H_3J(\mu_k^{(n)})=0,$$

$$\cot\frac{\nu_ml}{\sqrt{1+\omega_c^2}}=\frac{\nu_m^2-H_1H_2}{\nu_m(H_1+H_2)},$$

$$z_m=\arctan\frac{\nu_m}{H_1},\quad H_1=\sqrt{1+\omega_c^2}\left(h_1-\frac{qE_3}{4e_F}\right),$$

$$H_2=\sqrt{1+\omega_c^2}\left(h_2+\frac{qE_3}{4e_F}\right).$$

Ellipsoid of revolution

$$x=r\cos\theta\sin\varphi,\quad y=r\cos\theta\cos\varphi,$$

$$u=\frac{z}{\sqrt{1+\omega_c^2}}=r\cos\theta,$$

$$0\leqslant r\leqslant r_0,\quad 0\leqslant\varphi\leqslant 2\pi,\quad 0\leqslant\theta\leqslant\pi,$$

$$d^3x'=r'^2\sin\theta'dr'd\theta'd\varphi'.$$

The boundary conditions are $[\mathbf{M}(\mathbf{x},t)]_{r=r_0}=0$.

The initial conditions are $\mathbf{M}_{t=0}=(m(\mathbf{x})\cos\varphi(\mathbf{x}),-m(\mathbf{x})\sin\varphi(\mathbf{x}),m_3(\mathbf{x}))$. The propagation function is

$$g(t,r',\theta',\varphi',r,\theta,\varphi)=\frac{1}{\pi r_0^2}$$

$$\times\exp\left(-\frac{q(E_1+\omega_cE_2)(x'-x)}{4e_F}\right.$$

$$-\frac{q(E_2-\omega_cE_1)(y'-y)}{4e_F}-\frac{qE_3\sqrt{1+\omega_c^2}(u'-u)}{4e_F}$$

$$\left.-\frac{(1-\omega_c^2)q^2\mathbf{E}^2d_Ft}{16e_F^2}\right)$$

$$\times\left[\sum_{n=0,\ m=1}^{\infty}\sum_{k=1}^{n'}\frac{\varepsilon_k^{-1}\cos k\varphi\cos k\varphi'+\sin k\varphi\sin k\varphi'}{\frac{(n+k)!}{(2n+1)(n-k)!}[J'_{n+1/2}(\mu_m^{(n)})]^2}\right.$$

$$\times\exp(-(\mu_m^{(n)}/r_0)^2d_Ft)$$

$$\times\frac{J_{n+1/2}(\mu_m^{(n)}r/r_0)J_{n+1/2}(\mu_m^{(n)}r'/r_0)}{\sqrt{rr'}}$$

$$\left.\times P_{n,k}(\cos\theta)P_{n,k}(\cos\theta')\right],$$

$J_{\mu+1/2}$ are the Bessel functions of half-integral order, $P_{n,k}$ are the associated Legendre functions, and $\mu_m^{(n)}$ are the positive roots of the equation $J_{n+1/2}(\mu_m^{(n)})=0$.

APPENDIX 2

If the mismatch $\Delta=\Omega-\omega$, i.e. the difference between Larmor precession Ω and the frequency of the alternating magnetic field is not equal to zero, the general exact solution of the equation (12) has the form:

$$\mathbf{M}(\mathbf{x},\Delta,t)=\mathbf{m}^{(0)}(\mathbf{x},t)+\mathbf{m}(\mathbf{x},\Delta,t),$$

$$\begin{aligned}\mathbf{m}(\mathbf{x},\Delta,t)=&\left(\left(-A\cos\gamma t+\frac{\omega_1}{\gamma}m_3^{(0)}\sin\gamma t\right)\sin\omega t\right.\\&+A_1\cos\omega t-\frac{\Delta}{\gamma}A_1\sin\gamma t\sin\omega t-A_1\cos\Omega t\\&+A\sin\Omega t-\left(\frac{\Delta}{\gamma}A\sin\gamma t-(\omega_1\Delta m_3^{(0)}\right.\\&\left.\left.-\Delta^2A_1)\frac{1-\cos\gamma t}{\gamma}\right)\cos\omega t,\left(-A\cos\gamma t\right.\\&\left.+\frac{\omega_1}{\gamma}m_3^{(0)}\sin\gamma t\right)\cos\omega t-A_1\sin\omega t\\&+\left(\frac{\Delta}{\gamma}A\sin\gamma t-(\omega_1\Delta m_3^{(0)}\right.\\&\left.-\Delta^2A_1)\frac{1-\cos\gamma t}{\gamma^2}\right)\sin\omega t\\&-\frac{\Delta}{\gamma}A_1\sin\gamma t\cos\omega t+A_1\sin\Omega t\\&+A\cos\Omega t,m_3^{(0)}(\cos\gamma t-1)+\frac{\omega_1}{\gamma}A\sin\gamma t\\&\left.+(\Delta^2m_3^{(0)}+\omega_1\Delta A_1)\frac{1-\cos\gamma t}{\gamma^2}\right),\end{aligned}$$

where $\gamma=\sqrt{\omega_1^2+\Delta^2}$.

The dynamic shift is $\Omega'(\mathbf{x},\Delta,t)=\phi(\mathbf{x},\Delta,t)-\varphi(\mathbf{x})/t$, where

$$\varphi(x,\Delta,t)$$

$$=\arctan\frac{A\cos\gamma t-\omega_1m_3^{(0)}(\sin\gamma t/\gamma)+\Delta A_1\sin\gamma t/\gamma)}{A_1-\Delta A(\sin\gamma t/\gamma)+(\omega_1\Delta m_3^{(0)}-\Delta^2A_1)(1-\cos\gamma t)/\gamma^2}.$$

*E-mail: yevgeny@kipt.kharkov.ua

[1] V. P. Silin, Zh. Éksp. Teor. Fiz. **30**, 421 (1956) [Sov. Phys. JETP **3**, 305 (1956)].
[2] M. Ya. Azbel', V. I. Gerasimenko, and I. M. Lifshitz, Zh. Éksp. Teor. Fiz. **32**, 1212 (1957) [Sov. Phys. JETP **5**, 986 (1957)].
[3] L. V. Keldush, Zh. Éksp. Teor. Fiz. **48**, 1692 (1965) [Sov. Phys. JETP **21**, 1135 (1965)].
[4] E. A. Ivanchenko, V. V. Krasil'nikov, and S. V. Peletminskii, Fiz. Met. Metalloved. **57**, 441 (1984).
[5] G. D. Gaspari, Phys. Rev. **151**, 215 (1966).
[6] T. L. Andreeva and P. L. Rubin, Zh. Éksp. Teor. Fiz. **91**, 877 (2000) [Sov. Phys. JETP **91**, 761 (2000)].
[7] V. Baryakhtar and B. Ivanov, *Modern Magnetism*, Nauka, Moscow (1986).
[8] M. I. Kurkin and E. A. Turov, NMR in *Magnetically Ordered Materials and Its Application* [in Russian], Nauka, Moscow (1990), p. 148.
[9] N. M. Pomerantsev, V. M. Ryzhov, and G. V. Skrotskii, *Physical Principles of Quantum Magnetometry* [in Russian], Nauka, Moscow (1972), p. 142.
[10] K. R. Brownstein, and C. E. Tarr, Phys. Rev. **19**, A2446 (1979).
[11] Yi-Qiao Song, Phys. Rev. Lett. **85**, 38 (2000).
[12] B. M. Budak, A. A. Samarskii, and A. N. Tikhonov, *Collected Problems in Mathematical Physics* [in Russian], Nauka, Moscow (1980).

This article was published in English in the original Russian journal. Reproduced here with stylistic changes by AIP.

LOW-DIMENSIONAL AND DISORDERED SYSTEMS

Point-contact studies of the Kondo size effect in the alloys CuMn, CuCr, and AuFe in a magnetic field

V. V. Fisun* and I. K. Yanson

B. Verkin Institute for Low Temperature Physics and Engineering, National Academy of Sciences of Ukraine, pr. Lenina 47, 61103 Kharkov, Ukraine

J. M. van Ruitenbeek and J. A. Mydosh

Kamerlingh Onnes Laboratorium, Leiden University, PO Box 9504, NL-2300, RA Leiden, the Netherlands
(Submitted October 1, 2001)
Fiz. Nizk. Temp. **28**, 176–182 (February 2002)

The splitting of the Kondo peak on the differential resistance–voltage characteristic in a magnetic field is investigated in CuMn, CuCr, and AuFe point contacts of different diameter. Empirical formulas are obtained which can take into account the variation of the energy position of the maxima of the split Kondo peak, both in external and internal (the spin-glass state) magnetic fields, as a function of the temperature of the experiment and the Kondo temperature and also as the diameter of the contacts is decreased. © *2002 American Institute of Physics.* [DOI: 10.1063/1.1461924]

Point-contact spectroscopy (PCS) is now being used to investigate the characteristics of various dilute alloys exhibiting the Kondo effect.[1–5] At biases of the order of ± 10 mV the curves of the differential resistance versus the voltage across the point contacts ($dV/dI(V)$) have a Kondo peak at $V=0$ (Fig. 1). At biases above 10 mV a sharp increase of the differential resistance occurs due to the scattering of conduction electrons on phonons of the host metal, Cu or Au. The voltage dependence of the differential resistance at low biases has the form $dV/dI(V) \propto -\log V$. It is similar to the temperature dependence of the resistivity for a bulk Kondo alloy, $\rho(T) \propto -\log T$ (Fig. 1). The difference is that in the PCS method the interaction of the conduction electrons with paramagnetic impurities and phonons is investigated as a function of the voltage V across the point contact at low temperature, $k_B T < eV$ (k_B is Boltzmann's constant). The maximum energy in the inelastic scattering of conduction electrons is equal to eV, with an accuracy of several $k_B T$. Usually point contacts with ballistic electron transport are investigated.

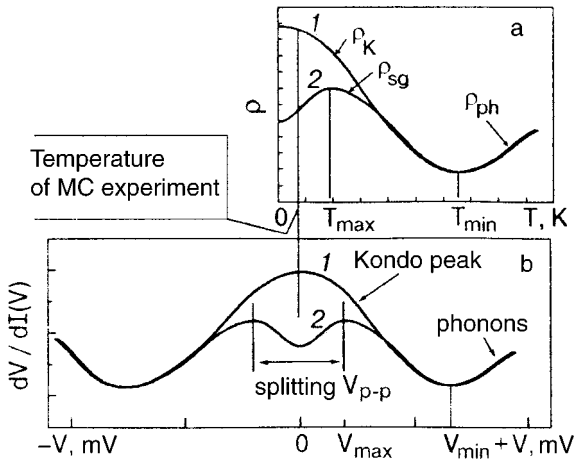

FIG. 1. Schematic illustration of the temperature dependence of the resistivity (a) and the dependence of the differential resistance on the applied voltage across the point contact (b) of a Kondo alloy: *1*—in the absence of magnetic field, *2*—in an external or internal magnetic field.

As the impurity concentration is increased in alloys with a low Kondo temperature, such as CuMn, AuMn, and AuFe, the Ruderman–Kittel–Kasuya–Yosida (RKKY) interaction will bring about a transition to a spin-glass state, which is characterized by an internal magnetic field. The $\rho(T)$ curves of such alloys have a maximum at a characteristic value of the temperature T_{max} (Fig. 1a). In the case of PCS the $dV/dI(V)$ characteristics exhibit a maximum at a certain finite bias V_{max}, and the spectrum of the Kondo peak splits (Fig. 1b, curve *2*), with an energy splitting V_{p-p} between the maxima.

A maximum on the $\rho(T)$ curve is also observed in an external magnetic field **H** in the paramagnetic state. The appearance of this maximum is due to the Zeeman energy $E_Z = g\mu_B H$ (g is the Landé factor and μ_B is the Bohr magneton), which prevent the spin of the magnetic impurity from flipping in its interaction with a conduction electron. The spins fixed by the external magnetic field do not participate in the Kondo scattering, and that leads to a decrease in the resistance as $T \to 0$. For the alloys mentioned above, the $dV/dI(V)$ characteristics also exhibit a splitting of the Kondo peak in an external magnetic field (curve *2* in Fig. 1b). Although the nature of this splitting in external and internal magnetic fields is different, their point-contact spectra $dV/dI(V)$ are qualitatively similar. For this reason they are represented in Fig. 1b by a single curve *2*.

Observation of the splitting of the Kondo peak in the point-contact spectra both in external and internal magnetic

fields is possible only at a temperature below the temperature of the maximum $T_{\max}$ on the $\rho(T)$ curves. Obviously, the simultaneous presence of both external and internal magnetic fields in a point-contact experiment will also lead to splitting of the Kondo peak. Changing the value of the temperature interval between $T_{\max}$ and the temperature T of the point-contact experiment should lead to a change in the value of V_{p-p} (Fig. 1). Decreasing this temperature interval should make V_{p-p} smaller, since qualitatively the relation $V \propto T$ is observed in PCS. Actually, however, in point-contact experiments in an external magnetic field for alloys with unscreened spins (such alloys were studied in Refs. 1–5), within a certain temperature range (for $k_B T < g\mu_B H$) the opposite occurs, on account of the smearing of the Fermi energy distribution of the conduction electrons and the fact that the experiments were done for $T \ll T_{\max}$.

In Ref. 3 the PCS method was used to study the behavior of several Kondo alloys as a function of external magnetic field in the both the spin-glass and paramagnetic states. The g factor was determined from the energy position of the maxima of the split Kondo peak and was always found to be greater than 2. On the other hand, in Ref. 6 a theory was given for calculating the $dV/dI(V)$ curves for point contacts containing magnetic impurities in an external magnetic field. A comparison of the theoretical curves of $dV/dI(V)$ with the experimental curves for the alloys AuFe (0.1 at.% Fe) in a field of 3 T at a temperature of 1.5 K (Ref. 6) shows that the distance between the maxima of the split Kondo peak, V_{p-p}, on the theoretical curves is smaller than on the experimental curves but is nevertheless greater than the value of $2g\mu_B H$ for $g=2$, indicating that the theory does not fully describe the splitting.

At present there is no theory that can predict the relation between the values of V_{p-p} and the internal and external magnetic fields at different temperatures of the experiment and different Kondo temperatures. Here we present empirical relations in which the value of V_{p-p} is determined by the physical quantities mentioned and also by the point-contact characteristics of the Kondo alloys CuMn, CuCr, and AuFe for different contact diameters.[1)] We arrived at these formula on the basis of our experiments and the experiments of other authors,[2–6] having found that the position of the maxima of the split Kondo peak on the point-contact characteristic $dV/dI(V)$ is determined not only by the Zeeman energy, as had been assumed previously, but also by the temperature of the experiment and the Kondo temperature. Another important consideration is whether or not the alloy under study is in the spin-glass state. We have found that the distance between the maxima of the split Kondo peak on the $dV/dI(V)$ curve in an external magnetic field in the spin-glass state is described by a simple empirical formula for alloys with unscreened magnetic impurities ($T \gg T_K$; $k_B T \ll g\mu_B H$):

$$V_{p-p} = 2[g\mu_B H + 3.63 k_B (T + T_K)] + V^{sg}_{p-p}, \qquad (1)$$

where $g=2$. The coefficient $3.63k_B$ agrees with the analogous coefficient for point contacts in the thermal limit, $eV = 3.63 k_B T_0$, where T_0 is the temperature at the center of the contact at voltage V and a bath temperature equal to zero;[7] V^{sg}_{p-p} is the distance between maxima on the point-contact characteristics of the Kondo alloy in the spin-glass state in zero magnetic field at the given temperature. In the case of low concentrations of a magnetic impurity, when the spin glass is not observed, $V^{sg}_{p-p}=0$. One can set $T_K=0$ for alloys with a negligibly low Kondo temperature in the bulk state, provided that the diameter of the contact is large enough, e.g., for CuMn for $d \leqslant 300$ nm and a Kondo temperature $T_k^{\text{bulk}}=0.01$ K. The above formula is applicable only in the case when the Kondo peak is split by an external field or by internal and external fields simultaneously. If the peak is split only by an internal field (for $H=0$), then $V_{p-p}=V^{sg}_{p-p}$.

It follows from formula (1) that $V_{p-p} \equiv 2g\mu_B H$ only for an alloy with a low T_K at $T=0$ in the paramagnetic state ($V^{sg}_{p-p}=0$). We have checked formula (1) for the alloys CuMn, AuMn, and AuFe.

The alloys studied were prepared at the Kamerlingh Onnes Laboratory of Leiden University, where the study of the point-contact spectra was also carried out with the use of the ''break-junction'' technology.[11] Low temperatures were achieved by pumping on ^{3}He vapor. The MC spectra were measured by the standard technique using a bridge circuit for higher resolution. Particular attention was paid to homogenization of the samples and to protecting the contacts from mechanical and thermal shocks. We also took into account that repeated cycling of the resistance of the point contacts from large to small values usually destroys the ballistic electron transport through a point contact. Increasing the temperature of the experiment above 10 K has a similar effect.

The validity of the proposed formula is illustrated below for the point-contact spectra of the alloy CuMn in the paramagnetic state (Fig. 2) and for the alloy AuFe, which is found in the spin-glass state at the same temperature (Fig. 3). These experimental data, and also the results of other authors,[2,3,5] agree with formula (1) to good accuracy, indicat-

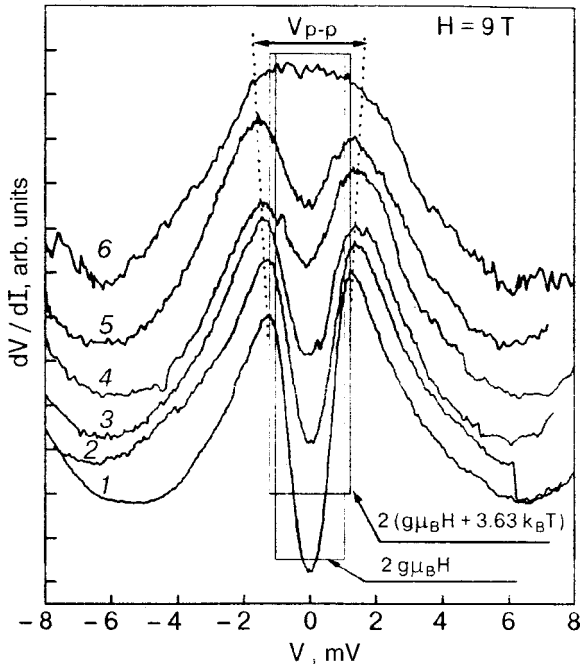

FIG. 2. $dV/dI(V)$ curves of a point contact of a CuMn alloy (0.1 at.% Mn) found in the paramagnetic state at $T=0.6$ K. The point contacts had diameters [nm]: 26.3 (*1*), 10.5 (*2*), 8.4 (*3*), 6.97 (*4*), 6.4 (*5*), 4.4 (*6*).

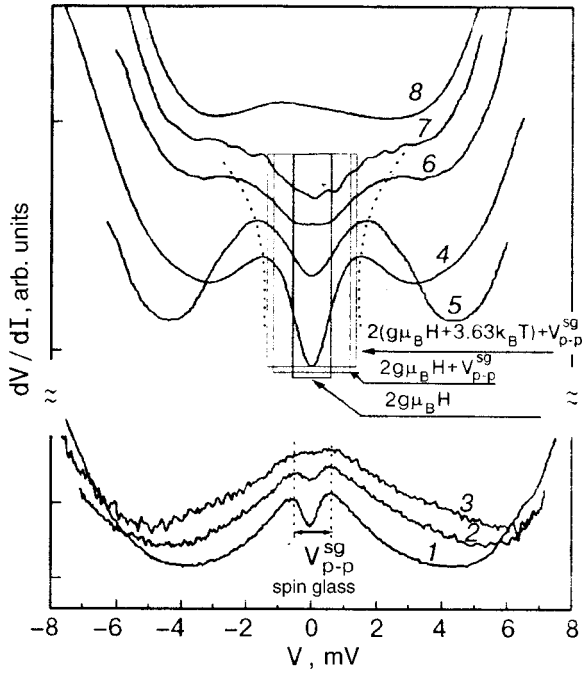

FIG. 3. $dV/dI(V)$ curves for different diameters of point contacts of the alloy AuFe (0.1 at.% Fe) found in the spin-glass state at $T=0.6$ K. The external magnetic field $H=0$ (*1–3*) and 5 T (*4–8*). The diameters of the point contacts [nm]: 23.1 (*1*), 10,2 (*2*), 6.7 (*3*), 12.7 (*4*), 6.5 (*5*), 5.3 (*6*) 4.8 (*7*), 3.8 (*8*).

ing that it is applicable in the temperature range $T<T_{\max}$ (Fig. 1).

The alloy CuCr, with a Kondo temperature of 2 K, is a special case. At helium temperature it undergoes a transition to the spin-glass state at a concentration of 0.5 at.% Cr.[8] Previously only a decrease in the resistivity was observed on the $\rho(T)$ curve for this alloy in an external magnetic field.[9] Negative magnetoresistance is also observed on the point-contact spectra of CuCr (0.1 at.% Cr) in fields up to 5 T.[10] In this alloy magnetic impurities are screened by conduction electrons, since $T\leqslant T_K$.

Let us consider the $dV/dI(V)$ characteristics shown in Fig. 2 for CuMn alloy point contacts of different diameter at a temperature of 0.6 K in an external magnetic field $H=9$ T. The splitting V_{p-p} of the Kondo peak in a field of 9 T for a point-contact diameter of 26.3 nm is larger than $2g\mu_B H$ and, with allowance for the temperature of the experiment, is in good agreement with the value determined by formula (1). For clarity the values of $2g\mu_{BH}$ and $2(g\mu_B H+3.63k_B T)$ are shown in the form of rectangles. Consequently, when the temperature of the experiment is taken into account according to the proposed formula (1), the value of V_{p-p} corresponds to the point contact of greatest diameter. For this diameter the Kondo temperature was neglected. The point-contact characteristics in Fig. 2 clearly show that decreasing the contact diameter leads to an increase in the value of V_{p-p} (the dotted curve), which is due to the increase of the Kondo temperature. Previously[4] we have shown for this alloy that decreasing the diameter of a point contact leads to an increase in T_K, which corresponds to formula (1). We see from Fig. 2 that for $d=4.4$ nm the splitting of the Kondo peak is destroyed, because the sum temperature $(T+T_K)$ becomes larger than $T_{\max}$. Thus the temperature of the experiment and the Kondo temperature lead to an increase in the energy position of the maxima of the split Kondo peak in an external magnetic field. The higher these temperatures, the larger the splitting V_{p-p}.

Let us demonstrate the validity of the proposed formula for the alloy AuFe, which is found in the spin-glass state at an experimental temperature of 0.6 K. Figure 3 shows the $dV/dI(V)$ characteristics of point contacts of different diameter for an AuFe alloy (0.1 at.% Fe) at $T=0.6$ K and $H=0$ (the three lower spectra) and $H=5$ T (the five upper spectra). At this temperature the bulk alloy AuFe is found in the spin-glass state, since the Kondo peak is split on the spectra of contacts of large diameter (curves *1* and *2*) on account of an internal field. Decreasing the diameter of the point contact leads to destruction of the spin glass, as is seen from the vanishing of the splitting of the Kondo peak on the $dV/dI(V)$ characteristics (curve *3* in Fig. 3). It is seen in the figure that under the influence of the size effect the spin glass is destroyed without affecting the position V^{sg}_{p-p}. It would seem that the size effect should lead to an increase in V^{sg}_{p-p} with decreasing diameter of the point contact, as occurs for the splitting of the Kondo peak in an external magnetic field (Fig. 2). We have observed analogous behavior of V^{sg}_{p-p} with decreasing diameter of the point contact for the alloy CuMn in the spin-glass state.

For lack of a theory of the size effect in point contacts found in the spin-glass state, we assume that this behavior of the position of the maxima V^{sg}_{p-p} is due to the fact that the relative (in comparison with the volume) number of Kondo impurities found on the surface of the contact increases with decreasing diameter of the contact. According to the theoretical and experimental studies[12] the spin of a Kondo impurity at the alloy surface does not scatter conduction electron. Therefore surface Kondo impurities do not take part in the formation of the spin-glass state in the contact region. This effect is equivalent to a decrease of the concentration of the Kondo impurities, which form a spin glass in the contact region, and this, in turn, should lead to a shift of the splitting V^{sg}_{p-p} of the maxima to lower values as the diameter decreases. Simultaneously, as the diameter decreases the size effect should cause a shift in the position of the maxima V^{sg}_{p-p} to larger values. It may be that the competition of these two effects leaves the value of V^{sg}_{p-p} approximately constant with decreasing diameter.

In an external field of 5 T (curves *4–8* in Fig. 3) the Kondo peak of an AuFe alloy (0.1 at.% Fe) is split, and the value of V_{p-p} is considerably greater than $2g\mu_B H$. At a temperature of 0.6 K this alloy is found in the spin-glass state, i.e., internal and external fields are simultaneously present. Consequently, the value of V_{p-p}, according to Eq. (1), is determined by the Zeeman energy, the temperature of the experiment, and the Kondo temperature, and also by V^{sg}_{p-p}. For clarity the values of the quantities are represented in Fig. 3 in the form of rectangles. We see that only when all of the quantities appearing in formula (1) are taken into account is there agreement with the experimental value of V_{p-p} (dotted lines). Here it is also necessary to take into account the Kondo temperature in the bulk alloy, $T_K^{\text{bulk}}(\text{AuFe})=0.2$ K. With decreasing diameter of the point contact the value V_{p-p} at a constant field increases (curves

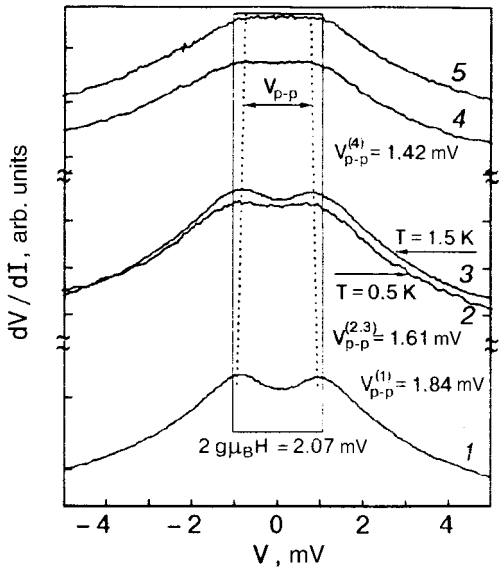

FIG. 4. $dV/dI(V)$ curves for different diameters of point contacts of the alloy CuCr at $T=0.5$ K (except for curve *3*, taken at $T=1.5$ K) in an external magnetic field $H=9$ T. The diameters of the point contacts [nm]: 21.8 (*1*), 10.5 (*2*), 24.1 (*3*), 9 (*4*), 9.8 (*5*).

4–7 in Fig. 3), since $T_K=T_K^{\text{bulk}}+\delta T_K$. At small diameter one observes the complete destruction of the splitting (curve *8*). The Kondo size effect in this alloy was investigated previously by the authors at $T=1.6$ K.[10] At that temperature the spin glass does not exist. It was shown that decreasing the diameter of the point contact leads to an increase in the Kondo temperature. Consequently, it is the increase of the Kondo temperature with decreasing diameter of the point contact that leads to the growth of V_{p-p}.

In contradistinction to the increase of V_{p-p} in a magnetic field for the alloys with unscreened impurities, viz., CuMn and AuFe, in CuCr alloys (0.1 at.% Cr) the distance between the maxima of the split Kondo peak is smaller than $2g\mu_B H$. Figure 4 shows the point-contact spectra of CuCr point contacts of different diameter in a magnetic field of 9 T at a temperature of 0.5 K (curves *1, 2, 4, 5*) and at 1.5 K for a contact of diameter 24.1 nm (curve *3*). From a comparison of the position V_{p-p} for spectra *1* and *3* we see that the higher the temperature at which the experiment is done, the greater the disparity between $2g\mu_B H$ and the value of V_{p-p}, which is getting progressively smaller.

As is shown in Fig. 1a, increasing the temperature T of the experiment decreases the interval between $T_{\max}$ and T, which leads to a decrease in the value of V_{p-p}. This is in good agreement with the fact that qualitatively $V\propto T$ in PCS. From a comparison of the position V_{p-p} of the spectra *1* and *2* (Fig. 4) it can be concluded that the smaller the diameter of the contact, the smaller the value of V_{p-p}. This tendency is opposite to what is observed for alloys with unscreened Kondo impurities (CuMn, AuMn, AuFe). Previously in studies of the size effect in the alloy CuCr we showed[10] that decreasing the diameter of a point contact leads to growth of the Kondo temperature (T_K for curve *2* is higher than for curve *1*). Thus the temperature of the experiment and the Kondo temperature tends to decrease the value of V_{p-p}.

It has been established previously[9] for the alloy CuCr that the dependence of the relative magnetoresistance on ($T+T_K$) is close to linear. Using this observation, we propose the following empirical formula for alloys with screened magnetic impurities:

$$V_{p-p}=2\left\{g\mu_B H-3.63k_B\left[\frac{(T+\delta T_K)T_K}{T+T_K+\delta T_K}\right]\right\}, \qquad (2)$$

where δT_K is the growth of the Kondo temperature relative to that of the bulk sample, T_K, as a result of the size effect. This formula is applicable only in the case of the splitting of the Kondo peak in an external magnetic field.

From the experimental curves presented in Fig. 4 we see that in a field $H=9$ T curves *2* and *3* have the same values of V_{p-p}, while curve *3* was obtained at a temperature 1 K higher than curve *2* for a point contact of smaller diameter. According to formula (2), this means that T_K is now 1 K higher for curve *2* than for curve *1*. In view of the large diameter of the contact, for curve *1* we can take $T_K=2$ K, as for the bulk alloy.

At present we do not know of any point-contact experiments on the study of the Kondo size effect in a magnetic field for the alloy CuCr in the spin-glass state, and the term V_{p-p}^{sg} is therefore absent in formula (2).

From an analysis of the point-contact characteristics and the formulas presented here, it follows that the energy position of the maxima of the split Kondo peak in an external magnetic field depends on T and T_K in a different way depending on the screening of the spin of the paramagnetic impurity. For alloys with unscreened spins, increasing the temperatures T and T_K leads to growth of the value of V_{p-p}. Before, for the alloy CuMn, we could neglect the small value of T_K and consider only the temperature of the experiment. For alloys with screened spins, increasing T or T_K leads to a decrease in the value of V_{p-p}. This behavior is in good agreement with the appearance of the Kondo peak on the point-contact spectra in analogy with the dependence $\rho(T)$ (Fig. 1). However, T and T_K enter the formula in such a way that in this case they cannot be taken into account independently, since a small value of one of these temperatures will make their total influence on the value of V_{p-p} even smaller.

Using the proposed formulas, one can estimate the increase of T_K in CuMn, AuFe, and CuCr point contacts with decreasing diameter if the values of V_{p-p} are known for the given value of the external magnetic field. Figure 5 shows the results obtained from the spectra of the splitting of the Kondo peak in an external magnetic field for different values of the parameters appearing in formulas (1) and (2). The increase in the Kondo temperature with decreasing diameter of the point contacts for these alloys is in qualitative agreement with the results presented in Refs. 4 and 10, in which T_K was systematically higher than the values given in Fig. 5. Thus we have studied the Kondo size effect on alloys consisting of various metals (Cu, Au) with magnetic impurities (Mn, Cu, Fe) both in the spin-glass state and in the case where the spin glass is absent. The Kondo temperatures of these alloys lie in the interval from 0.01 to 2 K. Magnetic impurities in the alloys CuMn and AuFe are not screened, while in CuCr they are screened by conduction electrons; in spite of this, in all the alloys a size effect is observed both in the presence and absence of a magnetic field.[4,10] It should be noted that in zero magnetic field, for all of the alloys listed

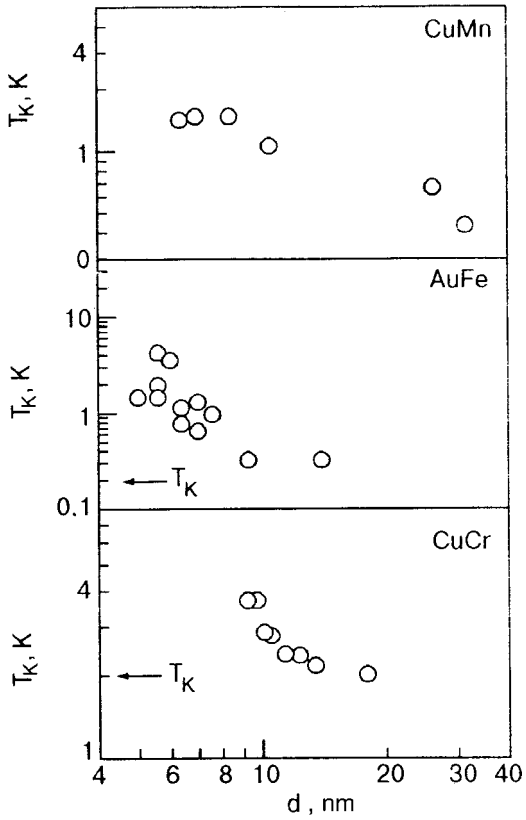

FIG. 5. Dependence of the Kondo temperature on the diameter of the point contact. The values were obtained with the use of formula (1) for the CuMn and AuFe alloys and formula (2) for the CuCr alloy.

and also for CuFe (Ref. 13), as a result of the size effect an energy broadening of the Kondo peak occurs, which is due to the increase of T_K in the point contact. The Kondo size effect in point contacts with ballistic electron transport leads to enhancement of the interaction of the conduction electrons with paramagnetic impurities, i.e., the sign of the size effect is opposite to that observed on films and nanowires in both the spin-glass and paramagnetic states.[14–19]

In an external magnetic field the splitting V_{p-p} of the Kondo peak behaves differently depending on the screening of the spin. For CuMn, AuFe, and AuMn alloys, having unscreened spins, $V_{p-p} \geqslant 2g\mu_B H$, whereas for the alloy CuCr, having screened spins, $V_{p-p} \leqslant 2g\mu_B H$. It is not yet clear why $V_{p-p} \geqslant 2g\mu_B H$ in an external magnetic field for alloys with unscreened spins, as that is at odds with the treatment of the point-contact characteristics by analogy with the $\rho(T)$ curve, since, qualitatively, $V \propto T$ for PCS. It may be that this is due to stimulation of the spin glass by the external magnetic field.

Of course, the empirical formulas presented here cannot claim to represent a complete description of the splitting of the Kondo peak on the point-contact characteristics in an external or internal magnetic field or in the case of the size effect. There is some justification for using them in that experimenters do not have any formulas available for describing the Kondo characteristics of point contacts of different diameter in an external or internal magnetic field, as they do, say, for the case of phonons.[20] We hope that further theoretical and experimental studies will lead to a deeper understanding of the observed point-contact characteristics.

*E-mail: fisun@ilt.kharkov.ua

[1)]The diameters of the point contacts (d, nm) were determined from the Sharvin formula: $d \approx 30/\sqrt{R_0}$ (for Cu) and $u = d \approx 28/\sqrt{R_0}$ (for Au). R_0 is measured at $V = 0$.

[1] A. A. Lysykh, I. K. Yanson, O. I. Shklyarevski, and Yu. G. Naydyuk, Solid State Commun. **35**, 987 (1980); A. G. M. Jansen, A. P. van Gelder, P. Wyder, and S. Srassler, J. Phys. F. **11**, L15 (1981); Yu. G. Naĭdyuk, O. I. Shklyarevskiĭ, and I. K. Yanson, Fiz. Nizk. Temp. **8**, 725 (1982) [Sov. J. Low Temp. Phys. **8**, 362 (1982)].
[2] D. C. Ralph, Thesis Cornell Univ. (1994) (unpublished).
[3] A. Duif, Thesis Kath. Univ. Nijmegen (1983) (unpublished).
[4] I. K. Yanson, V. V. Fisun, R. Hesper, A. V. Khotkevich, J. M. Krans, J. A. Mydosh, and J. M. van Ruitenbeek, Phys. Rev. Lett. **74**, 302 (1995).
[5] F. Roche, Thesis, Grenoble High Magnetic Field Laboratory, Max-Planck-Institut (1995) (unpublished).
[6] N. d'Ambrumenil and R. W. White, J. Appl. Phys. **53**, 2052 (1982).
[7] B. I. Verkin, I. K. Yanson, I. O. Kulik, O. I. Shklyarevskii, A. A. Lysykh, and Yu. G. Naidyuk, Solid State Commun. **30**, 215 (1979).
[8] K. R. Lane, M. Park, J. F. DiTusa, M. S. Isaacson, and J. M. Parpia, J. Low Temp. Phys. **93**, 7 (1993).
[9] M. D. Daybell and W. A. Steyert, Phys. Rev. Lett. **20**, 195 (1968).
[10] V. V. Fisun, I. K. Yanson, J. A. Mydosh, and J. M. van Ruitenbeek, Fiz. Nizk. Temp. **26**, 681 (2000) [Low Temp. Phys. **26**, 497 (2000)].
[11] C. J. Muller, J. M. van Ruitenbeek, and L. J. de Jongh, Physica C **191**, 485 (1992).
[12] O. Ujsaghy, A. Zawadowski, and B. L. Gyorffy, Phys. Rev. Lett. **76**, 2378 (1996); O. Ujsaghy and A. Zawadowski, Phys. Rev. B **57**, 11598 (1998).
[13] I. K. Yanson, V. V. Fisun, J. A. Mydosh, and J. M. van Ruitenbeek, in *Proceedings of NATO ARW on Size Dependent Magnetic Scattering*, edited by V. Chandrasekhar, Hungary (2001); cond-mat/008055.
[14] T. M. Jacobs and N. Giordano, Europhys. Lett. **44**, 74 (1998).
[15] J. F. DiTusa, K. Lin, M. Park, M. S. Isaacson, and J. M. Parpia, Phys. Rev. Lett. **68**, 678 (1992).
[16] G. Chen and N. Giordano, Phys. Rev. Lett. **66**, 209 (1998).
[17] C. Strun, M. Henny, and C. Schonenberger, Phys. Rev. Lett. **81**, 2982 (1998).
[18] V. Chandrasekhar, P. Santhaman, N. A. Penebe, R. A. Webb, H. Vloeberghs, C. Van Haesendonck, and Y. Bruynseraede, Phys. Rev. Lett. **72**, 2053 (1994).
[19] K. R. Lane, M. Park, M. S. Isaacson, and J. M. Parpia, Phys. Rev. B **51**, 945 (1995).
[20] I. O. Kulik, A. N. Omel'yanchuk, and R. I. Shekhter, Fiz. Nizk. Temp. **3**, 1543 (1977) [Sov. J. Low Temp. Phys. **3**, 740 (1977)].

Translated by Steve Torstveit

QUANTUM EFFECTS IN SEMICONDUCTORS AND DIELECTRICS

Dependence of semiconductor energy bands on the isotopic composition. A universal relation for monoatomic crystals

A. P. Zhenov†

Kurchatov Institute Russian Research Center, Institute of Superconductivity and Solid State Physics, pl. Kurchatova 4, 123182 Moscow, Russia

(Submitted June 3, 2001)
Fiz. Nizk. Temp. **28**, 183–193 (February 2002)

The influence of the isotopic composition of the components of semiconductor compounds on the structure of the energy bands $E_{\mathbf{f},n}$ is discussed. The respective roles of changes in the volume of the unit cell of the crystal and of renormalization of the electron–phonon interaction upon changes in the isotopic composition are considered. For the case of monoatomic systems in the virtual crystal approximation a universal relation is obtained for the dependence of the bands on the composition and temperature. © *2002 American Institute of Physics.*
[DOI: 10.1063/1.1461925]

1. INTRODUCTION

Currently a considerable amount of attention is being devoted to the study of the properties of chemically pure and structurally perfect semiconductor single crystals with different isotopic compositions. A large number of studies have been done on such classic and commercially important monoatomic semiconductors as diamond, silicon, and germanium. This has become possible thanks to the synthesis of nearly defect-free bulk single crystals highly enriched in the isotopes ^{12}C, ^{13}C, ^{28}Si, ^{70}Ge, and ^{76}Ge and also of crystals with other than the natural isotopic composition.[1–5] We note that diamond crystals of different isotopic composition have been grown in the laboratory at General Electric (USA), and their germanium counterparts by collaborative efforts at the Institute of Molecular Physics of the Kurchatov Institute Russian Research Center (Russia) and the Lawrence Berkeley National Laboratory (USA). Isotopically highly enriched crystals of silicon have been obtained in a cooperation of scientists from Russia, Germany, and Japan.

Varying the isotopic composition of the components of a compound gives rise to effects linear in the mass difference of the isotopes and to effects proportional to the mean-square atomic-mass fluctuation parameter (in other words, effects of first and second orders). The first-order effects can have an appreciable influence on the static and thermodynamic properties, while effects of both orders are manifested in an important way in the features of the behavior of the kinetic parameters and optical spectra.[6–8]

To a first approximation the harmonic phonon modes can be described in the virtual crystal model. For this the real lattice with randomly distributed isotopes is replaced by a lattice without isotopic disorder, in which the masses of the atoms of the components are replaced by their average values $\langle M\rangle = M_c^k = \Sigma_i c_i^k M_i^k$ (k is the number of the atom in the cell, and c_i^k is the concentration of the ith isotope of the given element). It is also assumed that the mean-square mass fluctuation parameter, $G_2 = (\langle M^2\rangle - \langle M\rangle^2)/\langle M\rangle^2$ is a small quantity. In the framework of the virtual crystal model, isotope effects involving phonons either directly or indirectly—through anharmonic phonon–phonon and electron–phonon interactions—can arise in the physical parameters.

In this paper we use the virtual crystal model in a quasiharmonic approach to consider the influence of the isotopic composition of a semiconductor compound on the structure and position of the energy bands.

It is well known that the temperature dependence of the energy bands and optical characteristics of a solid are determined by two main effects. First, the bands $E_{\mathbf{f},n}$ depend on the volume of the unit cell of the crystal, which changes on account of thermal expansion of the lattice. Second, the value of $E_{\mathbf{f},n}$ changes with increasing T on account of the electron–phonon interaction (EPI). Taking the EPI into account leads to a renormalization of the contribution of the elastic channel, which is due to the fact that the true amplitude of the electron–ion interaction contains the dynamic Debye–Waller (DW) factor in addition to the static part. The contribution of the inelastic intra- and interband EPI processes is also renormalized at the same time.[9,10]

It is clear from what we have said that upon variation of the isotopic composition, when the phonon spectrum is deformed, the energy of the bands should also be altered substantially. Here the influence of the isotopic composition on the energy of the bands is again determined by the change in volume of the unit cell and the renormalization of the EPI (the corresponding contributions will be denoted by subscripts $D\Omega$ and EP). At a certain value of the temperature T we have

$$\left(\frac{\partial E}{\partial M}\right)_T = \left(\frac{\partial E}{\partial M}\right)_{\text{tot}} = \left(\frac{\partial E}{\partial M}\right)_{D\Omega} + \left(\frac{\partial E}{\partial M}\right)_{EP}.$$

We note that in the last few years the influence of the isotopic composition on the electronic structure has been investigated in great detail experimentally by Cardona's group in Stuttgart (see the references to the work of this group and

others in Sec. 4). The author is aware of only three theoretical papers that discuss this problem. In Ref. 11 calculations were done for C and Ge by the NLPP method for electrons and a bond-charge model for phonons. There the renormalizations of the energies of the interband transitions on account of the changes in the factor $(\partial E/\partial M)_{EP}$ upon variation of the isotopic composition were determined. For Ge, GaAs, and ZnSe, estimates of both factors $(\partial E/\partial M)_{D\Omega}$ and $(\partial E/\partial M)_{EP}$ were made in Refs. 12 and 13 in the framework of the NLPP and LCAO methods. For describing the phonon modes the shell and rigid-ion models were used in addition to the bond-charge model. The goal of the present paper is different: to show that for monoatomic crystals of different isotropic composition the relation between the parameters of the band transitions arises from universal relations that are satisfied at any value of the temperature. The essence of these relations is as follows. If the data for the natural composition are known, then one can determine the parameters for enriched compositions very simply.

Section 2 presents a summary of the known results on the dependence of the energy bands on temperature and isotopic composition. The volume and EPI effects are considered. In Sec. 3 a universal relation is obtained for the dependence of the energy bands on the isotopic composition and temperature in the case of monoatomic crystals. The relations have a simple structure. The reason is that in crystals of this kind the polarization vectors are independent of the mass, and the frequency has a dependence $\omega(l)\sim M^{-1/2}$. For polyatomic crystals the situation is much more complicated, since the isotope shifts of the frequencies are proportional to the square of the corresponding modulus of the polarization vector (see Appendix), and these vectors themselves are also dependent on the mass. (The case of polyatomic crystals will be analyzed separately.) Section 4 presents a discussion of the data obtained by linear and nonlinear spectroscopy on the influence of the composition on the isotope shifts of the energies of the interband direct and indirect electronic transitions and also on the position of the critical points in the optical spectra.

2. DEPENDENCE OF THE ENERGY BANDS ON THE ISOTOPIC COMPOSITION AND TEMPERATURE

2.1. Volume effect

Let us determine the renormalization of the bands E due to the change in volume of the unit cell of the crystal on account of deformation of the phonon spectrum upon variation of the isotopic composition. For this purpose we introduce into the discussion a factor given by the derivative of the energy of the band with respect to the mass of one of the components of the compound at a constant temperature (see also Ref. 14):

$$\left(\frac{\partial E}{\partial M_c^k}\right)_{D\Omega} = -B\left(\frac{\partial E}{\partial P}\right)_V \left(\frac{\partial \ln \Omega}{\partial M_c^k}\right)_P . \tag{1}$$

Here Ω is the volume of the unit cell of the crystal, and $B = -V(\partial P/\partial V)_T$ is the bulk modulus of compression. Here $(\partial E/\partial P)_V$ is a coefficient characterizing the pressure dependence of the band. We note that the bulk modulus B and the coefficient $(\partial E/\partial P)_V$ are usually comparatively weak functions of T.

In the quasiharmonic approximation

$$\Omega(T) = \Omega_0 + \frac{1}{B}\sum_l \gamma(l)\epsilon(l). \tag{2}$$

Here Ω_0 is the volume of the "frozen" (static) lattice; the index l labels vibrational modes, $l=\{\mathbf{q},j\}$, where $\mathbf{q}$ is the quasimomentum and j is the polarization of the phonon mode; $\gamma(l) = -[\partial\omega_c(l)/\partial\Omega]/[\omega_c(l)/\Omega]$ is the partial Grüneisen factor for the lth vibrational mode, which takes into account the fact that the frequencies of the different modes $\omega_c(l)$ depend differently on the volume, and $\epsilon(l)$ denotes the contribution of each mode to the thermal energy:

$$\epsilon(l) = \hbar\omega_c(l)\left(n(l)+\frac{1}{2}\right), \tag{3}$$

($n(l)$ is the Bose–Einstein factor). We note that the frequencies $\omega_c(l)$ depend on the volume, the temperature T, and the mass of the atoms.

The factor $(\partial E/\partial M_c^k)_{D\Omega}$ (1) is a positive definite quantity, since the volume Ω of the cell usually decreases with increasing mass of the isotope.

If the factor $(\partial E/\partial M_c^k)_{D\Omega}$ is known, one can immediately determine the difference in the energies of the bands of crystals with masses M_c^k and $M_c^k+\Delta M^k$:

$$\Delta\tilde{E}^{D\Omega}(\Delta M^k) = \Delta E^{D\Omega}(M_c^k+\Delta M^k) - \Delta E^{D\Omega}(M_c^k) = \left(\frac{\partial E}{\partial M_c^k}\right)_{D\Omega}\Delta M^k. \tag{4}$$

It follows from relations (1) and (4) that as the mass of the isotope increases, the corresponding renormalization (decrease) of the volume leads to an increase in the energy of the band.

It should be noted that in the case of the monoatomic semiconductors C, Si, and Ge, all of the quantities appearing in the formula have been investigated repeatedly. Data for the different coefficients of the type $(\partial E/\partial P)_T$ can be found in the monograph of Sobolev and Nemoshkalenko.[10] As to the factor $(\partial \ln\Omega/\partial M_c^k)_V$, its behavior has been analyzed theoretically in a wide interval in the framework of microscopic models in Refs. 15–18, for example.

In view of what we have said, the renormalization of the band energy from the volume effect can be estimated using a formula of the form

$$\Delta E_{f,n}^{D\Omega} \propto -B\left(\frac{\partial E_{\mathbf{f},n}}{\partial P}\right)_V \frac{\Omega(T)-\Omega_0}{\Omega_0} = -\left(\frac{\partial E_{\mathbf{f},n}}{\partial P}\right)_V \sum_l \gamma(l)\epsilon(l). \tag{5}$$

The expression for $\Delta E_{\mathbf{f},n}^{D\Omega}$ in (5) is used in Sec. 3 in deriving a universal relation for the electron bands.

2.2. The Debye–Waller factor and inelastic electron–phonon scattering

In this Section we summarize the research results on the influence of temperature and isotopic composition of the constituents of compounds on the EPI and the associated renormalization of the energy bands. In the virtual crystal approximation the corresponding renormalizations were determined in Ref. 9. That paper set forth the basic principles of the theory of the temperature dependence of the electron band structure. The energy bands $E_{\mathbf{f},n}(T)$ were determined in the adiabatic approximation in the framework of second-order perturbation theory in the displacements of the atoms.

In view of what we have said, we shall assume that the crystalline potential $V(\mathbf{r},\mathbf{u})$ is a superposition of the potentials V_k of the individual ions. We note that the position of an ion in the lattice is specified by the radius vector of the equilibrium position of the unit cell $\mathbf{R}_{\mathbf{m}}^{(0)}$ and the number k of the ion within the cell. Here $\tilde{V}_k = V_k(\mathbf{r}-\mathbf{R}_{\mathbf{m}}^{(0)}-\mathbf{u}_{\mathbf{m},k})$, where the vector $\mathbf{u}_{\mathbf{m},k}$ describes the dynamic atomic displacements. We expand the potential $\tilde{V}_k$ in a series in the displacements $\mathbf{u}_{\mathbf{m},k}$. Then we determine the state of the electrons in the potential $V(\mathbf{r},\mathbf{u}=0)$ of the "frozen" lattice. The corresponding one-electron energy eigenvalues $\varepsilon_n(\mathbf{f})$ and eigenfunctions $|\mathbf{f},n\rangle$ of the Kohn–Sham type are classified according to the quasimomentum $\mathbf{f}$ and the number n of the band. For the sake of simplicity we shall drop the spin index.

It is customarily assumed that such one-electron states describe long-lived excitations. In principle, the concept of quasiparticles is justified if their energy is close to the Fermi energy. Experiment suggests that the domain of applicability of the theory is wider than that.

Let us consider how the electronic structure is affected by the presence of an electron–ion interaction Hamiltonian consisting of terms linear (H_1) and quadratic (H_2) in the dynamic atomic displacements. By definition

$$H_{\rm int} = H_1 + H_2 = \sum_{\mathbf{m},k} \frac{\partial V_k}{\partial R_{\mathbf{m}}^{(0)\alpha}} u_{\mathbf{m},k}^{\alpha} + \frac{1}{2} \sum_{\mathbf{m},k;\mathbf{m}'} \frac{\partial^2 V_k}{\partial R_{\mathbf{m}}^{(0)\alpha} \partial R_{\mathbf{m}'}^{(0)\beta}} u_{\mathbf{m},k}^{\alpha} u_{\mathbf{m}',k'}^{\beta} + \ldots, \tag{6}$$

where $V_k = V_k(\mathbf{r}-\mathbf{R}_{\mathbf{m}}^{(0)})$ (α and β are Cartesian coordinates).

In calculating the renormalization of the spectrum in the adiabatic approximation ($\sim (m_e/M)^{1/2}$), one can treat the displacements as classical parameters. Then, according to steady-state perturbation theory, the renormalization of the energy of a quasiparticle in the state $|\mathbf{f},n\rangle$ can be written in the form

$$\Delta E_{\mathbf{f},n}^{EP}(\{\mathbf{u}(\mathbf{m},k)\}) = \langle \mathbf{f},n|H_1+H_2|\mathbf{f},n\rangle + \sum_{\mathbf{f},n\neq\mathbf{f}',n'} \frac{|\langle \mathbf{f}',n'|H_1|\mathbf{f},n\rangle|^2}{\varepsilon_n(\mathbf{f})-\varepsilon_{n'}(\mathbf{f}')+i\eta}. \tag{7}$$

Performing the statistical averaging $\langle \ldots \rangle$ in (7) over an ensemble of small dynamic thermal atomic displacements, we can immediately determine the temperature dependence of the energy bands, i.e., we can go from $E_{\mathbf{f},n}(\{\mathbf{u}_{\mathbf{m},k}\})$ to $E_{\mathbf{f},n}(T)$. In the harmonic approximation for the atomic vibrations we obtain[9]

$$E_{\mathbf{f},n}(T) = \varepsilon_n(\mathbf{f}) + \Delta E_{\mathbf{f},n}^{EP}(T), \qquad E_{\mathbf{f},n}^{EP}(T) = \Delta E_{\mathbf{f},n}^{DW}(T) + \Delta E_{\mathbf{f},n}^{SE}(T), \tag{8}$$

where

$$\Delta E_{\mathbf{f},n}^{EP}(T) = \frac{1}{2}\sum_{\mathbf{m}} \left\langle \mathbf{f},n \left| \frac{\partial^2 V_k}{\partial R_{\mathbf{m}}^{(0)\alpha} \partial R_{\mathbf{m}}^{(0)\beta}} \right| \mathbf{f},n \right\rangle \langle u_{\mathbf{m},k}^{\alpha} u_{\mathbf{m},k}^{\beta} \rangle + \sum_{\mathbf{m},k;\mathbf{m}',k'} \sum_{\mathbf{f},n\neq\mathbf{f}',n'} \frac{\langle \mathbf{f},n|(\partial V_k/\partial R_{\mathbf{m}}^{(0)\alpha})|\mathbf{f}',n'\rangle\langle \mathbf{f}',n'|(\partial V_{k'}/\partial R_{\mathbf{m}'}^{(0)\beta})|\mathbf{f},n\rangle}{\varepsilon_n(\mathbf{f})-\varepsilon_{n'}(\mathbf{f}')+i\eta} \langle u_{\mathbf{m},k}^{\alpha} u_{\mathbf{m}',k'}^{\beta} \rangle. \tag{9}$$

We recall that the operator for the dynamic atomic displacements has the form

$$\mathbf{u}_{\mathbf{m},k} = \sum_{\mathbf{q}j} \left(\frac{\hbar}{2NM_c^k \omega_c(l)} \right)^{1/2} \times [\mathbf{e}^c(k|l) e^{i\mathbf{q}\mathbf{R}_m^{(0)}} b_l + \mathbf{e}^{c*}(k|l) e^{-i\mathbf{q}\mathbf{R}_{\mathbf{m}}^{(0)}} b_l^*], \tag{10}$$

where $\omega_c(l)$, $\mathbf{e}(k|l)$ are the frequency and polarization vector of the phonon mode $l=\{\mathbf{q}j\}$, and b_l (b_l^*) are the quasiparticle annihilation (creation) operators.

On the right-hand side of Eq. (9) are two terms. The first of these describes the contribution to the renormalization from the DW effect, i.e., an elastic interaction in which an electron in state $|\mathbf{f},n\rangle$ simultaneously emits and absorbs a phonon with wave vector $\mathbf{q}$ and polarization j. The corresponding correction to the electronic spectrum of a crystal with "frozen" atomic displacements is denoted by $\Delta E_{\mathbf{f},n}^{DW}$. The second term describes inelastic interaction processes between electrons and phonons (including inter- and intraband transitions) in the second order of perturbation theory. The correction to the electron spectrum $\Delta E_{\mathbf{f},n}^{SE}$ is a complex quantity. Here its real part characterizes the change of the effective mass of the electron, and the imaginary part determines the lifetime.

With allowance for what we have said, formula (9) can be written in the form

$$\Delta E_{\mathbf{f},n}^{EP}(T) = \Delta E_{\mathbf{f},n}^{DW} + \Delta E_{\mathbf{f},n}^{SE} + i\Gamma_{\mathbf{f},n}. \tag{11}$$

In Ref. 19 a so-called acoustic sum rule was established for metals and insulators in the long-wavelength limit; this

sum rule is a consequence of the condition of electrical neutrality of the system. On the basis of this sum rule, one can redefine the first term in formula (9), which characterizes the DW effect (see, e.g., Refs. 9 and 11). Then using the explicit representation for the dynamic displacements (10), we obtain in place of (9) (see also Refs. 12 and 20)

$$\Delta E^{EP}_{\mathbf{f},n}(T)=\sum_{\mathbf{q},j}\left\{\left[\frac{\partial E_{\mathbf{f},n}}{\partial n(\mathbf{q},j)}\right]_{DW}+\left[\frac{\partial E_{\mathbf{f},n}}{\partial n(\mathbf{q},j)}\right]_{SE}\right\}\times\left[\left(n(\mathbf{q},j)+\frac{1}{2}\right];\right. \tag{12}$$

$$\left[\frac{\partial E_{\mathbf{f},n}}{\partial n(\mathbf{q},j)}\right]_{DW}=-\frac{1}{2N}\sum_{n',k,k'}\frac{Q^*_\alpha(\mathbf{f},n,n',\mathbf{q}j,k)Q_\beta(\mathbf{f},n',n;\mathbf{q}j,k')}{\varepsilon_n(\mathbf{f})-\varepsilon_{n'}(\mathbf{f})+i\eta}\times\left[\frac{1}{M^k_c}e^c_\alpha(k|-\mathbf{q}j)e^c_\beta(k|\mathbf{q}j)+\frac{1}{M^{k'}_c}e^c_\alpha(k'|-\mathbf{q}j)e^c_\beta(k'|\mathbf{q}j)\right]; \tag{13}$$

$$\left[\frac{\partial E_{\mathbf{f},n}}{\partial n(\mathbf{q},j)}\right]_{SE}=\frac{1}{N}\sum_{n';k,k'}\frac{Q_\alpha(\mathbf{f},n,n';\mathbf{q}j,k)Q_\beta(\mathbf{f},nn';\mathbf{q}j,k')}{\varepsilon_n(\mathbf{f})-\varepsilon_{n'}(\mathbf{f}+\mathbf{q})}\times\frac{1}{(2M^k_cM^{k'}_c)^{1/2}}e^c_\alpha(k|-\mathbf{q}j)e^c_\beta(k'|\mathbf{q}j). \tag{14}$$

The quantity $\mathbf{Q}$ is defined as

$$\mathbf{Q}(f,n,n';\mathbf{q}j,k)=\left\{\frac{\hbar}{\omega_c(\mathbf{q},j)}\right\}^{1/2}\langle\mathbf{f}',n'|\nabla V_k|\mathbf{f},n\rangle, \tag{15}$$

where $\mathbf{f}'=\mathbf{f}+\mathbf{q}+\mathbf{G}$, and $\mathbf{G}$ is a reciprocal lattice vector.

The difference in the band energies of crystals with masses M^k_c and $M^k_c+\Delta M^k$ on account of the EPI can be written

$$\Delta\overline{E}^{EP}(\Delta M^k)=\Delta E^{EP}(M^k_c+\Delta m^k)-\Delta E^{EP}(M^k_c)=\left(\frac{\partial E^{EP}}{\partial M^k_c}\right)_{T,V}\Delta M^k. \tag{16}$$

We note that the factor $(\partial E^{EP}/\partial M^k_c)_{T,V}$ has a positive sign. The renormalizations of the energy bands due to the EPI decreases with increasing mass of the atoms. The increase in mass will actually lead to freezing of the vibrations of the crystal. This increases the energies of the interband transitions.

Thus, in this Section we have considered the influence of the renormalization of the electronic spectrum due to the EPI at a constant volume. Using relations (8), (9), and (12)–(14), one can study how the behavior of the energy bands is affected by the deformation of the EPI spectrum due to variation of the isotopic composition in a wide range of temperatures.

3. UNIVERSAL RELATION FOR THE DEPENDENCE OF THE ENERGY BANDS ON THE ISOTOPIC COMPOSITION. THE CASE OF MONOATOMIC CRYSTALS

Let us determine how the energy bands $E_{\mathbf{f},n}$ of a crystal containing atoms of only one element depend on the isotopic composition. It happens that in this case the dependence of $E_{\mathbf{f},n}$ on the isotopic composition can be described extremely simply in the virtual crystal approximation.

Let us consider the basic equation that determines the eigenfrequencies and polarization vectors of the vibrational modes $l=\{\mathbf{q}j\}$ of a monoatomic crystal of arbitrary isotopic composition (we label it with index c):

$$\omega^2_c(l)e^c_\alpha(k|l)=\sum_{k',\alpha'}\Phi^c_{\alpha\alpha'}(kk'|\mathbf{q})e^c_{\alpha'}(k'|l). \tag{17}$$

Here $\Phi^c_{\alpha\alpha'}(kk'|\mathbf{q})$ is the dynamical matrix of the crystal, and α,α' are Cartesian indices. The matrix Φ is specified by a relation of the form

$$\Phi^c_{\alpha\alpha'}(kk'|\mathbf{q})=\frac{1}{M_c}\tilde{\Phi}_{\alpha\alpha'}(kk'|\mathbf{q})=\frac{1}{NM_c}\times\sum_{\mathbf{mm}'}\varphi_{\alpha\alpha'}(\mathbf{m}k,\mathbf{m}'k')\times\exp(i\mathbf{q}(\mathbf{R}^{(0)}_{\mathbf{m}}-\mathbf{R}^{(0)}_{\mathbf{m}'})), \tag{18}$$

where $\varphi_{\alpha\alpha'}(\mathbf{m}k,\mathbf{m}'k')$ is the matrix of second-order spin parameters, and N is the number of unit cells. We note that the matrix $\tilde{\Phi}$ is independent of the value of the average mass M_c.

As is shown in the Appendix, in the case of a monoatomic crystal the frequencies of the vibrational modes obey a relation of the form

$$\frac{d\ln\omega^2_c(l)}{d\ln M_c}=-1+O\left[\left(\frac{|\Delta M|}{M_c}\right)^2,\ \frac{\Delta M}{M_c}\frac{\langle u^2\rangle}{a^2}\right] \tag{19}$$

from which it follows that

$$\omega_c(l)=w(l)M_c^{-1/2}. \tag{20}$$

By definition, the value of $w(l)$ is independent of M_c.

Substituting (20) into (17) and taking relation (18) into account, we obtain the equation

$$w^2(l)e^c_\alpha(k|l)=\sum_{k',\alpha'}\tilde{\Phi}^c_{\alpha\alpha'}(kk'|\mathbf{q})e^c_{\alpha'}(k'|l). \tag{21}$$

From this equation we see that, unlike the frequencies, the polarization vectors $e^c_\alpha(k|l)$ are independent of the value of the mass for a specific isotopic composition of the compound.

We denote the parameters for a certain isotopic composition by the index c_0. For an arbitrary isotopic composition we will continue to use the index c. In view of what was said above, we consider the expressions for the contributions to the renormalizations of the energy bands due to the change in volume and in the EPI as a result of a variation of the composition.

The contribution to the renormalization of the electronic structure from the volume is described by relation (5). Differentiating $\gamma(l)$ with respect to M_c and using (19), we see

that $\gamma(l)$ is independent of M_c. Consequently, for $T<T_D$ the following quantity which appears in the sum over l must depend on the average mass of the crystal (through $\omega(l)$):

$$X_c^{(1)}(l,T)=\omega_c(l)\left[n\left(\frac{\hbar\omega_c(l)}{k_BT}\right)+\frac{1}{2}\right]. \tag{22}$$

The contribution due to the EPI is given by formulas (12)–(14). In this case the following quantity depends on the average mass M_c of the crystal:

$$X_c^{(2)}(l,T)=\frac{1}{M_c\omega_c(l)}\left[n\left(\frac{\hbar\omega_c(l)}{k_BT}\right)+\frac{1}{2}\right]$$
$$\sim\omega_c(l)\left[n\left(\frac{\hbar\omega_c(l)}{k_BT}\right)+\frac{1}{2}\right]. \tag{23}$$

Thus in the case of an arbitrary phonon spectrum the contributions to the renormalization of the energy bands from the volume changes and from the EPI are described by the same dependence. By virtue of of relation (20), we obtain in an obvious way

$$X_c^{(i)}(l,T)=\sqrt{M_{c_0}/M_c}X_{c_0}^{(i)}(l,T'),\quad T'=T\sqrt{M_c/M_{c_0}}. \tag{24}$$

As a result, the change in band energy arising upon variation of the isotopic composition can be determined using the universal relation

$$\Delta E_{\mathbf{f},n}^{(c)}(T)=\sqrt{M_{c_0}/M_c}\Delta E_{\mathbf{f},n}^{(c_0)}(T'). \tag{25}$$

A relation analogous to (25) is also found for the factor $\Gamma_{\mathbf{f},n}$ that appears in Eq. (11) and which is inversely proportional to the electron lifetime.

Let us consider the case of the low-temperature limit, which is important from a practical standpoint. It follows from (22) and (23) that in this case the mass dependence of the energy and damping of an electron in state $\mathbf{f},n$ can be described by the formulas

$$E_{\mathbf{f},n}^{(c)}(T=0)=\varepsilon_n(\mathbf{f})+\frac{C_1}{\sqrt{M_c}},\quad \Gamma_{\mathbf{f},n}^{(c)}=\frac{C_2}{\sqrt{M_c}}. \tag{26}$$

We recall that $\varepsilon_n(\mathbf{f})$ is the energy of an electron in the ''frozen'' lattice. This energy and the parameters C_1 and C_2 are independent of the mass.

We note the following fact: it follows directly from relations (22)–(25) that in the classical temperature limit the structure of the electronic spectrum is independent of the isotopic composition.

Relations of a universal type are convenient to use in the analysis of experimental curves of the dependence of the parameters on the isotopic composition. If data are available for the natural composition $c_0=\mathrm{nat}$, then one can rather simply determine theoretically the values of the parameters for enriched compositions and compare the values obtained with the corresponding experimental results.

The universal relations obtained have an extremely simple structure. Their essence is that in monoatomic crystals, as we have said, the polarization vectors are independent of the mass, and the frequencies go as $\omega(l)\sim M^{-1/2}$. In the case of polyatomic crystals the situation is considerably more complicated, since the isotopic frequency shifts are proportional to the square of the corresponding moduli of the polarization vectors (see Appendix), and these vectors themselves also depend on the mass. The case of polyatomic structures requires special treatment.

For describing the temperature and mass dependences of the band energies E_i, a number of authors (see, e.g., Refs. 10, 21, and 22) have introduced an average phonon frequency θ_c and an average Bose–Einstein factor n_c, so that

$$E_i=E_i^0-B_i\left(\frac{M_{\mathrm{nat}}}{M_c}\right)^{1/2}(2n_c+1), \tag{27}$$

where $n_c=1/[\exp(\theta_c/T)-1]$, the E_i^0 are the values of the renormalized gap, and the B_i are parameters of some kind. By definition $\theta_c=\theta_{\mathrm{nat}}(M_{\mathrm{nat}}/M_c)^{1/2}$. (The damping of electrons due to the EPI is defined in an analogous way.) In the temperature region $T>T_D$ we have

$$E_i(T>T_D)=E_i^0-2B_i\frac{T}{T_D}, \tag{28}$$

where the E_i are independent of the mass, so that the parameters B_i can be determined from the dependence of E_i on T at high temperatures. (Relation (27) is an analog of Varshney's empirical formula.)

Let us comment on the results of Refs. 12 and 13 in connection with relation (27). In those papers the values of the band gap E_g of Ge were calculated as functions of the isotopic composition in the framework of the NLPP and LCAO methods. (The calculations done by the LCAO method[13] are apparently more precise. In particular, they describe to good accuracy the values of the factors $(\partial E_g/\partial T)_{\mathrm{tot}}$, which determine the temperature dependence of the gap.) The partial contributions to the isotope shift parameter of the gap due to the DW effect (the elastic channel) and to the effects of inelastic EPI processes were analyzed, and the role of the optical and acoustic phonon modes was examined. It was found that both elastic and inelastic EPI processes give contributions of the same order of magnitude to the isotope shifts. The influence of the acoustic and optical modes on the EPI turns out to be practically the same. The acoustic phonons influence the renormalization of the spectrum through the elastic scattering channel, the optical phonons through the inelastic channel. We call attention to the fact that, according to the results of Ref. 18, the value of the factor $(\partial\ln\Omega/\partial M_c^k)_P$ and, with it, the volume effect is largely determined by the contribution of the optical modes.

A comparison of the contributions of the volume and EPI effects to the values of the isotope shifts of the bands shows that they are of the same scale in the case of bands of the E_0 and E_g types, while in the case of critical points of the E_1 type the EPI mechanism is dominant.

In view of all we have said, it seems that the description of the isotopic and temperature dependences of the bands by relation (27) is rather crude and generally unreliable.

4. DISCUSSION OF THE RESULTS OF THE EXPERIMENTAL STUDIES

Precision measurements giving direct information about the energies of interband transitions and the critical points of the optical spectra in monoatomic semiconductors have now been made.

In Ref. 23 the influence of isotopic substitution of atoms on the optical properties of a germanium semiconductor was investigated for the first time. Only two sets of samples were studied: relatively highly enriched $^{75.7}$Ge crystals (with the isotopic composition 84% ^{76}Ge, 15% ^{74}Ge, remaining isotopes not more than 0.2% each) and a crystal with the natural isotopic composition. At $T=1.7$ K the photoluminescence spectra were measured in the short-wavelength part of the edge spectrum and the transmission spectra were measured in the region of direct excitonic transitions. The excitonic absorption spectra in the region of the edge of direct optical transitions was also determined. These experimental data were used to find the isotope shifts of the band gap ΔE_g at the Γ and L points of the Brillouin zone.

In Ref. 24 (see also Ref. 25) the luminescence spectra for diamond crystals were measured in the frequency region close to the energy of an indirect interband transition of the E_g type. At nitrogen temperatures only two groups of samples were studied: highly enriched ^{13}C, and the natural composition (98.9% ^{12}C and 1.1% ^{13}C). It was established how the spectral peaks corresponding specifically to free excitons are shifted for all three types of peaks (A, B, and C). The shift of the peaks for excitons localized around neutral boron impurities was also observed.

We note that the authors of Refs. 23 and 24 considered qualitatively the role of the volume effect and the EPI. According to their estimates the isotope shifts are due mainly to the EPI.

Further, in Ref. 14 the methods of modulation spectrometry were used to determine directly the values and isotope dependence of the energies of the direct transitions of the type $E_0(\Gamma_8^+-\Gamma_7^-)$ and of the indirect transitions $E_g(\Gamma_8^+-L_6^+)$ in Ge at helium temperatures. We note that the measurements were made on four highly enriched samples of germanium: ^{70}Ge, $^{72.9}$Ge, $^{73.9}$Ge, and $^{75.6}$Ge, and also a sample with the natural composition. Here the value of E_0 is determined from the photomodulated reflection coefficient. The energy of the indirect transitions E_g was found from the photoluminescence and electromodulated transmission spectra. According to the results obtained in Ref. 14, the isotope dependence of the parameters of the electronic spectrum at E_0 and E_g is well described by the relation $E=E_\infty+B/\sqrt{M}$ $(B<0)$.

Then in Ref. 26 the behavior of the critical points of the E_1 type was studied for samples of ^{70}Ge, $^{75.6}$Ge, and natural composition. The dielectric function ε_2 was determined by the method of ellipsometric spectroscopy. We note that in the case of germanium, according to the band calculations, the critical points E_1 (of the 2D-minimum and saddle-point type) on the graph of the imaginary part of the dielectric permittivity lie in the region 1.8–2.6 meV. The structure and value of ε_2 in this energy interval is almost entirely determined by the doublet transitions $\Lambda_3-\Lambda_1$. For the other transitions the energy intervals overlap one another, and their individual contributions cannot be seen.

It turned out that the change of E_1 upon variation of the isotopic composition, as in the previous case, is described by a formula of the form $E_1=E_\infty^1+B/\sqrt{M}$ $(B<0)$. A similar type of relation holds for the linewidths $\Gamma(M)$.

In Refs. 14 and 26 the contributions of the volume and EPI effects to the empirical parameter B were estimated. The volume contribution was estimated from the experimental data for $(1/V)(dV/dM)$ and the hydrostatic deformation potential V_g as $\Delta E\propto V_g(1/V)(\Delta V/\Delta M)$. The EPI contribution was determined as the difference between the experimental value of B and the volume contribution. It was found that in the case of optical transitions with energies E_0 and E_g the contributions to the isotope shifts from the volume and EPI effects are of the same order. At the same time, the isotope shifts for the critical points of the E_1 type are determined almost entirely by the EPI.

Let us summarize what we have said in this Section. The experimental results for diamond and germanium are in reasonable agreement with the theory. Thus a domain of applicability for the universal relations does indeed exist.

Questions of the spin–orbit interaction and the possible specific role of the d band, which remain outside the scope of this paper, are briefly discussed in the Conclusion.

5. CONCLUSION

We have investigated the influence of the isotopic composition of a compound on the structure of the energy bands $E_{\mathbf{f},n}$ in the virtual crystal approximation in the framework of a quasiharmonic approach. We have discussed the role of the changes in the volume of the unit cell of the crystal and the renormalization of the electron–phonon interaction (the elastic and inelastic channels) arising upon variation of the isotopic composition. For the case of monoatomic systems we have obtained a universal relation for the dependence of $E_{\mathbf{f},n}$ on the composition and temperature. We have made a comparison with the experimental data for the energies of interband transitions and the critical points for the optical spectra.

The electronic spectra actually depend in a substantial way on the spin–orbit interaction (this does not pertain to crystals containing atoms of light elements, such as diamond). The spin–orbit effects lead to doublet splitting of the p- and d-type bands at certain points of the Brillouin zone. Since the interaction of the spin and orbital moments occurs in the region of the atomic core, the parameters of the spin–orbit splitting Δ should in principle be determined by the core electronic levels, which are, generally speaking, weakly influenced by the crystalline potential. It is customarily assumed that the values of Δ for a free atom and an atom in a crystal differ by approximately 10%. Here it is known specifically that the parameter Δ in an atom is altered by the isotope shift of the levels.[27] However, according to the experimental data of Ref. 26, the isotope shifts of Δ in a crystal are significantly larger in magnitude that in the case of a free atom. In addition, a strong temperature dependence of the parameter Δ has also been observed in GaSb and α-Sn crystals (see the references cited in Ref. 26). Thus the question of the role of the spin–orbit interaction requires special handling.

We note that in monoatomic semiconductor crystals the structure and intensity of the densities of states of the upper valence bands and lower conduction bands are determined mainly by states of the s and p types, with a small admixture of d states (for germanium the typical energy differences between the valence p band and the d bands is around 20 eV), so that the role of the d orbitals in the optical transitions

is clearly weak. However, in a number of compounds, such as CuCl(Br) and CdS, the energy difference between the atomic p and d levels is of the order of 1 eV (see, e.g., Refs. 28 and 29). In that case the orbitals of the p and d types are mixed, and the hybridization effect is significant. For this reason the valence bands are substantially influenced by the d states. In such compounds upon isotopic substitution the situation is as follows:[28] in the matrix element V_{pd} responsible for the mixing of the levels of the p and d types the dominant role is played by the pseudopotential of the cation (copper), while the role of the pseudopotential of the anion is weak.[28] When the mass of the cation is increased, the DW factor $\exp(-W)$ changes. It decreases, since $\exp(-W)\propto 1-\frac{1}{2}\langle u^2\rangle G^2$. At the same time, the effective pseudopotential of the cation and the matrix element V_{pd} increase. Then the energy of the interband transition E_0 should decrease, i.e., $\partial E/\partial M_c<0$. As a result, a partial or even total compensation of the band renormalization effect due to the EPI can occur (the EPI leads to an effect of the opposite sign: $\partial E/\partial M_c>0$). At the same time, changing the mass of the anion has a weak effect on the matrix element V_{pd}, and the isotope shift as before is determined almost entirely by the EPI, and $\partial E/\partial M_a>0$. The role of the mixing of states of the p and d types also requires a detailed theoretical analysis.

The questions of the dependence of the structure of the electron spectrum on T and on the isotopic composition are of a general nature. Knowledge of the features of the behavior of the isotope shifts of the bands is extremely important, since it makes possible a more complete understanding of the nature of the electronic structure.

The author thanks L. A. Maksimov for interest in this study and helpful advice and Yu. M. Kagan for support. Assistance in this study from A. V. Inyushkin and D. A. Zhernov is gratefully acknowledged.

6. APPENDIX

Let us discuss the question of the isotope shift of the frequency of a vibrational mode in a crystal whose unit cell contains atoms of different elements. We use the average values of the atomic masses of the elements, the values of which vary, and we assume that the masses of the isotopes of a given element are close in value. We consider the effect linear in the mass difference of the isotopes. In this approximation the symmetry point group of the crystal lattice, generally speaking, remains unchanged, and, consequently, so does the vibrational spectrum, i.e., the degeneracy is not lifted. In reality, in a crystal lattice with isotopic disorder, because of the difference of the zero-point vibrations of the different isotopes, static displacement fields arise. In the presence of these fields the local symmetry is lowered. However, in standard crystals (as opposed to quantum crystals) these displacements are proportional to an additional small parameter $\langle u^2\rangle/a^2$ and their role can be neglected.

We consider a polyatomic crystal with isotopes of different kinds. We assume that the isotopic composition in respect to one of the elements, which occupies positions of type k_1, can vary.

Suppose that there exist two crystals, differing in the isotopic composition of the k_1 component of the compound. The quantities for the two crystals will be labeled with indices c and $c1$. The average atomic mass of the element k_1 is

$$M_c^{k_1}=\sum_i c_i^{k_1}M_i^{k_1} \tag{A1}$$

($c_i^{k_1}$ is the concentration of the ith isotope of the given element), and it is assumed that it differs little from the average mass for composition $c1$:

$$|M_c^{k_1}-M_{c1}^{k_1}|/M_c^{k_1}=|\Delta M^{k_1}|/M_c^{k_1}\ll 1. \tag{A2}$$

The dynamical matrix $\Phi_{\alpha\alpha}(kk'|\mathbf{q})$ of a polyatomic crystal is given by the relation

$$\Phi_{\alpha\alpha'}(kk'|\mathbf{q})=\frac{1}{N}\frac{1}{(M_c^kM_c^{k'})^{1/2}}\sum_{\mathbf{mm}'}\varphi_{\alpha\alpha'}(\mathbf{m}k,\mathbf{m}'k')\times\exp(i\mathbf{q}(\mathbf{R}_{\mathbf{m}}^{(0)}-\mathbf{R}_{\mathbf{m}'}^{(0)})), \tag{A3}$$

where $\varphi_{\alpha\alpha'}(\mathbf{m}k,\mathbf{m}'k')$ is the matrix of second-order force parameters. The dynamical matrix is a Hermitian matrix of dimension $3s\times 3s$ (s is the number of atoms in the unit cell), i.e.,

$$\Phi_{\alpha\alpha'}(kk'|\mathbf{q})=\Phi^*_{\alpha'\alpha}(k'k|\mathbf{q}). \tag{A4}$$

We shall assume that the eigenfrequencies $\omega_c(l)$ and the orthonormalized polarization vectors $\mathbf{e}^c(k|l)$ for the virtual crystal with the dynamical matrix Φ (A3) are known. Let us determine the isotope shift of the frequencies upon going to composition $c1$.

It is known that the calculation of the eigenvalues accurate to a certain order of smallness with respect to a perturbation requires knowledge of the eigenfunctions with an accuracy to the next lower order. Upon variation of the isotopic composition the change of the eigenvalues (square of the frequency) in the first approximation is equal to the sum of the corresponding diagonal elements of the energy of the perturbation over the unperturbed states:

$$\left(\frac{\Delta\omega^2(l)}{\Delta M^{k_1}}\right)_c=\sum_{k,\alpha}\sum_{k',\alpha'}e_\alpha^{c*}(k|l)\times\left(\frac{\Delta\Phi_{\alpha\alpha'}(kk'|q)}{\Delta M^{k_1}}\right)_c e_{\alpha'}^c(k'|l). \tag{A5}$$

Here, according to the definition of the dynamical matrix (A3), we have

$$\left(\frac{\Delta\Phi_{\alpha\alpha'}(kk'|\mathbf{q})}{\Delta M^{k_1}}\right)_c=-\frac{1}{2}\Phi^c_{\alpha\alpha'}(kk'|\mathbf{q})\left[\frac{\delta_{kk_1}}{M_c^k}+\frac{\delta_{k_1k'}}{M_c^{k'}}\right]. \tag{A6}$$

We substitute (A6) into (A5), taking into consideration that

$$\omega_c^2(l)e_\alpha^c(k|l)=\sum_{k',\alpha'}\Phi^c_{\alpha\alpha'}(kk'|\mathbf{q})e^c_{\alpha'}(k'|l). \tag{A7}$$

In addition, we take into account that, as a consequence of the Hermitianity of $\Phi(\mathbf{q})$ the polarization vectors satisfy orthonormality and completeness conditions of the form

$$\sum_{k,\alpha} e_\alpha^{c*}(k|\mathbf{q}j)e_\alpha^c(k|\mathbf{q}j') = \delta_{jj'},$$
$$\sum_{j} e_\alpha^{c*}(k|\mathbf{q}j)e_{\alpha'}^c(k'|\mathbf{q}j) = \delta_{kk'}\delta_{\alpha\alpha'}. \quad \text{(A8)}$$

We note that in principle the value of the average mass varies in a continuous manner, so that the symbol Δ can be changed to a differentiation sign. As a result, we obtain

$$\frac{d\ln\omega_c^2(l)}{d\ln M_c^k} = -\sum_\alpha |e_\alpha^c(k|l)|^2. \quad \text{(A9)}$$

We see from (A9) that in a polyatomic crystal the shift of the frequency of a vibrational mode due to a change of the average mass of one of the elements of the compound is proportional to the square modulus of the corresponding polarization vector.

Relations of this type were first obtained in Ref. 30, in an analysis of the influence of the isotopic composition on the properties of fullerenes.

In the case of a monoatomic crystal, when atoms of only one element are present in the unit cell of the crystal, we have instead of (A9)

$$\frac{d\ln\omega_c^2(l)}{d\ln M_c} = -1 + O\left[\left(\frac{|\Delta M|}{M_c}\right)^2, \frac{\Delta M}{M_c}\frac{\langle u^2\rangle}{a^2}\right]. \quad \text{(A10)}$$

[†]Deceased

[1] H. Holloway, K. C. Hass, M. A. Tamor, T. R. Anthony, and W. F. Banholzer, Phys. Rev. B **44**, 7123 (1991).
[2] W. S. Carpinski, H. J. Maris, E. Bauser, I. Siller, T. Ruf, M. A. Asen-Palmer, M. Cardona, and E. Gmelin, Appl. Phys. Lett. **71**, 2109 (1997).
[3] T. Ruf, R. W. Henn, M. A. Asen-Palmer, E. Gmelin, M. Cardona, H. J. Pohl, G. G. Devyatych, and P. G. Sennikov, Solid State Commun. **115**, 243 (2000).
[4] H. D. Fushs, C. Crein, R. I. Devien, J. Kuhl, and M. Cardona, Phys. Rev. B **44**, 8633 (1991).
[5] V. I. Ozhogin, A. V. Inyushkin, A. N. Taldenkov, G. É. Popov, E. Haller, and K. Itoh, JETP Lett. **63**, 490 (1996).
[6] H. Bettger, *Principles of the Theory of Lattice Dynamics*, Akademie-Verlag, Berlin (1983).
[7] G. Leibfried, in *Handbuch der Physik*, Vol. 7, Part 1, edited by S. Flügge, Springer-Verlag, Berlin (1955), p. 104; *Microscopic Theory of the Mechanical and Thermal Properties of Crystals* [Russian translation], GIL, Moscow (1963).
[8] M. Cardona, Physica B **263**, 376 (1999).
[9] P. B. Allen and V. Heine, J. Phys. C **9**, 2305 (1976).
[10] V. V. Sobolev and V. V. Nemoshkalenko, *Methods of Computational Physics in Solid State Theory. The Electronic Structure of Semiconductors* [in Russian], Naukova Dumka, Kiev (1988).
[11] S. Zollner, M. Cardona, and S. Gopalan, Phys. Rev. B **45**, 3376 (1992).
[12] N. Garro, A. Cantarero, M. Cardona, A. Göbel, T. Ruf, and K. Eberl, Phys. Rev. B **54**, 4732 (1996).
[13] D. Olguin, A. Cantarero, and M. Cardona, Phys. Status Solidi B **220**, 33 (2000).
[14] C. Parks, A. K. Ramdas, S. Rodríguez, K. M. Itoh, and E. E. Haller, Phys. Rev. B **49**, 14245 (1994).
[15] P. Pavone and S. Baroni, Solid State Commun. **90**, 295 (1994).
[16] G. M. Rignanese, J. P. Michenaud, and X. Gonze, Phys. Rev. B **53**, 4488 (1996).
[17] A. P. Zhernov, Zh. Éksp. Teor. Fiz., **114**, 6548 (1998) [JETP **87**, 1172 (1998)].
[18] A. P. Zhernov, Fiz. Nizk. Temp., **26**, 1226 (2000) [Low Temp. Phys. **26**, 908 (2000)].
[19] R. M. Pick, M. H. Cohen, and R. M. Martin, Phys. Rev. B **1**, 910 (1970).
[20] P. Lautenschlager, P. B. Allen, and M. Cardona, Phys. Rev. B **31**, 2163 (1985).
[21] L. F. Lastras-Martínez, T. Ruf, M. Konuma, M. Cardona, and D. E. Aspnes, Phys. Rev. B **61**, 12946 (1999).
[22] S. D. Yoo, D. E. Asphes, L. F. Lastras-Martínez, T. Ruf, M. Konuma, and M. Cardona, Phys. Status Solidi B **220**, 117 (2000).
[23] V. F. Agekyan, V. M. Asnin, A. M. Kryukov, I. I. Markov, N. A. Rud', V. I. Stepanov, and A. B. Churilov, Fiz. Tverd. Tela (Leningrad), **31**, 101 (1989) [Sov. Phys. Solid State **31**, 2082 (1989)].
[24] A. T. Collins, S. C. Lawson, D. Gordon, and H. Kanda, Phys. Rev. Lett. **65**, 891 (1990).
[25] T. Ruf, M. Cardona, H. Sternschulte, S. Wahl, K. Thonke, R. Sauer, P. Pavone, and T. R. Anthony, Solid State Commun. **105**, 311 (1998).
[26] D. Ronnow, L. F. Lastras-Martínez, and M. Cardona, Eur. Phys. J. B **5**, 29 (1998).
[27] I. I. Sobel'man, *Introduction to the Theory of Atomic Spectra* [in Russian], GIFML (1963).
[28] A. Gobel, T. Ruf, M. Cardona, C. T. Lin, J. Wrzesinski, M. Steube, K. Reimann, J.-C. Merle, and M. Joucla, Phys. Rev. B **57**, 15183 (1998).
[29] J. M. Zhang, T. Ruf, R. Lauck, and M. Cardona, Phys. Rev. B **57**, 9716 (1998).
[30] J. Menendez, J. B. Page, and S. Guha, Philos. Mag. B **70**, 651 (1994).

Translated by Steve Torstveit

PHYSICAL PROPERTIES OF CRYOCRYSTALS

Molar volume dependence of the thermal conductivity in mixed cryocrystals

V. A. Konstantinov,* E. S. Orel, and V. P. Revyakin

B. Verkin Institute for Low Temperature Physics and Engineering, National Academy of Sciences of Ukraine, pr. Lenina 47, 61103 Kharkov, Ukraine

(Submitted October 3, 2001)
Fiz. Nizk. Temp. **28**, 194–198 (February 2002)

The dependence of the thermal conductivity Λ of solid solutions of cryocrystals on the molar volume is investigated theoretically in the Callaway approach under the assumption that the heat is transferred by mobile low-frequency phonons and, above the phonon mobility edge, by ''localized'' modes which migrate randomly from site to site. The phonon mobility edge ω_0 is found from the condition that the phonon mean free path, which is governed by umklapp processes and scattering on point defects, cannot become smaller than one-half the phonon wavelength. The Bridgman coefficient $g=-(\partial \ln \Lambda/\partial \ln V)_T$ is the weighted mean over these modes, which have strongly different volume dependences. For the example of the solid solution $Kr_{1-c}(CH_4)_c$, where c is the mole fraction of the components, it is shown that with increasing methane concentration in krypton the Bridgman coefficient decreases, in good agreement with experiment, from $g\approx 9$, characteristic for the pure crystals, to $g\approx 4$. © *2002 American Institute of Physics.* [DOI: 10.1063/1.1461926]

INTRODUCTION

If a crystal is subjected to hydrostatic compression, the volume of the crystal decreases and the Debye temperature $\Theta_D=\hbar\omega_D$ (ω_D is the Debye frequency) increases. Therefore, the thermal conductivity Λ should increase with increasing pressure, as was first observed by Bridgman.[1] The volume dependence of the thermal conductivity can be described with the aid of the Bridgman coefficient

$$g=-(\partial \ln \Lambda/\partial \ln V)_T. \tag{1}$$

Subsequent studies of the thermal conductivity as a function of pressure for a wide range of substances[2–4] have shown that the values of the Bridgman coefficient vary, as a rule, in a range from 3–4 to 10–15. The general tendency is for g to decrease with increasing structural disorder; the weakest volume dependence of the thermal conductivity is found in glasses and polymers.[2] In three cases—the *Ih* phase of ice, the phase NH_4F(I), and CuCl—the Bridgman coefficient is negative.[2] This is explained by anomalous behavior of the transverse modes, the velocity of which decreases with increasing pressure.

Most often the high-temperature ($T\geqslant\Theta_D$) thermal conductivity of insulators is described with the use of the Leibfried–Schlömann (LS) formula and the Callaway integral,[5] which are also used for calculating the Bridgman coefficient.[4,6–11] According to the LS formula, the thermal conductivity of a crystal can be written as

$$\Lambda=\frac{K\bar{M}a\Theta_D^3}{\gamma^2 T}, \tag{2}$$

where $\bar{M}$ is the mean atomic (molecular) mass, a^3 is the volume per atom (molecule), $\gamma=-(\partial \ln \Theta_D/\partial \ln V)_T$ is the Grüneisen parameter, and K is a constant factor. Differentiating (2) with respect to volume and introducing the parameter $q=(\partial \ln \Gamma/\partial \ln V)_T$, we obtain

$$g=3\gamma+2q-1/3. \tag{3}$$

Usually at temperatures of the order of the Debye temperature and higher it is assumed that $\gamma\propto V$, and the second Grüneisen coefficient $q\approx 1$.[6,11]

Expressions (2) and (3) are valid for perfect insulators in the presence of only U-processes. They are not applicable to strongly disordered crystals and amorphous solids. Gerlich[10] used the Callaway integral to study the influence of point defects on the volume dependence of the thermal conductivity. He was able to describe qualitatively the slight decrease in g observed in the solid solution AgCl–AgBr.[2] In pure AgBr and AgCl the Bridgman coefficient is equal to 9.8 and 9.5, respectively, while in a solid 50% solution $g=8.1$. The theory of Ref. 10 predicted a decrease of g to 8.4.

In recent studies[12] of the isochoric thermal conductivity of the solid solution $Kr_{1-c}(CH_4)_c$ a strong decrease of the Bridgman coefficient was observed, from a value $g\approx 9$ characteristic for pure Kr and CH_4 to $g\approx 4$ at only a tiny impurity concentration (see Fig. 1). These experimental data cannot be adequately described by the approach used by Gerlich.[10] It was shown that as the molar volume of the components in the solid solution $Kr_{1-c}(CH_4)_c$ is changed, one observes a gradual transition from the thermal conductivity of a perfect crystal (the pure components) to the lower limit to the thermal conductivity $\Lambda_{\min}$ at $0.2<c<0.8$. The concept of a lower limit to the thermal conductivity[13] emerges from the assumption that in the case of strong scattering the phonons are weakly localized in regions of the order of $\lambda/2$, where λ is the phonon wavelength, and can

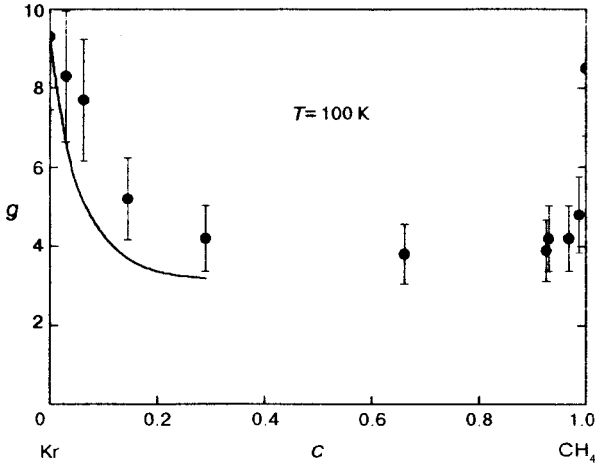

FIG. 1. Dependence of the Bridgman coefficient $g=-(\partial \ln \Lambda/\partial \ln V)_T$ on the concentration of the components in the solid solution $Kr_{1-c}(CH_4)_c$. The points are experimental, the solid curve theoretical.

migrate via neighboring sites in a random manner. To describe the temperature dependence of the isochoric thermal conductivity of the solid solution $Kr_{1-c}(CH_4)_c$, in Ref. 12 a combined model was proposed in which part of the heat is transferred by mobile low-frequency (acoustic) phonons and, above the mobility edge, by ''localized'' modes. In the present paper this model is used to describe the molar volume dependence of the thermal conductivity.

MODEL

We calculate thermal conductivity of the solid solution $Kr_{1-c}(CH_4)_c$ in the framework of the Callaway approach. Here we make the following assumptions: normal processes can be neglected; the temperature is assumed to be of the order of the Debye temperature or higher; heat is transferred only by phonons (acoustic and ''localized''); all phonons are described by the Debye model; all the modes have the same Grüneisen parameter γ; the medium is isotropic.

In the Callaway model the thermal conductivity Λ can be written as

$$\Lambda=\frac{k_B}{2\pi^2 v^2}\int_0^{\omega_D} l(\omega)\omega^2 d\omega, \tag{4}$$

where v is the averaged sound velocity, ω_D is the Debye frequency [$\omega_D=(6\pi^2)^{1/3}v/a$], $l(\omega)$ is the phonon mean free path, which is governed by U-processes and scattering on point defects:

$$l(\omega)=[l_u^{-1}(\omega)+l_i^{-1}(\omega)]^{-1}. \tag{5}$$

The phonon mean free paths corresponding to each scattering mechanism are expressed as[5]

$$l_u(\omega)=v/A\omega^2 T, \tag{6}$$

$$A=\frac{18\pi^3}{\sqrt{2}}\frac{k_B\gamma^2}{ma^2\omega_D^3}; \tag{7}$$

$$l_i(\omega)=v/B\omega^4, \tag{8}$$

$$B=\frac{3\pi\Gamma}{2\omega_D^3}. \tag{9}$$

When the mass difference ΔM of the atoms (molecules) of the impurity and host and the dilatation of the lattice are taken into account, the coefficient Γ can be written as

$$\Gamma=c(1-c)\left(\frac{\Delta M}{\overline{M}}+6\gamma\frac{\Delta a}{\overline{a}}\right)^2, \tag{10}$$

where Δa is the change of the lattice parameter upon introduction of the impurity.

Expression (5) does not apply if $l(\omega)$ becomes of the order of one-half the phonon wavelength ($\lambda/2=\pi v/\omega$) or smaller. A similar situation was discussed previously for the case of U-processes alone.[14] We assume that in the general case

$$l(\omega)=\begin{cases} v/(A\omega^2 T+B\omega^4), & 0\leqslant\omega\leqslant\omega_0, \\ \alpha\pi v/\omega=\alpha\lambda/2, & \omega_0<\omega\leqslant\omega_D, \end{cases} \tag{11}$$

where α is a numerical coefficient of the order of unity. Excitations whose frequencies lie above the phonon mobility edge ω_0 will be assumed ''localized.'' The frequency ω_0 can be found from the condition

$$v/(A\omega_0^2 T+B\omega_0^4)=\alpha\pi v/\omega_0. \tag{12}$$

It is determined by the expression

$$\omega_0=\frac{1}{(2\alpha\pi B)^{1/3}}\left(\sqrt[3]{1+\sqrt{1+u}}+\sqrt[3]{1-\sqrt{1+u}}\right), \tag{13}$$

where the dimensionless parameter u is given by

$$u=\frac{4\alpha^2\pi^2 A^3 T^3}{27B}. \tag{14}$$

The thermal conductivity integral (4) separates into two parts, describing the contribution to the heat transfer from acoustic and ''localized'' phonons:

$$\Lambda=\Lambda_{ph}+\Lambda_{loc}. \tag{15}$$

In the high-temperature ($T\geqslant\Theta_D$) limit these contributions are

$$\Lambda_{ph}=\frac{k_B}{2\pi^2 v}\frac{1}{\sqrt{ATB}}\arctan(\omega_0\sqrt{B/AT}) \tag{16}$$

and

$$\Lambda_{loc}=\frac{\alpha\kappa_B}{4\pi v}(\omega_D^2-\omega_0^2). \tag{17}$$

The problem of determining the thermal conductivity of a solid solution reduces to that of finding the volume derivative of expression (15). Taking into account that $(\partial \ln A/\partial \ln V)_T=3\gamma+2q-2/3$ and $(\partial \ln B/\partial \ln V)_T=3\gamma$ [this follows from Eqs. (7) and (9)] and also that $(\partial \ln\Gamma/\partial \ln V)_T\approx 0$, we have:

$$g=\frac{\Lambda_{ph}}{\Lambda}g_{ph}+\frac{\Lambda_{loc}}{\Lambda}g_{loc}, \tag{18}$$

where

$$g_{\rm ph}=-\left(\frac{\partial \ln \Lambda_{\rm ph}}{\partial \ln V}\right)_T=2\gamma+q+\frac{\omega_0\sqrt{B/AT}}{(1+\omega_0^2 B/AT)\arctan(\omega_0\sqrt{B/AT})}(\gamma_0+q-1/3), \tag{19}$$

$$g_{\rm loc}=-\left(\frac{\partial \ln \Lambda_{\rm loc}}{\partial \ln V}\right)_T=-\gamma+\frac{1}{3}\frac{2}{\omega_D^2-\omega_0^2}(\omega_D^2\gamma-\omega_0^2\gamma_0), \tag{20}$$

$$\gamma_0=-\left(\frac{\partial \ln \omega_0}{\partial \ln V}\right)_T=\gamma+\frac{u^{1/3}}{6\sqrt{1+u}}\times(\sqrt[3]{1+\sqrt{1+u}}-\sqrt[3]{1-\sqrt{1+u}})(6\gamma+6q-2). \tag{21}$$

RESULTS AND DISCUSSION

The isochoric thermal conductivity of the solid solution $Kr_{1-c}(CH_4)_c$ was recently investigated in the temperature interval from 40 K to temperatures ~150 K over a wide concentration interval for samples of different density.[12] In the concentration interval $0.2<c<0.8$ the thermal conductivity of the solid solution was practically equal to the lower limit to the thermal conductivity of the lattice $\Lambda_{\rm min}$ calculated according to Ref. 13. In pure methane and in methane containing a small amount of krypton there is an additional phonon scattering mechanism: scattering on fluctuations of the short-range orientational order, the efficiency of which is maximum immediately after the $\alpha\rightarrow\beta$ transition and decreases with increasing temperature.[15] The thermal conductivity of such a solution cannot be described adequately in the framework of the simple model discussed above. A CH_4 impurity in Kr can be treated as a point defect, since collective rotational excitations are absent in this case. Using the integral form of the model described above (without the simplifying assumption $T\geqslant\Theta_D$), the authors in Ref. 12 were able to describe adequately the temperature dependence of the thermal conductivity of the solid solution $Kr_{1-c}(CH_4)_c$ in the concentration interval $0<c<0.3$. The initial parameters for the fit were a, v, and the coefficient Γ calculated according to (10). The values of A and α were varied. This same scheme was also used in the present study. Initially the thermal conductivity determined by expressions (15)–(17) was fit by the least-squares method to the experimentally measured temperature dependence of the thermal conductivity[12] for the isochore with $T_0=75$ K (T_0 is the temperature at which the condition of isochoricity begins to hold) and different concentrations of the methane impurity. Then the Bridgman coefficient was calculated according to (18)–(21) under the assumption that $q=1$ and $\gamma=2.5$.[12] The parameters of the Debye model of the thermal conductivity which were used in the fitting (a, v, and Γ) and the values of A and α obtained as a result of the fitting are presented in Table I along with the calculated values of the Bridgman coefficient. A feature specific to isochoric studies of the thermal conductivity is that the coefficient g is determined most accurately near the triple points, where the change in volume is maximal. The values given for g correspond to a temperature of 100 K.

TABLE I. Parameters of the Debye model of the thermal conductivity used in the fitting: a, v, and Γ; the values of A and α obtained in the fitting, and the Bridgman coefficients calculated according to Eqs. (18)–(21).

				Adjustable parameters		
c	$a\cdot10^{-8}$ cm	v, km/s	Γ	$A\cdot10^{-15}$ s/deg	α	g
0.03	3.625	0.88	0.055	0.342	1.201	6.4
0.063	3.63	0.92	0.12	0.496	1.213	4.9
0.145	3.648	0.97	0.26	1.175	1.163	3.4
0.29	3.66	1.07	0.54	6.35	1	3.2

Figure 1 shows the smoothed values of the Bridgman coefficient calculated according to the procedure described above (solid curve) in comparison with the experimental values.[12] It is seen that the agreement is completely satisfactory for such a simple model, which does not include phonon dispersion and the real density of states. Figure 2 shows the temperature dependence of g calculated according to Eqs. (18)–(21). We see that the Bridgman coefficient should decrease with increasing temperature. Unfortunately, as we have already mentioned, the error in the determination of g in isochoric studies increases as the temperature moves away from the triple point, and the accuracy is too low to permit a comparison with the theory.

In our opinion, expression (18) is not only applicable to solid solutions but has a general character. The main idea pursued in this paper is that the contributions to the molar volume dependence of the thermal conductivity from mobile acoustic phonons and ''localized'' modes are sharply different. If the heat is transferred mainly by acoustic phonons (perfect crystals), then the Bridgman coefficient is described by expression (3). In the opposite case, when the thermal conductivity has reached its lower limit $\Lambda_{\rm min}$ and all the heat is transferred by ''localized'' modes (amorphous solids and

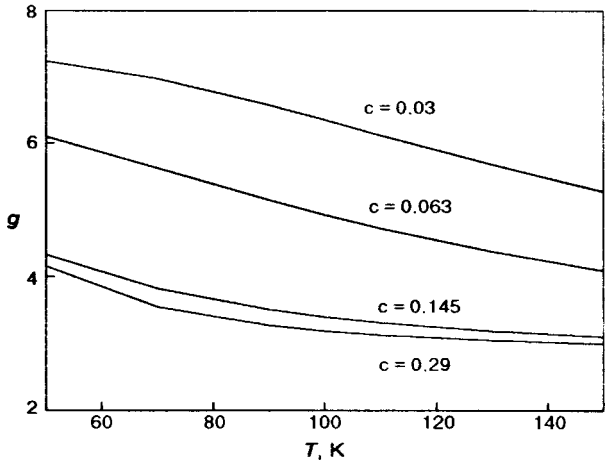

FIG. 2. Temperature dependence of the Bridgman coefficient of the solid solution $Kr_{1-c}(CH_4)_c$ for different concentrations of the components.

strongly disordered crystals), then for $T \geqslant \Theta_D$ the lower limit to the thermal conductivity is described by $\Lambda_{\min} \propto v/a^{2/3}$ (Ref. 13), and

$$g = \gamma + 1/3. \tag{22}$$

This also follows from Eq. (20) in the limit $\omega_0 \to 0$. In the general case the Bridgman coefficient g is a weighted average over the acoustic and ''localized'' modes.

CONCLUSION

We have proposed a simple model in which the Bridgman coefficient containing the molar volume dependence of the thermal conductivity is determined by a competition between heat transfer by mobile low-frequency phonons and by ''localized'' modes existing in regions of the order of $\lambda/2$. In the case of solid solutions of cryocrystals the phonon mobility edge ω_0 is found from the condition that the phonon mean free path, which is governed by umklapp processes and scattering on point defects, cannot be smaller than one-half the wavelength of the phonon. The Bridgman coefficient is a weighted average over these modes, which have very different volume dependences. For the example of the solid solution $Kr_{1-c}(CH_4)_c$ we have shown that as the fraction of heat transferred by ''localized'' modes increases, the Bridgman coefficient decreases from a value $g \approx 9$, characteristic for the pure crystals, to $g \approx 4$.

The authors thank Acad. V. G. Manzhelii and Prof. R. O. Pohl for their steady interest in this study and for a fruitful discussion. This study was supported by the Ukrainian Ministry of Education and Science, Project F7/286-2001.

*E-mail: konstantinov@ilt.kharkov.ua

[1] P. W. Bridgman, *The Physics of High Pressure*, McMillan, New York (1931), Ch. 11.
[2] R. G. Ross, P. A. Andersson, B. Sundqvist, and G. Backstrom, Rep. Prog. Phys. **47**, 1347 (1984).
[3] L. N. Dzhavadov and Yu. I. Krotov, Fiz. Tverd. Tela (Leningrad) **20**, 654 (1978) [Sov. Phys. Solid State **20**, 379 (1978)].
[4] A. A. Averkin, Yu. A. Logachev, A. V. Petrov, and N. S. Tsypkina, Fiz. Tverd. Tela (Leningrad) **19**, 1692 (1977) [Sov. Phys. Solid State **19**, 988 (1977)].
[5] R. Berman, *Thermal Conduction in Solids*, Oxford, Clarendon Press (1976).
[6] G. A. Slack, in *Solid State Physics*, Vol. 34, edited by H. Ehrenreich, F. Seitz, and D. Turnbull (Academic Press, New York, London (1979), p. 1).
[7] D. L. Money and R. G. Steg, High Temp.-High Press. **1**, 237 (1969).
[8] K. P. Roy, P. Mochazzabi, and P. C. Sharma, Can. J. Phys. **62**, 89 (1984).
[9] D. Gerlich, J. Phys. C **19**, 2877 (1986).
[10] D. Gerlich, J. Phys. C **20**, 5479 (1987).
[11] G. K. White, High Temp.-High Press. **21**, 233 (1989).
[12] V. A. Konstantinov, V. G. Manzhelii, V. P. Revyakin, and R. O. Pohl, Fiz. Nizk. Temp. **27**, 1159 (2001) [Low Temp. Phys. **27**, 858 (2001)].
[13] D. G. Cahill, S. K. Watson, and R. O. Pohl, Phys. Rev. B **46**, 6131 (1992).
[14] M. C. Roufosse and P. G. Klemens, J. Geophys. Res. **79**, 703 (1974).
[15] V. A. Konstantinov, V. G. Manzhelii, V. P. Reviakin, and S. A. Smirnov, Physica B **262**, 421 (1999)

Translated by Steve Torstveit

SHORT NOTES

Effect of impurity oxygen on the low-temperature plasticity of solid normal hydrogen

L. A. Alekseeva* and Yu. V. Butenko

B. Verkin Institute for Low Temperature Physics and Engineering, National Academy of Sciences of Ukraine, pr. Lenina 47, 61103 Kharkov, Ukraine

(Submitted October 4, 2001; revised October 15, 2001)
Fiz. Nizk. Temp. **28**, 199–202 (February 2002)

The features of the low-temperature plastic deformation of solid normal hydrogen (n-H_2) of 99.99% purity (the main impurity is oxygen) are investigated at liquid-helium temperature by the method of stepwise uniaxial loading under conditions of creep. It is shown that molecular oxygen has a significant influence on the parameters of the strain curves of n-H_2. A softening of the crystal lattice of solid n-H_2 is observed, which may be due to acceleration of the ortho–para conversion in the hydrogen samples as a result of the presence of impurity O_2 molecules. © *2002 American Institute of Physics.* [DOI: 10.1063/1.1461927]

The plasticity and strength of molecular hydrogen crystals are extremely sensitive to the orthohydrogen content in the samples[1,2] and also the concentration of isotopic and foreign impurities.[2] It is expected that doping of hydrogen with an oxygen impurity will lead to a substantial change in its resistance to plastic deformation, since the heavy molecules of impurity oxygen are can modify the dynamics of the lattice vibrations of H_2 significantly. In addition, oxygen is characterized by considerably higher shear stresses,[3] and therefore the presence of O_2 in H_2 should lead to hardening of the comparatively soft hydrogen matrix.

To study the character of the influence of oxygen impurities on the plasticity of n-H_2, in the present study we have measured its deformation parameters under uniaxial tensile loading for samples of 99.99% purity. The main impurity was oxygen. It was found that this impurity has a significant effect on the deformation parameters of n-H_2, which can be interpreted[4] as resulting from an appreciable acceleration of the spontaneous ortho–para transition in hydrogen in the presence of molecular O_2.

Samples with a diameter of 6 mm were grown from liquid n-H_2 (75% ortho modification), which was condensed beforehand in a liquid-helium cooled glass ampoule of the cryostat[5] from an external cylinder. We used a standard configuration of the samples for tensile testing—the ratio of the length of the working part to the diameter was equal to 5. The samples were polycrystalline, having grains with linear dimensions of up to 2 mm.

The samples were loosened from the walls of the ampoule by briefly pumping on the vapor over them (see Ref. 5 for details), annealed at a temperature of ~ 11 K, and slowly cooled to the testing temperature of 4.2 K. The n-H_2 crystals were held at this temperature for 15–20 min. The total time of the annealing and isothermal hold of the samples at $T = \text{const}$ reached 50 min.

The samples were tested under conditions of uniaxial stepwise tensile loading[6] with small load increments $\Delta\sigma$ ($0.2-0.6$ gf/mm^2) applied at equal time intervals $\Delta t = 2$ min. The load σ was applied by means of a quartz rod connected to a precision balance arm (sensitivity ± 200 mg) placed in the vacuum part of the cryostat. After each loading the samples were found in a transient creep regime under the influence of the gradually applied load. The increment in the length of the crystals achieved at the end of each time interval Δt was summed with the previous values and taken as the resultant value corresponding to the given total load. The length increments were measured by an inductive displacement sensor[7] to an accuracy of $\pm 10^{-4}$ cm and was recorded continuously by a KSP-4 electronic potentiometer.

The temperature of the lower and upper parts of the samples were measured by two semiconductor resistance thermometers to an accuracy of $\pm 2\times 10^{-2}$ K. The temperature was stabilized to within 0.1 K and its distribution along the sample was uniform to within the same accuracy. This level of stabilization was achieved by admitting gaseous ^{4}He into the ampoule containing the sample at a pressure of up to 10^{-1} torr.

Figure 1 shows the typical tensile stress–strain curves $\sigma(\varepsilon)$ for crystals of normal hydrogen with an oxygen impurity at a temperature of 4.2 K. For better comparison of the measured curves with the typical hardening curves traditionally obtained on testing machines under conditions of active tensile straining of the samples at a specified rate, the values of the stress σ are plotted along the vertical axis. The curves presented in Fig. 1 correspond to the limiting cases of the degree of dispersity of the O_2–n-H_2 samples. Also shown for comparison are the stress–strain curves of 99.999% pure n-H_2 and of p-H_2 with the orthohydrogen content reduced to $\simeq 0.2\%$, obtained under analogous loading conditions (see Refs. 8 and 9).

It is seen from Fig. 1 that the stress–strain curves for the O_2–n-H_2 samples lie between the $\sigma(\varepsilon)$ curves obtained for pure n-H_2 and p-H_2 and are clearly closer to the strain curve typical for p-H_2. Thus at $T = 4.2$ K, to obtain the same level

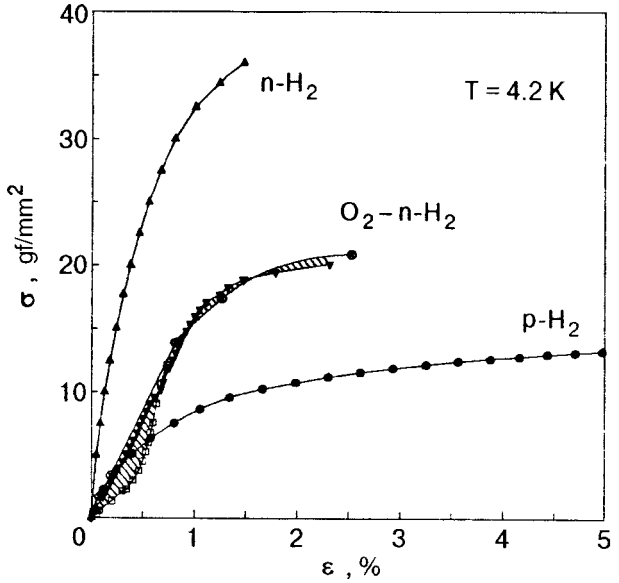

FIG. 1. Typical tensile stress–strain curves $\sigma(\varepsilon)$ of polycrystals of pure n-H_2 (Ref. 8) and p-H_2 (Ref. 9) ($\simeq 0.2\%$ o-H_2) and for polycrystalline samples of O_2–n-H_2.

of strain ε for samples of n-H_2 containing an oxygen impurity requires considerably lower values of the applied stress than for pure n-H_2. On the other hand, for a specified level of stress σ on the O_2–n-H_2 samples a considerably smaller value of the relative elongation is obtained than for a sample of pure p-H_2. The observed difference in the behavior of the stress–strain curves for O_2–n-H_2 and p-H_2 are due to the role of the oxygen impurity molecules in the processes governing the development of plastic deformation of these crystals.

To ascertain the analytical form of the relation between the deforming stress σ and the strain ε for the O_2–n-H_2 samples, we replotted the experimental $\sigma(\varepsilon)$ curves in logarithmic coordinates. Figure 2 shows the characteristic

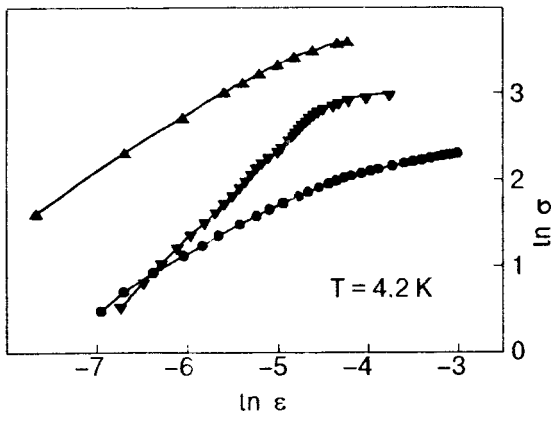

FIG. 2. Appearance of the $\sigma(\varepsilon)$ curves obtained for polycrystals of n-H_2 containing an O_2 impurity (▼) and also for polycrystalline samples of pure n-H_2 (Ref. 8) (▲) and p-H_2 (Ref. 9) (●) replotted on a logarithmic scale.

$\ln\sigma$–$\ln\varepsilon$ plot for the O_2–n-H_2 samples. Analysis showed that the tensile stress–strain curves $\sigma(\varepsilon)$ of our n-H_2 samples containing impurity oxygen are characterized by the presence of the two stages of deformation typical for polycrystalline hydrogen,[8,9] with different laws of variation of $\sigma(\varepsilon)$. The first stage is observed either immediately, or after a short delay in the case of an s-shaped trend of the $\sigma(\varepsilon)$ curves (see Fig. 1), and is characterized by a linear dependence of $\sigma(\varepsilon)$ with rather strong hardening of the crystals. The hardening coefficient $d\sigma/d\varepsilon$ is equal to 1.6×10^8 dynes/cm^2, which is practically an order of magnitude lower than the elastic modulus of n-H_2 at this temperature.[10]

Upon reaching a certain critical stress (17.7 gf/mm^2) a transition occurs in the deformed O_2–n-H_2 samples to a different stress–strain law. The deformation of the O_2–n-H_2 samples is characterized by a power law $\sigma \approx \varepsilon^n$ with a small exponent $n \approx 0.2$ all the way to failure, which occurs at considerably lower stresses than in the case of pure n-H_2 (Refs. 1 and 8). At a temperature of 4.2 K such a low value of n is more typical for p-H_2 polycrystals[9] and Ne–n-H_2 solid solutions[11] than for solid normal hydrogen ($n \simeq 0.4$).[8]

Thus, judging from the fact that the value of σ required to achieve a specified level of deformation for the O_2–n-H_2 samples studied here is lower than is typical for pure n-H_2, it can be concluded from these experiments that hardening of n-H_2 by molecular oxygen does not occur at liquid-helium temperature. Consequently, the motion of dislocations in these samples is facilitated to a significant degree in spite of the presence of the heavy impurity molecules of O_2 in the n-H_2. By analogy with the hydrogen crystals containing neon,[11] the observed softening of the hydrogen samples containing oxygen may be due to the formation of van der Waals complexes in these samples.[12,13] Another (in this case more likely) explanation for the observed softening is the presence of ortho–para conversion processes in the n-H_2. The fact that the O_2 molecules have a magnetic moment (see Refs. 14 and 15) as well as a quadrupole moment is a decisive factor for acceleration of a natural catalytic reaction[16] near the O_2 impurity molecules in n-H_2, which causes spontaneous transitions of o-H_2 molecules closest to the oxygen molecules to the para state, which has lower rotational energy. The ortho–para conversion usually includes two stages: a spin–nuclear transition (''flipping'' the spin of one of the protons in the H_2 molecule) and a vibrational–rotational transition, with the excess rotational energy being transferred to lattice vibrations in the form of two phonons ($T \approx 170$ K; see Ref. 14). Thus, owing to ortho–para conversion induced by the paramagnetic impurity of O_2 molecules in solid n-H_2 (Ref. 4), after several hours the o-H_2 molecules in a significant portion of the volume of the O_2–n-H_2 samples will have converted to the para state. For samples of p-H_2 individual oxygen molecules have a hardening effect (see Fig. 1), in agreement with the results of Ref. 17 for p-H_2 with the ortho content reduced to $\approx 0.2\%$.

The authors are deeply grateful to V. G. Manzhelii, M. A. Strzhemechny, V. D. Natsik, M. I. Bagatsky, and A. I. Prokhvatilov for a discussion of the results, and to T. F. Lemzyakova for the chromatographic analysis of the hydrogen.

*E-mail: alekseeva@ilt.kharkov.ua

[1] Yu. E. Stetsenko, D. N. Bol'shutkin, and L. A. Indan, Fiz. Tverd. Tela (Leningrad) **12**, 3636 (1970) [Sov. Phys. Solid State **12**, 2958 (1970)].
[2] I. N. Krupskiĭ, A. V. Leont'eva, L. A. Indan, and O. V. Evdokimova, JETP Lett. **24**, 266 (1976).
[3] S. C. Bates and T. L. Altshuler, Crystallogr. Rep. **35**, 559 (1995).
[4] V. Shevtsov, A. Shcherbakov, P. Malmi, E. Ylinen, and M. Punkkinen, J. Low Temp. Phys. **104**, 211 (1996).
[5] I. N. Krupskiĭ, A. V. Leont'eva, L. A. Indan, and O. V. Evdokimova, Fiz. Nizk. Temp. **3**, 933 (1977) [Sov. J. Low Temp. Phys. **3**, 453 (1977)].
[6] I. A. Gindin, V. M. Godzhaev, N. K. Nechvold, and Ya. D. Starodubov, Dokl. Akad. Nauk SSSR **174**, 73 (1967) [*sic*].
[7] L. I. Danilenko, M. V. Zinov'ev, and V. A. Koval', Prib. Tekh. Éksp., No. 2, 212 (1973).
[8] L. A. Alekseeva, O. V. Litvin, and I. N. Krupskiĭ, Fiz. Nizk. Temp. **8**, 316 (1982) [Sov. J. Low Temp. Phys. **8**, 158 (1982)].
[9] L. A. Alekseeva, Candidate's Dissertation [in Russian], FTINT, Kharkov (1986).
[10] R. Wanner and H. Meyer, J. Low Temp. Phys. **11**, 715 (1973).
[11] L. A. Alekseeva, M. A. Strzhemechny, and G. N. Shcherbakov, Fiz. Nizk. Temp. **21**, 983 (1995) [Low Temp. Phys. **21**, 758 (1995)]; L. A. Alekseeva, M. A. Strzhemechny, and Yu. V. Butenko, Fiz. Nizk. Temp. **23**, 448 (1997) [Low Temp. Phys. **23**, 329 (1997)].
[12] R. E. Boltnev, E. B. Gordon, I. N. Krushinskaya, A. A. Pel'menev, E. N. Popov, and O. F. Pugachev, Fiz. Nizk. Temp. **18**, 819 (1992) [Low Temp. Phys. **18**, 576 (1992)].
[13] A. S. Baryl'nik, A. I. Prokhvatilov, M. A. Strzhemechnyi, and G. N. Shcherbakov, Fiz. Nizk. Temp. **19**, 625 (1993) [Low Temp. Phys. **19**, 447 (1993)].
[14] V. G. Manzhelii and Yu. A. Freiman (Eds.), *Physics of Cryocrystals*, AIP Press, Woodbury New York (1996); B. I. Verkin and A. F. Prikhot'ko (Eds.), *Cryocrystals* [in Russian], Naukova Dumka, Kiev (1983).
[15] B. I. Verkin, V. G. Manzhelii, V. N. Grigoriev, V. A. Koval', V. V. Pashkov, V. G. Ivantsov, O. A. Tolkacheva, N. M. Zvyagina, and L. I. Pastur, *Handbook of Properties of Condensed Phases of Hydrogen and Oxygen*, Hemisphere Publishing Corporation, New York, Washington, Philadelphia, London (1991).
[16] E. Cremer and V. Polanyi, Trans. Faraday Soc. **28**, 435 (1932).
[17] L. A. Alekseeva and M. N. Kazeev, IAÉ Preprint 5299/7 [in Russian], Kurchatov Institute of Atomic Energy, Moscow (1991).

Translated by Steve Torstveit

NEWS ITEMS

XIV international seminar on high-temperature superconductivity and school of applied superconductivity (Kurchatovets vacation base, Protvino, Russia, May 28–31, 2001)

M. A. Belogolovskiĭ*

A. A. Galkin Donetsk Physico-Technical Institute, National Academy of Sciences of Ukraine, ul. R. Lyuksemburg 72, 83114 Donetsk, Ukraine

S. I. Bondarenko**

B. Verkin Institute for Low Temperature Physics and Engineering, National Academy of Sciences of Ukraine, pr. Lenina 47, 61103 Kharkov, Ukraine

L. S. Shirshov***

Institute of High-Energy Physics Government Research Center, Protvino, Moscow District, Russia
(Submitted August 2, 2001)
Fiz. Nizk. Temp. **28**, 203–206 (February 2002)

[DOI: 10.1063/1.1461928]

It has become traditional to hold an annual School of Applied Superconductivity at the Kurchatov Institute's vacation base near Protvino in the last week of May. This year the XIV International Seminar on High-Temperature Superconductivity was also held here. This seminar continued the tradition of annual joint meeting that have been held since the late 1970s alternately in Russia, Germany, and Ukraine. About a hundred participants came in from 28 academic institutions, research centers, and commercial enterprises in Moscow, St. Petersburg, Kiev, Kharkov, Ekaterinburg, and other cities. This meeting clearly demonstrated the international character of research in this field. Of the more than 80 papers presented at the Seminar and School, at least a quarter of them had a foreign colleague among the coauthors. Naturally, the greatest number of them were German, but researchers from Great Britain, the Netherlands, Slovakia, and other countries were also represented. In comparison with the previous trilateral seminars the number of reports from Ukraine has grown, and, most importantly, the first signs of a growing collaboration between Russian and Ukrainian colleagues were in evidence.

Since the Kurchatov Institute Russian Research Center, the organizer and administrator of the two programs, is known throughout the world as one of the leading institutions in the field of high-current superconductivity, it was only natural that a large part of these programs would be devoted to that topic. It was on the initiative of Acad. Evgeniĭ Velikkov, the Director of the Kurchatov Institute, that the International Thermonuclear Experimental Reactor (ITER) project was launched; besides Russia, participants in this project now include the European Union and Japan. The history of this project begins back in the 1950s, when the idea of the Tokamak was born. By 1978 the Tokamak T-7, with windings based on a NbTi alloy, had already been successfully tested, and by the end of 1988 the Tokamak T-15, with windings based on Nb_3Sn, was commissioned.

Last year in Japan a model coil for the central solenoid was successfully tested, and a record magnetic field of 13 T was obtained at a current of 46 kA. In addition, it was decided to prepare a superconducting coil insert for this solenoid, with a winding ~ 5 m in height and about 1.5 m in diameter. V. E. Sytnikov of the All-Russia Scientific Research Institute of the Cable Industry gave a presentation on the joint efforts of three Russian institutes in the preparation of the coil insert, which was delivered to Japan at the end of May. Workers at the A. A. Bochvar All-Russia Scientific Research Institute prepared one metric ton of Nb_3Sn wire, which was wound and placed in a titanium tube about 4 cm in diameter and over 100 m long. Such a cable is expensive, around $5000 per meter, so there is not much room for error. For high-temperature annealing of such large windings a special oven was built at the D. V. Efremov Scientific Research Institute of Electrophysical Apparatus (SRIEA) in St. Petersburg. This was a difficult task because it was necessary to satisfy a number of conflicting requirements. The windings were annealed for 22 days, with the outer surface of the helical winding held in a high vacuum while at the same time gaseous helium was blown through the inner ''tube'' to remove the impurities released during the heat treatment. The deviation of the temperature from the specified level during the multistep heat-treatment regime had to be maintained within a 5-degree interval over the entire volume of the coil.

A report entitled ''Accidents in superconducting magnets caused by electric arcing,'' presented by S. A. Lelekhov, V. E. Keilin, and B. N. Kolbasov of the Kurchatov Institute drew a great deal of interest. The ITER under development will contain toroidal fields windings based on 18 superconducting coils, in which the total magnetic energy stored will be around 41 GJ. To consider possible anomalous situations, they analyzed the experimental data on high-current electric arcs from tests of the coils of the Tokamak T-15, in which the design value of the stored energy is 800 MJ. The results of

their calculations will make it possible to prepare recommendations on the design of the superconducting coils of the magnet system of ITER.

Of the other talks pertaining to high-current superconductivity, we should mention the one entitled ''The magnet system of the electron lens of the Tevatron,'' which was given by L. M. Tkachenko of the Institute for High-Energy Physics (IHEP), Protvino. The magnet system, which includes a long superconducting solenoid with a field of 6.5 T, was developed and prepared in a collaboration between the IHEP and the Fermi National Laboratory (USA) for electron cooling of an antiproton beam. The electron lens should reduce the variance of betatron frequencies which arises in an antiproton beam as a result of the interaction of colliding beams. On March 23, 2001 at the Tevatron (USA) an electron beam was passed through a ''magnetic channel'' created by a chain of magnets, with a total channel length of more than 3 meters. Studies including measurements of the main characteristics of the beam interaction are planned with the goal of converting this into a working device.

The cryogenic system for the tests of the superconducting devices at a temperature of 1.8 K was the subject of an interesting report presented by V. V. Pleskach of IHEP. Unlike the magnet system, which was prepared for operation in the USA, this system was intended for operation at the oldest and most powerful proton accelerator, the U-70. The development of this system was prompted by a gift from physicists at CERN, who donated two large superconducting resonators with a working frequency at the 3 GHz level as part of the OKA complex for rf separation of K mesons, which is scheduled to go on stream at the U-70 in 2002.

L. K. Kovalev of the Moscow Aviation Institute presented new types of electric motors with rotor elements made of HTSC materials, various designs for hysteretic, reactive, trapped-flux, and composite synchrotron HTSC machines and the prospects for their application. A report on how thermobaric treatment can improve the properties of bulk 123 materials was presented by T. A. Prikhna of the Institute of Ultrahard Materials of the National Academy of Sciences of Ukraine. These studies were done jointly with scientists from German and Spain and resulted in the creation of bulk YBCO rotors for the electric motors spoken of by L. K. Kovalev. L. M. Fisher of the All-Russia Electrical Engineering Institute and his coauthors from Russia, Ukraine, and Norway spoke of an unusual phenomenon: macroturbulent instability, which is observed in flux-carrying superconductors upon their magnetization reversal. A theory using some ideas of classical hydrodynamics was proposed and confirmed in magnetooptic experiments on YBCO.

Two talks were devoted to one of today's ''hot'' topics: the transport properties properties of Josephson structures including superconducting and ferromagnetic layers. V. V. Ryazanov of the Institute of Solid State Physics of the Russian Academy of Sciences, reported on the creation of the so-called π contact, which should become a basic element of phase-based superconducting qubits, and V. N. Krivoruchko of the Donetsk Physico-Technical Institute presented a theoretical paper demonstrating the possibility of amplifying the Josephson current in superconductor/ferromagnet–insulator–ferromagnet/superconductor structures with an antiparallel orientation of the magnetic layers.

We must mention the next ''sensation'' in the field of HTSCs: superconducting borides. V. S. Kruglov of the Kurchatov Institute presented a survey entitled ''Superconductivity of MgB_2 compounds: results and prospects.'' The discovery of superconductivity in simple layered compounds of magnesium and boron, with a critical temperature four times as high as for the alloy NbTi, raises the questions: What type of superconductor is it, and how promising is this new material for use in electrical engineering? Samples of multistrand cable of diboride in a stainless-steel casing have already been prepared using the ''powder-in-tube'' method. The measured value of the transport current density in zero magnetic field exceeded the level of 10 kA/cm^2 at a temperature of 33 K. In spite of a certain skepticism above the future of this superconductor on account of its relatively low critical fields, it cannot be ruled out that in time magnesium diboride will squeeze out its niobium competitors. The discovery of this superconductor was stimulated by a search for new related materials and intensive studies of their characteristics. M. V. Indenbom of the Institute of Solid State Physics of the Russian Academy of Sciences reported the successful synthesis of MgB_2 in the form polycrystals and films and the magnetooptic visualization of the macroscopic critical currents in these samples. V. A. Gasparov of that same institute and coauthors reported the observation of superconductivity in ZrB_2, with $T_c = 6$ K.

Among the reports of pure basic research was the talk by A. M. Gabovich of the Institute of Physics of the National Academy of Sciences of Ukraine, who, together with colleagues from Ukraine, Great Britain, and Belgium interprets the anomalous properties of cuprates as a possible manifestation of instabilities of their electronic spectrum (charge- and spin-density waves, phase separation, etc.). The fundamental aspects of quasiparticle transport through the surface of high-temperature superconductors was discussed in the report by Yu. F. Revenko *et al.* of the Donetsk Physico-Technical Institute; those authors presented surprising proof that in this case there is a surface barrier with strong antiferromagnetic correlations. To confirm this hypothesis, V. E. Shaternik and É. M. Rudenko of the Kiev Institute of Metal Physics (IMP) of the National Academy of Sciences of Ukraine did studies of the layered structure of antiferromagnetic chromium oxide, which showed results identical to the contact characteristics of the HTSC materials. The results of calculations of the charge-density distribution in mercury HTSC compounds were presented by R. V. Lutsiv of Lvov University.

Research on HTSC films is actively continuing. Their properties under microwave irradiation and their practical applications as filters were the subject of a series of papers by Kiev scientists. G. A. Melkov of Kiev University proposed a tunable (by means of weak external magnetic fields) narrow-band microwave filter based on HTSC and ferrite films. Microwave filters based on YBCO films were made in collaboration with colleagues from the University of Leipzig; these filters and the influence of temperature on their selectivity were the subject of two reports by I. V. Korotash of IMP. The groups of V. M. Pan of IMP and G. A. Melkov of

Kiev University have investigated the microwave characteristics of YBCO films obtained by the method of laser deposition and elucidated the correlations between the deposition regime, the dislocation structure of the resulting layers, and their surface resistance. The report by A. V. Bobyl of SRIEA in St. Petersburg was devoted to the interrelation between the characteristics of electric noise of metallic layers and their structure, with the goal of prolonging the service life of 123 films. N. G. Cherpak of the Institute of Radio Electronics of the National Academy of Sciences of Ukraine in Kharkov, together with German colleagues from Jena, first used microwave and rf techniques for studying the characteristics of fused HTSC materials. The authors regard this as a promising technique for investigating objects of this class.

The report by S. I. Bondarenko of the Institute for Low Temperature Physics and Engineering of the National Academy of Sciences of Ukraine in Kharkov demonstrated the possibility of significantly (by a factor of some tens) improving the sensitivity of SQUIDs by means of ferromagnetic magnetic-field concentrators. This is particularly essential in the case of HTSC SQUIDs, which still remain inferior to helium-temperature devices in terms of sensitivity. It was also shown to be promising to make highly sensitive HTSC gradientometers utilizing magnetic circuits without multiturn coupling coils in the flux transformer. The results represent another step toward the creation of HTSC magnetoencephalographs.

The participants at the seminar showed particular interest in the report by S. I. Bondarenko on the state of development of a cryogenic automobile in the Ukraine. The energy source and coolant for the superconducting units of this automobile is liquid nitrogen in a transportable cryostat. As a result of gasification of a portion of the nitrogen when it comes into contact with the ambient medium, the high-pressure gas drives a pneumomachine with a shaft-mounted superconducting electrical generator. The generation supplies HTSC electric motors (it is assumed that their power does not exceed 10 kW per wheel), controlled individually and coordinated. Such an environmentally clean and fire-safe automobile is already economically justified today, especially as city transport for light- and medium-duty trucks. Considering the progress in the development of HTSC electric motors and generators, the cryogenic automobile can become yet another field of application of HTSC devices.

As was noted in the closing address by Prof. Viktor Efimovich Keilin, the Chairman of the Organizing Committee of the School, holding the two events simultaneously turned out to be very fortunate. In particular, the School had less of an applied character and a greater thematic range of topics addressed. There were many new faces not seen in the previous meetings, and the presence of young people instills hope for the successful development of superconductivity in the future.

The program of the School and Seminar were supported on the Russian side by the Ministry of Industry, Science, and Technology of the Russian Federation and by Minatom RF, and on the Ukrainian side by the National Academy of Sciences of Ukraine.

The next School of Applied Superconductivity will be held, as always, at the vacation base of the Kurchatov Institute at the end of May, 2002

*E-mail: bel@kinetic.ac.donetsk.ua
**E-mail: Bondarenko@ilt.kharkov.ua
***E-mail: shirshov@mx.ihep.su

Translated by Steve Torstveit

QUANTUM LIQUIDS AND QUANTUM CRYSTALS

Concentration dependence of the attenuation of first sound in supersaturated superfluid ^{3}He–^{4}He solutions under pressure

A. A. Zadorozhko, T. V. Kalko, É. Ya. Rudavskiĭ,* I. A. Usherov-Marshak, V. K. Chagovets, and G. A. Sheshin

B. Verkin Institute for Low Temperature Physics and Engineering, National Academy of Sciences of Ukraine, pr. Lenina 47, 61103 Kharkov, Ukraine
(Submitted September 28, 2001)
Fiz. Nizk. Temp. **28**, 107–114 (February 2002)

The concentration dependence of the attenuation coefficient of first sound in superfluid ^{3}He–^{4}He solutions in the saturation and supersaturation regions is investigated experimentally at pressures of 0–10 atm. An original technique of continuous variation of the concentration *in situ* by variation of the osmotic and thermomechanical pressures is used, permitting measurements to be made in the long-lived metastable phase of the superfluid solutions. It is shown that the data obtained are described well in terms of the theory of sound propagation in a gas of Fermi excitations without taking the Fermi-liquid corrections into account. The corresponding values of the effective mass and relaxation time of ^{3}He quasiparticles are taken from an analysis of the existing experimental data. Within the experimental error, no excess sound attenuation was found in the region of supersaturated solutions. © *2002 American Institute of Physics.* [DOI: 10.1063/1.1461917]

1. INTRODUCTION

One of the characteristic features of liquid solutions of ^{3}He–^{4}He is the presence of a first-order phase transition, phase separation, as a result of which the liquid separates into a lighter concentrated phase that is rich in ^{3}He and a dilute superfluid phase that is rich in ^{4}He. As $T\rightarrow 0$ the phase separation curve tends not to zero values of the concentration but to a finite solubility $x_0\approx 6.7\%$ ^{3}He. This means that at very low temperatures and $x<x_0$ the ^{3}He–^{4}He solution is a homogeneous quantum liquid comprising a solution of a normal Fermi liquid in a superfluid Bose liquid. The properties of such a system have been described in detail in several monographs.[1,2]

The kinetic properties of Fermi–Bose quantum liquids (degenerate solutions of ^{3}He in ^{4}He) are governed by processes of interaction between elementary excitations, among which the Fermi excitations—^{3}He quasiparticles—play the leading role at low temperatures. Important information about such solutions has been obtained as a result of experimental and theoretical studies of the acoustic properties of the system.[3–9] In particular, a relaxation process in the gas of Fermi excitations, with a characteristic relaxation time τ_{33}, has been registered, which is broadened and shifted to higher temperatures as the frequency of the sound increases. A subsequent analysis has shown that this relaxation process is due to the viscosity of the Fermi liquid, which is inversely proportional to the square of the temperature.

In recent years there has been a renewal of interest in the kinetic processes occurring in degenerate ^{3}He–^{4}He solutions after it was shown experimentally that the region of superfluidity of the solutions could be expanded through the realization of a long-lived metastable superfluid phase.[10,11] Even though the observed supersaturation has so far remained considerably less than predicted by the theory of homogeneous nucleation, this discovery has opened up the possibility, in particular, of continuing the study of sound attenuation to higher concentrations. Here the method of continuous variation of the concentration in the course of the experiment, proposed in Ref. 12, has permitted the first recording of the concentration dependence of sound attenuation at constant temperature and pressure. A topic of independent interest is to study the attenuation of sound in a supersaturated superfluid solution, where additional sources of dissipation are possible.[13] The present study was undertaken to investigate this circle of topics.

2. EXPERIMENTAL TECHNIQUE

Figure 1 shows a diagram of the experimental cell, together with the low-temperature part of the dilution refrigerator. The cell contains two chambers: a control chamber *1* and a measurement chamber *3*, which are connected by a capillary *2*. The latter chamber contains a sound cell *4* for the acoustic measurements and a capacitive concentration gauge *5*. The measurement chamber is in permanent thermal contact with the mixing chamber *6* through a threaded coupler, and the control chamber *1*, which is equipped with a heater *9*, is connected to the still through a thermal switch *13* containing superfluid ^{4}He. In the closed state the switch was filled with superfluid, and the control chamber rapidly took on the temperature of the still. The switch was opened by removing the liquid ^{4}He from the switch by means of a thermomechanical pump.

The temperature of the measurement chamber was recorded by means of an ^{3}He melting-curve thermometer *12*.

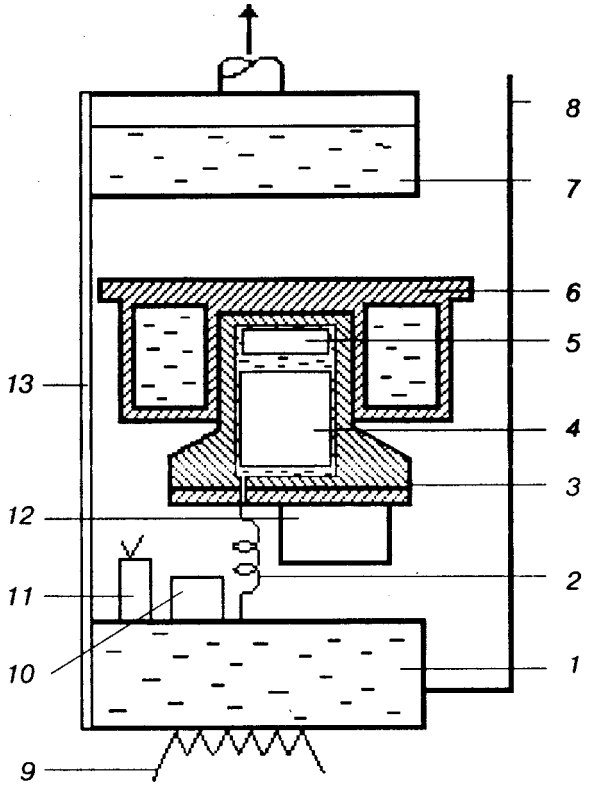

FIG. 1. Diagram of the experimental cell and its position in the dilution refrigerator: *1*—control chamber; *2*—connecting capillary; *3*—measurement chamber; *4*—sound cell; *5*—capacitive concentration gauge; *6*—mixing chamber; *7*—still; *8*—filling capillary; *9*—heater; *10*—liquid thermometer containing ^{3}He; *11*—carbon resistance thermometer; *12*—^{3}He melting-curve thermometer; *13*—thermal switch.

The temperature of the control chamber was determined by means of a liquid thermometer *10*, which registered the ^{3}He vapor pressure, and a carbon resistance thermometer *11*. The solution under study was condensed in both chambers – the measurement chamber (volume 6.17 cm^3) and the control chamber (volume 53.04 cm^3). When the two chambers were at the same temperature, the concentrations of the solution in them were also the same. When the control chamber was heated (after opening of the thermal switch) an additional osmotic pressure and the fountain pressure arose in it, causing ^{3}He to leak from the control chamber into the measurement chamber. The ^{3}He concentration in the measurement chamber can be measured in the course of the experiment by means of a capacitive gauge *5* from the change in the dielectric constant. This method also made it possible to decrease the concentration in the measurement chamber by turning off heater *9* and cooling chamber *1* through the thermal switch *13*. A small heat exchanger made of sintered copper powder (not shown in Fig. 1) was used in the measurement chamber to decrease the Kapitsa thermal boundary resistance between the solution under study and the wall of the mixing chamber.

The attenuation of first sound was measured at a frequency of 30 MHz by a pulsed technique described previously.[14] The method of measurement is based on a comparison of the amplitudes of two radio pulses—the pulse under study and a measuring pulse—which were formed in the same generator and were sent through the same amplifying devices. The sound emitter was an X-cut quartz slab with a fundamental frequency of 10 MHz, which was operated as a sound receiver in the intervals between emissions. The quartz slab and the reflector were adjusted to a parallel alignment in a separate experiment with ^{4}He. The sound propagated in a cavity 10 mm in diameter and 7.15 mm long. To preclude any heating of the liquid by the radio pulses, the low-temperature measurements were made at 10-second intervals with a pulse duration of 10 μs. We also checked for the lack of any dependence on the signal amplitude and for the absence of nonlinear effects. The error of measurement of the sound attenuation coefficient was not over 5%.

The construction of the experimental cell permitted making measurements under pressure, which was produced by means of a gasifier (or "bomb"). For measurement and stabilization of the pressure we used a piston manometer which was equipped with a visual oil indicator to improve accuracy. Constancy of the pressure was achieved by maintaining an established oil level in the tube to an accuracy of ± 1 mm of the oil column. The pressure was determined to within an error of 0.1 bar.

3. CHANGE OF THE CONCENTRATION OF THE SOLUTION AND THE CORRESPONDING CHANGE IN SOUND ATTENUATION

At the start of the experiment both the measurement and control chambers of the experimental cell were filled with solution of equal concentration, and then the measurement cell was cooled together with the dilution chamber; the control chamber was cooled through the thermal switch *13* and had the temperature of the still of the refrigerator. Then the control chamber was heated at a rate of $\sim 3-4$ mK/min, raising the concentration in the measurement chamber (see Fig. 2a). The change in concentration, Δx, was measured from the change in capacitance, ΔC, of a special capacitive gauge *5* (Fig. 1), which was placed so that after phase separation it was located completely in the dilute phase. The concentration change Δx caused a change in the dielectric constant ε of the solution, which is related to the molar volume by the well-known Clausius–Mossotti equation, with the molar volume V_x of the solution expressed in terms of the molar volume V_4 of ^{4}He:

$$V_x(P,T,x)=V_4(P,T)(1+\alpha_{PT}x), \tag{1}$$

where the parameter α_{PT} plays a part in the theory of degenerate solutions[15] and is equal to the relative change of the molar volume of the solution when a ^{4}He atom is replaced by a ^{3}He atom. In the limit of low ^{3}He concentrations at $P\to 0$ and $T\to 0$, one has $\alpha_{00}=0.284\pm 0.005$.[16] The detailed $P-V-T$ measurements made in Ref. 17 permit determination of the pressure dependence of α_{PT} for $T>0$. It has been shown that α_{P0} decreases strongly with increasing pressure. The temperature dependence of α_{PT} can be taken into account as

$$\alpha_{PT}=\alpha_{P0}-\alpha_T T, \tag{2}$$

where the parameter $\alpha_T=0.032\pm 0.003$ K^{-1} was determined in Ref. 16. Here we assume that α_{PT} is independent of concentration in the concentration region under study. Then the Clausius–Mossotti equation will be a relation between the dielectric constant and the concentration of the solution:

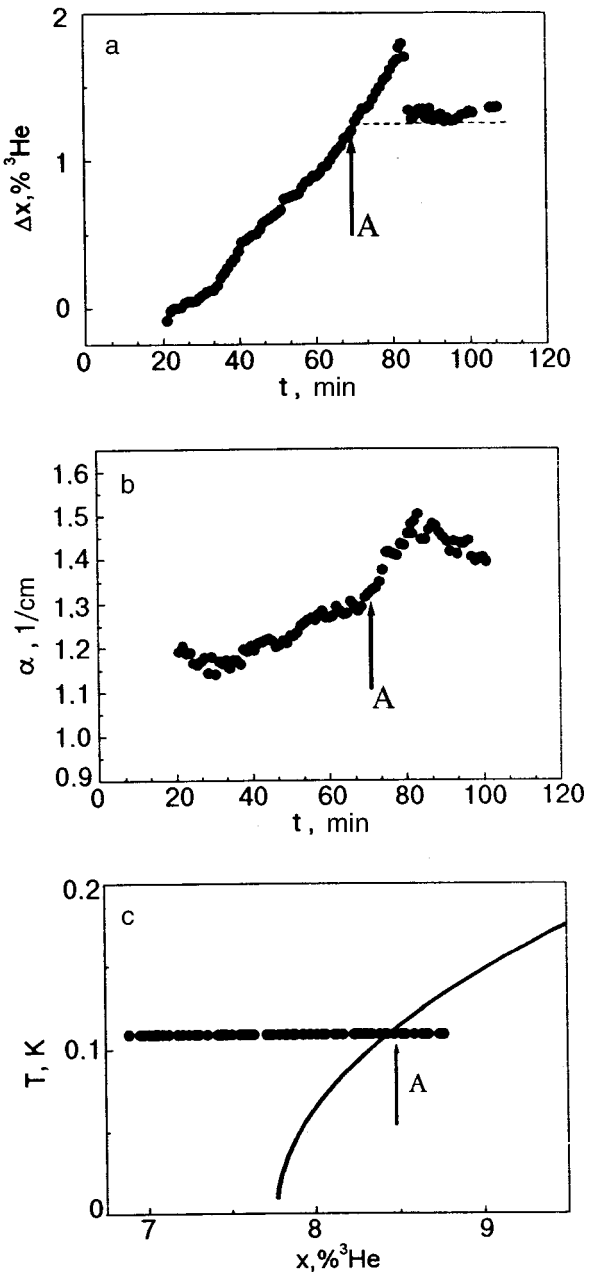

FIG. 2. Variation of the concentration of the solution under study with time (a); the corresponding variation of the sound attenuation coefficient with time at a temperature of 109 mK and a pressure of 2 bar (b); the variation of the concentration of the solution in the course of the experiment relative to the equilibrium phase separation line (solid curve) (c). In each case the intersection with the phase separation line is indicated by an arrow.

$$\frac{\varepsilon-1}{\varepsilon+2}=\frac{4\pi}{3}\frac{\gamma}{V_4(P,T)[1+(\alpha_{00}-\alpha_T T)x]}, \tag{3}$$

where γ is the polarizability of the solution, which was assumed equal to 0.1232 cm^3/mole.[18] Taking into account that the change in capacitance of the flat capacitive sensor is $\Delta C/C=\Delta\varepsilon/\varepsilon$, we obtain from (3) the final formula for determining the change in concentration, Δx, in terms of the corresponding change in capacitance of the concentration sensor, ΔC:

$$\Delta x=A(P)\Delta C, \tag{4}$$

where

$$A(P)=\frac{3\varepsilon(P)}{[\varepsilon(P)-1][\varepsilon(P)+2]}\frac{1+\alpha_{PT}(P)x}{\alpha_{PT}(P)C}.$$

Usually the value of $A(P)$ at each pressure was determined at a point corresponding to the saturated solution on the equilibrium phase-separation line (point A in Fig. 2). The concentration change Δx was reckoned from the initial concentration in the measurement chamber, and the absolute value of the concentration was obtained using the same reference point A.

The values of Δx calculated according to formula (4), which are plotted as a function of time in Fig. 2a, do not show any anomaly upon crossing of the equilibrium line of phase separation (point A in Fig. 2c). This point is indicated by an arrow in the figure. The jump in Δx is observed later, after an appreciable supersaturation Δx_s has been attained. As before,[10] the observed metastable state is long-lived, and far from the point of rapid nucleation the characteristic scale of its lifetime is in hours.

The time dependence of the sound attenuation coefficient in the investigated solution of changing concentration is shown in Fig. 2b. The character of the dependence is practically the same as that of $x(t)$ (see Fig. 2a). Since we measured the relative sound attenuation, the absolute values of α were obtained by normalizing at the point A, where the attenuation of sound in the saturated solution was investigated previously[4,8,9] and it was shown that it is described well by the relation[5]

$$\alpha=\frac{2}{3}\frac{\lambda^2 P_F(T)}{\rho c^3}\frac{\omega^2\tau_{33}}{1+\omega^2\tau_{33}^2}, \tag{5}$$

where ρ_4 is the density of ^{4}He, c and ω are the velocity and frequency of the sound, $P_F(T)$ is the pressure of the gas of Fermi excitations at temperature T, τ_{33} is the characteristic relaxation time in the system of ^{3}He quasiparticles, and the parameter λ is expressed in terms of the effective mass m^* of the Fermi excitations:

$$\lambda=\left(1+\alpha_{PT}+\frac{m^*-m_3}{m_3}\right)\frac{m_4}{m^*}, \tag{6}$$

where m_3 and m_4 are the masses of the ^{3}He and ^{4}He atoms. Expression (5) was obtained under the assumption that the sound is propagating in a gas of Fermi excitations of mass m^* and pressure $P_F(T)$. All but two of the parameters appearing in expression (5) are well known. The exceptions, τ_{33} and m^*, must be chosen from an independent analysis.

4. RELAXATION TIME AND EFFECTIVE MASS OF FERMI EXCITATIONS IN THE SOLUTION

First, the ^{3}He–^{3}He relaxation time in the solution was investigated for the nondegenerate case. An important role in determining the impurity relaxation time in the degenerate region was played by acoustic experiments[4] in which the maximum in the sound attenuation due to relaxation in the gas of Fermi excitations was recorded at a temperature of $\sim$50 mK. A subsequent analysis of the mechanisms of sound attenuation in this region[5] showed that the relaxation time τ_{33} can be written in the form

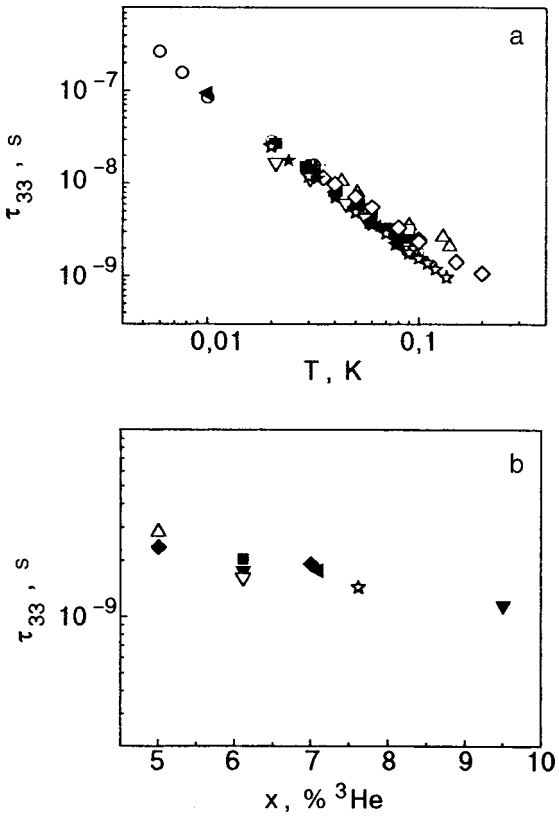

FIG. 3. Relaxation time τ_{33} for various pressures, as a function of temperature at a ^{3}He concentration of $\sim 5-7\%$ (a) and as a function of concentration at a temperature of 100 mK (b). △—$x=5\%$ ^{3}He, $P=0$ from sound attenuation;[4] □—$x=5.73\%$ ^{3}He, $P=0$ from sound attenuation;[8] ●—$x=5.73\%$ ^{3}He, $P=10$ bar from sound attenuation;[8] ○—saturated solution, $P=0$ from viscosity;[9] ♦—$x=5\%$ ^{3}He, $P=0$ from viscosity;[19] ▼—$x=6.12\%$ ^{3}He, $P=9.8$ bar from viscosity;[20] ◀—$x=7.1\%$ ^{3}He, $P=0$ from viscosity;[20] ▽—$x=6.12\%$ ^{3}He, $P=19.4$ bar from viscosity;[20] ☆, ★—saturated solution, $P=0$ from viscosity and osmotic pressure, respectively.[21]

$$\tau_{33}=\frac{A(P,x)}{T^2}\left[1+B(p,x)\left(\frac{T}{T_F}\right)^2\right], \tag{7}$$

where

$$T_F=\frac{\hbar^2}{2km^*}\left(3\pi^2\frac{N_A x}{V_m}\right)^{2/3}$$

is the Fermi degeneracy temperature of the solution, N_A is Avogadro's number, and the coefficients $A(P,x)$ and $B(P,x)$, which depend on the concentration and pressure, were chosen so that the maximum observed in the sound attenuation at low temperatures corresponded to the calculated one. Subsequent experiments on sound attenuation in ^{3}He–^{4}He solutions[8,9] have substantially expanded the investigated region of concentrations, temperatures, pressures, and frequencies. The values of τ_{33} obtained from acoustic experiments[4,8,9] are given in Fig. 3. It is seen from the plots that the data of the three groups of authors are in good agreement with one another.

Another independent way of determining the relaxation time of the Fermi excitations in solutions involves the use of the experimental data on their viscosity.[19–21] If the viscosity of the solution is due solely to the ^{3}He quasiparticles, then its relation to the time τ_{33} can be written in the form[5]

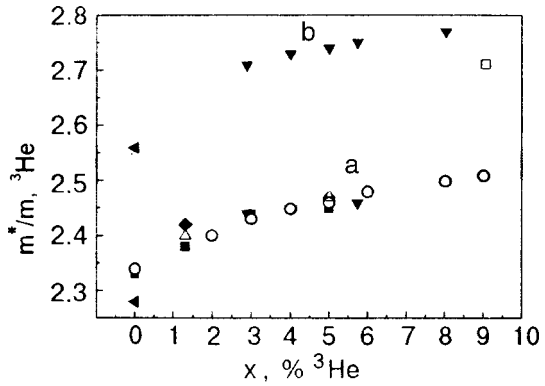

FIG. 4. Concentration dependence of the effective mass of impurity excitations in solutions at $P=0$ (a) and $P=10$ bar (b). ▼—Ref. 8; ■—Ref. 22; △—Ref. 23; ♦—Ref. 24; ◀—Ref. 25; □—Ref. 26; ○—Ref. 27.

$$\eta_3=P_F(T)\tau_{33}, \tag{8}$$

and the pressure of the gas of ^{3}He quasiparticles in the degenerate region is given by the formula

$$p_F(T)=\frac{2}{3}\frac{kT_F N_A x}{V_x}\left[1+\frac{5\pi^2}{12}\left(\frac{T}{T_F}\right)^2-\frac{\pi^4}{16}\left(\frac{T}{T_F}\right)^4\right]. \tag{9}$$

The values of τ_{33} calculated from the experimental values of the viscosity[18,19] according to formulas (8) and (9) are also shown in Fig. 3. It is seen from these data that the value of τ_{33} decreases quite markedly with increasing temperature, has a weak concentration dependence, and is practically independent of pressure.

As to the other parameter appearing in Eqs. (5) and (6), the effective mass m^* of a ^{3}He quasiparticle, the existing data for two pressures are summarized in Fig. 4, which shows the values of m^* obtained from the measurements of first-sound attenuation,[8] the heat capacity,[22–24] the velocity of second sound,[25] and the line of phase separation at high pressures.[26] Also shown in Fig. 4 are the smoothed values of the effective mass which were calculated in Ref. 27 using the ^{3}He–^{3}He interaction potential proposed in Ref. 15. One notices that, according to the data of Ref. 26, at high concentrations there is a deviation of $m^*(x)$ from a monotonically increasing trend. Otherwise the agreement of the experimental data of the different studies is completely satisfactory. Here it is assumed that the value of m^* is independent of temperature.

5. CONCENTRATION DEPENDENCE OF THE SOUND ATTENUATION COEFFICIENT. COMPARISON WITH THEORY

Figure 5 shows the experimental data on the sound attenuation α in the saturated and supersaturated solutions (the boundary of their coexistence region is indicated by an arrow) and the values of α calculated according to formulas (5) and (6) with the values of τ_{33} and m^* given in Figs. 3 and 4. Also shown are the experimental results obtained in Ref. 8 at the same sound frequency and the same pressure but at lower ^{3}He concentrations.

It follows from the plots that the experimental concentration dependence of the sound attenuation agrees within the total error limits with the predictions of the theory of Refs. 5 and 6, which uses a gas model of the ^{3}He quasiparticles

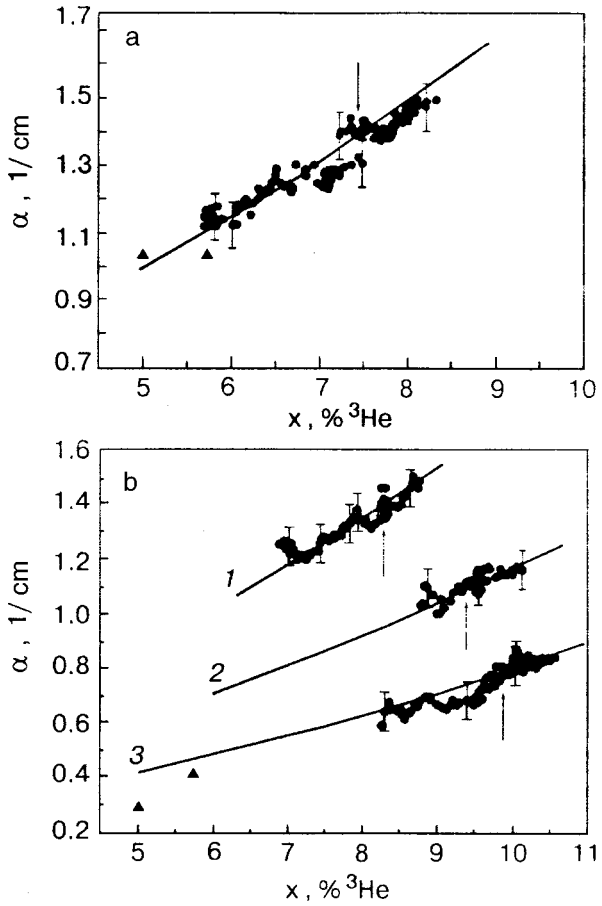

FIG. 5. Concentration dependence of the first-sound attenuation at $T=120$ mK and sound frequency 30 MHz, for various pressures P [atm]: 0.55 (a), 2 (*1*), 5 (*2*), 10 (*3*) (b); ●—present study; ▲—Ref. 8. The arrows indicate the concentration corresponding to phase separation at the given pressure, and the curves were calculated according to Eq. (5).

without taking the Fermi-liquid corrections into account. This means that in the investigated regions of concentrations and pressures the main mechanism for the attenuation of first sound is the direct absorption of an acoustic phonon by ^{3}He quasiparticles. In the region of high pressures and concentrations, however, agreement between experiment and theory is observed if the effective mass of the impurity excitations decreases markedly with increasing concentration, which correlates with the conclusions of Ref. 26.

We also note that, within the experimental error, the data do not show any anomaly at the transition from the region of the saturated solution to the region of the supersaturated solution. Excess sound attenuation can appear in the supersaturation region if the metastable supersaturated solution becomes inhomogeneous, i.e., if suspended droplets of the condensed phase (almost pure ^{3}He) appear in it. These droplets float upward on account of buoyant forces, and the kinetics of the process depend strongly on the droplet size R, which determines their rate of ascent.

The problem of sound propagation in such a system was solved in Ref. 13. That paper considered three possible dissipative processes that lead to additional sound attenuation in the supersaturated solution. The first mechanism is based on the different compressibility of the droplet and the surrounding solution, which leads to absorption of sound. In this case the expression for the sound attenuation has the form

$$\alpha_I=\frac{2\pi}{9}k_1^4\left(1-\frac{\rho_1 c_1^2}{\rho_2 c_2^2}\right)^2 R^6 N_d, \tag{10}$$

where k is the wave vector of the sound, ρ is the density, and c is the sound velocity in each phase (the subscripts 1 and 2 refer to the solution and the droplets, respectively), and N_d is the number of droplets per unit volume.

The second mechanism of sound attenuation involves the vibrational motion of the solution with respect to the droplet, which leads to entrainment of the droplet. The corresponding sound attenuation is expressed as

$$\alpha_{II}=\frac{2\pi}{3}\left(\frac{\rho_1-\rho_2}{\rho_1+2\rho_2}\right)^2 N_d\left[k_1^4R^6+9k_1\lambda_1R^2\left(1+\frac{\lambda_1}{\lambda_2}\right)^{-1}\right], \tag{11}$$

where $\lambda_{1,2}=(2\eta_{1,2}/\rho_{1,2}\omega)^{1/2}$ is the penetration depth of the viscous wave for the respective phase.

The third dissipative process considered describes the sound attenuation due to the excitation of natural modes of the droplet, with frequency ω_2, by the incident sound wave with frequency ω. This leads to additional attenuation, which depends on the relationship between the values of ω_1 and ω_2 and is an extremely complicated function of λ_i, ρ_i, and k_i.

We note that the treatment in Ref. 13 is valid only for droplets of size R satisfying the condition

$$\lambda_{1,2}\ll R\ll\frac{1}{k_{1,2}}. \tag{12}$$

An analysis of these three mechanisms of sound attenuation on droplets with allowance for (12) showed that the first mechanism is the main dissipative process under the conditions of the given experiment, and the other two are negligible in comparison with it. As we see from Eq. (10), $\alpha_{\rm I}$ increases monotonically with increasing R. However, at large R, when $R\sim 1/k_{1,2}\sim 10^{-4}$ cm, the time of buoyant ascent of the droplets is short ($\sim$100 s), and the contribution of such droplets to the sound attenuation is very difficult to detect. As to the small droplets ($R\sim 10^{-5}$ cm), which ascend quite slowly, their contribution to $\alpha_{\rm I}$ according to (10) is so small that it is less than the measurement error. Thus, under the conditions of the given experiment, the predicted[13] excess sound attenuation is the supersaturated solution cannot be detected.

CONCLUSION

The technique of continuous variation of the concentration of superfluid ^{3}He–^{4}He solutions has enabled us to measure for the first time the concentration dependence of the attenuation of first sound at constant temperature and different pressures. It is found that in the investigated concentration region, which also includes metastable supersaturated solutions, the sound attenuation is described well by the theory of impurity–impurity absorption for the degenerate temperature region in the framework of a gas model of the Fermi excitations. Under the experimental conditions the excess sound attenuation due to the appearance of suspended droplets of the concentrated phase in the region of supersaturated solutions was not manifested. It seems advisable to

continue the measurements into a higher frequency range with the use of automated detection equipment.

The authors are grateful to Prof. I. N. Adamenko and K. E. Nemchenko for a helpful discussion of the results of this study.

This study was supported as part of the NATO Science Fellowships Program, Grant PST.CLG.978495.

*E-mail: rudavskii@ilt.kharkov.ua

[1] I. M. Khalatnikov, *Theory of Superfluidity* [in Russian], Nauka, Moscow (1971).
[2] B. N. Esel'son, V. N. Grigor'ev, V. G. Ivantsov, E. Ya. Rudavskiĭ, D. G. Sanikidze, and I. A. Serbin, *Solutions of Quantum Liquids* [in Russian], Nauka, Moscow (1971).
[3] I. M. Khalatnikov and V. N. Zharkov, Zh. Éksp. Teor. Fiz. **32**, 1108 (1957) [Sov. Phys. JETP **5**, 905 (1957)].
[4] B. M. Abraham, Y. Ekstein, J. B. Ketterson, and J. H. Vignos, Phys. Rev. Lett. **17**, 1254 (1966); **20**, 251 (1968); **21**, 422 (1968).
[5] G. Baym, W. F. Saam, and C. Ebner, Phys. Rev. **173**, 306 (1968); G. Baym and C. Pethick, *Physics of Liquid and Solid Helium*, edited by K. H. Bennemann and J. B. Ketterson, Wiley, New York (1978), p. 123.
[6] I. N. Adamenko and V. I. Tsyganok, Zh. Éksp. Teor. Fiz. **87**, 865 (1984); **88**, 1641 (1985); [Sov. Phys. JETP **60**, 491 (1984)]; **61**, 978 (1985)].
[7] É. Ya. Rudavskii and V. K. Chagovets, Fiz. Nizk. Temp. **10**, 1031 (1984) [Sov. J. Low Temp. Phys. **10**, 538 (1984)]; V. K. Chagovets, É. Ya. Rudavskiĭ, and V. A. Goncharov, Fiz. Nizk. Temp. **11**, 266 (1985) [Sov. J. Low Temp. Phys. **11**, 145 (1985)].
[8] I. Fuji, A. J. Ikushima, M. Fukuhara, and K. Kanako, J. Low Temp. Phys. **57**, 179 (1984); **63**, 535 (1986).
[9] S. A. J. Wiegers, R. Jochemsen, C. C. Kranenburg, and G. Frossati, J. Low Temp. Phys. **71**, 69 (1988).
[10] V. A. Mikheev, É. Ya. Rudavskiĭ, V. K. Chagovets, and G. A. Sheshin, Fiz. Nizk. Temp. **17**, 444 (1991) [Sov. J. Low Temp. Phys. **17**, 233 (1991)].
[11] T. Satoh, M. Morishita, and M. Ogata, Physica B **169**, 513 (1991); Physica B **197**, 397 (1994).
[12] A. A. Golub, V. A. Mikheev, É. Ya. Rudavskiĭ, and V. K. Chagovets, Inventor's Certificate (USSR) 1469292 SSSR; publ. Byull. Izobret., No. 12 (March 30, 1989).
[13] I. N. Adamenko, O. E. Gusev, K. E. Nemchenko, and V. I. Tsyganok, Fiz. Nizk. Temp. **18**, 1085 (1992) [Sov. J. Low Temp. Phys. **18**, 760 (1992)].
[14] V. K. Chagovets, É. Ya. Rudavskiĭ, and V. A. Goncharov, Fiz. Nizk. Temp. **11**, 266 (1985) [Sov. J. Low Temp. Phys. **11**, 145 (1985)].
[15] J. Bardeen, G. Baym, and D. Pines, Phys. Rev. **156**, 207 (1967).
[16] D. O. Edwards, E. M. Ifft, and R. E. Sarwinski, Phys. Rev. **177**, 380 (1969).
[17] H. A. Kierstead, J. Low Temp. Phys. **24**, 497 (1976).
[18] G. E. Watson, J. D. Reppy, and R. C. Richardson, Phys. Rev. **188**, 384 (1969).
[19] K. A. Kuenhold, D. B. Crum, and R. E. Sarwinski, Phys. Rev. Lett. **41A**, 13 (1972).
[20] R. Konig and F. Pobell, J. Low Temp. Phys. **89**, 465 (1992); **97**, 287 (1994).
[21] J. C. H. Zeegers, A. Th. A. M. de Waele, and H. M. Gijsman, J. Low Temp. Phys. **112**, 199 (1998).
[22] E. Polturak and R. Rosenbaum, J. Low Temp. Phys. **43**, 477 (1981).
[23] R. M. Mueller, H. Chocholacs, Ch. Buchal, M. Kubota, J. R. Owers-Bradley, and F. Pobell, in *Proceedings LT-17*, Amsterdam (1984), p. 1247.
[24] A. C. Anderson, D. O. Edwards, and W. R. Roach, J. Low Temp. Phys. **63**, 535 (1966).
[25] R. A. Sherlock and D. O. Edwards, Phys. Rev. **8**, 2744 (1973).
[26] H. Fukuyama, I. Kurikawa, H. Ishimoto, and S. Ogawa, Phys. Rev. B **45**, 12942 (1992).
[27] R. Radebaugh, NBC Technical Note, No. 362 (1967), p. 137.

Translated by Steve Torstveit

Self-consistent calculation of the spectrum of quasiparticles in a superfluid Bose liquid with a quenched Bose–Einstein condensate

É. A. Pashitskiĭ[a)]

Institute of Physics, National Academy of Sciences of Ukraine, pr. Nauki 46, 03650 Kiev, Ukraine

S. I. Vilchinsky[b)]

T. Shevchenko Kiev University, pr. Glushkova 2, 03142 Kiev, Ukraine

S. V. Mashkevich[c)]

N. N. Bogolyubov Institute of Theoretical Physics, National Academy of Sciences of Ukraine, ul. Metrologicheskaya 14-b, 03143 Kiev, Ukraine

(Submitted October 15, 2001)
Fiz. Nizk. Temp. **28**, 115–122 (February 2002)

An iterative method is used in a self-consistent calculation, at $T=0$, of the normal Σ_{11} and anomalous Σ_{12} self-energy parts, the boson polarization operator Π on the ''mass shell,'' and the quasiparticle spectrum $E(p)$ in a superfluid Bose liquid with an interaction-quenched single-particle Bose–Einstein condensate (BEC). The calculation is based on a system of ''truncated'' integral equations for Σ_{11} and Σ_{12} with allowance for terms of first order in the density $n_0/n \ll 1$ of the BEC and with the ''bare'' interaction between bosons taken in the form of the repulsive pseudopotential in the ''semitransparent spheres'' model, for which the Fourier component of the pseudopotential is an oscillatory sign-varying function of the momentum transfer. By fitting with a single adjustable parameter—the amplitude of the initial repulsive pseudopotential—one can achieve completely satisfactory agreement of the theoretical quasiparticle spectrum $E(p)$ with the measured spectrum of elementary excitations in superfluid helium from neutron-scattering experiments over a wide momentum range ($0 \leqslant p \leqslant p_{\max} \simeq 4$ Å^{-1}). © *2002 American Institute of Physics.* [DOI: 10.1063/1.1461918]

1. INTRODUCTION

An exact *ab initio* calculation of the spectrum of elementary excitations in a superfluid Bose liquid with a strong interaction between particles is an extremely complex (if not hopeless) problem of many-body quantum theory. Therefore, it is necessary to look for various simplified (model) approaches to the solution of this problem with the aid of various approximate analytical and numerical methods exploiting the small parameters available. One such parameter for a Bose liquid at a temperature close to zero ($T \to 0$) is the ratio of the density n_0 of the single-particle Bose–Einstein condensate (BEC), which is quenched on account of the interaction between bosons, to the total particle density n in the Bose liquid. According to the experimental data,[1,2] in ^{4}He at $T \ll 1$ K the ratio n_0/n is not more than 10% and can serve as an initial small parameter for constructing an approximate theoretical model of the superfluid state of a Bose liquid.

This paper is devoted to the further development of methods of numerical calculation of the quasiparticle spectrum in a superfluid Bose liquid with a quenched BEC in the framework of the approach proposed in Ref. 3 on the basis of the ''truncated'' Belyaev equations.[4] An iterative method is used to calculate the normal Σ_{11} and anomalous Σ_{12} self-energy parts and the boson polarization operator Π on the ''mass shell.'' As the zeroth iteration in calculating the polarization operator Π we use the Bogolyubov spectrum[5] for a repulsive potential in the ''semitransparent spheres'' model with a subsequent renormalization (''screening'') of this interaction due to many-particle (collective) effects in the process of a self-consistent calculation of the quasiparticle spectrum. It is shown that in the framework of this model, by the fitting of a single adjustable parameter—the amplitude of the repulsive pseudoparticle—one can achieve completely satisfactory agreement of the theoretical spectrum with the measured spectrum of elementary excitations in liquid ^{4}He from inelastic neutron-scattering experiments.[6,7]

2. CHOICE OF THE INITIAL INTERACTION POTENTIAL BETWEEN BOSONS

It was shown in Ref. 3 (see also Ref. 8) that at a low density of the BEC ($n_0 \ll n$) in the Bose liquid one can obtain a closed self-consistent system of integral equations for the normal $\Sigma_{11}(\mathbf{p},\omega)$ and anomalous $\Sigma_{12}(\mathbf{p},\omega)$ self-energy parts by truncating the infinite series of perturbation theory in powers of $\sqrt{n_0}$ (i.e., in the number of condensate lines), keeping only the leading terms of first order in the small parameter n_0/n.

In analytical form this system of ''truncated'' Belyaev–Dyson equations[4] has the form[3,8]

$$\tilde{\Sigma}_{11}(\mathbf{p},\varepsilon) = n_0 \Lambda(\mathbf{p},\varepsilon)\tilde{V}(\mathbf{p},\varepsilon) + n_1 V(0) + \Phi(\mathbf{p},\varepsilon); \quad (1)$$

$$\tilde{\Sigma}_{12}(\mathbf{p},\varepsilon) = n_0 \Lambda(\mathbf{p},\varepsilon)\tilde{V}(\mathbf{p},\varepsilon) + \Psi(\mathbf{p},\varepsilon). \quad (2)$$

Here $\tilde{V}(\mathbf{p},\varepsilon)$ is the renormalized (''screened'' on account of many-particle collective effects) pair interaction between bosons,

$$\tilde{V}(\mathbf{p},\varepsilon)=\frac{V(p)}{1-V(p)\Pi(\mathbf{p},\varepsilon)}; \tag{3}$$

$\Pi(\mathbf{p},\varepsilon)$ is the polarization operator of the bosons (see below), $\Gamma(\mathbf{p},\varepsilon;\mathbf{k},\omega)$ is the vertex part (three-pole) describing many-particle correlations of the local-field-effects type, $\Lambda(\mathbf{p},\varepsilon)=\Gamma(\mathbf{p},\varepsilon,0,0)$ is the vertex part with zero values of the incoming momentum and energy corresponding to the interaction with the BEC, $n_1=n-n_0$ is the number of ''above-condensate'' particles, and the functions Φ and Ψ, with allowance for the contribution of the poles of the single-particle normal $G_{11}(\mathbf{p},\varepsilon)$ and anomalous $G_{12}(\mathbf{p},\varepsilon)$ Green's functions, are determined by the integral equations

$$\Phi(\mathbf{p},\varepsilon)=-\frac{1}{2}\int\frac{d^3\mathbf{p}'}{(2\pi)^3}\Gamma(\mathbf{p},\varepsilon;\mathbf{p}',E(\mathbf{p}'))\times\tilde{V}(\mathbf{p}-\mathbf{p}',\varepsilon-E(\mathbf{p}'))\left[\frac{A(\mathbf{p}',E(\mathbf{p}'))}{E(\mathbf{p}')}-1\right]; \tag{4}$$

$$\Psi(\mathbf{p},\varepsilon)=-\frac{1}{2}\int\frac{d^3\mathbf{p}'}{(2\pi)^3}\Gamma(\mathbf{p},\varepsilon;\mathbf{p}',E(\mathbf{p}'))\times\tilde{V}(\mathbf{p}-\mathbf{p}',\varepsilon-E(\mathbf{p}'))\times\frac{n_0\Lambda(\mathbf{p}',E(\mathbf{p}'))\tilde{V}(\mathbf{p}',E(\mathbf{p}'))+\Psi(\mathbf{p}',E(\mathbf{p}'))}{E(\mathbf{p}')}, \tag{5}$$

where

$$A(\mathbf{p},E(\mathbf{p}))=n_0\Lambda(\mathbf{p},E(\mathbf{p}))\tilde{V}(\mathbf{p},E(\mathbf{p}))+\frac{\mathbf{p}^2}{2m}+\Phi(\mathbf{p},E(\mathbf{p}))-\Phi(0,0)+\Psi(0,0), \tag{6}$$

and $E(\mathbf{p})$ is the quasiparticle spectrum, which corresponds to the poles of the functions G_{11} and G_{12} and in general form is determined by the following relations:[9]

$$E(\mathbf{p})=\left\{\left[\frac{\mathbf{p}}{2m}+\Sigma_{11}^{s}(\mathbf{p},E(\mathbf{p}))-\mu\right]^2-\left|\Sigma_{12}(\mathbf{p},E(\mathbf{p}))\right|^2\right\}^{1/2}+\tilde{\Sigma}_{11}^{a}(\mathbf{p},E(\mathbf{p})), \tag{7}$$

where

$$\tilde{\Sigma}_{11}^{s,a}(\mathbf{p},\varepsilon)=\frac{1}{2}[\Sigma_{11}(\mathbf{p},\varepsilon)\pm\Sigma_{11}(-\mathbf{p},-\varepsilon)], \tag{8}$$

$$\mu=\Sigma_{11}(0,0)-\Sigma_{12}(0,0). \tag{9}$$

In the framework of the approximation under consideration, with allowance for Eqs. (1), (2), and (6), expression (7) takes the form

$$E(p)=\{A^2(\mathbf{p},E(p))-[n_0\Lambda(\mathbf{p},E(p))\tilde{V}(\mathbf{p},E(p))+\Psi(\mathbf{p},E(p))]^2\}^{1/2}+\frac{1}{2}[\Phi(p,E(p))-\Phi(-p,-E(p))]. \tag{10}$$

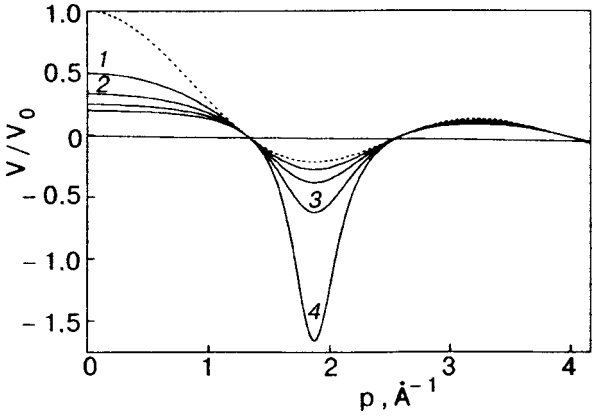

FIG. 1. Bare interaction (11) in the ''hard spheres'' model (dotted line) and the renormalized (''screened'') Fourier component of the pair interaction of bosons in the approximation of a constant screening parameter (22) for different values of α (solid curves): $\alpha=1$ (*1*), 2 (*2*), 3 (*3*), 4 (*4*).

In Ref. 10 an iterative method was used to calculate the quasiparticle spectrum $E(p)$ with the use of an initial interaction potential $V(p)$ in the form the renormalized Fourier component of the infinite repulsion $V(r)\to\infty$ for $r\leqslant a$ in the ''hard spheres'' model (Fig. 1); this Fourier component was obtained in Refs. 11 and 12 in the framework of the ''ladder'' approximation as

$$V(p)=V_0\frac{\sin pa}{pa}. \tag{11}$$

We note that the presence of the excluded volume for $r<a$ leads to a restriction on the applicability of potential (11) to the region of momentum space $p\leqslant 2\pi/a$, which corresponds to the accessible volume $r\geqslant a$.

In the numerical calculations in Ref. 10 the polarization operator $\Pi(\mathbf{p},\varepsilon)$ was calculated using as the zeroth iteration of the spectrum, $E_0(p)$, the Bogolyubov spectrum[5]

$$E_B(p)=\left\{\frac{p^2}{2m}\left[\frac{p^2}{2m}+2nV(p)\right]\right\}^{1/2} \tag{12}$$

with the oscillatory sign-varying potential (11), with a best fit to the experimental spectrum of the elementary excitations, $E_{\exp}(p)$, in liquid ^{4}He by adjustment of the two parameters V_0 and a (Fig. 2).

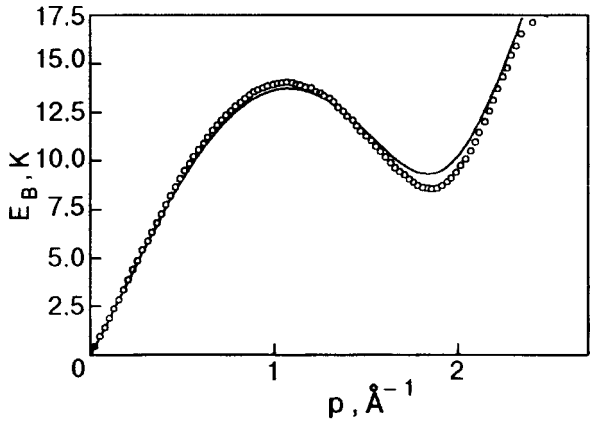

FIG. 2. Bogolyubov spectrum (12) (continuous curve) that best fits the experimental spectrum (data points) for $V_0/a^3=169$ K with $a=2.44$ Å.

In particular, for this spectrum $E_B(p) \cong E_{\exp}(p)$, the functions in the integrand in the expression for $\Pi(\mathbf{p},\omega)$ were calculated on the "mass shell" $\varepsilon = E(p)$:

$$\Pi(\mathbf{p},E(p)) = \frac{1}{2}\int \frac{d^3\mathbf{k}}{(2\pi)^3}\frac{[I_{11}(\mathbf{p},\mathbf{k})+I_{12}(\mathbf{p},\mathbf{k})]}{E(\mathbf{k})-E(\mathbf{k}-\mathbf{p})-E(\mathbf{p})}\Gamma(\mathbf{p},\mathbf{k}), \tag{13}$$

where

$$I_{11}(\mathbf{p},\mathbf{k}) = \frac{F_{11}(\mathbf{p},\mathbf{k})}{E(\mathbf{k})[E(\mathbf{k})+E(\mathbf{k}-\mathbf{p})-E(\mathbf{p})]} - \frac{D_{11}(\mathbf{p},\mathbf{k})}{E(\mathbf{k}-\mathbf{p})[E(\mathbf{k})+E(\mathbf{k}-\mathbf{p})+E(\mathbf{p})]}, \tag{14}$$

$$I_{12}(\mathbf{p},\mathbf{k}) = \frac{F_{12}(\mathbf{p},\mathbf{k})}{E(\mathbf{k})[E(\mathbf{k})+E(\mathbf{k}-\mathbf{p})-E(\mathbf{p})]} - \frac{D_{12}(\mathbf{p},\mathbf{k})}{E(\mathbf{k}-\mathbf{p})[E(\mathbf{k})+E(\mathbf{k}-\mathbf{p})+E(\mathbf{p})]}, \tag{15}$$

and the functions F_{11}, F_{12}, D_{11}, and D_{12} are given by the relations

$$F_{11}(\mathbf{p},\mathbf{k}) = \left[E(\mathbf{k})+\frac{k^2}{2m}-\mu+\Sigma_{11}(-\mathbf{k},-E(\mathbf{k}))\right] \times\left[E(\mathbf{k})-E(\mathbf{p})+\frac{(\mathbf{k}-\mathbf{p})^2}{2m}-\mu+\Sigma_{11} \times(-\mathbf{k}+\mathbf{p},-E(\mathbf{k})+E(\mathbf{p}))\right]; \tag{16}$$

$$D_{11}(\mathbf{p},\mathbf{k}) = \left[E(\mathbf{k}-\mathbf{p})+\frac{(\mathbf{k}-\mathbf{p})^2}{2m}-\mu+\Sigma_{11}(-\mathbf{k}+\mathbf{p}, -E(\mathbf{k}-\mathbf{p}))\right]\left[E(\mathbf{k}-\mathbf{p})-E(\mathbf{p}) +\frac{\mathbf{k}^2}{2m}-\mu+\Sigma_{11}(-\mathbf{k}-E(\mathbf{k}-\mathbf{p})+E(\mathbf{p}))\right]; \tag{17}$$

$$F_{12}(\mathbf{p},\mathbf{k}) = \Sigma_{12}(\mathbf{k},E(\mathbf{k}))\Sigma_{12}(\mathbf{k}-\mathbf{p},E(\mathbf{k})-E(\mathbf{p})); \tag{18}$$

$$D_{12}(\mathbf{p},\mathbf{k}) = \Sigma_{12}(\mathbf{k}-\mathbf{p},E(\mathbf{k}-\mathbf{p}))\Sigma_{12}(\mathbf{k},E(\mathbf{k}-\mathbf{p})-E(\mathbf{p})). \tag{19}$$

We used the approximation of a nondecaying spectrum of He II, which holds for $\varepsilon > \varepsilon_c \sim 10$ K. This approach is justified because the given model is not intended to be a detailed description of the phonon part of the spectrum at low phonon energies. Since

$$E(\mathbf{k}) < E(\mathbf{p})+E(\mathbf{k}-\mathbf{p}), \tag{20}$$

the total denominator in the integrand of Eq. (13) is negative at all momenta, while the functions $I_{11}(\mathbf{p},\mathbf{k})$ and $I_{12}(\mathbf{p},\mathbf{k})$ are positive, so that $\Pi(\rho) \equiv \Pi(\mathbf{p},E(p)) < 0$. Because of this, in the boson pair interaction renormalized ("screened") by collective effects,

$$\tilde{V}(p) \equiv \tilde{V}(\mathbf{p},E(p)) = \frac{V(p)}{1-V(p)\Pi(p)}, \tag{21}$$

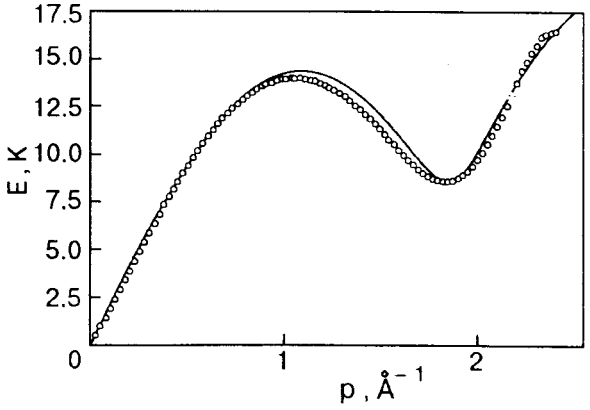

FIG. 3. Quasiparticle spectrum calculated in Ref. 10 in the "hard spheres" model (continuous curve) for parameter values $V_0/a^3 = 147$ K, $\alpha = 3.65$, $a = 2.44$ Å, and $m^* = 550m$. The data points show the experimental spectrum in ^{4}He.

the repulsion is weakened in the region $0 \leqslant pa \leqslant \pi$, where $V(p) > 0$, and the effective attraction is enhanced in the region $\pi < pa \leqslant 2\pi$, where $V(p) < 0$ (see Fig. 1). To simplify the calculations, in Ref. 10 the expression for $V(p)$ with allowance for (11) was approximated by the potential

$$\tilde{V}(p) = \frac{V(p)\sin(pa)}{pa+\alpha\sin(pa)}, \tag{22}$$

where $\alpha = V_0\overline{|\Pi(p)|}$ is a positive dimensionless parameter determined by the average value of the modulus of $\Pi(p)$ in the region $0 \leqslant pa \leqslant 2\pi$. The volume $\tilde{V}(p)$ is shown in Fig. 1 for various values of α.

Iterative numerical calculations were carried out in Ref. 10 for different values of the adjustable parameters V_0 and α at fixed values $a = 2.44$ Å, equal to twice the quantum radius of the ^{4}He atom, and $n_0 = 0.09n$, in accordance with the experimental data.[1,2] A third adjustable parameter was the effective mass m^* of the bosons in the Bose liquid, which was used in expression (6) in place of the mass m of the ^{4}He atom. The best agreement with $E_{\exp}(p)$ was achieved at the values $V_0/a^3 = 147$ K and $\alpha = 3.65$ (Fig. 3). The value obtained for the total particle density, 2.2×10^{22} cm^{-3}, is close to the experimental value; it was calculated by the formula

$$n = n_0 + n_1 = n_0 + \frac{1}{2}\int \frac{d^3\mathbf{p}}{(2\pi)^3}\left[\frac{A(\mathbf{p},E(\mathbf{p}))}{E(\mathbf{p})}-1\right]. \tag{23}$$

However, in order for the group velocity of the quasiparticles to agree with the velocity of first (hydrodynamic) sound $c_1 = 236$ m/s for $p \to 0$ an anomalously large value of the effective mass ratio, $m^*/m \cong 550$, is required. This is indicative of an unsatisfactory situation that arises with the use of the simplified potential (22) with a constant value of the "screening" parameter α. In addition, it is inconsistent to calculate the interaction in the framework of the "hard spheres" model with the use of formula (11), since the latter was obtained in the "ladder" approximation,[5,12] which is valid only for dilute Bose systems.

For a Bose liquid it is more suitable to use an approach analogous to the pseudopotential method in the theory of the solid state and which takes into account the quantum diffraction effects in the scattering of particles on one another. The

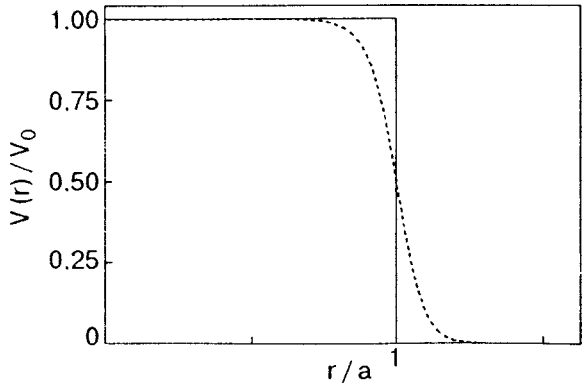

FIG. 4. Potential with finite repulsion in the ''semitransparent spheres'' model (solid curve) and the form of the ''Lindhard'' function (25) (dashed curve) in real space.

simplest example of such a ''quantum pseudopotential'' is the ''semitransparent spheres'' model with a finite repulsion $V(r)=V_0=\text{const}$ in the region $r\leqslant a$ and $V(r)=0$ for $r>a$ (Fig. 4). The Fourier component of such a potential has the form (Fig. 5)

$$W(p)=W_0\frac{\sin(pa)-pa\cos(pa)}{(pa)^3}, \tag{24}$$

where $W_0=3W(0)=6\pi V_0/a^3$. It should be emphasized that precisely such a Fourier component is obtained[13] for a smoother potential in the form of a ''Lindhard'' function of the radius r (see Fig. 4):

$$W(r)=\frac{V_0}{2}\left[1+\frac{1-r^2/a^2}{2r/a}\ln\left|\frac{a+r}{a-r}\right|\right], \tag{25}$$

which has an inflection point with an infinite derivative at $r=a$. This substantially widens the class of pseudopotentials characterized by sign-varying Fourier components with oscillations in momentum space, which are formally analogous to the well-known Ruderman–Kittel and Friedel oscillations in real space.[13,14]

We note that an oscillatory pseudopotential of the ''semitransparent spheres'' type (24) has been used previously[15] for calculating the Bogolyubov spectrum (12) with a ''roton'' minimum and is more convenient than the ''hard spheres''

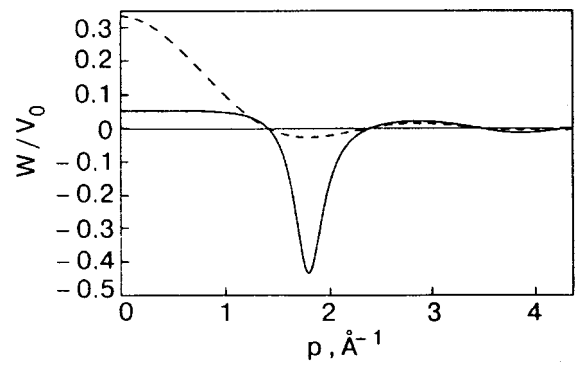

FIG. 5. Fourier component of the bare interaction $W(p)$ in the ''semitransparent spheres'' model (24) (dashed curve) and the renormalized interaction $\tilde{W}(p)$ with allowance for the momentum dependence of the polarization operator Π on the ''mass shell'' (solid curve).

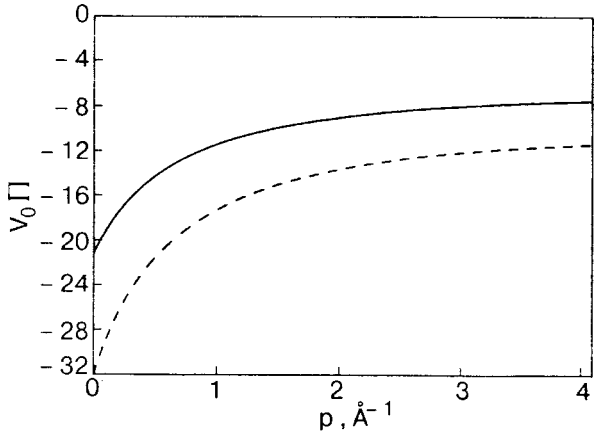

FIG. 6. Momentum dependence of the boson polarization operator on the ''mass shell,'' $\Pi(p)\equiv\Pi(\mathbf{p},E(p))$, obtained as a result of self-consistent calculations for $\Gamma=1$ and multiplied by V_0 (solid curve). The dashed curve shows $V_0\Pi(p)\Gamma$ for $\Gamma=1.5$.

potential (11), from the standpoint of both stability of the spectrum and its similarity to the empirical spectrum in ^{4}He.

In view of what we have said, in this paper we have used the pseudopotential (24) for calculating the quasiparticle spectrum (10) in a Bose liquid by self-consistent solution of the system of nonlinear integral equations (4)–(6).

3. ITERATION SCHEME AND THE QUASIPARTICLE SPECTRUM

For calculating the quasiparticle spectrum we first carried out a numerical calculation of the functions $\Phi_1(p)\equiv\Phi(p,E_0(p))$ and $\Psi_1(p)\equiv\Psi(p,E_0(p))$ to a first approximation with the use of the zeroth approximation for the ''screened'' pseudoparticle

$$\tilde{W}_0(p)=\frac{W(p)}{1-W(p)\Pi_0} \tag{26}$$

with a constant negative value of Π_0 and with the use of potential (24) and the Bogolyubov spectrum (12), which is close to $E_{\text{exp}}(p)$. Then, on the basis of the functions $\Phi_1(p)$ and $\Psi_1(p)$ obtained and the functions $\Sigma_{11}^1(p)$ and $\Sigma_{12}^1(p)$ corresponding to them we calculated the polarization operator $\Pi_1(0)$ using relations (13)–(19) for $\Gamma=1$. In this stage of the calculation, as in Ref. 10, as the zeroth iteration for the spectrum $E(p)$ we chose the Bogolyubov spectrum (12), which gives the best agreement of $E_{\text{exp}}(p)$ for liquid ^{4}He, but with potential (24) used instead of (11).

The limiting value $\Pi_1(0)$ was compared with the exact thermodynamic value of the polarization operator of a ^{4}He Bose liquid, which determines the compressibility of the Bose system, at $p=0$ and $\omega=0$:[16]

$$\Pi(0,0)=-\frac{n}{mc_1^2}. \tag{27}$$

The absolute value of (27) turned out to be almost one-and-one-half times as large as the calculated value of $|\Pi_1(0)|$. This made it possible to estimate the mean value of the vertex Γ_1 in the first approximation.

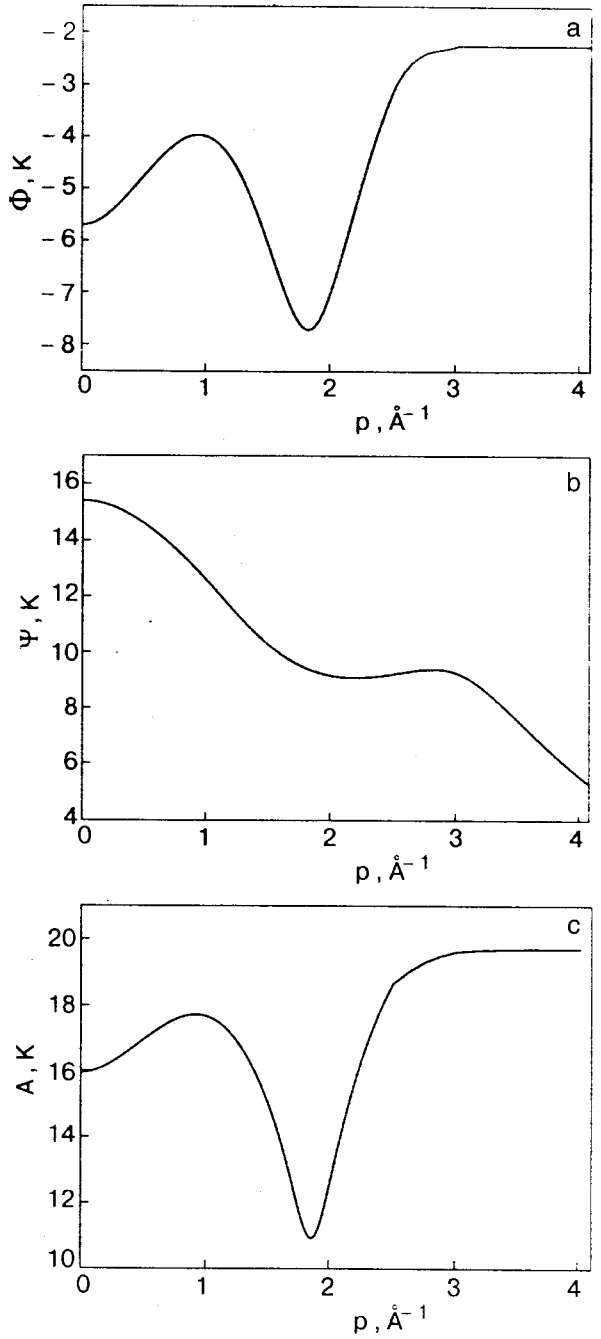

FIG. 7. Momentum dependence of the functions $\Phi(p)$ (a), $\Psi(p)$ (b), and $A(p)$ (c), all obtained as a result of self-consistent calculations with the parameter value $V_0/a^3=1552$ K.

The second approximation, $\Phi_2(p)$ and $\Psi_2(p)$, was obtained on the basis of Eqs. (4) and (5) using the constant value $\Gamma_1 \equiv \Lambda_1$ and the renormalized pseudopotential of the first approximation:

$$\tilde{W}_1(p)=\frac{W(p)}{1-W(p)\Pi_1(p)\Gamma_1}. \tag{28}$$

This iteration procedure was repeated several times (from 4 to 6) and was used to refine the polarization operator. At each step formulas (6) and (10) were used to reconstruct the quasiparticle spectrum $E(p)$ and to track the rate of convergence of the iterations and the degree of proximity of $E(p)$ to the empirical spectrum $E_{\exp}(p)$.

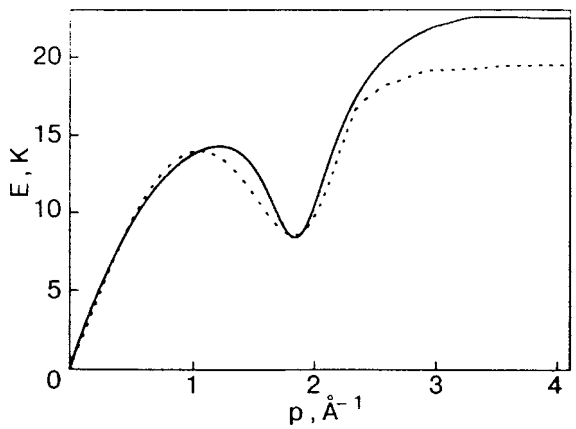

FIG. 8. Theoretical quasiparticle spectrum $E(p)$ obtained as a result of self-consistent calculations in the framework of the "semitransparent spheres" model. The dotted curve is the empirical spectrum of elementary excitations in liquid ^{4}He.

The only adjustable parameter of the fit was the amplitude V_0 of the initial pseudoparticle (24) for $a=2.44$ Å and $n_0=0.09n$ in (23). The theoretical spectrum $E(p)$ from the computer calculations was in completely satisfactory agreement with $E_{\exp}(p)$. Figures 6 and 7 show the final result (after 5 iterations) for the function $\Pi(p)$ and the self-consistent results for the functions $\Phi(p)$, $\Psi(p)$, and $A(p)$ found using relations (4)–(6).

The solid curve in Fig. 8 shows the theoretical quasiparticle spectrum $E(p)$ obtained after 5 iterations, and the dotted curve the experimental data[7] from inelastic neutron scattering in liquid ^{4}He up to momenta $p\simeq 4$ Å^{-1}. We see that completely satisfactory agreement of $E(p)$ with $E_{\exp}(p)$ is observed in the region $p\leqslant 2.5$ Å^{-1}. In the region $p>2.5$ Å^{-1} the theoretical spectrum $E(p)$ lies somewhat lower than $E_{\exp}(p)$, apparently because the vertex function $\Gamma(\mathbf{k},\mathbf{p})$, which falls off with increasing p, has been replaced by the constant value $\tilde{\Gamma}\simeq 1.5$ in the entire range of p. A characteristic feature of the spectrum obtained is the presence of weak oscillations in the region $p>2$ Å^{-1} (with a maximum $E_{\max}=22.63$ K at $p>2.98$ Å^{-1} and a minimum $E_{\min}=22.53$ K at $p=3.39$ Å^{-1}). The corresponding region of the spectrum is shown on an expanded scale in Fig. 9. The

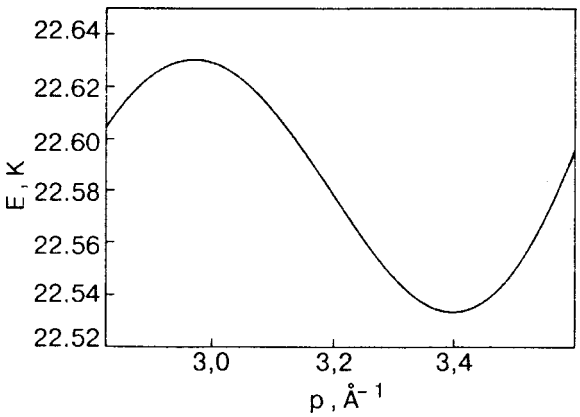

FIG. 9. Additional oscillations of the theoretical quasiparticle spectrum $E(p)$ in the region of large momenta (on an expanded scale).

presence of the ''repeated'' maximum and minimum is due to the oscillatory character of the initial potential (24) at large p.

The parameter V_0 was chosen such that the phase velocity $E(p\to 0)/p$ would agree with the hydrodynamic sound velocity $c_1 \simeq 236$ m/s in liquid ^{4}He, and it corresponds to a value $V_0/a^3 = 1552$ K for $a = 2.44$ Å. Then the value found from (22) for the total particle density, 2.12×10^{22} cm^{-3} at $n_0 = 0.09n$, is close to the experimental value of the total particle density in liquid ^{4}He.

4. CONCLUSIONS

In this study we have implemented a self-consistent iterative procedure for computer calculation of the spectrum of quasiparticles in a Bose liquid on the basis of the model developed in Refs. 3, 8, and 10: a closed model of the superfluid state with a quenched BEC ($n_0 \ll n$) and with a simple pseudopotential pair interaction in the ''semitransparent spheres'' approximation. We have shown that this approximation is much better than the ''hard spheres'' model, since it can give completely satisfactory agreement of the theoretical quasiparticle spectrum $E(p)$ with the empirical spectrum $E_{\rm exp}(p)$ for liquid ^{4}He over a wide range of momenta and with only one adjustable parameter.

The authors thank I. N. Adamenoko, É. R. Rudavskii, I. V. Simenog, and P. I. Fomin for helpful discussions.

One of the authors (V.S.I.) gratefully acknowledges the financial support for this study from DAAD of Germany.

[a)]E-mail: pashitsk@iop.kiev.ua
[b)]sivil@phys.univ.kiev.ua
[c)]E-mail: mash@mashke.org

[1] H. R. Glyde and E. C. Swensson, in *Neutron Scattering*, edited by D. L. Price and K. Skold, Vol. 23B of Methods of Experimental Physics, Academic Press, New York (1987), p. 303.
[2] A. F. G. Wyatt, Nature (London) **391**, 56 (1998).
[3] Yu. A. Nepomnyashchii and E. A. Pashitskii, Zh. Éksp. Teor. Fiz. **98**, 178 (1990) [Sov. Phys. JETP **71**, 98 (1990)].
[4] S. T. Belyaev, Zh. Éksp. Teor. Fiz. **34**, 417, 433 (1958) [Sov. Phys. JETP **289**, 299 (1958)].
[5] H. H. Bogolyubov, Izv. Akad. Nauk SSSR Ser. Fiz. **11**, 77 (1947); Physica (Amsterdam) **9**, 23 (1947).
[6] H. R. Glyde and W. G. Stirling, Phys. Rev. B **42**, 4224 (1990).
[7] K. H. Andersen, W. G. Stirling, R. Scherm, A. Stanault, B. Fak, H. Godfrin, and A. J. Dianoux, J. Phys.: Condens. Matter **6**, 821 (1994).
[8] É. A. Pashitskiĭ, Fiz. Nizk. Temp. **25**, 115 (1999) [Low Temp. Phys. **25**, 81 (1999)].
[9] A. A. Abrikosov, L. P. Gor'kov, and I. E. Dzyaloshinskiĭ, *Methods of Quantum Field Theory in Statistical Physics* [Prentice-Hall, Englewood Cliffs, NJ (1963); Fizmatgiz, Moscow (1962)].
[10] É. A. Pashitskiĭ and S. I. Vil'chinskiĭ, Fiz. Nizk. Temp. **27**, 253 (2001) [Low Temp. Phys. **27**, 185 (2001)].
[11] K. A. Bruckner and K. Sawada, Phys. Rev. **106**, 1117, 1128 (1957).
[12] K. A. Bruckner, *Theory of Nuclear Matter* [Russian translation], Mir, Moscow (1964).
[13] J. R. Schrieffer, *Theory of Superconductivity* [Benjamin, New York (1964); Nauka, Moscow (1970)].
[14] R. M. White, *The Quantum Theory of Magnetism* [McGraw-Hill, New York (1970); Mir, Moscow (1985)].
[15] É. A. Pashitskiĭ, Ukr. Fiz. Zh. (Russ. Ed.) **18**, 1439 (1973).
[16] Yu. A. Nepomnyashchiĭ and A. A. Nepomnyashchiĭ, Zh. Éksp. Teor. Fiz. **75**, 976 (1978) [Sov. Phys. JETP **48**, 493 (1978)].

Translated by Steve Torstveit

Asymmetry of relaxation processes and the creation of high-energy phonons in the anisotropic phonon systems of He II

I. N. Adamenko* and K. É. Nemchenko

V. N. Karazin Kharkov National University, pl. Svobody 4, 61077 Kharkov, Ukraine

A. F. G. Wyatt**

School of Physics, University of Exeter, Exeter, EX4 4QL, UK
(Submitted October 18, 2001)
Fiz. Nizk. Temp. **28**, 123–137 (February 2002)

A study is made of relaxation processes in anisotropic phonon systems in superfluid helium. The rates of creation and annihilation of high-energy (h) phonons in all possible processes in an anisotropic phonon system are obtained as functions of momentum, temperature, and the anisotropy parameter. The physical causes of the asymmetry in the creation and annihilation of h phonons are elucidated. All of the processes of interaction of h phonons with low-energy phonons (l phonons) and h phonons with each other are investigated, and the role of each of these processes in the formation of the distribution function of h phonons is determined. All of the processes that do not conserve the total number of h phonons are taken into account in constructing an equation describing the change in energy density of the h phonons in the main beam, and a quasistationary solution of this equation is found. The solution of this equation can be used to find the energy density of the created h phonons at any point in space at an arbitrary time and the energy density of l phonons in the main beam. © *2002 American Institute of Physics.* [DOI: 10.1063/1.1461919]

1. INTRODUCTION

The interaction of phonons in superfluid ^{4}He (He II) is determined by the dependence of the phonon energy ε on the momentum $\mathbf{p}$, which is written in the form

$$\varepsilon_i = c(p_i + f_i), \tag{1}$$

where c is the velocity of sound, and $f_i \equiv f(p_i)$ is a function describing the deviation of this dependence from linear. Although this deviation is small ($f_i \ll p_i$), it is what governs the different relaxation mechanisms in the phonon system of He II.

For momenta p_i less than a critical value p_c, the function $f_i(p_i < p_c) > 0$ (anomalous dispersion). At the saturated vapor pressure one has $cp_c/k_B = 10$ K.[1,2] In the case of anomalous dispersion the energy and momentum conservation laws allow processes that do not conserve the number of phonons. The fastest of these is a three-phonon process ($3pp$), in which one phonon decays into two or in which one phonon is obtained as a result of the interaction of two phonons. The rate ν_{3pp} of such a process in the limiting cases was obtained in Refs. 3 and 4 and was calculated in the general case in Ref. 5.

For $p_i > p_c$ the function $f_i < 0$. In this case the dispersion is normal, and three-phonon processes are forbidden by the energy and momentum conservation laws. As a result, for high-energy (h) phonons with $p_i > p_c$ the fastest process in the four-phonon process ($4pp$), in which the energy and momentum conservation laws hold:

$$\varepsilon_1 + \varepsilon_2 = \varepsilon_3 + \varepsilon_4, \tag{2}$$

$$\mathbf{p}_1 + \mathbf{p}_2 = \mathbf{p}_3 + \mathbf{p}_4. \tag{3}$$

Here and below we shall assume that phonon ''1'' has a momentum $p_1 \geqslant p_c$ (i.e., is an h phonon, denoted h_1), while the other three phonons can be h phonons or low-energy phonons (l phonons), for which $p_i < p_c$.

The rate ν_{3pp} of the three-phonon process can be calculated from the Landau Hamiltonian[6] in first order of perturbation theory, while the rate of the four-phonon processes is found in second order. In view of this we have the strong inequality

$$\nu_{3pp} \gg \nu_{4pp}. \tag{4}$$

As a result, the phonons of superfluid helium form two subsystems with substantially different relaxation times:

1) a subsystem of l phonons with $p_i < p_c$, in which equilibrium is rapidly established;

2) a subsystem of h phonons, with $p_i > p_c$, in which equilibrium is established relatively slowly.

The three-phonon processes only involve small angles. Therefore, in isotropic phonon systems they only slowly can bring about the establishment of equilibrium. As a result, the thermodynamic parameters of the l phonons are functions of direction.[7] The establishment of total equilibrium in the system of l phonons in the isotropic case is brought about by four-phonon processes and by diffusion in angular space, which is due to three-phonon processes.[8–10]

The situation is different in highly anisotropic phonon systems, in which the momenta of all the phonons lie within a narrow cone of solid angle Ω_p of the order of the characteristic angle of the three-phonon processes. In this case the presence of two phonon subsystems leads to the unique properties of the anisotropic phonon systems of He II observed in

experiments.[11–15] A theoretical description of anisotropic phonon systems was first given in Refs. 16 and 17.

Systems with a highly anisotropic distribution of phonons in momentum space have been created in liquid helium at such low temperatures that the presence of thermal excitations in it could be neglected.[11–15] Phonons were injected into this pure and isotropic superfluid liquid (superfluid vacuum) by means of a heater. The injected phonons move in the direction normal to the surface of the heater, so that in momentum space all of the phonons were found only in a narrow cone with solid angle $\Omega_p \ll 1$.

The experimental apparatus[11–15] for investigating the properties of highly anisotropic phonon systems contains a heater and a detector, both immersed in liquid ^{4}He at zero pressure and a temperature of the order of 0.05 K. The heater is a metal film deposited on glass. When a current pulse passes through the metallic film, a phonon pulse moving toward the detector is injected into the superfluid helium (superfluid vacuum). In the case when a gold film is used for the heater, all of the injected phonons occupy a solid angle $\Omega_p = 0.125$ sr in momentum space.[14] The dimensions of this highly anisotropic system in real space are determined by the area of the heater and the duration of the thermal pulse.

For thermal pulses with a duration of the order of 10^{-7} s at a power of the order of 10 mW/mm^2 released in the heater, a single phonon pulse at the heater gave two phonon pulses at the detector.[13] The appearance of two pulses at the detector, as was noted in Refs. 14 and 16, is explained by relation (1) and inequality (4). As a result of fast three-phonon processes the l phonons move as a unified whole at a velocity $c = 238$ m/s and give the first narrow pulse at the detector. The group velocity of the h phonons is less than 190 m/s. Because of the difference in group velocities of the l and h phonons, the h phonons form a second pulse, which moves toward the detector at a lower velocity and broadens as a result of the weak interaction and relatively large dispersion of the h phonons.

Subsequent experiments[18,19] showed irrefutably that the h phonons arriving at the detector are not injected by the heater together with the l phonons but are created in the main beam of l phonons. This raised the question of how could a cold beam of l phonons with a temperature of the order of 1 K create h phonons with energies $\varepsilon \geqslant 10$ *K*, an order of magnitude higher than the temperature of the main beam? The answer to this question was provided by the theory proposed in Refs. 16 and 17.

The subsequent development of the theory[20–22] showed that the relaxation time of h phonons in anisotropic phonon systems is substantially different from that in ordinary isotropic phonon systems, for which there is no preferred direction in momentum space. As a result, according to the estimates made in Ref. 22, in anisotropic phonon systems the steady-state energy distribution function of h phonons at $\varepsilon \approx \varepsilon_c$ is two orders of magnitude greater than the Bose–Einstein distribution and has a different momentum dependence.

In Ref. 22 the rates of creation and annihilation were calculated for the first two processes, in which the h phonons interact only with l phonons (see Sec. 3). In the present paper we give the results of calculations of the creation and annihilation rates in slightly anisotropic phonon systems for all five processes describing the interaction of h phonons with l phonons and h phonons with each other. This allows one to consider the conversion of l phonons into h phonons with all five processes taken into account. In addition, unlike Refs. 16 and 17, we have taken into account the increase in volumes occupied by the beams of l and h phonons. The results obtained in this paper show that it is important to take the volume change into account when comparing the calculated values with the experimental data,[11–15] which were obtained using a heater of the order of 1 mm^2 in area, with a distance of more than 10 mm from the heater to the detector.

2. ASYMMETRY OF THE CREATION AND ANNIHILATION PROCESSES FOR *h* PHONONS IN ANISOTROPIC PHONON SYSTEMS

The strong inequality (4) and all of the characteristic times of the problem allow us to assume that the establishment of equilibrium in the l-phonon subsystem occurs instantaneously, and the energy distribution of the l phonons is described by the Bose–Einstein function

$$n_i^{(0)} = (e_i^{\varepsilon}/T - 1)^{-1}. \tag{5}$$

The establishment of equilibrium in the h-phonon subsystem is described by the kinetic equation

$$\frac{dn_i}{dt} = N_b - N_d. \tag{6}$$

Here $n_i \equiv n(\mathbf{p}_i)$ is the distribution function of phonons with momentum $\mathbf{p}_i$,

$$N_b = \int_{\Omega_b} W n_3 n_4 (1+n_1)(1+n_2)\,\delta(\varepsilon_1+\varepsilon_2-\varepsilon_3-\varepsilon_4) \times \delta(\mathbf{p}_1+\mathbf{p}_2-\mathbf{p}_3-\mathbf{p}_4)\,d^3p_2 d^3p_3 d^3p_4 \tag{7}$$

is the increase per unit time in the number of h_1 phonons with momentum $\mathbf{p}_1$ as a result of the four-phonon interaction,

$$N_d = \int_{\Omega_d} W n_1 n_2 (1+n_3)(1+n_4)\,\delta(\varepsilon_1+\varepsilon_2-\varepsilon_3-\varepsilon_4) \times \delta(\mathbf{p}_1+\mathbf{p}_2-\mathbf{p}_3-\mathbf{p}_4)\,d^3p_2 d^3p_3 d^3p_4 \tag{8}$$

is the decrease in the number of h_1 phonons per unit time, $W = W(\mathbf{p}_1, \mathbf{p}_2 | \mathbf{p}_3, \mathbf{p}_4)$ is a function that determines the transition probability density, Ω_b and Ω_d form the set of maximum possible values of the angle variables Ω_{bi} and Ω_{di} ($i = 2,3,4$) of the phonons taking part in the creation (b) and annihilation (d) processes, respectively, for phonons with momentum $\mathbf{p}_1$. In the isotropic case $\Omega_{bi} = \Omega_{di} = 4\pi$. In the anisotropic case Ω_{bi} and Ω_{di} are determined by Ω_p.

According to Eq. (6), the steady state of the h-phonon subsystem is determined by the equation

$$N_b = N_d. \tag{9}$$

In the isotropic case, when $\Omega_b = \Omega_d$, relations (7)–(9) yield the equation

$$n_3 n_4 (1+n_1)(1+n_2) = n_1 n_2 (1+n_3)(1+n_4). \tag{10}$$

The solution of equation (10) with Eqs. (2) and (3) taken into account is the Bose–Einstein distribution (5).

We define the rate of creation $\nu_b^{(n)}$ and annihilation $\nu_d^{(n)}$ of phonons with momentum $\mathbf{p}_1$ for an arbitrary distribution function $n(\mathbf{p})$ by the relations

$$N_b = n_1^{(0)} \nu_b^{(n)}; \quad N_d = n_1 \nu_d^{(n)}. \tag{11}$$

The creation and annihilation rates calculated for the Bose–Einstein distribution (5) according to formulas (7), (8), and (11) will be denoted by $\nu_b^{(0)}$ and $\nu_d^{(0)}$, respectively. In an isotropic phonon system, according to Eqs. (9) and (10), these rates are equal. However, in an anisotropic phonon system, when $\Omega_b \neq \Omega_d$, these rates are not equal, and, according to Eqs. (6) and (11), their difference

$$\nu_b^{(0)} - \nu_d^{(0)} = \frac{1}{n_1^{(0)}} \frac{dn_1}{dt} \tag{12}$$

governs the relative rate of change of the initial Bose–Einstein distribution in the phonon system.

We give the results of calculations of the rates of creation $\nu_b^{(0)}$ and annihilation $\nu_d^{(0)}$ for phonons whose momentum $\mathbf{p}_1$ is directed along an axis of symmetry of an anisotropic phonon system with $\Omega_p \ll 1$. We shall drop the superscript (0) from the notation for these rates, denoting them $\nu_{b,d}$.

We write the integrals (7) and (8) in a spherical coordinate system with the polar axis along the symmetry axis z of the phonon system, so that $\mathbf{p}_i = (p_i, \theta_i, \varphi_i)$. In Eqs. (7) and (8) we do the integration over the variables p_4, φ_3, and φ_4, making use of the δ functions. The integration over φ_2 involves rather complicated integrals containing special functions. The situation is simplified considerably if $\theta_1 = 0$. In that case relations (7), (8), and (11) yield the following relation for the rates of creation (b) and annihilation (d) of a phonon moving along the z axis:

$$\nu_{b,d} = \int dp_2 \int dp_3 \int_0^{\zeta_{b,d}^{(2)}} d\zeta_2 \int_0^{\zeta_{b,d}^{(3)}} d\zeta_3 \int_0^{\zeta_{b,d}^{(4)}} d\zeta_4 W \frac{n_0}{c} \times \delta(p_2\zeta_2 - p_3\zeta_3 - p_4\zeta_4 - \Phi) p_2^2 p_3^2 p_4^2 \frac{8\pi}{\sqrt{R}} \eta(R), \tag{13}$$

where the upper limits of integration for the variables $\zeta_i = 1 - \cos\theta_i$ are determined by the anisotropy parameter,

$$\zeta_p = 1 - \cos\theta_p = \frac{\Omega_p}{2\pi}, \tag{14}$$

and have the values

$$\zeta_b^{(2)} = 2, \quad \zeta_b^{(3)} = \zeta_p, \quad \zeta_b^{(4)} = \zeta_p, \tag{15}$$

$$\zeta_d^{(2)} = \zeta_p, \quad \zeta_d^{(3)} = 2, \quad \zeta_d^{(4)} = 2. \tag{16}$$

The function $n_0 = n_2^{(0)}(1 + n_3^{(0)})(1 + n_4^{(0)})$ contains the distribution function (5); $p_4 = p_1 + p_2 - p_3 - \Phi$ is a function of the independent variables p_2 and p_3,

$$\Phi = f_3 + f_4 - f_1 - f_2; \tag{17}$$

$\eta(R)$ is a step function, equal to 1 for a positive value of the argument and to zero for a negative value, and

$$R = 4p_{3\perp}^2 p_{4\perp}^2 - (p_{2\perp}^2 - p_{3\perp}^2 - p_{4\perp}^2)^2 \quad \text{and} \quad p_{nt} = p_i \sin\theta_i.$$

The function W was obtained in Ref. 22 and is given by

$$W = \frac{(u+1)^4}{2^7 \pi^5 \hbar^7 \rho^2} p_1 p_2 p_3 p_4 m^2. \tag{18}$$

where ρ is the density of the liquid helium, $u = (\rho/c) \times (\partial c/\partial \rho)$ is the Grüneisen constant, and

$$m = \frac{(p_1+p_2)^2}{\zeta_2 p_1 p_2 + (p_1+p_2)(f_1+f_2-f_{1+2})} - \frac{(p_1-p_3)^2}{\zeta_3 p_1 p_3 + (p_1-p_3)(f_3+f_{1-3}-f_1)} - \frac{(p_1-p_4)^2}{\zeta_4 p_1 p_4 + (p_1-p_4)(f_4+f_{1-4}-f_1)} \tag{19}$$

is the matrix element corresponding to the three different intermediate states.

The asymmetry of the creation and annihilation processes in anisotropic phonon systems comes in through the different upper limits of integration in (15) and (16) for the variables ζ_i. Because of this asymmetry, the integration of the delta function in (13) for ν_b should be done with respect to the variable ζ_2 which has the largest accessible range; similarly for ν_d it should be done with respect to the variable ζ_4.

Integrating (13) over the variable ζ_2, we obtain

$$\nu_b = N p_1 \int dp_2 \int dp_3 n_0 \frac{p_2^2 p_2^3 p_4^3}{|p_1 - p_4|} I_b. \tag{20}$$

Here

$$I_b = \int_0^{\zeta_p} d\zeta_3 \int_0^{\zeta_p} d\zeta_4 m^2 \frac{\pi^{-1}}{\sqrt{R_b}} \eta(R_b), \tag{21}$$

where

$$R_b = (\zeta_3 - \zeta_{3-}^{(b)})(\zeta_{3+}^{(b)} - \zeta_3), \tag{22}$$

$$\zeta_{3\pm}^{(b)} = \left(\frac{p_4}{p_1 - p_4}\right)^2 \times [\sqrt{\zeta_4} \pm \sqrt{p_1 p_2 / p_3 p_4}\sqrt{\zeta_4 - [(p_2 - p_3)/p_1 p_4]\Phi}]^2; \tag{23}$$

$$N = \frac{2(1+u)^4}{(4\pi)^3 \rho^2 \hbar^7 c}.$$

The integration in (13) over the variable ζ_4 gives

$$\nu_d = N p_1 \int dp_2 \int dp_3 n_0 \frac{p_2^3 p_3^2 p_4^2}{p_1 + p_2} I_d. \tag{24}$$

Here

$$I_d = \int_0^{\zeta_p} d\zeta_2 \int_0^{2} d\zeta_3 m^2 \frac{\pi^{-1}}{\sqrt{R_d}} \eta(R_d), \tag{25}$$

where

$$R_d = (\zeta_3 - \zeta_{3-}^{(d)})(\zeta_{3+}^{(d)} - \zeta_3); \tag{26}$$

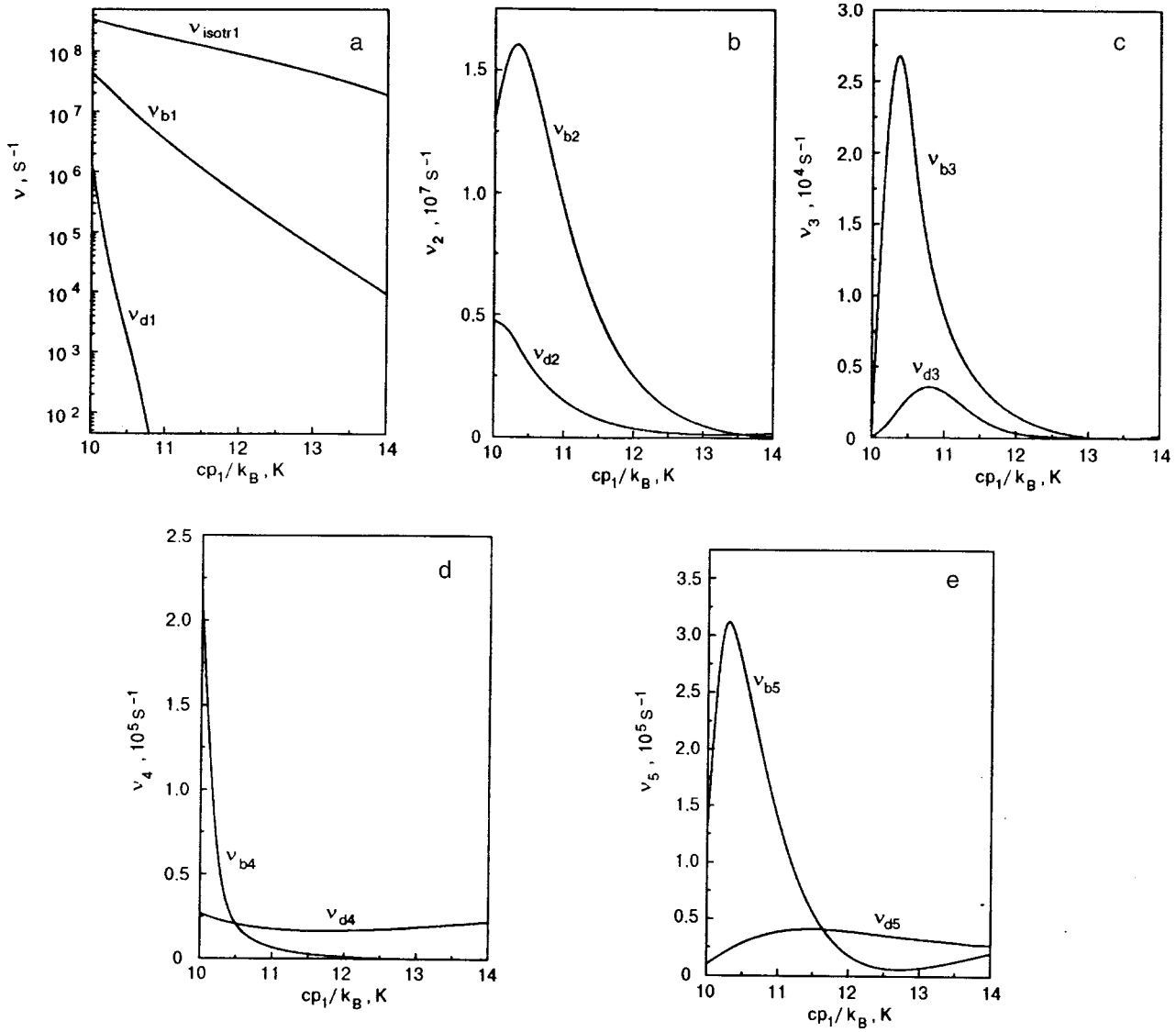

FIG. 1. Momentum dependence of the rates of creation and annihilation at $T=1$ K and $\theta_p=11.4°$ for the five types of processes (a–d for processes 1–5, respectively).

$$\zeta_{3\pm}^{(d)}=\left(\frac{p_2}{p_1+p_2}\right)^2 \times[\sqrt{\zeta_2}\pm\sqrt{p_1p_4/p_2p_3}\sqrt{\zeta_2-[(p_1+p_2)/p_1p_2]\Phi}]^2. \tag{27}$$

According to (27)

$$\zeta_2\geqslant\zeta_{2\,\min}=\frac{p_1+p_2}{p_1p_2}\Phi. \tag{28}$$

For $\Phi>0$ the annihilation process can occur only in systems with

$$\zeta_p>\zeta_{2\,\min}. \tag{29}$$

According to (23), the process of creation of an h_1 phonon can occur in the case when

$$\zeta_4\geqslant\zeta_{4\,\min}=\frac{p_2-p_3}{p_1p_4}\Phi. \tag{30}$$

Inequality (30) leads to a restriction different from (29) on the anisotropy parameter for creation processes:

$$\zeta_p>\zeta_{4\,\min}. \tag{31}$$

In anisotropic phonon systems at certain values of p_1 a situation can arise in which inequality (29) does not hold but (31) does. In that case the lifetime of the h_1 phonons will be infinite, while the rate of creation is nonzero (see Fig. 1a). As a result, the number of these h_1 phonons will increase, and a steady state can be established in the h-phonon subsystem only by other processes. We note that relations (28) and (30) can be obtained from the conservation laws (2) and (3), since inequalities (27) and (23) are the result of integrating (13) with delta functions containing the conservation laws for energy (2) and momentum (3).

In the majority of cases considered below, restriction (31) for the creation of h_1 phonons is weaker than restriction (29). Furthermore, relation (20) contains the difference $|p_1-p_4|$ in the denominator, while relation (24) contains the sum (p_1+p_2). Therefore, in the majority of cases the rate ν_b is higher than rate ν_d. As a result, the steady-state energy distribution function of the h phonons in highly anisotropic phonon systems for $\varepsilon\approx\varepsilon_c$ is substantially larger than the

Bose–Einstein distribution and has a different momentum dependence.

It should be stressed particularly that this asymmetry of the creation and annihilation processes arises only in highly anisotropic phonon systems, when $\zeta_p \ll 1$. In isotropic phonon systems, when $\zeta_p = 2$, Eq. (20) will give the same result as Eq. (24), since they differ from each other only by the different ways of integrating Eq. (13), which for $\zeta_p = 2$ is identical for creation and annihilation processes. As a result, the steady-state distribution function in isotropic phonon systems is the Bose–Einstein distribution.

3. RATES OF CREATION AND ANNIHILATION IN SLIGHTLY ANISOTROPIC PHONON SYSTEMS

There are five different types of four-phonon interaction processes between an h_1 phonon and l phonons and other h phonons:

$$1)\ h_1 + l_2 \leftrightarrow l_3 + l_4; \quad 2)\ h_1 + l_2 \leftrightarrow h_3 + l_4;$$
$$3)\ h_1 + l_2 \leftrightarrow h_3 + h_4; \quad 4)\ h_1 + h_2 \leftrightarrow h_3 + l_4;$$
$$5)\ h_1 + h_2 \leftrightarrow h_3 + h_4. \tag{32}$$

A rightward arrow indicates a decay process, and a leftward arrow the creation of an h_1 phonon.

The limits of integration in (20) and (24) over the variables p_2 and p_3 are determined by: 1) the type of creation or annihilation process; 2) the conservation laws (2) and (3); 3) the sign of Φ, which determines the ''switching on'' of the η functions in the integrands of (20) and (24) in association with inequality (31) for creation and (29) for annihilation processes.

After the limits of integration are found, the integration of expressions (20) and (24) can be done numerically to obtain the dependence of the rates of creation and annihilation in processes (32) on the main parameters of the problem: p_1, T, and θ_p. Figure 1 shows the dependence on p_1 thus obtained for fixed values $T = 1$ K and $\theta_p = 11.4°$ ($\zeta_p = 2 \times 10^{-2}$), which are typical for the experiments of Refs. 14 and 15. At constant values of the temperature and p_1, all of the rates are monotonically decreasing functions of the parameter ζ_p. Figure 1a shows the rate for the first process in the isotropic case,

$$\nu_{\text{isotr}} = \nu_{b1}(\zeta_p = 2,\ T = 1K) = \nu_{d1}(\zeta_p = 2,\ T = 1K). \tag{33}$$

At fixed values of p_1 and ζ_p all of the rates are monotonically decreasing functions of temperature.

To elucidate the physical causes of the dependences obtained for the creation and annihilation rates, it is necessary to supplement the computer calculations with analytical calculations according to formulas (20), (21) and (24), (25). Such calculations for the processes of the first and second types (32) were carried out in Ref. 22. Since the analytical calculations for processes of the third, fourth, and fifth types are analogous to those in Ref. 22, here we shall describe only the main steps and the results of the calculations.

In expression (25) the integration can be done over both variables ζ_2 and ζ_3 in terms of elementary functions.[22] However, the awkwardness of the result makes it very difficult to use for further analytical calculations in (24). Expression (21) can be integrated with respect to the variable ζ_3. Further integration with respect to the variable ζ_4 for $\zeta_p \ll 1$ cannot be done in terms of elementary functions. For this reason we made an analytical approximation of integrals (21) and (25) by calculations that go essentially as follows.

For each of the five creation processes $j = b1$, $b2$, $b3$, $b4$, $b5$ and annihilation processes $j = d1$, $d2$, $d3$, $d4$, $d5$ we find the values of all the typical angles $\zeta_{ti}^{(j)}$ ($i = 2, 3, 4$). The angles $\zeta_{ti}^{(j)}$ for $\zeta_p \ll 1$ are calculated by proceeding from expressions (23) and (27) and the delta function contained in (13). Then the ζ_i in expressions (21) and (25) are replaced by their typical values $\zeta_{ti}^{(j)}$. Then the integration is performed.

The analytical approximations (21) and (25) were substituted into Eqs. (20) and (24), respectively. For the functions f_i contained in (13), (21), and (25), we used the analytical approximation proposed in Ref. 22. The integrals (20) and (24) thus obtained cannot be expressed in terms of elementary functions. Therefore, in this case also the analytical approximation was carried out by an analogous scheme. In the integrands of (20) and (24) the arguments in the slowly varying functions of p_2 and p_3 were replaced by their typical values p_{2t} and p_{3t}. Then the integration over the variables p_2 and p_3 was performed.

The analytical expressions thus obtained for all ten rates give numerical values close to the results of the computer calculations. We will not write out these analytical expressions here but will only give a brief discussion of what they imply about the physical causes of the the observed dependence of the creation and annihilation rates on the parameters p_1, ζ_p, and T.

The first process, which involves an exchange of phonons between the h and l subsystems, is extremely important in the formation of the distribution function of the h phonons. As we shall show below, it is the first process that is mainly responsible for the conversion of l phonons into h phonons, the process by which the beam of h phonons detected in Ref. 13 was produced by the main beam of l phonons.

The decrease of ν_{b1} with increasing p_1 (Fig. 1a) is due to the momentum dependence of the matrix element m (19), which is contained in Eq. (21). The inequality $\nu_{b1} \ll \nu_{\text{isotr1}}$ and its increase with increasing p_1 is due to the strong anisotropy of the system ($\zeta_p \ll 1$) and to restriction (31). In contrast to the isotropic case (33), for $\zeta_p \ll 1$ the creation rate is substantially higher than the annihilation rate. At the parameter values realized in the experiments,[15] viz., $\theta_p = 11.4°$ ($\zeta_p = 2 \times 10^{-2}$) and $T = 1$ K, the minimum ratio $(\nu_{b1}/\nu_{d1})_{p_1 = p_c} = 30$, and this ratio goes to infinity for $cp_1/k_B = cp_0/k_B \approx 11$ K. The great difference in the values and momentum dependence of the rates ν_{b1} and ν_{d1}, which may be seen in Fig. 1a, is due to the strong anisotropy of the system and to the fact that in the first process it is always the case that $p_1 > p_2$ and $\Phi > 0$. As a result, for $\zeta_p \ll 1$ inequality (29) leads to much greater restrictions than (31). For example, according to (30), for any p_1, values of p_2 and p_3 are always found for which inequality (31) holds, and the rate ν_{b1} is nonzero for any p_1. The situation is different for the annihilation process, when, according to (28), there exists a momentum $p_1 = p_0$ such that inequality (29) does not hold above this value. As a result, $\nu_{d1}(p_1 > p_0) = 0$, and the lifetime of such phonons in respect to the first process is infinite.

An analytical expression for p_0 can be obtained from relations (28) and (29) as follows. We expand the functions f_i contained in Φ (17) about the following characteristic values of the momenta: the functions $f_{1,3}$ about p_c, and f_4 about p_2. We find the minimum value $\zeta_{2\ \min}$ by substituting in the right-hand side of (28) the maximum value of the momentum p_2, which for the first process, according to Eq. (2), is equal to $p_{2\,\mathrm{up}}=2p_c-p_1$. Proceeding from Eq. (29), we obtain the equation

$$\zeta_p=\zeta_{2\ \min}(p_2=p_{2\mathrm{up}};\ \ p_1=p_0),$$

which can be used to estimate an upper bound on p_0:

$$p_0=p_c\left(1+\sqrt{\zeta_p c/2p_c}\left|\frac{\partial^2\varepsilon}{\partial p^2}\right|^{-1/2}_{p=p_c}\right). \tag{34}$$

For $\zeta_p=2\times10^{-2}$ relation (34) gives a value $cp_0/k_B=11$ K, which agrees with the results of a computer calculation, which are presented in Fig. 1a.

Because of the infinite lifetime and finite creation rate of phonons with $p_1>p_0$, the first process cannot bring about dynamic equilibrium between the h- and l-phonon subsystems in an anisotropic phonon system. This equilibrium must be established by other processes.

For the second process, as follows from Fig. 1b, $\nu_{b2}>\nu_{d2}$ in the entire momentum range for the reasons indicated above. Unlike the case of the first process, ν_{d2} does not vanish at any values of p_1, since in the second process for $p_1<p_3$ the function $\Phi<0$, and restriction (29) is absent, since here, according to (28), $\zeta_{2\ \min}<0$.

The second process conserves the total number of h phonons. It is therefore obvious that as the momentum p_1 deviates from the symmetry axis z of the anisotropic phonon system (i.e., with increasing θ_1) the rate ν_{b2} should decrease and ν_{d2} increase, so that, starting at a certain value $\theta_1=\theta_{c1}$, the rate of creation of h_1 phonons should become smaller than the rate of annihilation. As a result, the second process will lead to a concentration of h phonons near the z axis in momentum space.

The fifth process (Fig. 1e) is largely analogous to the second. The function Φ (17) can have different signs, depending on the relationship between the momenta of the phonons taking part in the process. The fifth process, like the second, conserves the total number of h phonons and also leads to a concentration of h phonons near the z axis in momentum space.

The tendency of h phonons to concentrate near the z axis was observed in the experiments of Ref. 14, where the h phonons moved in a 4° cone while the l phonons moved in an 11.4° cone.

For the third process (Fig. 1c) $\nu_{b3}>\nu_{d3}$, since at all values of the momenta the function $\Phi>0$ and restriction (29) is always present. The rates ν_{b3} and ν_{d3} go to zero for $p_1\to p_c$, since the variable p_3 has a vanishing volume in momentum space, which in the third process is delimited by the inequality $p_c\leqslant p_3\leqslant p_1$. For this reason, at $p_1\to p_c$ the rate ν_{b5} (Fig. 1e) goes to zero and the rates ν_{d5} (Fig. 1e) and ν_{b2} (Fig. 1b) decrease. The presence of a maximum in the momentum dependence of these rates and their subsequent monotonic decrease with increasing momentum, like the monotonically decreasing character of the momentum dependence of the other rates (Fig. 1), is mainly due to the momentum dependence of the matrix element m (19). The decrease of m with increasing momentum is explained by the mutual compensation of the different terms in (19). In a number of cases this compensation breaks down for $cp_1/k_B>13$ K, and the matrix element becomes an increasing function of momentum. In particular, this leads to a minimum on the momentum dependence of the rates ν_{d4} (Fig. 1d) and ν_{b5} (Fig. 1e).

Along with the first process, the fourth process also plays an important role in the formation of the distribution function of h phonons in anisotropic phonon systems. For the fourth process (Fig. 1d) the rate $\nu_{d4}>\nu_{b4}$ in that region of momenta where $\nu_{d1}=0$. This result is due to the fact that for any relationship between the momenta of the phonons taking part in the fourth process, the function Φ is always less than zero. As a result, for the annihilation processes, according to (28), restriction (29) is absent, while at the same time for the creation processes, according to (30), restriction (31) comes into play for $p_2<p_3$. It should be kept in mind here that, unlike ν_{b1}, the rate $\nu_{d4}^{(n)}$ increases with increasing number of h phonons and in the steady state is substantially larger than the rate ν_{d4} calculated with the Bose–Einstein distribution. This circumstance leads to the appearance of a multiplicative factor containing the annihilation rate for the fourth process in the expression for the average value of the energy density of h phonons in the quasisteady case (see Sec. 5).

For all five processes the creation and annihilation rates decrease monotonically with decreasing temperature. Thus, in the temperature region of interest for the experiments of Refs. 11–15, from 1 to 0.7 K, the rates ν_{b1} and ν_{d1} decrease by factors of ≈5 and ≈6, respectively, while ν_{b2} and ν_{d2} decrease by ≈9 and ≈6 times, ν_{b3} and ν_{d3} by ≈70 and ≈65 times, ν_{b4} and ν_{d4} by ≈80 and ≈95 times, and ν_{b5} and ν_{d5} by ≈85 and ≈100 times.

The temperature dependence is stronger for processes involving four h phonons or three h phonons and one l phonon. As a result, for the fourth and fifth processes in the indicated temperature region the dependence is close to $\exp(-10.5/T)$, and for the third process it is close to $\exp(-10/T)$. This type of temperature dependence for the third, fourth, and fifth processes is mainly due to the presence of the function n_0 in the integrands of (20) and (24).

The second process involves two h phonons and two l phonons. In this case the temperature dependence of the rates looks smoother,[22] but in the interval $0.7\ \mathrm{K}\leqslant T\leqslant1\ \mathrm{K}$ it is approximated quite well by an $\exp(-5/T)$ dependence.

For the first process the temperature dependence is weaker than for the rest, since here only one h_1 phonon and three l phonons take part. For the first process, as for the second, the temperature dependence is rather complicated,[22] but for $0.7\ \mathrm{K}\leqslant T\leqslant1\ \mathrm{K}$ it is well approximated by the function $\exp(-4/T)$.

The dependence of the rates on ζ_p derives, first, from the circumstance that in the initial state the phonons move at angles smaller than θ_p to the z axis. This requirement leads to a linear dependence on ζ_p. Second, additional restrictions on the integration volumes in momentum space are imposed by the conservation laws (2) and (3) and the inequality

$\zeta_p \ll 1$. This restriction leads to an additional power-law dependence on ζ_p and in a number of cases is quite restrictive.

These requirements and restrictions cause the creation and annihilation rates in anisotropic phonon systems with $\zeta_p \ll 1$ to be substantially lower than the corresponding rates in the isotropic case.

4. EVOLUTION OF A PHONON BEAM PRODUCED BY A HEATER IN He II

The phonon beam produced by the heater in the experiments of Refs. 11–15 is an anisotropic phonon system. Let us briefly describe the main stages in the evolution of such a phonon beam.

When a current pulse of duration t_p is passed through a metal film immersed in liquid helium at $T \approx 0.05$ K, every point of the heated film emits phonons into the He II within a narrow cone of solid angle Ω_p, the value of which is determined by the small parameter c/c_s. Here c_s is the speed of sound in the film material. In the experiments of Refs. 11–15 the film was made of gold, for which $\Omega_p = 0.125$ sr, and pulses of various durations from 10^{-8} to 10^{-5} s were used.

The phonons emitted by a solid have the distribution function[23]

$$n_s = A(e^{\varepsilon/T_s} - 1)^{-1}, \tag{35}$$

where $A \approx 4\rho c/\rho_s c_s \ll 1$, and T_s and ρ_s are the temperature and density of the solid. The function (35) is a nonequilibrium distribution with respect to three-phonon processes. Therefore, over a time $\tau_{3pp} \approx 10^{-10}$ s the l phonons instantaneously (on the scale of t_p) come to a state of equilibrium with respect to energies and have a Bose–Einstein distribution (5) with a temperature $T = A^{1/4} T_s$, which was of the order of 1 K in the experiments.[11–15] Then the h phonons produced by the heater essentially disappears into the so-called "background"[18] that forms near the heater on account of, in particular, the nonideality of its surface.[24,25] Experimental studies of this "background" were carried out in Refs. 26 and 27.

The beam of l phonons formed, with an energy distribution function (5), move toward the detector as a unified whole ($\tau_{3pp} \ll t_p$) with a velocity $c = 238$ m/s. However, such an anisotropic phonon system containing only l phonons is not in equilibrium, since the distribution distribution function must also contain a "tail" formed by h phonons. Therefore, the main part of the beam, consisting of l phonons, generates this "tail" at a rate ν_{b1} (see Fig. 2).

The h phonons created have a group velocity $c_h \approx 190$ m/s, which is less than c, and are relatively weakly coupled ($\nu_{3pp} \gg \nu_{4pp}$) with the l phonons. As a result, the h phonons leave the main beam through its rear plane. The escape of the h phonons leads to a deficit of such phonons in the main beam, which the l phonons compensate by forming new h phonons at the rate ν_{b1}. These newly formed h phonons then leave the beam, and so on.

The intensity of the process of creation of h phonons in the main beam depends on the temperature of the l phonons, which decreases with time for two reasons. First, because of conversion of l phonons into h phonons. Second, under the experimental conditions[11–15] the beam cools relatively rapidly because of the increase of its volume occurring as the phonons move in a cone with solid angle Ω_p. At sufficiently low temperatures ($T < 0.7$ K) the conversion of l phonons into h phonons can be neglected.[16,17] Then the l and h phonons propagate in the helium as pulses moving toward the detector independently of each other at different velocities. The sequence of events described above is shown in Fig. 2 for three different values of t_p.

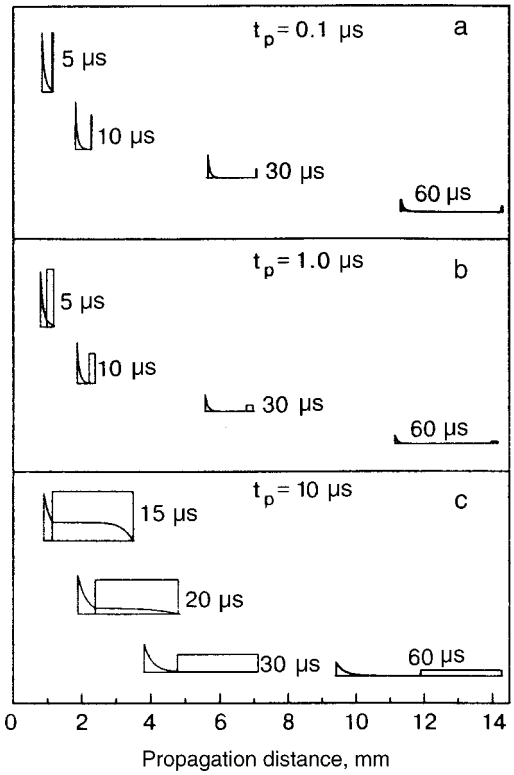

FIG. 2. Evolution of the beams of l and h phonons in their propagation from the heater toward the detector for pulse durations t_p [μs]: 0.1 (a), 1.0 (b), 10 (c).

5. ENERGY DENSITY OF *h* PHONONS IN THE BEAM

Experiments that attest to the asymmetry of the creation and annihilation processes in anisotropic phonon systems are unquestionably of interest. According to the results of Sec. 3, such asymmetry leads to high densities of h phonons in long phonon beams, and these may be observable in experiments. In planning experiments of this kind it is important to calculate the energy density of h phonons in beams of different lengths, and that is our goal in this Section.

The process of conversion of l phonons into h phonons is described by the kinetic equation (6), which in a coordinate system moving with the beam of l phonons is written

$$\frac{\partial n_1}{\partial t} + \mathbf{u}_1 \nabla n_1 = n_1^{(0)} \sum_{i=1}^{5} \nu_{bi}^{(n)} - n_1 \sum_{i=1}^{5} \nu_{di}^{(n)}, \tag{36}$$

where $\mathbf{u}_1 = \mathbf{c}_1 - \mathbf{c}$ is the relative velocity of the h_1 and l phonons.

We multiply Eq. (36) by the energy ε_1 and perform the integration over the momentum space of the h phonons, $0 \leqslant \Omega_1 \leqslant \Omega_p$, $p_c \leqslant p_1 \leqslant \infty$. As a result, we obtain an equation for the energy density E_h of h phonons in the main beam:

$$\frac{\partial E_h}{\partial t}+u_c\frac{\partial E_h}{\partial z_p}=E_h^{(0)}\overline{\nu}_{b1}-E_h\nu_d^{(1)}-\frac{E_h^2}{E_h^{(0)}}\nu_d^{(2)}. \tag{37}$$

In view of the exponential energy dependence of the distribution function, we can assume that the average velocity $u_c=c-c_c\approx 50\text{m/s}$, where $c_c=c_h$ $(p_1=p_c)$;

$$E_h^{(0)}=\frac{\Omega_p k_B^4 T\varepsilon_c^3}{(2\pi\hbar c_c)^2}e^{-\varepsilon_c/T} \tag{38}$$

is the energy density of h phonons with a Bose–Einstein energy distribution function (5). In Eq. (37) we have used a one-dimensional approximation with the z_p axis directed antiparallel to the motion of the beam, and we have introduced the average rates $\overline{\nu}$ in such a way that they can be assumed independent of E_h:

$$\overline{\nu}_{b1}=\frac{1}{E_h^{(0)}}\int \varepsilon_1 n_1^{(0)}\nu_{b1}^{(0)}d\Gamma_1, \text{ where } d\Gamma_1=\frac{d^3p_1}{(2\pi\hbar)^3}; \tag{39}$$

$$\nu_d^{(1)}=\overline{\nu}_{d1}+\overline{\nu}_{d3}-\overline{\nu}_{b4}, \text{ where } \overline{\nu}_{d1}=\frac{1}{E_h}\int \varepsilon_1 n_1\nu_{d1}^{(0)}d\Gamma_1; \tag{40}$$

$$\overline{\nu}_{d3}=\frac{1}{E_h}\int \varepsilon_1 n_1\nu_{d3}^{(0)}d\Gamma_1, \quad \overline{\nu}_{b4}=\frac{1}{E_h}\int \varepsilon_1 n_1^{(0)}\nu_{b4}^{(n)}d\Gamma_1; \tag{41}$$

$$\nu_d^{(2)}=\overline{\nu}_{d4}-\overline{\nu}_{b3}, \text{ where } \overline{\nu}_{d4}=\frac{E_h^{(0)}}{E_h^2}\int \varepsilon_1 n_1\nu_{d4}^{(n)}d\Gamma_1; \tag{42}$$

$$\overline{\nu}_{b3}=\frac{E_h^{(0)}}{E_h^2}\int \varepsilon_1 n_1^{(0)}\nu_{b3}^{(n)}d\Gamma_1. \tag{43}$$

In relations (39) and (41) it is taken into account that for $\varepsilon_c\gg T$ one can assume $\nu_{b1}^{(n)}=\nu_{b1}^{(0)}$ and $\nu_{d3}^{(n)}=\nu_{d3}^{(0)}$. On the right-hand side of Eq. (37) the contributions of the second and fifth processes have not been taken into account, since they conserve the total number of h phonons.

Equation (37) is supplemented with a boundary condition that follows from an analysis of the given situation. The beam volume V is bounded by the planes $z_p=0$ and $z_p=L_p$. Here the h phonons move relative to the beam from the plane $z_p=0$ to the plane $z_p=L_p$. Consequently,

$$E_h(z_p=0,t)=0. \tag{44}$$

After the initial, rapid stage of formation of the h phonons in the main beam is completed and the energy E_h varies slowly with time, a quasisteady situation arises for the h phonons, where one can neglect the first term on the left-hand side of Eq. (37). Then the integration of Eq. (37) with the boundary condition (44) will give the following energy density distribution of h phonons in different z_p planes of the beam in the quasisteady situation:

$$E_h(z_p)=E_h^{(0)}\frac{2\overline{\nu}_{b1}}{\nu_{\text{eff}}+\nu_d^{(1)}}\left[1-\exp\left(-\nu_{\text{eff}}\frac{z_p}{u_c}\right)\right]\times\left[1+\frac{\nu_{\text{eff}}-\nu_d^{(1)}}{\nu_{\text{eff}}+\nu_d^{(1)}}\exp\left(-\nu_{\text{eff}}\frac{z_p}{u_c}\right)\right]^{-1}, \tag{45}$$

where $\nu_{\text{eff}}=[\nu_d^{(1)^2}+4\overline{\nu}_{b1}\nu_d^{(2)}]^{1/2}$.

In long beam, for $z_p\gg u_c/\nu_{\text{eff}}$, the energy density (45) reaches saturation:

$$E_h^{(s)}=\frac{2\overline{\nu}_{b1}}{\nu_{\text{eff}}+\nu_d^{(1)}}E_h^{(0)}. \tag{46}$$

This $E_h^{(s)}$ differs from the equilibrium factor, which can be estimated by replacing the rates $\overline{\nu}_{b,di}$ $(i=1,\ 2,\ 3)$ by the corresponding average values of the rates described in Sec. 3:

$$\widetilde{\nu}_{b,d1}=\int_{p_c}^{\infty}n_1^{(0)}\nu_{b,di}p_1^2dp_1\Big/\int_{p_c}^{\infty}n_1^{(0)}p_1^2dp_1. \tag{47}$$

Figure 3 shows the temperature dependence of $\widetilde{\nu}_{b,di}$ calculated according to formula (47) with the analytical expressions for the rates $\nu_{b,di}$ obtained by the scheme described in Sec. 3. The average value of the rates for the third process, which are not shown in Fig. 3, are found from the data given for the fourth process with the aid of the relations

$$\widetilde{\nu}_{b3}=\frac{1}{2}\widetilde{\nu}_{d4};\quad \widetilde{\nu}_{d3}=\frac{1}{2}\widetilde{\nu}_{b4}. \tag{48}$$

Relations (48) were obtained by relabeling the variables of integration and reflect the fact that the third process is the inverse of the fourth.

At $T=1$ K the replacement of $\overline{\nu}_{b,di}$ by $\widetilde{\nu}_{b,di}$ in relation (46) gives $E_h^{(s)}/E_h^{(0)}\approx 30$. The large value of $E_h^{(s)}$ in comparison with $E_h^{(0)}$ calculated for the Bose–Einstein distribution (5) is a consequence of the asymmetry of the creation and annihilation processes in anisotropic phonon systems (the causes of this asymmetry were described in Sec. 2).

6. CREATION OF *h* PHONONS IN A BEAM OF *l* PHONONS

The amplitude of the h-phonon signal at the detector (the left-hand pulse in Fig. 2) is determined by the energy flux of h phonons per unit time from a unit area of the $z_p=L_p$ plane of the main beam:

$$Q=u_cE_h(z_p=L_p). \tag{49}$$

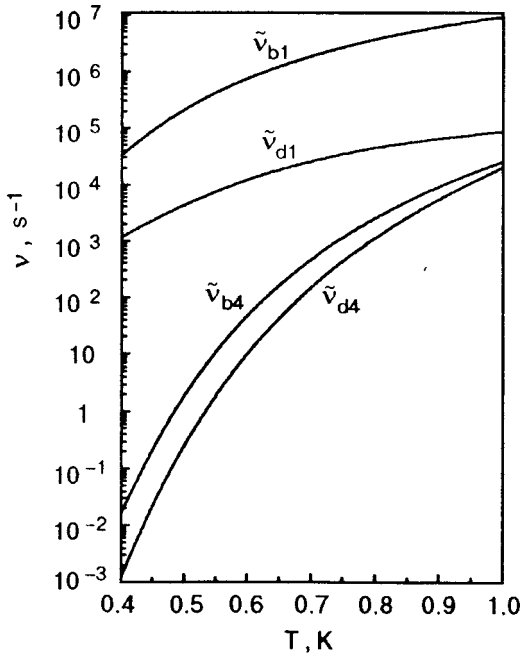

FIG. 3. Temperature dependence of the average values of the rates.

It follows from Eqs. (45) and (49) that the energy flux density Q of h phonons increases with increasing pulse duration $t_p = L_p/c$ to a maximum value

$$Q_{\max} = u_c E_h^{(s)} \quad \text{for} \quad L_p \gg u_c/\nu_{\text{eff}}. \tag{50}$$

When $t_p > u_c/c\nu_{\text{eff}}$ the energy flux density is close to the maximum value (50) and falls off relatively slowly as t_p is increased further. This result agrees with the saturation of the h-phonon signal observed in the experiments[14] for $t_p \approx 2 \times 10^{-7}$ s.

The cooling of the l phonons in the main beam, with a resulting decrease in the flux of h phonons (49), is described by the phonon energy conservation law

$$\frac{\partial(E_l^{(0)} V)}{\partial t} = -\frac{V}{L} Q, \tag{51}$$

where $E_l^{(0)} = \Omega_p \pi k_B^4 T^4/120\hbar^3 c^3$ is the energy density of l phonons with a Bose–Einstein energy distribution function (5). According to Eq. (51), the temperature of the l phonons decreases for two reasons. First, because of the energy flux of h phonons through the rear plane of the beam. Second, because of the increase of the volume $V = V(t)$ of the main beam as the phonons move toward the detector in a cone of solid angle Ω_p.

The volume V is bounded by two planes with coordinates z_1 and z_2 and the surface of the cone formed by a generator making an angle θ_p with the axis z of the cone. The volume of this solid of revolution for $\theta_p \ll 1$ is

$$V = \pi \theta_p^2 (z_2^3 - z_1^3) \frac{1}{3}. \tag{52}$$

Since $z_2 - z_1 = L_p$ at all times, we write expression (52) in the form

$$V = \pi L_p \left(r_t^2 + r_t L_p \theta_p + \frac{1}{3} L_p^2 \theta_p^2 \right), \tag{53}$$

where $r_t = z_1 \theta_t = r + ct\theta_p$ is the radius of the rear surface of the beam at time t, and r is the radius of the surface of the heater, equal to 0.57 mm in the experiments of Refs. 11–15.

Substituting expressions (49) and (53) into Eq. (51), we obtain

$$\frac{\partial E_l^{(0)}}{\partial t} = -\frac{u_c}{L_p} E_h(z_p = L_p) - \frac{E_l^{(0)} c \theta_p (2r_t + L_p \theta_p)}{r_t^2 + r_t L_p \theta_p + L_p^2 \theta_p^2/3}. \tag{54}$$

Equation (54) and relation (45), with allowance for the temperature dependence of the rates, can be used to calculate the density of h phonons at any time and at any point in space (see Fig. 2) and the energy density of l phonons in the main beam.

Figure 4 shows the results obtained when Eqs. (54) and (45) are used to calculate the energy density of h phonons at the end (solid curve *1*) and at the beginning (solid curve *3*) of the h-phonon beam and the energy density of the l phonons in the main beam (solid curve *2*) for three different values of t_p. Curves *1* were constructed with allowance for the increase in volume of the h-phonon beam, which, according to the experimental data,[14] moves in a cone with $\theta_h = 4°$.

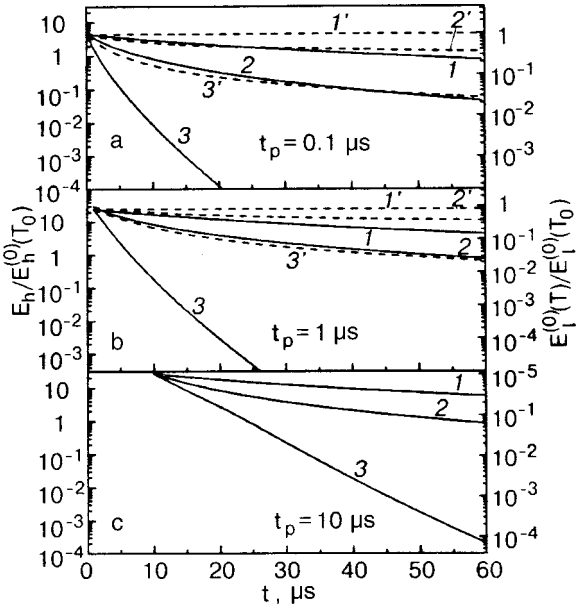

FIG. 4. Dependence of the energy densities in the beams of h and l phonons on the time of motion for different pulse durations t_p [μs]: 0.1 (a), 1.0 (b), 10 (c). Curve *1* is the variation of the relative energy density (left-hand axis) at the end of the beam of h phonons (the maximum of the left-hand pulse in Fig. 2) due solely to the increase in volume of the beam of h phonons as a result of its motion in a cone with $\theta_p = 4°$. Curve *2* describes the cooling of the main beam of l phonons due to the loss of energy to the formation of h phonons and to the increase in volume of the beam of l phonons in its motion in a cone with $\theta_p = 11.4°$. The relative value of the energy density in the beam of l phonons is given on the right-hand axis. Curve *3* is the decrease of the relative density density (left-hand axis) of the h phonons with time at the rear plane of the main beam of l phonons. The dashed curves $1'$, $2'$, and $3'$ show the variation of the corresponding relative densities without allowance for the increase in the volumes occupied by the beams of h and l phonons.

Figure 4 also shows the results of calculations of the corresponding energy densities (dashed curves) without allowance for the expansion of the beams of l and h phonons. The dashed curve $2'$ indicates that in the absence of expansion of the beam, a large fraction of the energy of the l phonons goes to the formation of h phonons. For example, for $t_p = 0.1$ μs in a beam with $T = 1$ K over a time of 10 μs more than 60% of the energy of the l phonons is converted into the energy of created h phonons. As a result, the main beam of l phonons is cooled so much ($T \leqslant 0.7$ K) that further conversion becomes insignificant. The physical reason for such intense conversion of l phonons into h phonons at $T = 1$ K and the sharp decline in this process for $T \leqslant 0.7$ K are described in detail in Refs. 16 and 17.

It follows from a comparison of the solid and dashed curves *2* that the cooling of the beam of l phonons due to expansion leads to a sharp decrease in the fraction of the energy of l phonons converted into the energy of created h phonons. Because of the rapid cooling of the beam of l phonons due to its increase in volume, the creation of h phonons will have practically ceased at a short distance from the heater, in agreement with the experimental results.[11–15] The theory developed in the present paper suggests some obvious ways of changing the experimental conditions to

increase the efficiency of creation of h phonons by a beam of l phonons.

7. CONCLUSION

A beam of phonons moving in superfluid helium from a heater towards a detector is a highly anisotropic system of phonons whose momenta lie in a narrow cone with solid angle Ω_p with its axis along the direction of motion of the beam. It follows from relations (29) and (31) that in an anisotropic phonon system there is an asymmetry of the creation and annihilation processes. The physical reason for this asymmetry is that the restrictions on the creation (31) and annihilation (29) processes are different. As a result, it can turn out that inequality (29) is not satisfied for $\Omega_p \ll 1$. Then there are no phonons in the beam with which the high-energy h phonons can interact, and the lifetime of such an h phonon is infinite. Here inequality (31) can be met, and the rate of creation of these h phonons is finite. This situation is demonstrated in Fig. 1a for $cp_1/k_B \geqslant 11$ K. In this situation, on account of the annihilation of l phonons, there is unbounded growth of the h phonons, which can be restrained only by other processes in the phonon system.

The results of the calculations of the momentum dependence (Fig. 1) for all ten rates pertaining to the five possible processes (32) make it possible to understand the role of each process in the formation of the distribution function of the h phonons in an anisotropic phonon system. For example, the first process leads to intense conversion of l phonons into h phonons; the second and fifth processes to concentration of the h phonons near the axis of anisotropy; the fourth process restrains the unbounded growth of the number of h phonons caused by the first process and brings about dynamic equilibrium between the l- and h-phonon subsystems; the third process is the inverse of the fourth and partially compensates it. As a result, the energy density of the h phonons in long beams (45) is substantially greater than the density obtained in the case of a Bose–Einstein distribution function.

All of the rates decrease with decreasing temperature and decreasing anisotropy parameter Ω_p. However, it follows from calculations that the dependence is different for different rates. This circumstance makes it possible to obtain different distributions of h phonons in the main beam by varying the parameters T and Ω_p.

We have shown that the increase of the beam volume has a substantial effect on the evolution of the phonon beams (Fig. 2). When all of the processes that do not conserve the number of h phonons are taken into account, one obtains Eq. (37), which can account for the experimentally observed saturation of the h-phonon signal amplitude and allows one to calculate its maximum value (46).

We have obtained an equation (54) describing the cooling of the beam of l phonons due to the increase of its volume and to the creation of h phonons. The solution of this equation can be used to find the energy density of the created h phonons at any time and at any point in space and the energy density of the l phonons in the main beam (Fig. 4). We have shown that under the conditions of the experiments, the increase in the beam volume leads to its rapid cooling, so that the creation of h phonons practically ceases by the time the beam has reached a distance of less than 3 mm from the heater.

The creation of h phonons by a beam of l phonons was observed[2,11–15] long before the foundations of the theory of this process were laid.[16,17] As to the large values of the energy density of h phonons in long beams (45) due to the asymmetry of the creation and annihilation processes, this conclusion of the theory awaits experimental confirmation. Such experiments are being planned at the University of Exeter, UK.

We are deeply grateful to EPSRC (Grants GR/N18796 and GR/N20225) and to the Ukrainian Government Foundation for Basic Research (Grant N02.07/000372) for support making this research possible.

*E-mail: adamenko@pem.kharkov.ua
**E-mail: a.f.g.wyatt@exeter.ac.uk

[1] R. C. Dynes and V. Narayanamurti, Phys. Rev. Lett. **33**, 1195 (1974).
[2] A. F. G. Wyatt, N. A. Lockerbie, and R. A. Sherlock, Phys. Rev. Lett. **33**, 1425 (1974).
[3] S. Havlin and M. Luban, Phys. Lett. A **42**, 133 (1972).
[4] H. J. Maris, Phys. Rev. A **8**, 1980 (1973).
[5] M. A. H. Tucker, A. F. G. Wyatt, I. N. Adamenko, A. V. Zhukov, and K. É. Nemchenko, Fiz. Nizk. Temp. **25**, 657 (1999) [Low Temp. Phys. **25**, 488 (1999)].
[6] L. D. Landau, Zh. Éksp. Teor. Fiz. **11**, 592 (1941).
[7] I. M. Khalatnikov, *Theory of Superfluidity* [in Russian], Nauka, Moscow (1971).
[8] I. N. Adamenko and M. I. Kaganov, Zh. Éksp. Teor. Fiz. **53**, 886 (1967) [Sov. Phys. JETP **26**, 537 (1968)].
[9] V. L. Gurevich and B. D. Laĭkhtman, Zh. Éksp. Teor. Fiz. **69**, 1230 (1975) [Sov. Phys. JETP **42**, 628 (1975)].
[10] V. L. Gurevich and B. D. Laĭkhtman, Zh. Éksp. Teor. Fiz. **70**, 1907 (1976) [Sov. Phys. JETP **43**, 993 (1976)].
[11] Y. Korczynski and A. F. G. Wyatt, J. Phys. Colloq. **39**, C6-230 (8;1978).
[12] A. F. G. Wyatt, J. Phys.: Condens. Matter **1**, 8629 (1989).
[13] M. A. H. Tucker and A. F. G. Wyatt, J. Phys.: Condens. Matter **4**, 7745 (1992).
[14] M. A. H. Tucker and A. F. G. Wyatt, J. Phys.: Condens. Matter **6**, 2825 (1994).
[15] M. A. H. Tucker and A. F. G. Wyatt, J. Low Temp. Phys. **113**, 621 (1998).
[16] I. N. Adamenko, K. E. Nemchenko, A. V. Zhukov, M. A. H. Tucker, and A. F. G. Wyatt, Phys. Rev. Lett. **82**, 1482 (1999).
[17] A. F. G. Wyatt, M. A. H. Tucker, I. N. Adamenko, K. E. Nemchenko, and A. V. Zhukov, Phys. Rev. B **62**, 9402 (2000).
[18] M. A. H. Tucker and A. F. G. Wyatt, Physica B **165–166**, 493 (1990).
[19] M. A. H. Tucker and A. F. G. Wyatt, J. Phys.: Condens. Matter **6**, 2813 (1994).
[20] A. F. G. Wyatt, M. A. H. Tucker, I. N. Adamenko, K. E. Nemchenko, and A. V. Zhukov, Phys. Rev. B **62**, 3029 (2000).
[21] A. F. G. Wyatt, M. A. H. Tucker, I. N. Adamenko, K. E. Nemchenko, and A. V. Zhukov, Physica B **280**, 36 (2000).
[22] A. F. G. Wyatt, I. N. Adamenko, and K. E. Nemchenko, J. Low Temp. Phys. **125**, 1 (2001).
[23] I. N. Adamenko, K. E. Nemchenko, A. V. Zhukov, M. A. H. Tucker, and A. F. G. Wyatt, Physica B **284–288**, 33 (2000).
[24] I. N. Adamenko and I. M. Fuks, Zh. Éksp. Teor. Fiz. **59**, 2071 (1970) [Sov. Phys. JETP **32**, 1123 (1971)].
[25] I. M. Khalatnikov and I. N. Adamenko, Zh. Éksp. Teor. Fiz. **63**, 745 (1972) [Sov. Phys. JETP **36**, 391 (1973)].
[26] R. A. Sherlock, A. F. G. Wyatt, N. G. Mills, and N. A. Lockerbie, Phys. Rev. Lett. **29**, 1299 (1972).
[27] R. A. Sherlock, N. G. Mills, and A. F. G. Wyatt, J. Phys. C **8**, 300 (1975).

Translated by Steve Torstveit

SUPERCONDUCTIVITY, INCLUDING HIGH-TEMPERATURE SUPERCONDUCTIVITY

On the criteria for superconductivity in $PrBa_2Cu_3O_{6.6}$

F. A. Boyko, G. V. Bukin, V. A. Voloshin,* and A. A. Gusev

A. A. Galkin Donetsk Physicotechnical Institute, National Academy of Sciences of Ukraine, ul. R. Lyuksemburg 72, 83114 Donetsk, Ukraine

(Submitted May 7, 2001; revised September 25, 2001)
Fiz. Nizk. Temp. **28**, 138–142 (February 2002)

The structure of $RBa_2Cu_3O_x$ is analyzed to ascertain the reason for the absence of superconductivity in $PrBa_2Cu_3O_7$ or for its presence in $PrBa_2Cu_3O_{6.6}$. An empirical formula with a single adjustable parameter is proposed which describes the temperature dependence of the resistance at different pressures. The character of the temperature variation of the superconducting transition temperature at pressures higher than those attained experimentally is predicted. © *2002 American Institute of Physics.* [DOI: 10.1063/1.1461920]

INTRODUCTION

Before 1998 it was assumed that all of the rare-earth compounds of the HTSC type $RBa_2Cu_3O_7$ (where R is a rare earth element) except $PrBa_2Cu_3O_7$ are superconducting (Ce and Tb do not form such a compound). In 1998, superconducting crystals of $PrBa_2Cu_3O_{6.6}$ were obtained.[1,2] The mechanism for the onset of superconductivity in $PrBa_2Cu_3O_{6.6}$ crystals has remained unclear. Some of these crystals have set records for growth of the superconducting transition temperature T_c under compression. The temperature dependence of the resistance of $PrBa_2Cu_3O_{6.6}$ at different pressures is shown in Fig. 1. Two questions arise:

1) How is praseodymium different from the other rare-earth elements?
2) What is the mechanism for the suppression of superconductivity in the system $PrBa_2Cu_3O_7$?

The superconducting crystals of $PrBa_2Cu_3O_{6.6}$ were obtained by a new radiation method. This raises a third question: What effect does this new method of obtaining crystals have on the structure?

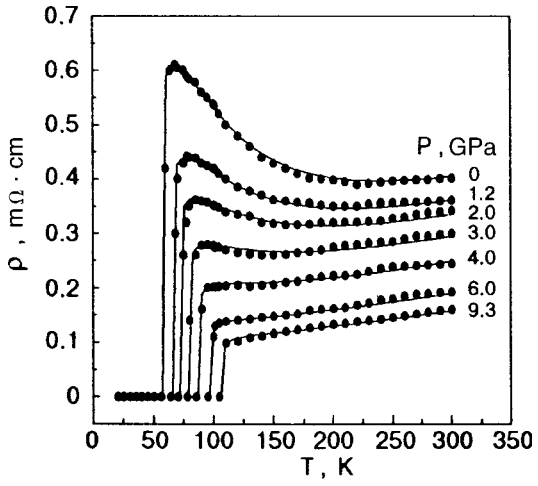

FIG. 1. Temperature dependence of the conductivity of $PrBa_2Cu_3O_{6.6}$ at various pressures. The continuous curves are calculated according to formula (1). The experimental points are the results of Ref. 2.

FEATURES OF THE STRUCTURE OF $PrBa_2Cu_3O_{6.6}$

As was shown in Ref. 3, the system $RBa_2Cu_3O_7$, can be found in different states, depending on the distance between the rare-earth ion and the oxygen ion:
— the $4f^n$ electronic configuration is isolated from its surroundings: an electronic state;
— the electronic and nuclear motions of the rare-earth ion and oxygen ions are inextricably mixed: a vibronic state.[4,5]

In constructing their theorem, Jahn and Teller[6] excluded rare earths from consideration on account of the practical isolation of the $4f$ electrons from the surroundings, although at high pressure and in certain other cases this isolation is destroyed and the Jahn–Teller theorem and all its consequences extends to the $4f$ configuration as well. In such cases vibronic motion can be formed.[3]

Two conditions are necessary for the formation of a vibronic state: degeneracy (but not Kramers degeneracy) of the ground state, and a distance equal to the critical distance between the rare-earth ion and the ligand ion. For the pair Pr–O the critical distance is 2.38 Å.

As we know, a characteristic of Kramers degeneracy is that it is lifted only in a magnetic field and is possible only in the case when an odd number of electrons are found in the f shell of the ion. Among the rare-earth elements, europium is a special case. Its ground state is nondegenerate even though it has an odd number of electrons in the f shell. Therefore it cannot form a vibronic state.

In the isomorphic series $RBa_2Cu_3O_7$, only the crystals whose ions have Kramers degeneracy or no degeneracy at all (like europium) are superconducting. Table I lists the superconducting transition temperatures for $RBa_2Cu_3O_7$ samples with Kramers and non-Kramers (*) ions.

The data in the table indicate that the vibronic state prevents the formation of superconductivity: seven of the eight

TABLE I. Values of T_c and R_{cr} for $RBa_2Cu_3O_7$ samples with Kramers and non-Kramers (*) ions.

R	$4f^n$	T_c, K	R_{Cr}, Å
Ce	$4f^1$	···	2.40
Pr*	$4f^2$	-	2.38
Nd	$4f^3$	96	2.36
Pm*	$4f^4$	···	2.34
Sm	$4f^5$	94	2.33
Eu	$4f^6$	95	2.32
Gd	$4f^7$	94	2.31
Tb*	$4f^8$	···	2.30
Dy	$4f^9$	92	2.29
Ho*	$4f^{10}$	90	2.28
Er	$4f^{11}$	90	2.27
Tm*	$4f^{12}$	90	2.26
Yb	$4f^{13}$	90	2.25

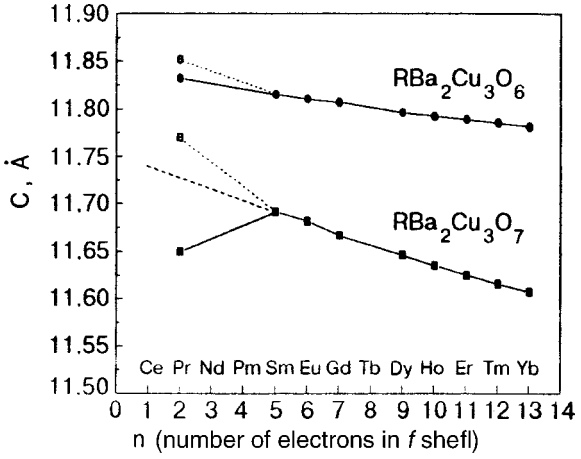

FIG. 2. Dependence of the crystal lattice parameter C of $RBa_2Cu_3O_6$ (tetragonal symmetry) and $RBa_2Cu_3O_7$ (orthorhombic symmetry) on the number of electrons of the f configuration. The average value of the parameter C is shown for $PrBa_2Cu_3O_x$ samples with $x=6.0$ (○) and $x=6.6$ (□).[1,2]

crystals for which the ions have Kramers degeneracy or no degeneracy at all are superconducting.

As we have said, for formation of a vibronic state it is necessary that the distance between the R ion and the ligand ions be equal to the critical value.[7] The critical distances in Å for the different rare-earth ions are listed in Table I.

Of the five crystals whose rare-earth ions have an even number of electrons in the f shell, only $HoBa_2Cu_3O_7$ and $TmBa_2Cu_3O_7$ are superconducting. Here the Ho and Tm ions do not form a vibronic state, since the critical distances indicated in Table I are not reached.

The question arises: Is praseodymium in a vibronic state in $PrBa_2Cu_3O_7$? According to the neutron-diffraction data,[8] of all eight of the praseodymium–oxygen bonds have lengths of approximately 2.45 Å, whereas according to the x-ray absorption fine-structure (XAFS) data, a fraction of them have a length of 2.27 Å, i.e., less than the critical distance.[9] The apparent inconsistency of the structural data[8,9] is important to note. As was shown in Ref. 10, this inconsistency may be explained by the circumstance that the $PrBa_2Cu_3O_7$ system is found in a state of electronic–vibronic dynamic equilibrium, i.e., some of the time the system is found in a vibronic state ($R<R_{cr}$), and some of the time it is in an ordinary electronic state ($R>R_{cr}$).[11] The XAFS method (with a time resolution of 10^{-17} s) registers both of these states, while the low-temperature neutron-diffraction method only measures their average values. Thus it can be assumed that the vibronic state prevents the formation of superconductivity.

Let us examine how the structure of the compounds changes as one goes from $RBa_2Cu_3O_6$ (compounds which are not superconductors) to the superconducting $RBa_2Cu_3O_7$ for samples grown by the conventional method.[8] Figure 2 shows the dependence of the unit cell parameter C of the crystal lattice of the compounds ($x=6$ or $x=7$) on the number of electrons in the $4f$ configuration.

For the nonsuperconducting $PrBa_2Cu_3O_6$ samples obtained by the conventional and new methods the dependence of the parameter C hardly deviates from the linear dependence for other $RBa_2Cu_3O_6$ systems. For $PrBa_2Cu_3O_7$ the character of this dependence breaks down both for samples obtained by the conventional technique and for samples obtained in Ref. 1 by a radiation method. In the first case the parameter C is much less than expected (by 0.08 Å), and this may be ascribed to the shortening of the chemical bonds upon the formation of a vibronic state, and so the decrease of the parameter C may be linked with the absence of superconductivity. In the second case the parameter C is larger than expected.

As we have shown above, the existence of a vibronic state is a condition for the suppression of superconductivity, and the destruction of this state may lead to the onset of superconductivity. For this it is necessary to ''stretch'' the praseodymium–oxygen bond. Therefore, to answer the third question it is necessary to assess whether the Pr–O bond length has increased in the superconducting crystals obtained by the radiation method. Here it should be noted that the authors of Refs. 1 and 2 came to the conclusion that the length of this bond is the same as for crystals grown by the conventional technique. However, for technical reasons, in Refs. 1 and 2 the detailed structural analysis was done for nonsuperconducting crystals unsaturated with oxygen (i.e., for $PrBa_2Cu_3O_6$), but, as we have shown above, the marked disparity in the parameter C occurs for the oxygen-saturated samples. For the samples obtained by the new method the value of the parameter C is even somewhat larger than expected. When these $PrBa_2Cu_3O_{6.6}$ samples are compressed, the superconductivity will persist until the parameter C has decreased to 11.65 Å, whereupon the superconductivity vanishes.

Thus the answer to the third question is that saturation of the samples with oxygen does not lead to an anomalously sharp decrease in the parameter C, and so apparently the praseodymium–oxygen bond length is considerably greater.

RESISTIVITY

Figure 1 shows the experimental data of Refs. 1 and 2 on the temperature dependence of the resistivity of superconducting crystals of $PrBa_2Cu_3O_{6.6}$. A description of these data was given in Ref. 12 on the basis of an empirical formula proposed in Ref. 13:

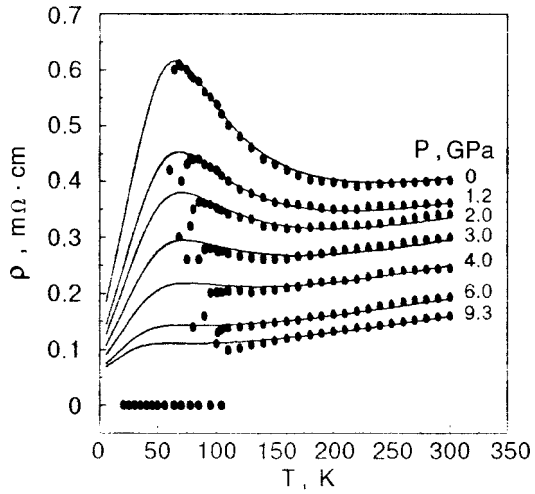

FIG. 3. Temperature dependence of the resistivity of $PrBa_2Cu_3O_{6.6}$ at different pressures. The continuous curves are calculated on the assumption that superconductivity is suppressed ($\beta=0$).

$$\rho=\frac{\rho_0+\alpha T}{1-n[1-\exp(-\Delta E/2kT)]}-\frac{\beta T_c}{T-T_c}, \tag{1}$$

where the first term describes a metallic or semiconductor temperature dependence of the resistivity at different pressures in the normal state, and the second term, which was proposed in Ref. 14, takes into account the fluctuational formation of local superconducting regions at temperatures above the temperature of the transition to the superconducting state. Based on an analysis of this formula, it was hypothesized for the first time in Ref. 13 that the transition of the system to the superconducting state occurs upon a change of the conductivity from semiconductor to metallic. It should be noted that the experimental curve was obtained in a temperature region far below T_c. In this case the resistivity was measured for $T>20$ K, i.e., in the temperature region $T<T_c$. The description of the experimental $\rho(T)$ curve by the proposed formula (1) is broken off after the transition to the superconducting state, since at $T=T_c$ the second term goes to infinity and the formula loses meaning. However, if the conditions of formation of the superconducting state are disrupted (the second term equals zero), then the curve is extended on (Fig. 3).

The experimental $\rho(T)$ curves are well described by formula (1), as one would naturally expect with six adjustable parameters. It is somewhat surprising, though, that five of them (all but T_c) are linear functions of a certain parameter, denoted as p. If one considers that the adjustable parameter T_c is very close to the experimentally determined value of T_c, then we can regard Eq. (1) as a single-parameter formula:

$$\begin{aligned}
&\rho_0=\rho_0'+0.000667p,\\
&\alpha=\alpha_0-0.0000258p,\\
&n=n_0-0.0185p,\\
&\Delta E/2k=[(\Delta E/2k)_0-13.978p]>0,\\
&\beta=\beta_0-0.0001p,
\end{aligned} \tag{2}$$

TABLE II. Comparison of T_c and T_x for different values of the adjustable parameter p for the superconducting crystal $PrBa_2Cu_3O_{6.6}$ under various pressures P.

P, GPa	p, GPa	T_c, K	T_x, K
0	0	56.33	96.83
1.2	1.1	64.75	103.3
2.0	1.85	71.19	106.74
3.0	3.1	78.1	111.21
4.0	4.7	85.98	115.28
6.0	7.3	95.3	117.43
9.3	9.3	104.74	115.92

where $\rho_0'=0.0078$ mΩ·cm, $\alpha_0=0.00057$ mΩ·cm/K, $n_0=0.942$, $(\Delta E/2k)_0=270$ K, and $\beta_0=0.00183$. Numerically the parameter p is very close to the pressure P at which the temperature curves of the resistivity were measured. These values and the superconducting transition temperatures corresponding to them are presented in Table II.

In formula (1) the numerical parameter n varies from 0 to 1. At $n=0$ the first term describes a metallic trend of the temperature dependence of the resistivity. At $n=1$ this dependence becomes that of a semiconductor. If we adopt the hypothesis of an electronic–vibronic dynamic equilibrium,[11] wherein the lifetime of the vibronic (or electronic) state varies from zero to infinity and the fraction of the state is proportional to its lifetime and varies from zero to unity, the experimental curve of the conductivity can be represented as a sum of semiconductor and metallic conductivities:

$$\sigma_1=\frac{1-n}{\rho_0+\alpha T}\ \text{ and }\ \sigma_2=\frac{n}{(\rho_0+\alpha T)\exp(\Delta E/2kT)}, \tag{3}$$

where $(1-n)$ is the metallic-phase fraction and n is the semiconductor fraction.

Figure 4 shows examples of the temperature dependence of these conductivities, i.e., each curve in Fig. 3 is represented as a sum of two curves, with semiconductor and me-

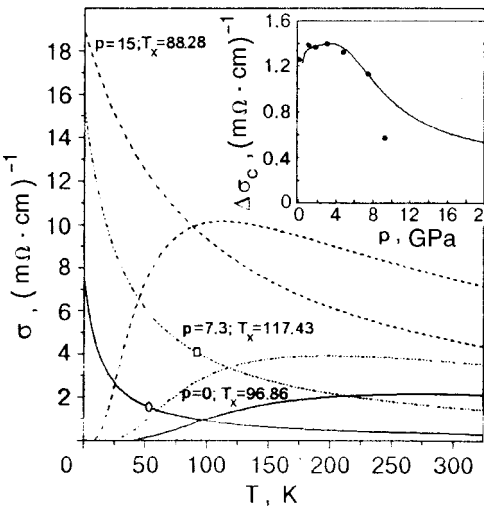

FIG. 4. Temperature dependence of the semiconductor and metallic components of the conductivity of $PrBa_2Cu_3O_{6.6}$ for $p=0$, 7.3, and 15 GPa. The symbols (○) and (□) denote T_c. The inset shows $\Delta\sigma_c=f(p)$, where $\Delta\sigma_c$ is the difference of the metallic and semiconductor components of the conductivity at which the system undergoes a transition to the superconducting state.

tallic conductivity. It should be noted that the decomposition of the curves for $p=0$ and 7.3 GPa was done with the experimental data taken into account, while for $p=15$ GPa the decomposition was done for the curve obtained from formula (1) without the second term but with allowance for the dependence of all five parameters on p. T_x is the temperature at which these conductivities are equal. Two fundamentally different regions exist:

— for $T<T_x$ the metallic conductivity is greater than the semiconductor conductivity;

— for $T>T_x$ the metallic conductivity is less than the semiconductor conductivity.

The values of T_x found for the states of the superconducting crystal $PrBa_2Cu_3O_{6.6}$ at different pressures[1,2] are given in Table II. One notices that, while the transition from the metallic to the semiconductor phase occurs in different cells of the crystal at different times, at the temperature T_x the resistivity is the same throughout the entire crystal. It cannot be ruled out that the relationship between the values of these conductivities and also the time spent in one phase or the other is related to a transition to the superconducting state.

Analysis of all the experimental data[1,2] up to $P=9.3$ GPa shows that the transition to the superconducting state occurs only under the condition $\Delta\sigma=(\sigma_1-\sigma_2)>0$, i.e., when the metallic conductivity is greater than the semiconductor. We assume that this condition will persist as the pressure is increased further. The data points in the inset to Fig. 4 show the amount $\Delta\sigma_c$ by which the metallic conductivity exceeds the semiconductor conductivity, according to the experimental data, at the temperature T_c of the transition to the superconducting state at different pressures, and the continuous curve shows one of the possible pressure dependences of this quantity at pressures from atmospheric to $p_{\max}=19.3$ GPa. The value of $p_{\max}$ is determined from formula (2) for $\Delta E=0$. The form of the function $\Delta\sigma_c=f(p)$ was obtained by fitting formula (1) without the second term, on the basis of three conditions: 1) $\Delta\sigma$ is always greater than zero; 2) the curve must conform to the experimental data; 3) the continuous curve $T_c=f(p)$ for $0<p<p_{\max}$ must conform to the experimental data. Under these conditions the form of the curve $\Delta\sigma_c=f(p)$ will be described by the following expression:

$$f(x)=\frac{0.23+0.000286\,x}{x/(x-0.04)-1.1[0.755-\exp(-220/x)]}. \qquad (4)$$

Figure 5 shows the experimental data for $T_c=f(P)$ (data points) in the region $0<P<9.3$ GPa and the proposed values of T_c (continuous curve) derived from the values of $\Delta\sigma$, for values of p from atmospheric pressure to 16.5 GPa. It turns out that for $p=10$ GPa the maximum value is $T_c=98.7$ K, after which a baric suppression of the superconductivity begins. It can be assumed that as the Pr–O distance is decreased to 1.73 Å in correspondence with the decrease in the parameter C, compression will promote an increase in T_c. This assumption needs to be checked, of course. Also shown in Fig. 5 is the curve of $T_x=f(p)$, the value of which was obtained from calculations of the semiconductor and metallic components of the conductivity. This curve bounds the region $\Delta\sigma>0$. Thus the value of T_c is always less than

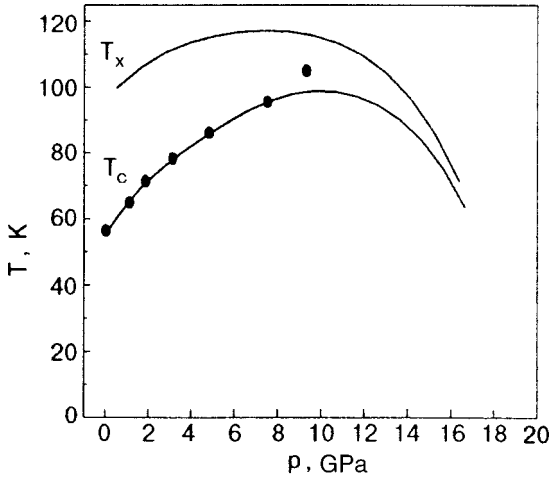

FIG. 5. The temperatures T_x and T_c as functions of the parameter p for $PrBa_2Cu_3O_{6.6}$.

T_x. For $p>19.3$ GPa the parameter $\Delta E/2k$ changes sign, and the σ_1 and σ_2 curves do not cross, i.e., the situation falls outside of our adopted hypothesis.

CONCLUSION

We have noted that the superconductivity in $PrBa_2Cu_3O_{6.6}$ sets in under the following conditions: the parameter C is greater than the value expected in the $RBa_2Cu_3O_7$ series; the metallic component of the conductivity is greater than the semiconductor component.

The function $T_c=f(p)$ obtained can be used to predict the temperature at which the transition to the superconducting state will occur anywhere in the region $0<p<19.3$ GPa. These predictions agree with the experimental data except in the region $p\approx 9.3$ GPa, where a disagreement with experiment is observed.

*E-mail: voloshin@host.dipt.donetsk.ua

[1] Z. Zou, J. Ye, K. Oka, and Y. Nishihara, Phys. Rev. Lett. **80**, 1074 (1998).
[2] J. Ye, Z. Zou, A. Matsushita, K. Oka, Y. Nishihara, and T. Matsumoto, Phys. Rev. B **58**, R620 (1998).
[3] V. A. Voloshin, Zh. Éksp. Teor. Fiz. **90**, 1336 (1986) [Sov. Phys. JETP **63**, 782 (1986)].
[4] W. Moffit and W. Thorson, Phys. Rev. **108**, 1251 (1957).
[5] I. B. Bersuker and V. Z. Polinger, *Vibronic Interactions in Molecules and Crystals* [in Russian], Nauka, Moscow (1983).
[6] H. A. Jahn and E. Teller, Proc. R. Soc. London, Ser. A **161**, 220 (1937).
[7] V. A. Voloshin, P. N. Mikheenko, and A. A. Gusev, Semicond. Sci. Technol. **11**, 1146 (1998).
[8] M. Guillaume, P. Allenspach, W. Henggeler, J. Mesot, B. Roessli, U. Staub, P. Fischer, A. Furrer, and V. Trouno, J. Phys.: Condens. Matter **6**, 7963 (1994).
[9] C. H. Booth, F. Bridges, J. B. Boyce, T. Claeson, Z. X. Zhao, and P. Cervantes, Phys. Rev. B **49**, 3432 (1994).
[10] V. A. Voloshin, A. A. Gusev, A. I. D'yachenko, and I. M. Reznik, Zh. Éksp. Teor. Fiz. **110**, 2135 (1996) [JETP **83**, 1175 (1996)].
[11] V. A. Voloshin, A. A. Gusev, I. A. Danilenko, L. I. Medvedeva, A. D. Prokhorov, and S. I. Khartsev, Phys. Lett. A **271**, 121 (2000).
[12] V. A. Voloshin, A. A. Gusev, and G. G. Levchenko, Fiz. Tekh. Vysokikh Davlenii. **10**, 3, 56 (2000).
[13] V. A. Voloshin, I. S. Abalesheva, G. Yu. Bochkovaya, F. A. Boĭko, N. A. Doroshenko, and Ya. I. Yuzhelevskiĭ, Fiz. Tverd. Tela (St. Petersburg) **38**, 1553 (1996) [Phys. Solid State **38**, 855 (1996)].
[14] L. G. Aslamazov and A. I. Larkin, Phys. Lett. A **26**, 238 (1968).

Translated by Steve Torstveit

Fluctuation conductivity in $YBa_2Cu_3O_{7-y}$ films with different oxygen content. II. YBCO films with $T_c \approx 80$ K

A. L. Solovjov*

B. Verkin Institute for Low Temperature Physics and Engineering, National Academy of Sciences of Ukraine, pr. Lenina 47, 61103 Kharkov, Ukraine

H.-U. Habermeier and T. Haage

Max-Planck-Institut für Feskorperforschung, Heisenbergstr. 1, 70569 Stuttgart, Germany
(Submitted June 6, 2001; revised November 22, 2001)
Fiz. Nizk. Temp. **28**, 144–156 (February 2002)

The fluctuation conductivity in $YBa_2Cu_3O_{7-y}$ (YBCO) films with $T \approx 80$ K is investigated for the first time. Unlike the optimally doped samples, these films exhibit a transition from a Maki–Thompson (MT) mechanism for the scattering of fluctuational pairs to a Lawrence–Doniach (LD) mechanism and, as the temperature approaches T_c, to an Aslamazov–Larkin (AL) mechanism. It is shown that the coherence length $\xi_c(0)$ along the c axis and the phase relaxation time $\tau_\varphi(100\ \mathrm{K})$ of the fluctuational pairs are determined by the temperature of this second transition. The features observed on both the fluctuation conductivity and resistive behavior are sharply enhanced as T_c approaches 80 K, probably because of a significant increase in the intensity of the magnetic interaction in high-T_c superconductors at these temperatures. In spite of this, for two samples a value $\tau_\varphi(100\ \mathrm{K}) = (3.35 \pm 0.01) \times 10^{-13}$ s is measured, i.e., the same value as for optimally doped YBCO films. It is shown that the dependence of $\xi_c(0)$ on T_c obeys the standard theory of superconductivity. The mechanisms for the scattering of charge carriers and the superconducting pairing in YBCO are analyzed. © *2002 American Institute of Physics.* [DOI: 10.1063/1.1461921]

INTRODUCTION

It is well known[1–4] that the longitudinal resistivity $\rho_{xx}(T)$ in $YBa_2Cu_3O_{7-y}$ (YBCO) systems is proportional to T over an anomalously wide temperature interval. However, with decreasing temperature the $\rho_{xx}(T)$ curve ultimately deviates downward from the linear trend at a certain characteristic temperature $T_{*0} \geqslant T_c$ (T_c is the temperature of the resistive transition), giving rise to an excess conductivity $\sigma' = \sigma(T) - \sigma_N(T)$, or

$$\sigma'(T) = [\rho_N(T) - \rho(T)]/[\rho_N(T)\rho(T)]. \quad (1)$$

Here $\rho(T) = \rho_{xx}(T)$ is the measured resistivity, and $\rho_N(T) = \alpha T + b$ is the normal-state resistivity of the sample extrapolated to the low-temperature region. As was shown in detail in Part I of this paper,[5] the linear temperature dependence of the resistivity of a high-T_c superconductor (HTSC) finds explanation in the framework of the ''nearly antiferromagnetic Fermi liquid'' (NAFL) model,[6] which also explains the anomalous temperature dependence of the Hall coefficient, $R_H \propto 1/T$. The NAFL theory assumes that the scattering in the HTSC is governed by an antiferromagnetic interaction V_{eff} existing in these substances. According to the NAFL theory, a linear dependence of $\rho_{xx}(T)$ at high temperatures can be regarded as a reliable sign of the normal state of the system, which is characterized by stability of the Fermi surface, and consequently, by stability of the normal–carrier scattering intensity. When the temperature is decreased below $T_*(T_* \geqslant T_{*0})$ the magnetic behavior of the system passes into a pseudogap (PG) regime, which is characterized by a change in the spectrum of magnetic fluctuations and by the presence of a strong variation of the band structure of the quasiparticles with temperature. This should lead to evolution of the Fermi surface[6,7] and, as a consequence, to a decrease of the scattering intensity. Here the parameters of the HTSC vary so unpredictably that neither the NAFL nor any other theory can describe experiment in this temperature range. It should be stressed that the intensity of V_{eff} and its influence on the temperature dependence of the resistivity decrease markedly with increasing oxygen index $\Delta y = (7 - y)$ in YBCO, probably because of the decreasing influence of spin correlations with doping,[1] as is confirmed by the results of recent optical measurements.[8,9] Accordingly, T_* should also decrease. For example, for optimally doped YBCO systems with $T_c \cong 90$ K the theory[6,7] gives $T_* \cong 110$ K, showing that in this case the crossover in the magnetic behavior of the system and the transition to the PG regime occur very close to T_c. Thus, with decreasing intensity of the magnetic interaction in a HTSC the temperature region of spin-gap behavior shrinks rapidly,[10] while T_c increases. This result suggests that the interaction mechanisms underlying the superconducting pairing in HTSCs have not been considered in the NAFL nor in other theories treating the mechanisms for the scattering of normal carriers in HTSCs.[6]

Usually the excess conductivity is interpreted[5] as the fluctuation conductivity predicted by the Aslamazov–Larkin (AL) theory,[11] and Eq. (1) is widely used to calculate $\sigma'(T)$ from experiment.[12–18] As was shown in Refs. 5 and 18, for optimally doped YBCO systems this assertion is justified, at

least in the temperature interval $T_c < T < T_{c0} = (105 \pm 5)$ K. Thus by studying the fluctuation conductivity one can obtain information about the scattering mechanism and the superconducting pairing as the temperature approaches T_c (Ref. 5). However, despite the considerable number of papers devoted to this problem, there is still no clarity on the question of whether the excess conductivity in HTSCs at $T > T_{c0}$ is entirely fluctuation conductivity, since $T_{*0} \cong (160 \pm 30)$ K for optimally doped YBCO films[19] and single crystals[14,15] and increases rapidly to $T_{*0} \cong 250$ K (Ref. 5) with decreasing oxygen content in the sample.[20] We have attempted to answer this question on the basis of an analysis of the fluctuation conductivity, which was first measured on a set of specially prepared well-structured $YBa_2Cu_3O_{7-y}$ films with different oxygen content.

In Ref. 5 we analyzed the fluctuation conductivity in a sample F1 ($T_c \cong 87.4$ K) which was close to an optimally doped system, and in a sample F6 ($T_c \cong 54.2$ K) which represented a very lightly doped system, and we also set forth the basic principles of analysis of the fluctuation conductivity in HTSCs. However, the behavior of the fluctuation conductivity in cuprates with intermediate T_c ($T_c \cong 80$ K) was not investigated. It should be stressed that the study of such YBCO systems is also of independent interest. As we have said, the intensity of the magnetic interaction and, hence, the intensity of the scattering of charge carriers in HTSCs decrease with increasing oxygen content.[1,5,8,10] Thus, while the scattering intensity in lightly doped samples with $T_c \leqslant 60$ K is determined by the magnetic interaction,[6] in optimally doped systems it is mainly due to strong electron correlations.[9,18,21] It has been found that the dependence of T_c on the oxygen content is nonmonotonic,[9,20,22] indicating a change in the mechanism for the scattering of normal carriers in the HTSC at $\Delta y \cong 0.12$,[9,22] i.e., precisely in samples with $T_c \cong 80$ K.

Consequently, in YBCO films with T_c of the order of 80 K it is conjectured that a coexistence of the magnetic and correlation interactions should occur, and that that probably accounts for their extremely peculiar properties manifested in measurements of $\rho_{xx}(T)$[1,20] and the Hall effect.[22,23] It was natural to expect that the corresponding features would also be observed in a study of the fluctuation conductivity in such samples.

In this paper the new approach to the analysis of fluctuation conductivity in HTSCs which was developed in Ref. 5 is used to investigate the temperature dependence of $\sigma'(T)$ in YBCO films with $T_c \cong 80$ K. Our previous results, including measurements of the fluctuation conductivity on optimally and lightly doped films of YBCO[5] and on YBCO–PrBCO superlattices,[16,18] are also compared and analyzed. On the basis of this analysis the possible mechanisms for the nucleation of superconducting pairing in HTSCs are considered.

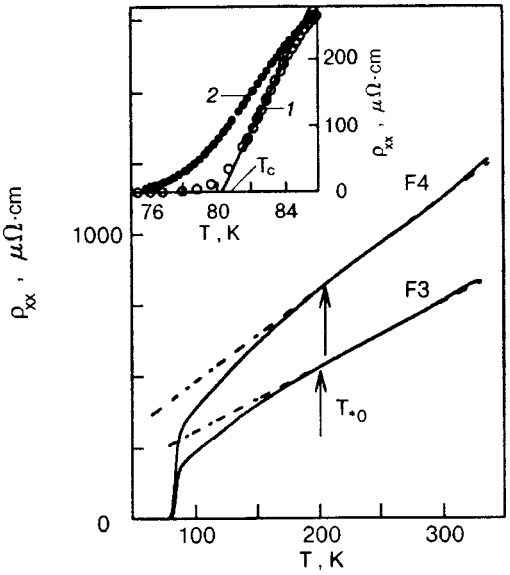

FIG. 1. Temperature dependence of the resistivity for samples F3 and F4; the dashed lines show the extrapolation of the resistivity in the normal state to the low-temperature region; the inset shows the resistive transition of sample F4 in zero magnetic field (curve 1) and in a field $B = 0.6$ T (curve 2).

EXPERIMENTAL RESULTS

In preparing the samples our task was to obtain YBCO films with different oxygen content and with the good structural quality necessary to ensure a high probability of observing the Maki–Thompson fluctuation contribution to $\sigma'(T)$.[5] The films were prepared by laser deposition on $SrTiO_3$ (100) substrates. This method[24] reproducibly yields *c*-oriented epitaxial films of YBCO, as was monitored by investigating the corresponding x-ray and Raman spectra. The technique used to prepare the samples is described in detail in Ref. 5.

The temperature dependence of ρ_{xx} was investigated for samples F3 ($T_c \cong 81.4$ K) and F4 ($T_c \cong 80.3$ K), of thickness $d_0 = 850$ Å (Fig. 1). The inset in Fig. 1 shows $\rho_{xx}(T)$ for sample F4 in zero magnetic field (curve *1*, on which we have indicated how T_c is determined) and at $B = 600$ mT (curve *2*), which confirms the phase homogeneity of the samples. The parameters of the samples are given in Table I. By comparing these results with the analogous curves obtained for single crystals,[20] we can estimate the oxygen index of the samples as follows: $\Delta y \cong 6.8$ (sample F3) and $\Delta y \cong 6.78$ (sample F4).

As we see in Fig. 1, decreasing T_c by only 1 K leads to a sharp increase in the resistivity: $\rho(100\text{ K})(\text{F4})/\rho(100\text{ K})(\text{F3}) \approx 1.6$ (see Table I), which can likely be attributed to

TABLE I. Resistive properties of the samples.

Sample	d_0, Å	T_c, K	ΔT, K	T_c^{mf}, K	ρ (100 K), μΩ·cm	ρ (300 K), μΩ·cm	$d\rho/dT$, μΩ·cm·K^{-1}	T_{*0}, K
F3	850	81.4	5.0	84.55	237	760	2.61	200
F4	850	80.3	5.5	83.4	386	1125	3.55	210

the expected enhancement of the influence of spin fluctuations on the scattering mechanism.[6] Here T_{*0} increases to 210 for sample F4, and above $T\sim 250$ K there is a noticeable "buckling" of the $\rho_{xx}(T)$ curve due to the enhancement of the electron–electron interaction at high temperatures.[6] Thus the resistive curve takes the typical form for 80-kelvin YBCO films,[23] with a relatively short linear part (210–250 K). In accordance with the NAFL model and the approach we developed in Ref. 5 for the analysis of fluctuation conductivity in HTSCs, this linear segment, extrapolated to the low-temperature region (the dashed line in Fig. 1), determines the normal-state resistivity $\rho_N(T)$ used for calculating $\sigma'(T)$ according to Eq. (1). In the same way $\rho_N(T)$ was determined for sample F3, for which, as expected, the $\rho_{xx}(T)$ curve has a longer linear region (200–270 K). Actually, however, the resistivity curve for sample F3 exhibits the same features as that for sample F4, only less pronounced. In summary, one can say that the resistive measurements evidently confirm the predicted sharp change in the parameters of YBCO films when T_c approaches 80 K.

ANALYSIS OF THE RESULTS

The general theory of fluctuation conductivity in layered superconductors was developed by Hikami and Larkin (HL)[25] and predicts a transition (crossover) from a Maki–Thompson (MT)[26] fluctuation mechanism to a Lawrence–Doniach (LD)[27] mechanism as the temperature approaches T_c. Knowing the crossover temperature, one can determine both the coherence length $\xi_c(0)$ and the phase relaxation time τ_φ of the fluctuational pairs, since the MT contribution depends on τ_φ.[26] A comparison of τ_φ with the charge carrier transport time τ is crucial for understanding the mechanisms for scattering and superconducting pairing in HTSCs. Thus the presence of a MT contribution is extremely important for deciding the nature of the superconducting pairing in HTSCs. In particular, in a number of theoretical works it is assumed that the presence of appreciable MT fluctuations rules out the possibility of non-*s* pairing in cuprates.[28] However, the question of whether a fluctuation contribution of the MT type is present in cuprates remains in dispute, since, except for measurements on YBCO–PrBCO superlattices,[18] it has not been possible to observe the MT contribution and, hence, the MT–AL crossover, in measurements on YBCO single crystals[14,15] and thin films.[13,17,19] At best it has been reported that the experimental data can be extrapolated by a smooth curve consisting of a sum of the AL and MT contributions.[15,19] Strictly speaking, this result seems rather strange, since the MT contribution is clearly observed in studies of the magnetoresistance on the same single crystals[15] and superlattices[29] and also on thin films of YBCO.[30–32]

In our view, this is due to at least two causes. The first is the poor structure of the ceramics[12] and of the first HTSC thin films.[13] As a consequence, such samples are characterized by a strong inelastic scattering[33,34] and, hence, strong pair breaking. Because of this, the temperature dependence of the fluctuation conductivity in those samples is described by the LD model,[27] which predicts a smooth transition of the fluctuation mechanism of the AL type from 2D to 3D behavior as $T\to T_c$. Here it is assumed that the MT contribution to the fluctuation conductivity is absent. The second cause is the indeterminacy in the choice of T_c^{mf} (the critical temperature in the mean field approximation), which is used in calculating $\sigma'(T)$,[13–19] and the consequent indeterminacy in the choice of methods of analysis.[14,17,19] As was shown in Ref. 17, the choice of T_c^{mf} has a very strong influence on the resulting slope of the $\sigma'(T)$ curve in the 3D region. As a consequence, the values of $\tau_\varphi(100\ \mathrm{K})$ measured by different authors lie in an interval from 1×10^{-13} s (Ref. 32) to 3.5×10^{-14} s (Refs. 18 and 29). To eliminate the second cause, theoretical models considering a different approach to the description of the fluctuation conductivity in HTSCs have been proposed in a number of papers;[17,34,35] the detailed analysis of these models is beyond the scope of this study. However, a common feature of these models is the assumption that the MT contribution is absent, and, in view of what we have said, that assumption is poorly founded.

It was shown in Ref. 5 that, in contrast to previous studies, the $\sigma'(T)$ curve of well-structured YBCO films for $T_0<T<T_{c0}$ is in fact extrapolated by the 2D MT contribution of the Hikami–Larkin theory[25]

$$\sigma'_{MT}=\left[\frac{e^2}{8\hbar d(1-\alpha/\delta)}\right]\ln\left\{\frac{(\delta/\alpha)[1+\alpha+(1+2\alpha)^{1/2}]}{1+\delta+(1+2\delta)^{1/2}}\right\}\varepsilon^{-1}. \tag{2}$$

Here $\alpha=2\xi_c^2(T)/d^2=2[\xi_c(0)/d]^2\varepsilon^{-1}$ is the coupling parameter, $\varepsilon=\ln(T/T_c^{mf})\approx(T-T_c^{mf})/T_c^{mf}$ is the reduced temperature, $d\cong11.7$ Å is the distance between the CuO_2 conducting layers in YBCO, and

$$\delta=1.203(l/\xi_{ab})(16/\pi\hbar)[\xi_c(0)/d]^2k_BT\tau_\varphi \tag{3}$$

is the pair-breaking parameter. The factor $1.203(l/\xi_{ab})$, which will henceforth be denoted as β (here l is the mean free path and ξ_{ab} is the coherence length in the ab plane), takes into account the clean-limit approximation introduced in the theory by Bieri, Maki, and Thompson[36] under the condition that nonlocal effects can be neglected. At the same time, near T_c ($T<T_0$) the 3D AL fluctuation mechanism,[11] which governs the fluctuation conductivity in any 3D system, is always present, and

$$\sigma'_{AL}=\frac{2}{32\hbar\xi_c}\varepsilon^{-1/2}. \tag{4}$$

Thus the MT–AL crossover, and not the MT–LD transition predicted by the HL theory, was observed in the experiment of Ref. 5. Here it is significant that the scale factor C_{3D} introduced in the calculations to take into account the inhomogeneous current distribution in the sample in the presence of structural distortions,[13–19] is equal to 1. On physical arguments it is clear that as the temperature is raised, the 3D fluctuation regime will persist as long as it remains possible for the Josephson interaction to occur between CuO_2 conducting planes, i.e., as long as $\xi_c(T)\geqslant d$ (Ref. 37). Consequently, in this case the 2D–3D crossover should occur at $\xi_c(T)\cong d$, i.e., at

$$\xi_c(0)\cong d\varepsilon^{1/2}, \tag{5}$$

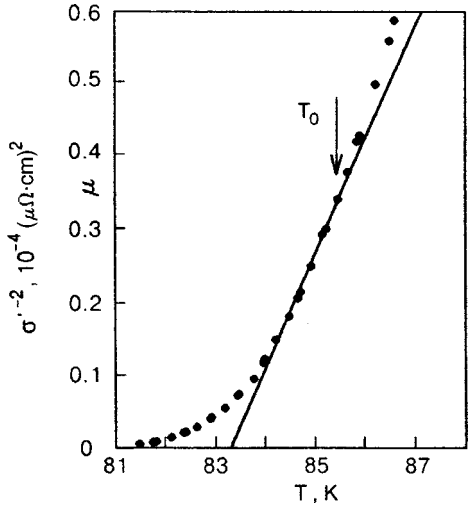

FIG. 2. Plot of σ'^{-2} versus T for sample F4 (points); the straight line shows the extrapolation of the 2D region; its intercept with the T axis gives T_c^{mf}.

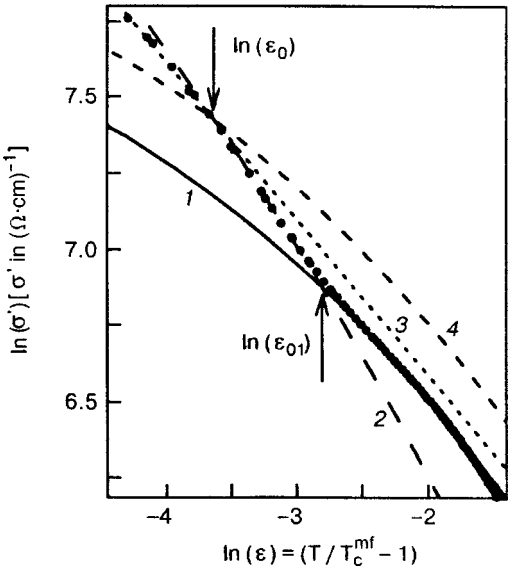

FIG. 3. Comparison of the experimental curve of $\ln(\sigma')$ versus $\ln(\varepsilon)$ (points) for sample F4 ($T_c^{mf}=83.4$ K) with the fluctuation theories: curve *1*—the MT contribution ($C_{2D}=0.272$, $d=11.7$ Å), curve *2*—the LD contribution ($C_{3D}=0.71$, $d=11.7$ Å), curve *3*—the AL (3D) contribution ($C_{3D}=0.632$), and curve *4*—the MT contribution ($C_{2D}=0.347$, $d=11.7$ Å). $\xi_c(0)=(1.78\pm0.01)$ Å.

which is twice as large as predicted by the HL[25] and LD[27] theories. Moreover, for well-structured samples the LD model does not correspond to experiment in any of the temperature intervals of interest.[5]

In this paper we have carried out the first studies of YBCO films with $T_c\approx80$ K, which turn out to have a much more complicated dependence $\sigma'(T)$ than that measured for the optimally and lightly doped films.[5] As we have said, for analysis of the fluctuation conductivity it is extremely important to determine T_c^{mf}, since outside the region of critical fluctuations, $\sigma'(T)$ is a function only of $\varepsilon=(T-T_c^{mf})/T_c^{mf}$ (Ref. 25). As before, we determined T_c^{mf} by extrapolation of the linear part of the $\sigma'^{-2}(T)$ curve to its intercept with the temperature axis.[5,13] In this case $T_c^{mf}>T_c$ and is that temperature which separates the region of fluctuation conductivity from the region of critical fluctuations.[13] Figure 2 shows the $\sigma'^{-2}(T)$ curve (data points) for sample F4. The 3D region, which is extrapolated by a straight line, is clearly visible. Its intercept with the temperature axis gives $T_c^{mf}\cong83.4$ K. However, in comparison with the optimally doped films,[5] for sample F4 the 3D region is somewhat shorter, and above $T_0\approx85.33$ K the experimental data deviate to the left from the straight line, as is characteristic for the LD model.[12–15,19] If a fluctuation mechanism of the MT type is realized for $T>T_0$, the data always deviate to the right.[5]

Figure 3 shows the $\sigma'(T)$ curve for sample F4, for which the behavioral features of the fluctuation conductivity are expressed more clearly than for F3. It is seen that, as in the optimally doped samples, below $T_{c0}\approx97.9$ K the $\sigma'(T)$ curve is well extrapolated by the MT contribution of HL theory (curve *1* in Fig. 3). However, here $\ln(\varepsilon_{c0})\cong-1.75$, i.e., the region of 2D fluctuations is considerably longer. Moreover, upon further lowering of the temperature one observes an unexpected transition from MT fluctuational behavior to behavior of the LD type (curve *2*) for $\ln\varepsilon_{01}\cong-2.81$ ($T_{01}\approx88.4$ K), which is denoted by an arrow in Fig. 3. Having determined ε_{01} it is easy to obtain $\xi_c(0)=(2.87\pm0.02)$ Å from (5) and $\tau_\varphi(100\text{ K})\beta\cong4.98\times10^{-13}$ s from Eq. (6) of Ref. 5. However, using these parameters one cannot match the calculated and experimental curves in a reasonable way in any of the temperature intervals. The $\sigma'(T)$ curve for $\ln\varepsilon_0\cong-3.766$ ($T_0=85.33$ K) has a second crossover, from LD to the expected 3D AL behavior (2), also indicated by an arrow (curve *3* in Fig. 3). Using the value found for ε_0, we obtain $\xi_c(0)=(1.78\pm0.01)$ Å and $\tau_\varphi(100\text{ K})\beta\cong13.24\times10^{-13}$ s. For these values of the parameters the calculated and experimental curves agree in all three temperature intervals (Fig. 3). Consequently, in this case it is the crossover at $\ln\varepsilon_0$ that determines the value of the parameters of the fluctuation theory, while the crossover at $\ln\varepsilon_{01}$ signifies only a changeover of the scattering mechanism for fluctuational pairs in the 2D region as the temperature is lowered. Sample F3 manifests the same fluctuational behavior (the data points in Fig. 4) with crossovers at $\ln\varepsilon_{01}\cong-3.2$ ($T_{01}\approx88.0$ K) and $\ln\varepsilon_0\cong-3.80$ ($T_0\approx86.44$ K). Using the value of ε_0 found from the second crossover, one can calculate the values $\xi_c(0)=(1.75\pm0.01)$ Å and $\tau_\varphi(100\text{ K})\beta\cong13.40\times10^{-13}$ s and describe completely the $\sigma'(T)$ curve below $T_{c0}\approx98.8$ K ($\ln\varepsilon_{c0}\cong-1.78$) (Fig. 4). However, all of the behavioral features of the fluctuation conductivity mentioned above for sample F3 (Fig. 4) are much less pronounced than for sample F4 (Fig. 3), in complete agreement with the results of the resistive measurements (Fig. 1).

We assume that the type of behavior of $\sigma'(T)$ found above, with an intermediate fluctuation region of the LD type, is typical for 80-kelvin YBCO films and, as mentioned, is probably due to the coexistence of magnetic and correlation interactions in such samples. However, as we have said, the LD model doesn't work for well-structured YBCO films[5]—it describes HTSC systems with an inhomogeneous structure[11,12] and samples with artificially created defects.[38,39] In all of these cases $C_{3D}\ll1$, which indicates the presence of strong structural distortions a percolation nature of the current flow through the sample.[23,40] As a result, in

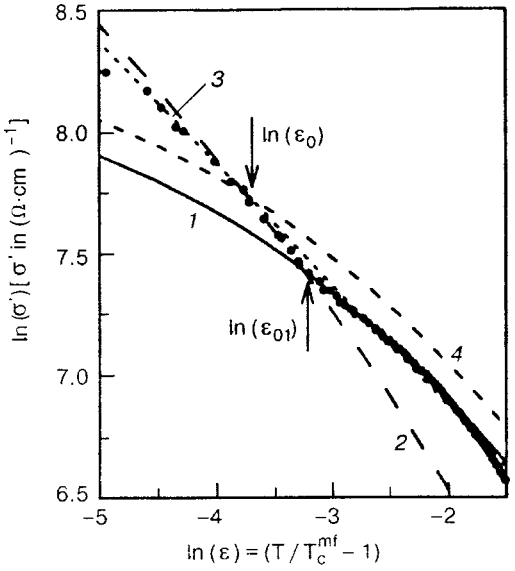

FIG. 4. Comparison of the experimental curve of $\ln(\sigma')$ versus $\ln(\varepsilon)$ (points) for sample F3 ($T_c^{mf}=84.55$ K) with the fluctuation theories: curve *1*—the MT contribution ($C_{2D}=0.391$, $d=11.7$ Å), curve *2*—the LD contribution ($C_{3D}=0.918$, $d=11.7$ Å), curve 3—the AL (3D) contribution ($C_{3D}=0.82$), and curve *4*—the MT contribution ($C_{2D}=0.45$, $d=11.7$ Å). $\xi_c(0)=(1.75\pm0.01)$ Å.

these HTSC systems there should be appreciable scatter in the effective distances between superconducting planes. It is clear that in that case it is hard to assign some definite dimensionality to the electronic system of the sample. Evidently it is only in this case that the temperature dependence of the fluctuation conductivity will be determined by the ratio $\xi_c(T)/d$, as follows from the LD model.[27]

Thus the contribution of the fluctuation mechanism of the LD type to $\sigma'(T)$ for samples F3 and F4 is a definite indication of the presence of inhomogeneities in the structure of 80-kelvin YBCO systems. For both samples $C_{3D}<1$ (Table II), and the ratio $C^*=C_{3D}/C_{2D}=2.1$ (F3) and 2.3 (F4), much larger than the typical value for well structured films: $C^*=(1.82\pm0.02)$.[5] It should also be noted that $\ln(\delta_{th})=\ln(\varepsilon_{c0})\cong(-1.75\pm0.05)$ for samples F3 and F4, indicating that in those samples T_c is almost 15 K lower than T_{c0} and presupposing a stronger pair-breaking mechanism than in optimally doped systems. All three results confirm the validity of the conclusion reached. We assume that while the inequality $C_{3D}<1$ reflects the inhomogeneity of the structure of any HTSC sample regardless of the oxygen content, the condition $C^*>1.82$ characterizes some specific inhomogeneity of 80-kelvin systems, which may result from the appearance of oxygen vacancies in the 1D CuO chains as Δy is decreased.[22] At the same time, the results of a study of the fluctuation conductivity (see Figs. 3 and 4) shows that this process follows definite rules that are hard to explain solely in terms of structural distortions. Indeed, the features of the behavior of the fluctuation conductivity and the inhomogeneity of the structure arise only for $T_c\leqslant 82$ K, whereas the carrier density and the value of T_c (see Tables I and II) decrease monotonically as Δy goes from 6.9 ($T_c\cong 90$ K) to 6.78 ($T_c\cong 80$ K). Furthermore, the observed features increase sharply as T_c approaches 80 K, in complete agreement with the ideas of Refs. 8, 9, and 22 about a change of mechanisms for the interaction of charge carriers in YBCO at oxygen concentrations corresponding to $T_c\cong 82$ K. Most likely the transformation of the structure and the changeover of interaction mechanisms with decreasing carrier concentration are two interrelated processes.[1,8,32] As a consequence, the behavior of the fluctuation conductivity in such samples becomes rather complex, since a fluctuation contribution of the MT type, which, as we have said, is characteristic for samples with good structure, is observed simultaneously with the LD contribution.

It is of interest to find out what will happen if for sample F4 one constructs Eq. (2), which describes the MT contribution, with the same parameters of the fluctuation conductivity but with $C_{2D}=C_{3D}/1.82=0.347$. As expected, in this case the $\sigma'(T)$ curve corresponding to the MT contribution (curve *4* in Fig. 3) intersects the experimental curve of $\sigma'(T)$ precisely at the crossover point at $\ln\varepsilon_0\cong-3.766$. An analogous result is obtained for sample F3 (curve *4* in Fig. 4) if one chooses $C_{2D}=C_{3D}/1.82=0.45$. Thus it can be assumed that in the absence of this specific inhomogeneity, the experimental curve of $\sigma'(T)$ in the 2D region, as in the case of optimally doped films, would coincide with curve *4*, i.e., it would be determined by the MT distribution alone. This result confirms the conclusion of Ref. 5 that the ratio $C^*=(1.82\pm0.02)$ is universal for YBCO, and it indicates that, by analogy with optimally doped systems,[5] the crossover at $\varepsilon=\varepsilon_0$ is just of the MT–AL type which is responsible for the fluctuation parameters of the sample. An additional argument in favor of this assertion is the fact that the values of $\xi_c(0)$, which are determined by ε_0, obey the relation $\xi_c(0)\propto 1/T_c$ (Fig. 5). Thus for $T_c\leqslant(82\pm1)$ K the specific inhomogeneity of YBCO films begins to be manifested, accompanied by

TABLE II. Electronic parameters of the samples.

Sample	C_{3D}	R_H (100 K), 10^{-9} m^3/C	n (100 K), 10^{21} cm^{-3}	n_0	r	l (100 K), Å	μ_H (100 K), cm^2/V·s
F1	1	2.45	2.7	0.47	1.06	48.6	16.55
F3	0.82	3.26	2.42	0.42	1.26	46.6	16.80
F4	0.632	4.04	2.3	0.40	1.49	44.8	16.56
F6	2 (1)	5.80	1.15	0.20	1.07	30.5	15.92
S1	3.8	3.28	2.36	0.41	1.24	20.1	7.32

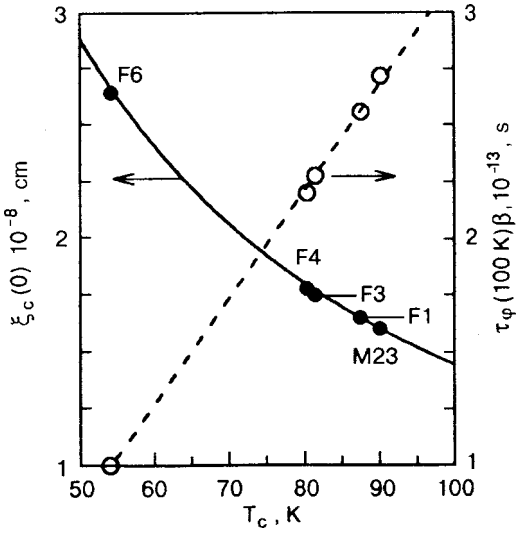

FIG. 5. $\xi_c(0)$ (filled circles) and $\tau_\varphi(100\ \mathrm{K})\beta$ (unfilled circles) versus T_c; the solid curve is calculated by Eq. (6) with the parameters for sample F1.

enhancement of the magnetic interaction in the HTSC.[6,9] As a result, the fluctuation mechanism of the MT type is gradually suppressed, giving way to the LD mechanism (see Figs. 3 and 4). The closer T_c is to 80 K, the larger is the region described by the LD model, and the larger are the values of C_{3D}, C^*, and $\rho_{xx}(T)$; the other parameters of the sample also change significantly (see Tables I and II); this, we believe, is a consequence of the growing influence of spin fluctuations[6,10] and reflects the complex dynamics of the coexistence of antiferromagnetic ordering and superconductivity in HTSCs.

At the same time, it remains an open question of how to explain the presence of fluctuation processes governed by the MT and LD contributions in the same sample. Obviously, the CuO_2 should not contain defects, since otherwise the MT mechanism will not be realized. At the same time, the number of oxygen vacancies in the CuO chains is already extremely large.[22] As a result, the current will flow through the sample in a percolational manner,[40] leading to scatter in the effective distances d_i between conducting planes, which, as we have said, is necessary for realization of the fluctuation mechanism of the LD type. Apparently, in YBCO systems of this type the evolution of $\sigma'(T)$ occurs as follows. With decreasing temperature the 2D MT regime exists until at $\varepsilon \cong \varepsilon_{01}$ the quantity $\xi_c(T)$ becomes equal to the smallest possible distance d^* between conducting planes. After this a Josephson interaction is realized between planes, and the 2D MT mechanism gives way to the LD mechanism. It is clear that in the given case $d^* < d$. From Eq. (5) one can easily estimate that $d^*(\varepsilon_{01}) \cong 8.2$ Å for sample F3 and $d^*(\varepsilon_{01}) \cong 7.2$ Å for sample F4. As the temperature is lowered further, a smooth transition of the LD type occurs from the 2D MT to the 3D AL fluctuation mechanism. Here, as a result of the growth of $\xi_c(T)$, an ever greater number of conducting layers are coupled by the Josephson interaction, until at ε_0, where $\xi_c(T) \cong d = 11.7$ Å, the system undergoes a transition to a 3D electronic state. It should be emphasized that samples F3 and F4 do not have any conducting layers with $d_i > 11.7$ Å, since the crossover at ε_0 is quite distinct. On the other hand, we have been unable to approximate the $\sigma'(T)$ curve in the 2D region by the MT contribution in a reasonable way using different $d_i < 11.7$ Å as a fitting parameter. Consequently, the possible scatter in the distances between conducting layers ($d^* < d_i < 11.7$ Å), giving rise to a fluctuation mechanism of the LD type, is extremely specific and relatively small, as is confirmed by the good quality of the film samples. In samples with a distinctly poor structure[11,12,37,38] this scatter is much larger, since the MT mechanism is completely suppressed and a fluctuation mechanism of the LD type is realized instead. It is important to note that these samples are optimally doped YBCO systems, and the LD type of dependence of $\sigma'(T)$ observed in them is due specifically to structural defects and not to a change of the stoichiometric state of the samples.

In spite of the above-noted complexity of the fluctuation conductivity, the experimental observation of the MT contribution allows one to determine the values of the parameter $\tau_\varphi(100\ \mathrm{K})\beta$; however, to determine the values of $\tau_\varphi(100\ \mathrm{K})$ in explicit form, it is necessary to find $\beta = [1.203(l/\xi_{ab})]$.[5] For this we have used the results of measurements of the Hall coefficient R_H and the approach developed in Ref. 5. Using the formula $l = (\hbar \mu_H / e)(2\pi n_s)^{1/2}$, where μ_H is the mobility of the Hall carriers and n_s is the surface density of the carriers, we find the mean free path of the charge carriers in sample F4: $l(100\ \mathrm{K}) = v_F \tau \cong 44.8$ Å, where v_F is the Fermi velocity. From published data[31,41,42] for sample F1 the average value of $\xi_{ab}(0)$ was chosen equal to 13.0 Å.[5] Assuming that $\xi_{ab}(\mathrm{F4})/\xi_{ab}(\mathrm{F1}) \sim \xi_c(\mathrm{F4})/\xi_c(\mathrm{F1})$, we obtain $\xi_{ab}(0) = 14.2$ Å for sample F4. Hence we find that $\beta = 3.85$ and, using the value $\tau_\varphi(100\ \mathrm{K})\beta \cong 12.95 \times 10^{-13}$ s found above, we obtain the desired value: $\tau_\varphi(100\ \mathrm{K}) \cong 3.36 \times 10^{-13}$ s, in excellent agreement with the values of $\tau_\varphi(100\ \mathrm{K})$ calculated for optimally and lightly doped YBCO films.[5] Doing the analogous calculations for sample F3, we obtain $\tau_\varphi(100\ \mathrm{K}) \approx 3.3 \times 10^{-13}$ s (Table III), i.e., practically the same as for sample F4. All of the parameters calculated for samples F3 and F4 are presented in Tables II and III.

For analysis of the parameters of the fluctuation conductivity and Hall effect for YBCO samples with different oxygen content, the tables also include the results obtained for samples F1 and F6 in Ref. 5 and for a 7YBCO–7PrBCO superlattice (sample S1 from Ref. 18), recalculated in the new approach to the analysis of fluctuation conductivity. Since the main parameters of a HTSC are temperature dependent, the estimates have been made for $T = 100$ K, as is customary in the literature.[15,30] It is clearly seen that as T_c decreases (with decreasing oxygen content), R_H increases noticeably, while the carrier density n and n_0, the carrier density normalized by the volume of the unit cell, decrease, and also that the measured parameter values agree with the analogous results reported in Refs. 20 and 22. At the same time, l and $\tau(100\ \mathrm{K})$ decrease. Nevertheless, $l(0) > l(100\ \mathrm{K}) \gg \xi_{ab}$, as before, and we can therefore state that the films studied here are indeed type-II superconductors in the clean limit. At the same time, μ_H and v_F remain practically unchanged with decreasing oxygen content. This result can be regarded as an additional argument in favor of the correctness of the approach developed in this paper for analysis of the fluctuation conductivity, since we indeed have

TABLE III. Electronic parameters of the samples.

Sample	v_F, 10^7 cm/s	m^*/m_0, (100 K)	τ (100 K), 10^{-13} s	$\xi_c(0)$, Å	β (100 K)	τ_φ (100 K), 10^{-13} s	C^*
F1	1.17–1.28	4.68–4.26	0.42–0.38	1.65	4.5	3.35	1.84
F3	1.15–1.27	5.33–4.84	0.40–0.36	1.75	4.06	3.30	2.1 (1.82)
F4	1.15–1.27	6.11–5,56	0.38–0.34	1.78	3.85	3.36	2.3 (1.82)
F6	1.16–1.28	3.10–2.81	0.26–0.24	2.64	1.76	3.36	1.81
S1	1.14–1.26	5.2–4.72	0.18–0.16	2.8	1.74	3.3	1.82

$\mu_H = R_H/(\rho C_{3D})$, where all of the parameters are measured independently. It follows that for well-structured HTSC samples with different T_c the ratio of their Hall coefficients R_H should be equal to the ratio of the values of ρC_{3D} in them, as is confirmed by our experiment. For example, the ratio $R_H(\mathrm{F3})/R_H(\mathrm{F1}) = 1.33$, and $\rho C_{3D}(\mathrm{F3})/\rho C_{3D}(\mathrm{F1}) = 1.31$. Similar ratios are obtained for the other samples as well, including for sample F6, which eliminates the question of whether C_{3D} should be chosen equal to 1 rather than 2 in estimating the value of ρC_{3D} in that case.[5] From these considerations it can be assumed that for the YBCO–PrBCO superlattice ($T_c = 80.3$ K, $\rho(100\ \mathrm{K}) = 118\ \mu\Omega\cdot\mathrm{cm}$) the value of the factor C_{3D} is overestimated by about a factor of two. However, if we set $C_{3D} = 1.74$, then the value of $\tau_\varphi(100\ \mathrm{K})$ comes out a factor of two smaller, which seems unlikely in view of the results of the analysis of the fluctuation conductivity[18] and magnetoresistance[29] for this sample. Thus the small values of μ_H in the given case can most likely be ascribed to the influence of the Pr layers, which typically cause such effects in HTSC systems of this kind.[43]

In Table II and III we see that the r factor[5] and, more importantly, the effective mass m^* of the carriers depend nonmonotonically on T_c, and n and m^* have their maximum values for 80-kelvin samples (F3 and especially F4). In our view, this result confirms the earlier conjecture that the scattering intensity in the 80-kelvin YBCO superconductor is much higher than in the optimally doped systems, increasing sharply as T_c approaches 80 K because of the enhancement of the magnetic interaction, which can also result in an increase in the effective mass of the carriers. Apparently the increase in m^* can also explain other behavior features of 80-kelvin YBCO systems. Interestingly, m^* decreases noticeably for lightly doped systems (sample F6). This result seems reasonable, since there is a simultaneous decrease in the r factor, which characterizes the carrier scattering intensity in the sample[5] and is measured independently. Consequently, the decrease of m^* and of the r factor is probably due to the decrease in the carrier concentration (see Table II). As a result, the r factor for sample F6 is practically the same as for sample F1.

Finally, in spite of the significant difference in the parameters, it is found for all of the YBCO films studied that $\tau_\varphi(100\ \mathrm{K}) = (3.33 \pm 0.03) \times 10^{-13}$ s and $C^* = (1.82 \pm 0.02)$. This value of $\tau_\varphi(100\ \mathrm{K})$ correlates with the results of recent measurements of the magnetoresistance in YBCO–PrBCO superlattices[29] and optimally doped YBCO films.[42] Consequently, it can be concluded that the values found for $\tau_\varphi(100\ \mathrm{K})$ and C^* are universal for YBCO oxides, independent of the oxygen content in the samples. This is the main experimental result of the study of fluctuation conductivity in well-structured YBCO systems. Thus the spin fluctuations and other possible types of interactions of quasiparticles in YBCO superconductors, while substantially determining the operative scattering mechanism for normal carriers in samples of different oxygen content, have practically no influence on the mechanism for the superconducting pairing, which is characterized by the quantity τ_φ.

We also note that the ratio between $\xi_c(0)$ and T_c for the samples obeys the general theory of superconductivity,[44] which implies that

$$\xi_0 \sim \hbar v_F/[\pi\Delta(0)], \tag{6}$$

where $\Delta(0)$ is the order parameter at $T = 0$ K. Taking into account that $2\Delta(0)/k_B T_c \approx 5$ in YBCO oxides[45] and assuming that $\xi_0 = \xi_c(0)$, we can rewrite Eq. (6) as

$$\xi_c(0) = G/T_c, \tag{7}$$

where $G = 2K\hbar v_F/(5\pi k_B)$, and $K \approx 0.12$ is a coefficient of proportionality. The experimentally determined ratio for samples F1 and F6 investigated in Ref. 5 can be written as follows: $T_c(\mathrm{F1})/T_c(\mathrm{F6}) = 1.61$, and $\xi_c(0)(\mathrm{F6})/\xi_c(0)(\mathrm{F1}) = 1.6$. Analogous ratios are obtained for the remaining samples as well, i.e., the relation $\xi_c(0) \propto 1/T_c$ holds for all of the YBCO films. It is clear that in this case v_F should be constant, as we confirmed in the calculation (see Table III). A plot of $\xi_c(0)$ as a function of T_c, calculated for sample F1 according to Eq. (7) with $G = 1.46 \times 10^{-6}$ Å·K, is shown by the solid curve in Fig. 5. The filled circles are the experimental values of $\xi_c(0)$ for all of the samples studied, including sample M-23 of Refs. 38 and 39 ($T_c = 90$ K), with specially introduced defects. It should be stressed that, as we have said, for the 80-kelvin samples these are precisely those values of $\xi_c(0)$ which are determined by the crossover at $\varepsilon = \varepsilon_0$. Since $\tau_\varphi(100\ \mathrm{K})$, like $\xi_c(0)$, is determined by the temperature at which the MT–AL crossover takes place, we believe that the result obtained is another piece of evidence that the values of $\tau_\varphi(100\ \mathrm{K})$ have been calculated correctly, and it no doubt indicates that the pairing mechanisms in high-temperature superconductivity to a large degree obey the general theory of superconductivity. Figure 5 also shows the dependence of $\tau_\varphi(100\ \mathrm{K})\beta$ on T_c (unfilled circles) for these same samples, normalized to the value $\tau_\varphi(100\ \mathrm{K})\beta$

$=5.9\times10^{-13}$ s for sample F6 in order to make the scales coincide. We see that the experimental dependence of $\tau_\varphi(100\text{ K})\beta$ increases linearly with increasing T_c, which is apparently a property of YBCO systems. It follows from Fig. 5 that for $T_c \geqslant 130$ K the value of $\xi_c(0)$ should become less than 1 Å, which is unphysical. Thus it is probably the small values of $\xi_c(T)$ in HTSCs that impose limitations on the attainment of high values of T_c. In other words, to achieve higher T_c, substances with large values of the coherence length are needed.

It is clearly seen from Table III that $\tau_\varphi(100\text{ K})/\tau(100\text{ K}) \gg 1$, in qualitative agreement with the theory of Ref. 36, but the real value of the ratio is approximately three times larger than predicted by the theory and increases with decreasing T_c. This result clearly shows that the coupling constant $\lambda_{e\text{ph}}$ of the normal carriers, which is characterized by τ, and λ_{cor}, which governs the interaction of the fluctuational pairs with the normal excitations[18] and is characterized by τ_φ, are very different, and it allows us to discuss the physics of the superconducting pairing in HTSCs. The effective coupling constant can be written as $\lambda_{\text{eff}}=\lambda_{e\text{ph}}+\lambda_{\text{cor}}$ (Ref. 33), where $\lambda_{e\text{ph}}$ and λ_{cor} are determined by the expression[46]

$$\hbar\tau^{-1}=2\pi\lambda k_B T \tag{8}$$

but using $\tau(100\text{ K})$ or $\tau_\varphi(100\text{ K})$, respectively.[5] As a result, for sample F1 the calculated $\lambda_{e\text{ph}}\approx 0.3$. As the T_c value of the sample decreases, $\lambda_{e\text{ph}}$ gradually increases to 0.47 (sample F6). Both values are found in good agreement with the results of resistive and optical measurements on optimally doped[47] and lightly doped[48] YBCO films. At the same time, from Eq. (8) we obtain $\lambda_{\text{cor}}\approx 0.037$ for all of the samples studied. We see that λ_{cor} is extremely small. This means that the interaction of fluctuational pairs with normal excitations, which governs the pair-breaking processes, is extremely weak. It follows that at sufficiently high temperatures the possibility of fluctuational pairing becomes extremely likely. Taking into account that $\delta_{\text{th}}(\varepsilon_{c0})=(T_{c0}-T_c)/T_c=2$ [see Eq. (3)], we can conclude that the theory indeed admits the existence of fluctuational pairs up to a temperature T_{c0} equal to $\sim$264 for sample F1, $\sim$240 K for sample F4, and $\sim$165 K for sample F6. Strictly speaking, the experimentally measured $\sigma'(T)$ goes to zero precisely at T_{*0} (Fig. 1), confirming the conjecture. The fact that for $T>(110\pm10)$ K the experimental $\sigma'(T)$ deviates from the theoretical curve is probably explained by the necessity of taking short-wavelength fluctuations into account in this region of temperatures.[49]

The possibility that paired holes exist in HTSCs at $T \gg T_c$ is widely discussed at the present time.[42,50–52] The observation of a coherent-boson current at $T \geqslant 120$ K[52] and the observation of magnetoresistance described by the fluctuation theories all the way to $T\sim 230$ K[42] have recently been reported for nearly optimally doped YBCO systems. It has been shown theoretically[7,10,53] that pair correlations in HTSCs above T_c can give rise to a highly anisotropic pseudogap in the spectrum of electronic states and lead to distortion of the Fermi surface.[6,50] Studies of Bi-2212 compounds by the method of angle-resolved photoemission spectroscopy (ARPES)[54] and by resistivity[55] and tunneling conductivity[56] measurements have shown the presence of such a pseudogap in samples at temperatures $T_c<T<T_{*0}\cong 170$ K. Thus the presence of fluctuational pairs in HTSCs, at least up to $T\sim(200\pm20)$ K, seems extremely likely.

Summing up, we can conclude that in HTSCs at $T \leqslant T_{*0}$ there are at least two mechanisms that lead to a deviation of $\rho_{xx}(T)$ from the linear trend in the normal state. The first is a rearrangement of the Fermi surface leading to a reduction in the normal-hole scattering of normal carriers.[6,7] The second is the formation of paired holes (fluctuational pairs); in optimally doped YBCO systems this mechanism presumably begins to operate at the same temperature.[49] Thus for $T<T_{*0}$ two different types of charge carriers should exist in a HTSC: normal holes and fluctuational pairs. With decreasing temperature the number of fluctuational pairs n_{sc} should increase and the number of normal holes n should, of course, decrease. Indeed, from Hall effect measurements we find for sample F1, for example, that $n(240\text{ K})\approx 5.4\times10^{21}$ cm^{-3} and $n(100\text{ K})\approx 2.7\times10^{21}$ cm^{-3}. It is most likely this effect that accounts for the anomalous ($\propto 1/T$) temperature dependence of the Hall coefficient usually observed in HTSCs below $T_{*0}\approx(220\pm20)$ K,[19,20,39] whereas for $T_{*0}<T<320$ K both n and R_H remain practically unchanged. In 60-kelvin samples (e.g., sample F6), where n is small from the start, R_H increases smoothly as the temperature is lowered from 320 K. This same result is obtained for lightly doped YBCO systems in Refs. 20 and 22, as well. Most likely in this case the temperature dependence of $R_H(T)$ and $\rho_{xx}(T)$ is mainly determined by the magnetic interaction, and the influence of fluctuational pairs is manifested much closer to T_c, presumably below $\sim$80 K (see Fig. 1 in Ref. 5).

Taking these arguments into consideration together with the universality of the values found for $\tau_\varphi(100\text{ K})$ and C^*, we can present the following picture of the superconducting pairing in optimally doped YBCO superconductors. The fluctuational pairs are apparently nucleated inside the CuO_2 planes at $T \leqslant T_{*0}$, leading to growth of n_{sc}. Since n_{sc} and especially $\xi_c(T)$ are extremely small at temperatures in the range $T_{c0}<T<T_{*0}$, there is most likely no interaction between pairs. The corresponding electronic state of the fluctuational pairs can be treated as zero-dimensional,[57] although such a state is not described by the existing theories of fluctuation conductivity.[49] For $T \leqslant T_{c0}$ the fluctuational pairs begin to overlap, but, as before, only within the CuO_2 planes, forming a 2D electronic state which is described by the MT contribution to HL theory.[25] For $T \leqslant T_0$ the growing value of $\xi_c(T)$ becomes larger than d, and the conducting planes are coupled by a pair tunneling interaction of the Josephson type. Now the fluctuational pairs interact throughout the entire volume of the superconductor, forming a 3D electronic state that is well described by the 3D contribution of AL theory.[11] Indeed, it is only now that the system is fully prepared to complete the transition to the superconducting state. A similar picture is observed in lightly doped systems, the only difference being that the influence of the fluctuational pairs begins to be manifested at a temperature much closer to T_c. The only difference shown by the 80-kelvin films is the presence of the LD fluctuation mechanism together with the

MT one in the 2D fluctuation region, as mentioned above.

Summarizing, we note once again that in a HTSC at $T_c<T<T_{*0}$ there should exist two types of excitations—normal carriers and fluctuational pairs. Thus we see an explicit analogy both between the fluctuational pairs and the spinons predicted by the ''resonant valence bands'' model,[58] which should pair at T_{*0} (Ref. 50), and also between the normal holes and holons,[58] which should condense at T_c (Ref. 50).

CONCLUSION

We have made the first investigation of fluctuation conductivity σ' in $YBa_2Cu_3O_{7-y}$ films with $T_c \approx 80$ K. Unlike the optimally doped films, the $\sigma'(T)$ curves of these samples exhibit a distinct transition from a 2D Maki–Thompson mechanism for the scattering of the fluctuational pairs to a Lawrence–Doniach mechanism and, as the temperature approaches T_c, to a 3D Aslamazov–Larkin mechanism. The closer T_c is to 80 K, the more strongly is the fluctuation mechanism of the MT type suppressed, and it gradually gives way to a LD mechanism. This behavior is probably due to enhancement of the magnetic interaction in YBCO superconductors as $T_c \to 80$ K, which can also result in an increase in the effective mass of the carriers.

With the results obtained we were able to carry out a comparative analysis of the measurements of the fluctuation conductivity and Hall effect on YBCO films with different oxygen content, including a YBCO–PrBCO superlattice. We showed that, in spite of the fact that the value of T_c for the samples varies from 88 K (sample F1) to 54 K (sample F6), for all the samples the values $\tau_\varphi(100\text{ K}) = (3.33 \pm 0.03) \times 10^{-13}$ s and $C^* = (1.82 \pm 0.02)$ were obtained, and the dependence of the coherence length along the c axis, $\xi_c(0)$, on T_c conforms to the general theory of superconductivity. This result suggests that spin fluctuations and other possible types of interactions of quasiparticles in a HTSC, while to a large degree determining the scattering mechanism for normal carriers at different oxygen content, have practically no influence on the mechanism for the superconducting pairing, which is characterized by the value of τ_φ.

A large value of τ_φ leads to small values of the coupling constant λ_{cor} for fluctuational pairs. This means that the interaction of fluctuational pairs with the normal excitations, which substantially governs the pair-breaking processes, is rather weak. Thus at sufficiently high temperatures there is a strong possibility of fluctuational pairing. Based on the likelihood that two types of carriers exist in a HTSC at $T \lesssim 200$ K, viz., normal holes and fluctuational pairs, we have proposed a possible mechanism for the transition from the normal to the superconducting state in HTSCs.

In closing, the authors thank Prof. V. M. Dmitriev for valuable comments in a discussion of the results of this study.

*E-mail:solovjov@ilt.kharkov.ua

[1] Y. Iye, in *Physical Properties of High Temperature Superconductors III*, edited by D. M. Ginsberg, World Scientific, Singapore (1992), p. 285.
[2] C. P. Slichter, in *Strongly Correlated Electronic Systems*, edited by K. S. Bedell, Addison-Wesley, New York (1994).
[3] M. Acquarone (Ed.), *High Temperature Superconductivity, Models and Measurements*, World Scientific, Singapore (1994).
[4] T. R. Chien, Z. Z. Wang, and N. P. Ong, Phys. Rev. Lett. **67**, 2088 (1991).
[5] A. L. Solov'ev and H.-U. Habermeier, and T. Haage, Fiz. Nizk. Temp. **28**, 24 (2002) [Low Temp. Phys. **28**, 18 (2002)].
[6] B. P. Stojkovic and D. Pines, Phys. Rev. B **55**, 8576 (1997).
[7] V. Barzykin and D. Pines, Phys. Rev. B **52**, 13585 (1995).
[8] V. V. Eremenko, V. N. Samovarov, V. N. Svishchev, V. L. Vakula, M. Yu. Libin, and S. A. Uyutnov, Fiz. Nizk. Temp. **26**, 739 (2000) [Low Temp. Phys. **26**, 541 (2000)].
[9] V. V. Eremenko, V. N. Samovarov, V. L. Vakula, M. Yu. Libin, and S. A. Uyutnov, Fiz. Nizk. Temp. **26**, 1091 (2000) [Low Temp. Phys. **26**, 809 (2000)].
[10] B. Bucher, P. Steiner, J. Karpinski, E. Kaldis, and P. Wachter, Phys. Rev. Lett. **70**, 2012 (1993).
[11] L. G. Aslamazov and A. I. Larkin, Phys. Lett. A **26**, 238 (1968).
[12] Y. Matsuda, T. Hirai, and Komiyama, Solid State Commun. **68**, 103 (1988).
[13] B. Oh, K. Char, A. D. Kent, M. Naito, M. R. Beasley, T. H. Geballe, R. H. Hammond, A. Kapitulnik, and J. M. Graybeal, Phys. Rev. B **37**, 7861 (1988).
[14] T. A. Friedmann, J. P. Rice, John Giapintzakis, and D. M. Ginsberg, Phys. Rev. B **39**, 4258 (1989).
[15] K. Winzer and G. Kumm, Z. Phys. B Condensed Matter **82**, 317 (1991).
[16] H.-U. Habermeier, A. L. Solovjov, and V. M. Dmitriev, Physica C **235–240**, 1959 (1994).
[17] A. Gauzzi and D. Pavuna, Phys. Rev. B **51**, 15420 (1995).
[18] A. L. Solovjov, V. M. Dmitriev, H.-U. Habermeier, and I. E. Trofimov, Phys. Rev. B **55**, 8551 (1997).
[19] W. Lang, G. Heine, P. Schwab, X. Z. Wang, and D. Bauerle, Phys. Rev. B **49**, 4209 (1995).
[20] T. Ito, K. Takenaka, and S. Uchida, Phys. Rev. Lett. **70**, 3995 (1993).
[21] G. M. Eliashberg, J. Supercond. **7**, 525 (1994).
[22] Z. Z. Wang, J. Clayhold, and N. P. Ong, Phys. Rev. B **36**, 7222 (1987).
[23] A. L. Solovjov, Fiz. Nizk. Temp. **24**, 215 (1998).
[24] H.-U. Habermeier, Appl. Surf. Sci. **69**, 204 (1993).
[25] S. Hikami and A. I. Larkin, Mod. Phys. Lett. B **2**, 693 (1998).
[26] K. Maki, Prog. Theor. Phys. **39**, 897 (1968); R. S. Tompson, Phys. Rev. B **1**, 327 (1970).
[27] W. E. Lawrence and S. Doniach, in *Proceedings of the Twelfth International Conference on Low Temperature Physics*, Kyoto 1971, p. 361.
[28] S. K. Yip, Phys. Rev. B **41**, 2612 (1990).
[29] W. Volz, F. S. Razavi, G. Quirion, H.-U. Habermeier, and A. L. Solovjov, Phys. Rev. B **55**, 6631 (1997).
[30] Y. Matsuda, T. Hirai, S. Komiyama, T. Terashima, Y. Bando, K. Iijima, K. Yamamoto, and K. Hirata, Phys. Rev. B **40**, 5176 (1989).
[31] J. Sugawara, H. Iwasaki, N. Kabayashi, H. Yamane, and T. Hirai, Phys. Rev. B **46**, 14818 (1992).
[32] W. Holm, O. Rapp, C. N. L. Johnson, and U. Helmersson, Phys. Rev. B **52**, 3748 (1995).
[33] P. A. Lee and N. Read, Phys. Rev. Lett. **58**, 2691 (1987).
[34] M. L. Horbach, F. L. J. Vos, and W. van Saarloos, Phys. Rev. B **49**, 3539 (1994).
[35] D. Neri, E. Silva, S. Sarti, R. Marcon, M. Giura, R. Fastampa, and N. Sparvieri, Phys. Rev. B **58**, 14581 (1998).
[36] J. B. Bieri, K. Maki, and R. S. Thompson, Phys. Rev. B **44**, 4709 (1991).
[37] V. M. Dmitriev, A. L. Solov'ev (Solovjov), and A. I. Dmitrenko, Fiz. Nizk. Temp. **11**, 374 (1985) [Sov. J. Low Temp. Phys. **11**, 374 (1985)].
[38] T. Haage, J. Q. Li, B. Leibold, M. Cardona, J. Zegenhagen, H.-U. Habermeier, A. Forkl, Ch. Jooss, R. Warthmann, and H. Kronmuller, Solid State Commun. **99**, 553 (1996).
[39] A. L. Solovjov, H.-U. Habermeier, and T. Haage (to be published).
[40] G. Doornbos, R. J. Wijngaarden, and R. Griessen, Physica C **235–240**, 1371 (1994).
[41] K. Semba and A. Matsuda, Phys. Rev. B **55**, 11103 (1997).
[42] J. Axnas, B. Lundqvist, and O. Rapp, Phys. Rev. B **58**, 6628 (1998).
[43] M. Affronte, J.-M. Triscone, O. Brunner, L. Antognazza, L. Mieville, M. Decroux, and Q. Fischer, Phys. Rev. B **43**, 11484 (1991).
[44] P. G. De Gennes, *Superconductivity of Metals and Alloys*, Benjamin, New York–Amsterdam (1966).

[45] V. M. Dmitriev, A. L. Solov'ev (Solovjov), and A. I. Dmitren-ko, Fiz. Nizk. Temp. **15**, 356 (1989) [Sov. J. Low Temp. Phys. **15**, 200 (1989)].
[46] P. B. Allen, T. B. Beaulac, F. S. Khan, W. H. Butler, F. J. Pinski, and J. H. Swihart, Phys. Rev. B **34**, 4331 (1986).
[47] D. B. Tanner and T. Timusk, in *Physical Properties of High Temperature Superconductors III*, edited by D. M. Ginsberg, World Scientific, Singapore (1992), p. 285.
[48] Z. Schlesinder, R. T. Collins, F. Holtzberg, C. Feild, S. H. Blanton, U. Welp, G. W. Crabtree, Y. Fang, and J. Z. Liu, Phys. Rev. Lett. **65**, 801 (1990).
[49] C. Carballeira, S. R. Curras, J. Vina, J. A. Veira, M. V. Ramallo, and F. Vidal, Phys. Rev. B **63**, 144515-1 (2001).
[50] J. R. Engelbrecht, A. Nazarenko, M. Randeria, and E. Dagotto, Phys. Rev. B **57**, 13406 (1998).
[51] V. J. Emery and S. A. Kivelson, Nature (London) **354**, 434 (1995).
[52] K. Kawabata, S. Tsukui, Y. Shono, O. Mishikami, H. Sasakura, K. Yoshiara, Y. Kakehi, and T. Yotsuya, Phys. Rev. B **58**, 2458 (1998).
[53] T. Timusk and B. Start, Rep. Prog. Phys. **62**, 61 (1999).
[54] H. Ding, T. Yokoya, J. C. Campuzano, T. Takahashi, M. Randeria, M. R. Norman, T. Mocchiki, K. Kadowaki, and J. Giapintzakis, Nature (London) **382**, 51 (1996).
[55] T. Watanabe, T. Fujii, and A. Matsuda, Phys. Rev. Lett. **79**, 2113 (1997).
[56] M. Suzuki, T. Watanabe, and A. Matsuda, Phys. Rev. Lett. **82**, 5361 (1999).
[57] I. O. Kulik and A. G. Pedan, Fiz. Nizk. Temp. **14**, 700 (1988) [Sov. J. Low Temp. Phys. **14**, 384 (1988)].
[58] P. W. Anderson and Z. Zou, Phys. Rev. Lett. **60**, 132 (1988); P. W. Anderson, Phys. Rev. Lett. **67**, 2092 (1991).

Translated by Steve Torstveit